



KADIR HAS UNIVERSITY  
SCHOOL OF GRADUATE STUDIES  
DEPARTMENT OF BIOINFORMATICS AND GENETICS

**IN SILICO DESIGNING OF ISOFORM-SELECTIVE  
INHIBITORS AGAINST CLASS IIA HISTONE  
DEACETYLASES**

AMMAR DAWOUD ELMEZAYEN  
PROF. DR. KEMEAL YELEKÇİ

PHD THESIS

ISTANBUL, FEBRUARY, 2021

Ammar Dawoud Elmezayen

PhD Thesis

2021

KADIR HAS UNIVERSITY  
SCHOOL OF GRADUATE STUDIES  
DEPARTMENT OF BIOINFORMATICS AND GENETICS

**IN SILICO DESIGNING OF ISOFORM-SELECTIVE  
INHIBITORS AGAINST CLASS IIA HISTONE  
DEACETYLASES**

AMMAR DAWOUD ELMEZAYEN  
PROF. DR. KEMAL YELEKÇİ

PHD THESIS

SUBMITTED TO THE SCHOOL OF GRADUATE STUDIES  
WITH THE AIM TO MEET THE PARTIAL REQUIREMENTS REQUIRED TO  
RECEIVE A PhD IN THE DEPARTMENT OF BIOINFORMATICS AND GENETICS

ISTANBUL, FEBRUARY, 2021

NOTICE ON RESEARCH ETHICS AND  
PUBLISHING METHODS

I, AMMAR DAWOUD ELMEZAYEN;

- hereby acknowledge, agree and undertake that this PhD Thesis that I have prepared is entirely my own work and I have declared the citations from other studies in the bibliography in accordance with the rules;
- that this PhD Thesis does not contain any material from any research submitted or accepted to obtain a degree or diploma at another educational institution;
- and that I commit and undertake to follow the "Kadir Has University Academic Codes of Conduct" prepared in accordance with the "Higher Education Council Codes of Conduct".

In addition, I acknowledge that any claim of irregularity that may arise in relation to this work will result in a disciplinary action in accordance with the university legislation.

Furthermore, both printed and electronic copies of my work will be kept in Kadir Has Information Center under the following condition as indicated below:

The full content of my thesis/project will not be accessible for one year. If no extension is required by the end of this period, the full content of my thesis/project will be automatically accessible from everywhere by all means.

AMMAR DAWOUD ELMEZAYEN

---

09/02/2021



## ACCEPTANCE AND APPROVAL

This study, titled **IN SILICO DESIGNING OF ISOFORM-SELECTIVE INHIBITORS AGAINST CLASS IIA HISTONE DEACETYLASES**, prepared by the **AMMAR DAWOUD ELMEZAYEN**, was deemed successful with the **UNANIMOUS/MAJORITY VOTING** as a result of the thesis defense examination held on the **09/02/2021** and approved as a **PHD THESIS** by our jury.

JURY:

SIGNATURE:

(Prof. Dr. Kemal Yelekçi) (Advisor) (Kadir Has University) \_\_\_\_\_

(Prof. Dr. Demet Akdoğan) (Kadir Has University) \_\_\_\_\_

(Prof. Dr. Safiye Erdem) (Marmara University) \_\_\_\_\_

(Asst. Prof. Deniz Erođlu) (Kadir Has University) \_\_\_\_\_

(Asst. Prof. Vildan Atalay) (Uskudar University) \_\_\_\_\_

I confirm that the signatures above belong to the aforementioned faculty members.

\_\_\_\_\_  
Director of the School of Graduate Studies

APPROVAL DATE: 09/02/2021

## TABLE OF CONTENTS

TABLE OF CONTENTS.....	i
LIST OF TABLES .....	v
LIST OF FIGURES .....	vii
LIST OF EQUATIONS .....	xiii
LIST OF ABBREVIATIONS .....	xiv
ABSTRACT .....	xix
ÖZET.....	xx
ACKNOWLEDGEMENTS.....	xxi
DEDICATION.....	xxiii
1. INTRODUCTION.....	1
1.1. CANCER: AN OVERVIEW .....	1
1.2. EPIGENETIC REGULATION .....	3
1.3. HISTONE DEACETYLASES .....	9
1.3.1. Action Mechanisms of Histone Deacetylase.....	11
1.3.2. Class IIa HDACs .....	12
1.4. THE ROLE OF CLASS IIA HDACS IN HUMAN DISEASES .....	15
1.4.1. Nervous System and Neurological Disorders .....	16
1.4.2. Immune System and Immunological Disease .....	17
1.4.3. Cardiovascular System and Related Diseases .....	18
1.4.4. Musculoskeletal System and Related Diseases .....	21
1.4.5. Cancer .....	22
1.4.6. Diabetes .....	27
1.5. HISTONE DEACETYLASE KNOWN INHIBITORS .....	28
1.5.1. Class IIa HDAC Inhibitors.....	33
1.6. COMPUTER-AIDED DRUG DESIGN TECHNIQUES .....	38
1.6.1. Virtual Screening .....	39
1.6.2. Molecular Docking .....	40
1.6.3. Homology Modeling .....	42
1.6.4. Pharmacophore Modeling .....	43

1.6.5.	ADMET Prediction in CADD .....	44
1.6.6.	Molecular Dynamics (MD) Simulation .....	45
1.6.7.	MM-PBSA Binding Free Energy .....	48
	AIM AND OBJECTIVES.....	50
2.	MATERIALS AND METHODS .....	51
2.1.	HOMOLOGY MODELING OF CLASS IIA HDAC5 AND HDAC9, AND THE DESIGN OF DUAL ACTING INHIBITOR .....	51
2.1.1.	Selection of The Template .....	52
2.1.2.	Template and Target Sequences Alignment .....	52
2.1.3.	Homology Model Building.....	52
2.1.4.	Homology Model Validation .....	53
2.1.5.	Molecular Docking with Known Inhibitors .....	54
2.1.6.	Dataset Preparation .....	55
2.1.7.	Molecular Docking and Structure-Based Virtual Screening .....	55
2.1.8.	Physicochemical Properties Description .....	55
2.1.9.	Pan-Assay Interference Compounds (PAINS) Filtration.....	56
2.1.10.	Molecular Dynamics MD Simulation .....	56
2.1.11.	Binding Free Energy (MM-PBSA) Calculations.....	57
2.2.	STRUCTURE-BASED DRUG DESIGNING OF ISOFORM SELECTIVE CLASS IIA HDACS INHIBITORS.....	58
2.2.1.	Class Iia Proteins Preparation.....	58
2.2.2.	Class Iia HDACs Structural and Sequence Alignment .....	59
2.2.3.	Dataset Preparation .....	62
2.2.4.	Structure-Based Virtual Screening Approach .....	63
2.2.4.1.	First stage of SBVS .....	63
2.2.4.2.	Second stage of SBVS .....	64
2.2.4.3.	Third stage of SBVS.....	67
2.2.5.	ADMET Profile Description.....	70
2.2.6.	Pan-Assay Interference Compounds (PAINS) Filter .....	70
2.2.7.	Molecular Dynamics (MD) Simulation .....	70
2.2.8.	Binding Free Energy Calculations.....	71

<b>2.3.</b>	<b>LIGAND-BASED PHARMACOPHORE MODELING FOR DESIGNING OF ISOFORM SELECTIVE HDAC5 AND HDAC9 INHIBITORS.....</b>	<b>72</b>
2.3.1.	Training Set Compounds Selection .....	73
2.3.2.	Pharmacophore Hypothesis Generation .....	75
2.3.3.	Pharmacophore Hypotheses Validation.....	76
2.3.4.	3D Database Search for New Hits .....	79
2.3.5.	Molecular Docking Study .....	80
2.3.6.	ADMET Description and Drug-Likeness .....	80
2.3.7.	Pan-Assay Interference Compounds (PAINS) Filter .....	81
2.3.8.	Molecular Dynamics Simulation.....	81
2.3.9.	Binding Free Energy Calculations.....	82
<b>3.</b>	<b>RESULTS .....</b>	<b>83</b>
<b>3.1.</b>	<b>HOMOLOGY MODELING OF CLASS IIA HDAC5 AND HDAC9, AND THE DESIGN OF DUAL ACTING INHIBITOR .....</b>	<b>83</b>
3.1.1.	Sequence Alignment of The Template with The Targets .....	83
3.1.2.	Generated Homology Models.....	84
3.1.3.	Homology Model Validation .....	86
3.1.4.	Molecular Docking with Known Inhibitors.....	89
3.1.5.	Molecular Docking and Structure-Based Virtual Screening .....	98
3.1.6.	Physicochemical Properties Description .....	102
3.1.7.	Pan-Assay Interference Compounds (PAINS) Filtration.....	103
3.1.8.	Molecular Dynamics MD Simulation .....	103
3.1.9.	Binding Free Energy (MM-PBSA) Calculations.....	109
<b>3.2.</b>	<b>STRUCTURE-BASED DRUG DESIGNING OF ISOFORM SELECTIVE CLASS IIA HDACS INHIBITORS.....</b>	<b>109</b>
3.2.1.	Class Iia HDACs Structural and Sequence Alignment .....	109
3.2.2.	Virtual Screening Results .....	112
3.2.3.	ADMET Profile and PAINS Filtration .....	126
3.2.4.	Molecular Dynamics MD Simulation .....	127
3.2.5.	Binding Free Energy (MM-PBSA) Calculations.....	135
<b>3.3.</b>	<b>LIGAND-BASED PHARMACOPHORE MODELING FOR DESIGNING OF ISOFORM SELECTIVE HDAC5 AND HDAC9 INHIBITORS.....</b>	<b>136</b>

<b>3.3.1.</b>	<b>Generated Pharmacophore Hypotheses.....</b>	<b>136</b>
<b>3.3.2.</b>	<b>Molecular Docking Study .....</b>	<b>140</b>
<b>3.3.3.</b>	<b>Drug-Likeness Prediction and PAINS Filtration .....</b>	<b>148</b>
<b>3.3.4.</b>	<b>Analysis of The MD Simulations .....</b>	<b>149</b>
<b>4.</b>	<b>DISCUSSION .....</b>	<b>156</b>
<b>4.1.</b>	<b>HOMOLOGY MODELING OF CLASS IIA HDAC5 AND HDAC9, AND THE DESIGN OF DUAL-ACTING INHIBITORS .....</b>	<b>156</b>
<b>4.2.</b>	<b>STRUCTURE-BASED DRUG DESIGNING OF ISOFORM SELECTIVE CLASS IIA HDACS INHIBITORS.....</b>	<b>159</b>
<b>4.3.</b>	<b>LIGAND-BASED PHARMACOPHORE MODELING FOR SELECTIVE HDAC5 AND HDAC9 INHIBITORS .....</b>	<b>163</b>
<b>5.</b>	<b>CONCLUSIONS .....</b>	<b>166</b>
	<b>REFERENCES.....</b>	<b>170</b>
	<b>CURRICULUM VITAE.....</b>	<b>210</b>
	<b>ANNEX A.....</b>	<b>211</b>

## LIST OF TABLES









Table 1.1. Type of histone modifications (Kouzarides, 2007).....	6
Table 1.2. Class IIa HDACs expression level and tissue distribution (Kasler & Verdin, 2006). .....	13
Table 1.3. Structural classification of HDACs inhibitors. ....	30
Table 2.1. Conserved amino acid residues in class IIa HDACs' catalytic domains. ....	62
Table 2.2. Coordinate parameters and grid box size used for QuickVina 2.0. ....	66
Table 2.3. Coordinate parameters and grid box size used for AutoDock 4.2. ....	67
Table 3.1. DOPE and Normalized DOPE scores for generated HDACs 5 and 9 models. ....	85
Table 3.2 A comparative study between the experimental catalytic activities ( $K_i$ or $IC_{50}$ ) (Exp.) of the HDAC5 known inhibitors and their corresponding in silico calculated $K_i$ values.....	90
Table 3.3 A comparative study between the experimental catalytic activities ( $K_i$ or $IC_{50}$ ) (Exp.) of the HDAC5 known inhibitors and their corresponding in silico calculated $K_i$ values.....	90
Table 3.4. In silico calculations of the binding energy and the inhibitory constant $K_i$ of the 18 molecules.....	99
Table 3.5. In silico AMDET properties prediction of the novel 18 compounds.....	102
Table 3.6. Calculated binding free energy (MM-PBSA) of HDAC5 and HDAC9 complexes.....	109
Table 3.7. Comparative analysis of sequence similarity (SIM) and identity (IDN) among class IIa HDACs in percentage %.....	110
Table 3.8. Comparative analysis of the structural superimpose of class IIa HDACs. RMSD (Å) calculations are shown in Blue cells. Overlapping amino acid residues are shown in GREEN.....	110
Table 3.9. Calculated binding energy by AutoDock 4.2 of the hit compounds against each member of class IIa HDACs. HDAC4 selective compounds are in green color, HDAC5 selective compounds are in blue color, HDAC7 selective compounds are in orange color, and HDAC9 selective compound is in yellow color.....	113

Table 3.10. Selectivity index of class IIa HDACs. $K_i$ of specific HDAC is compared to the nearest $K_i$ of others for the same compound. ....	113
Table 3.11. Physicochemical properties of the 15 hits, including ADMET profiles and Lipinski's rule of five parameters. ....	127
Table 3.12. Calculated binding free energy (MM-PBSA) of the selected isoform HDACs selective complexes.....	136
Table 3.13. Common features of the 10 generated pharmacophore hypotheses for the HDAC5 known inhibitors. ....	138
Table 3.14. Guner-Henry scoring method results for validating the 10 generated pharmacophore hypotheses based on the HDAC5 known inhibitors. ....	138
Table 3.15. Common features of the 10 generated pharmacophore hypotheses for the HDAC9 known inhibitors. ....	139
Table 3.16. Guner-Henry scoring method results for validating the 10 generated pharmacophore hypotheses based on the HDAC9 known inhibitors. ....	139
Table 3.17. Top ranked compounds with their calculated binding energy using QuickVina 2.0. Selective isoform compounds for HDAC5 are highlighted in green, and selective isoform compounds for HDAC9 are highlighted in yellow.....	141
Table 3.18. Selectivity indices of class IIa HDACs. Inhibition constant of one HDAC is compared to the closest inhibition constant of other HDACs for the same inhibitor. ...	148
Table 3.19. The drug-likeness and the physicochemical properties of the 6 isoform selective compounds. ....	149

## LIST OF FIGURES

Figure 1.1. Chromatin Organization. Double-stranded DNA coiled around octameric core of histone proteins to produce the nucleosomes. Nucleosomes go through multiple levels of folding to produce the chromatin (Annunziato, 2008). .....	4
Figure 1.2. Histone acetylation and deacetylation epigenetic modifications. HDACs positively charge the deacetylated histone tails so that the DNA strands strongly wrapped around histone proteins ( <i>top</i> ). HATs neutralize the positively charged histones in order to loosen the double-stranded DNA (Boron & Boulpaep, 2016).....	8
Figure 1.3. (a) Different classes of HDAC enzymes based on their cellular localization and similarity. Length of bar represents the number of amino acids in a protein from N- to C-terminal; DAC: is the deacetylase domain location; black bars are the nuclear localization domain; UB: ubiquitin binding; TDAC: tubulin deacetylase domain (Khan & La Thangue, 2012). (b) Phylogenetic tree of human HDACs (De Ruijter et al., 2003). .....	10
Figure 1.4. Proposed mechanism for charge-relay system and the interactions among the active residues within the active sites of the HDACs (Somoza et al., 2004). .....	11
Figure 1.5. Schematic diagram of the proposed mechanism of HDACs (Lombardi et al., 2011). .....	12
Figure 1.6. Representative crystal structure of the catalytic domain of HDAC7. Four loops are surrounding the active site of HDAC7: L1 and L2 loops are shown in yellow; L3 and L4 loops are shown in orange. Catalytic zinc ion is shown as yellow sphere. ....	15
Figure 1.7. HDACs inhibitors pharmacophore model features (M. A. Choi et al., 2019). Also, this model represents the chemical structure of suberanilohydroxamic acid (SAHA), the HDAC inhibitor. ....	28
Figure 1.8. Carboxylic acid based HDAC inhibitors. ....	31
Figure 1.9. Benzamide derivative HDAC inhibitors.....	32
Figure 1.10. Electrophilic ketones derivative HDAC inhibitors.....	32
Figure 1.11. Main pharmacophore model of cyclic peptide derivative HDAC inhibitors. ....	33
Figure 1.12. Classical workflow of drug design techniques (W. Lu et al., 2018). ....	39



Figure 1.13. Graphical representation of the force field interactions. Dark lines display covalent bonds. Dash line represents nonbonded interaction (Ponder & Case, 2003). ..	47
Figure 2.1. Flowchart of the homology modeling and the search for HDACs 5 and 9 dual-acting inhibitors.....	51
Figure 2.2. Structure-based virtual screening workflow.....	58
Figure 2.3. Structural alignment of class IIa HDAC enzymes. HDAC4: red, HDAC5: blue, HDAC7: green, HDAC9: yellow. ....	60
Figure 2.4. Amino acid sequence alignment of class IIa HDAC proteins. Amino acids identity is shown as dark green, similarity is represented as light green and no similarity is shown in white. Overall sequence identity among this class of HDACs is 55.6% and sequences similarity is 71.5%. [  $\beta$ -sheet,  $\alpha$ -helix]. ....	61
Figure 2.5. Phylogenetic tree of human class IIa HDAC enzymes. The tree shows that HDAC5 and HDAC9 are related as they share one node with their ancestral origin HDAC4, whereas they share two nodes and with HDAC7. ....	62
Figure 2.6. Pharmacophore modeling and virtual screening workflow.....	73
Figure 2.7. 2D structures of HDAC5 known inhibitors collected for the training set along with their IC <sub>50</sub> values in nM.....	74
Figure 2.8. 2D structures of HDAC9 known inhibitors collected for the training set along with their IC <sub>50</sub> values in nM.....	75
Figure 2.9. 2D structures of HDAC5 known inhibitors collected for the test set used in pharmacophore hypothesis validation.....	78
Figure 2.10. 2D structures of HDAC9 known inhibitors collected for the test set used in pharmacophore hypothesis validation.....	79
Figure 3.1. Sequences alignment of human (a) HDACs 4 and 5; and (b) HDACs 4 and 9.  Identical identity  Strong  Weak  Non-matching  $\beta$ -sheet  $\alpha$ -helix.....	83
Figure 3.2. The 20 generated homology models of (a) HDAC5:M0014; and (b) HDAC9:M0020 based on the X-ray crystallography structure of human HDAC4 (PDB ID: 2VQM_A).....	85
Figure 3.3. HDAC4 structural superimpose with (a) HDAC5:M0014 with RMSD value of 0.53 Å; and (b) HDAC9:M0020 with RMSD of 0.34 Å RMSD.....	86
Figure 3.4. Validation of the homology models. Black dots describe the generated models among native conformations of all PDB database, where (a) M0014 has a Z-score of -	

8.12; and (b) M0020 has a Z-score of -8.04. ProSA's energy plots of (c) M0014 model; and (d) M0020 model. Ramachandran plots displays allowed and favored regions for (e) M0014 model; and (f) M0020 model.....	88
Figure 3.5. ERRAT plots for the generated homology models (a) HDAC5:M0014 (b) HDAC9:M0020. Green bars describe the perfectly folded regions in the protein; Yellow bars refer to the 95% confidence misfolded regions; Red bars are 99% confidence of misfolded regions. ....	89
Figure 3.6. 3D presentations of the binding pose of (a) HDAC5-Rac26; and (b) HDAC9-TMP269. ....	91
Figure 3.7. The 2D Structures of the selected HDACs 5 and 9 known inhibitors.....	92
Figure 3.8. (“a” to “m”) The 3D schemes of the binding pose of the selected HDAC5 known inhibitors and their interactions to the active site of M0014 model.....	95
Figure 3.9. (“a” to “o”) The 3D schemes of the binding pose of the selected HDAC9 known inhibitors and their interactions to the active site of M0020 model.....	98
Figure 3.10. 3D presentations of the binding modes and 2D schemes of the chemical interactions of HDAC5 complexes: (a) docked pose of CHEMBL2114980 and (b) MD simulation snapshot (c) docked pose of CHEMBL217223 and (d) MD simulation snapshot.....	100
Figure 3.11. 3D presentations of the binding modes and 2D schemes of the chemical interactions of HDAC9 complexes: (a) docked pose of CHEMBL2114980 and (b) MD simulation snapshot (c) docked pose of CHEMBL217223 and (d) MD simulation snapshot.....	101
Figure 3.12. RMSD plots of (a) free HDAC5 and HDAC5 complex with the Rac26 known inhibitor, CHEMBL2114980, CHEMBL217223; (b) free HDAC9 and HDAC9 complex with the TMP269 known inhibitor, CHEMBL2114980, CHEMBL217223..	104
Figure 3.13. RMSF plots of (a) free HDAC5 and HDAC5 complex with the Rac26 known inhibitor, CHEMBL2114980, CHEMBL217223; (b) free HDAC9 and HDAC9 complex with the TMP269 known inhibitor, CHEMBL2114980, CHEMBL217223. ....	105
Figure 3.14. Radius of gyration (Rg) plots of (a) free HDAC5 and HDAC5 complex with the Rac26 known inhibitor, CHEMBL2114980, CHEMBL217223; (b) free HDAC9 and HDAC9 complex with the TMP269 known inhibitor, CHEMBL2114980, CHEMBL217223. ....	106

Figure 3.15. Potential energy graphs of (a) free HDAC5 and HDAC5 complex with the Rac26 known inhibitor, CHEMBL2114980, CHEMBL217223; (b) free HDAC9 and HDAC9 complex with the TMP269 known inhibitor, CHEMBL2114980, CHEMBL217223. ....	107
Figure 3.16. Plots of the number of hydrogen bonds in ligand-protein complexes: (a) HDAC5-CHEMBL217223, (b) HDAC5-CHEMBL2114980, (c) HDAC9-CHEMBL217223, (d) HDAC9-CHEMBL2114980. ....	108
Figure 3.17. Hydrophobic surface illustrations of the active sites of class IIa HDAC proteins. The hydrophobicity degree varies from complete hydrophilicity (BLUE) to entirely hydrophobic (BROWN). ....	111
Figure 3.18. Hydrogen bonds surface illustrations of the active sites of class IIa HDAC proteins. H-bond acceptor residues are represented in GREEN, while H-bond donor residues are in PINK. ....	112
Figure 3.19. Top two-ranked selective compounds for HDAC4. ....	115
Figure 3.20. 2D and 3D illustrations of CHEMBL2177655 bound to HDAC4 (a) after molecular docking study; (b) after MD simulation. ....	116
Figure 3.21. 2D and 3D illustrations of CHEMBL3126309 bound to HDAC4 (a) after molecular docking study; (b) after MD simulation. ....	117
Figure 3.22. The top two-ranked selective compounds for HDAC5. ....	118
Figure 3.23. 2D and 3D schemes of ZINC000033260361 bound to HDAC5 (a) after molecular docking study; (b) after MD simulation. ....	119
Figure 3.24. 2D and 3D illustrations of CHEMBL2426361 bound to HDAC5 (a) after molecular docking study; (b) after MD simulation. ....	120
Figure 3.25. The top two-ranked HDAC7 selective compounds. ....	121
Figure 3.26. 2D and 3D presentations of ZINC000009640741 bound to HDAC7 (a) after molecular docking study; (b) after MD simulation. ....	122
Figure 3.27. 2D and 3D illustrations of CHEMBL1968496 bound to HDAC7 (a) after molecular docking study; (b) after MD simulation. ....	123
Figure 3.28. The 2D structure of compound CHEMBL1761559. ....	124
Figure 3.29. 2D and 3D illustrations of CHEMBL1761559 bound to HDAC9 (a) after molecular docking study; (b) after MD simulation. ....	125

Figure 3.30. The root mean squared deviation (RMSD) plots of (a) HDAC4 systems; (b) HDAC5 systems; (c) HDAC7 systems; and (d) HDAC9 systems.....	129
Figure 3.31. The root mean squared fluctuation (RMSF) plots of (a) HDAC4 systems; (b) HDAC5 systems; (c) HDAC7 systems; and (d) HDAC9 systems.....	130
Figure 3.32. The radius of gyration (Rg) plots of (a) HDAC4 systems; (b) HDAC5 systems; (c) HDAC7 systems; and (d) HDAC9 systems. ....	132
Figure 3.33. The potential energy plots of (a) HDAC4 systems; (b) HDAC5 systems; (c) HDAC7 systems; and (d) HDAC9 systems. ....	133
Figure 3.34. Number of hydrogen bonds profile of (a) HDAC4 complexes; (b) HDAC5 complexes; (c) HDAC7 complexes; and (d) HDAC9 complex. ....	135
Figure 3.35. 14 of selected HDAC5 known inhibitors from the training set mapped onto the generated pharmacophore hypothesis Hypo1. ....	137
Figure 3.36. Four of selected HDAC9 known inhibitors from the training set mapped onto the generated pharmacophore hypothesis Hypo2. ....	140
Figure 3.37. The top six selective inhibitors and their mapping onto their respective pharmacophore hypothesis. (a) HDAC5 selective inhibitors mapped onto Hypo1. (b) HDAC9 selective inhibitors mapped onto Hypo2. ....	141
Figure 3.38. The two top-ranked HDAC5 selective inhibitors. ....	142
Figure 3.39. 3D and 2D presentations of the ZINC000257282664 compound interaction with HDAC5 (a) after molecular docking; and (b) after MD simulation. ....	143
Figure 3.40. 3D and 2D presentations of the ZINC000008918470 compound interaction with HDAC5 (a) after molecular docking; and (b) after MD simulation. ....	144
Figure 3.41. The two top-ranked HDAC9 selective inhibitors. ....	145
Figure 3.42. 3D and 2D presentations of the ZINC000016012342 compound interaction with HDAC9 (a) after molecular docking; and (b) after MD simulation. ....	146
Figure 3.43. 3D and 2D presentations of the ZINC000020942817 compound interaction with HDAC9 (a) after molecular docking; and (b) after MD simulation. ....	147
Figure 3.44. Presentation of the root mean squared deviation (RMSD) for (a) HDAC5 complex systems; and (b) HDAC9 complex systems. ....	151
Figure 3.45. Illustration of the root mean squared fluctuation (RMSF) for (a) HDAC5 complex systems; and (b) HDAC9 complex systems. ....	152

Figure 3.46. Representation of the radius of gyration ( $R_g$ ) for (a) HDAC5 complex systems; and (b) HDAC9 complex systems.....	153
Figure 3.47. Potential Energy profiles for (a) HDAC5 complex systems; and (b) HDAC9 complex systems. ....	153
Figure 3.48. Number of hydrogen bonds profile of (a) HDAC5-ZINC000257282664 complex; (b) HDAC5-ZINC000008918470 complex; (c) HDAC9-ZINC000016012342 complex; and (d) HDAC9-ZINC000020942817 complex.....	154
Figure A.1. Correlation between the experimental catalytic activities ( $K_i$ or $IC_{50}$ ) of HDAC5 known inhibitors with the in silico predicted $K_i$ values for the same inhibitors. Experimental values are presented in blue color, while in silico calculations are given in orange color.....	211
Figure A.2. A comparison chart between the experimental catalytic activities ( $K_i$ or $IC_{50}$ ) of the HDAC9 known inhibitors and their corresponding in silico predicted $K_i$ values.....	211

## LIST OF EQUATIONS

(1.1) Molecular mechanics.....	46
(1.2) Association constant $K_i$ .....	48
(1.3) Free-energy change at constant temperature and pressure .....	48
(1.4) Free energy and the equilibrium constant .....	48
(1.5) Binding free energy .....	49
(1.6) Calculation of the average free energy .....	49
(2.1) The binding free energy calculation .....	57
(2.2) ChemPLP scoring function .....	63
(2.3) QuickVina 2.0 scoring function .....	65
(2.4) Selectivity index for the SBVS .....	69
(2.5) Free energy of the non polar.....	72
(2.6) Guner-Henry scoring system.....	77
(2.7) CaFE tools free binding energy.....	82
(3.1) Selectivity index for the pharmacophore VS.....	148

## LIST OF ABBREVIATIONS

2D: Two-dimensional  
3D: Three-dimensional  
3DCRT: 3D conformal radiotherapy  
5-mC: 5-methylcytosine  
ADMET: Absorption, distribution, metabolism, excretion, toxicity  
AIDS: Acquired immunodeficiency syndrome  
ALL: Acute lymphoblastic leukemia  
AML: Acute myelocytic leukemia  
APHA: Aroyl-pyrrolyl-hydroxyamide  
ASP: Astex statistical potential  
BAX: Bcl-2 associated x-protein  
BCL: B-cell lymphoma  
BDMR: Brachydactyly mental retardation  
BLAST: Basic local alignment search tool  
BMP: Bone morphogenic protein  
BP: Base pair  
CADD: Computer-aided drug design  
CaMK: Ca<sup>2+</sup>/calmodulin-dependent kinase  
cAMP: Cyclic adenosine monophosphate  
Caspase: Cysteine-aspartic protease  
CD4+: Cluster of differentiation 4  
CD8+: Cluster of differentiation 8  
CDKN1A: Cyclin-dependent kinase inhibitor 1a  
CF: Cystic fibrosis  
CGenFF: CHARMM general force field  
CGN: Cerebellar granule neuron  
CHARMM: Chemistry at Harvard macromolecular mechanics  
CLL: Chronic lymphocytic leukemia  
CpG: Cytosine-guanine dinucleotides cluster  
CRPC: Castrate-resistant prostate cancer

CTCL: Cutaneous T-cell lymphoma  
Da: Dalton  
DAC: Deacetylase  
DDR: DNA damage response  
DNA: Deoxyribonucleic acid  
DNMT: DNA methyltransferase  
DOPE: Discrete optimized potential energy  
DPF: Docking parameter file  
DS: Discovery studio  
EBCTCG: Early Breast Cancer Trialists' Collaborative Group  
EC: Endothelial cell  
EGF: Epidermal growth factor  
eNOS: Endothelial nitric oxide synthase  
ER+: Estrogen receptor positive  
FDA: Food and Drug Administration  
FEP: Free energy perturbation  
FOXO: Forkhead box protein O  
G6Pase: Glucose 6-phosphatase  
GLUT4: Glucose transporter type 4  
GPCR: G protein-coupled receptor  
GPF: Grid parameter file  
GRK5: G protein-coupled receptor kinase-5  
HAT: Histone acetyltransferase  
HBA: Hydrogen bond acceptor  
HBD: Hydrogen bond donor  
HDAC: Histone deacetylase  
HDACi: HDAC inhibitor  
HIF-1 $\alpha$ : Hypoxia-inducible factor 1 alpha  
HMT: Histone methyltransferases  
HSP: Heat shock protein  
HTS: High-throughput screening  
HTT: Huntingtin gene



IC50: half-maximal inhibitory concentration  
IGRT: Image-guided radiotherapy  
IMRT: Intensity-modulated radiation therapy  
IUPAC: International union of pure and applied chemistry  
Kd: Dissociation constant  
Ki: Inhibitory constant  
LIE: Linear interactions energy  
LINAC: Linear accelerator  
lncRNA: Long non-coding RN  
MBP: Methyl-CpG-binding protein  
MD: Molecular dynamics simulation  
MeCP2: Methyl-CpG binding protein 2  
MEF2: Myocyte enhancer factor 2  
MEF2C: Myocyte enhancer factor 2C  
Mirk/dyrk1B: Minibrain-related kinase/dual-specificity tyrosine-regulated kinase 1B  
MITR: MEF2-interacting transcription repressor  
MM-PBSA: Molecular mechanics Poisson-Boltzmann surface area  
MPI: Message passing interface  
MW: Molecular weight  
MyoD: Myoblast determination  
NADH: Nicotinamide adenine dinucleotide + hydrogen  
NADPH: Nicotinamide adenine dinucleotide phosphate + hydrogen  
NAMD: Nanoscale molecular dynamics  
NCBI: National center for biotechnology information  
NCI: National cancer institute  
N-CoR: Nuclear receptor co-repressor  
NFAT: Nuclear factor of activated T-cell  
NKT: Natural killer T cell  
NMR: Nuclear magnetic resonance  
NPT: Number of atoms, pressure, temperature  
NSCLC: Non-small cell lung cancer  
NVT: Number of atoms, volume, temperature

OQF: Overall quality factor  
PAINS: Pan-assay interference compounds  
PBC: Periodic boundary conditions  
PBMC: Peripheral blood mononuclear cell  
PDB: Protein Data Bank  
PDBQT: Protein data bank, partial charge (Q) & atom type (T)  
PDGF-B: Platelet-derived growth factor B  
PDGFR $\beta$ : Platelet-derived growth factor receptor beta  
PHA: Phytohemagglutinin  
PKC: Protein kinase C  
PKD: Protein kinase D  
polyQ: Polyglutamine  
PP2A: Protein phosphatase 2A  
ProSA: Protein structure analysis  
PTCL: Peripheral T-cell lymphoma  
PTHrP: Parathyroid hormone-related peptide  
PTM: Posttranscriptional modification  
QSAR: Quantitative structure-activity relationship  
QSPR: Quantitative structure–property relationship  
Rg: Radius of gyration  
RMSD: Root mean square deviation  
RMSF: Root mean square fluctuation  
RNA: Ribonucleic acid  
RNAi: RNA interference  
Rpd3: Reduced potassium dependency-3  
Runx2: Runt-related transcription factor 2  
SAHA: Suberoylanilide hydroxamic acid  
SASA: Solvent-accessible surface area  
SBDD: Structure-based drug design  
SCD: Sickle cell disease  
SIK1: Salt-inducible kinase 1  
siRNA: Small interfering RNA

SMRT: Silencing mediator for retinoic acid and thyroid hormone receptors  
SRS: Stereotactic radiosurgery  
STAT1: Signal transducer and activator of transcription 1  
TDAC: Tubulin deacetylase  
TDG: Thymine DNA glycosylase  
TET: Ten-eleven translocation methylcytosine dioxygenase  
TFMK: Trifluoromethylketone  
TFMO: Trifluoromethyloxadiazolyl  
TI: Thermodynamic integration  
TIP3: Transferable intermolecular potential with 3 points  
TNF: Tumor necrosis factor  
TNFRSF10A: TNF receptor superfamily-member 10a  
TPSA: Total polar surface area  
TSA: Trichostatin A  
UB: Ubiquitin binding  
VEGF: Vascular endothelial growth factor  
VMD: Visual Molecular Dynamics  
VS: Virtual screening  
VSMC: Vascular smooth muscle cell  
ZBG: zinc-binding group  
 $\beta$ 1-AR:  $\beta$ 1-adrenergic receptor

# IN SILICO DESIGNING OF ISOFORM-SELECTIVE INHIBITORS AGAINST CLASS IIA HISTONE DEACETYLASES

## ABSTRACT

The fundamental cause of human cancer is strongly influenced by down- or upregulations of epigenetic factors. Upregulated histone deacetylases (HDAC) have been shown to be effectively neutralized by the action of HDACs inhibitors (HDACi). However, cytotoxicity has been reported in normal cells because of non-specificity of several available HDACis that are in clinical use or at different phases of clinical trials. Constant Search for specific HDAC isoform inhibitors is increasingly developing to avoid this side effect. Because of the high amino acid sequence and structural similarity among HDAC enzymes, it is believed to be a challenging task to obtain isoform-selectivity. The essential aim of the present study was to examine the similarity of class IIa HDACs (4, 5, 7, and 9) by aligning their structures and amino acid sequences, active site extraction, and recognition of the key amino acid residues within the catalytic channel. X-ray crystal structure of the human HDAC4 was used as a template for homology modeling of human HDACs 5 and 9. Consequently, isoform-selective inhibitors against class IIa HDACs were identified via structure- and ligand-based drug design. Based on the highest binding affinity and isoform-selectivity, the top-ranked inhibitors were in silico tested for their absorption, distribution, metabolism, elimination, and toxicity (ADMET) properties, which were classified as drug-like compounds. Later, molecular dynamics simulation (MD) was carried out for all compound-protein complexes to evaluate the structural stability and the binding mode of the inhibitors, which showed high stability throughout the 100 ns simulation. Free binding energy predictions by MM-PBSA method showed the high binding affinity of the identified compounds towards their respective targets. Hence, these inhibitors could be used as drug candidates or as lead compounds for more in silico or in vitro optimization to design safe isoform-selective HDACs inhibitors.

**Keywords:** Homology modeling, structure-based drug design, ligand-based pharmacophore modeling, ADMET, selective HDAC inhibitors.

# SINIF IIA HISTON DEASETİLAZLARINA KARŞI ISOFORM SEÇİCİ İNHİBİTÖRLERİNİN SİLİKO TASARIMI

## ÖZET

Yüksek regüle edilmiş histon deasetilazların (HDAC), HDAC inhibitörleriyle (HDACi) etkisiyle etkili bir şekilde azaltıldığı gösterilmiştir. Bununla birlikte, sitotoksitenin, klinik kullanımda olan veya klinik araştırmaların farklı safhalarında bulunan mevcut çeşitli HDAC inhibitörlerinin seçimli olmaması nedeniyle normal hücrelerde de olduğu görülmüştür. Seçimli HDAC izoform inhibitörlerinin geliştirilmesiyle birlikte gölenen bu an etkilerin de önleneneğine inanılmaktadır. Bu çalışmanın temel amacı, sınıf Iia HDAC'lerin (4, 5, 7 ve 9) benzerliğini, yapılarını ve amino asit dizilerini hizalayarak, aktif bölgede ve katalitik kanal içindeki anahtar amino asit kalıntılarının tanımlanmasını incelemektir. İnsan HDAC4'ün X ışını kristal yapısı, şablon olarak kullanılarak insan HDAC5 ve HDAC9'un homoloji modellemesi yapılmıştır. Sonuç olarak, sınıf Iia HDAC'lere karşı izoform seçici inhibitörler, yapı ve ligand bazlı ilaç tasarımı yoluyla tasarlanmıştır. En yüksek bağlanma afinitesi ve izoform seçiciliğine dayalı olarak, en üst sıradaki inhibitörler, ilaç olabilecek bileşikler olarak değerlendirilerek onların absorpsiyon, dağılım, metabolizma, eliminasyon ve toksisite (ADMET) özellikleri in-siliko yöntemler kullanılarak tespit edilmiştir. Daha sonra, inhibitörlerin yapısal stabilitesini ve bağlanma modunu değerlendirmek için tüm bileşik-protein komplekslerinin moleküler dinamik simülasyonu (MD) gerçekleştirildi. 100 ns simülasyonu süresi boyunca bütün kompleksler yüksek stabilite davranışları göstermişlerdir. MM-PBSA yöntemiyle serbest bağlanma enerjisi tahminleri, tanımlanan bileşiklerin ilgili hedeflerine karşı yüksek bağlanma afinitesini gösterdiği tespit edilmiştir. Bu nedenle, bu inhibitörler ilaç adayları olarak kullanılabilirler veya ilaç öncüleri olarak daha ileri in siliko veya in vitro optimizasyonlarla güvenilir ve izoform seçimli inhibitör olarak tasarlamada kullanılabilirler.

**Anahtar Kelimeler** Homoloji modelleme, Yapı bazlı ilaç tasarımı, Ligand bazlı farmakofor modelleme, ADMET, seçimli HDAC inhibitörleri.

## ACKNOWLEDGEMENTS

بِسْمِ اللَّهِ الرَّحْمَنِ الرَّحِيمِ

In the Name of **ALLAH**, the Most Beneficent, the Most Merciful. First, all the thanks and praises be to Almighty **ALLAH** Subhanahu Wa Ta'ala (SWT) for His greatness and for granting me the courage and power throughout this study and to finish my dissertation. All the gratitude be to **ALLAH** (SWT) for his endless grace that kept me on the right path throughout my live and during my doctoral research.

My endless gratefulness to my father **Dr. Dawoud Ahmed Elmezayen** and to my mother **Somaia Abdulkaksoud Bass**, for their unconditional love, courteous raising, and great support they provided me through my life, and still do, which I would not be in this place if it were not for them.

I am deeply gratitude to my beloved wife, **Nesrine Mohamed Abdelwahed**. I enormously in debt to her, for her continuous support to my dreams and for her enormous care and patience throughout this difficult journey, and certainly to my precious son, **Yamin**, who filled our lives with love since his born.

My sincere thanks to my brothers and sister, **Dr. Ahmed Dawoud Elmezayen**, **Dr. Halimah Dawoud Elmezayen**, and **Yasser Dawoud Elmezayen**, for their constant encouragement and support during my research.

I would like to express my deepest appreciation to my great and exceptional supervisor, **Professor Dr. Kemal Yelekçi**, for his guidance during my study. Professor **Kemal** was not just my supervisor, but he was as a caring father and a role model who I will always be inspired by his work, passion, and kindness. He offered me an opened and welcomed environment to pursue my study since my first day at the department.

I am deeply thankful to my PhD thesis steering committee and thesis defense jury members **Prof. Dr. Safiye Sağ Erdem** from Marmara University, **Asst. Prof. Deniz**

**Erođlu** from Kadir Has University, **Prof. Dr. E. Demet Akdođan** from Kadir Has University, and **Asst. Prof. Vildan Enisođlu Atalay** from Uskudar University, for their invaluable inputs and enriched contribution to my dissertation.

My sincere gratitude to my best friend, the master student, **Anas Al-Obaidi**, for his continuous backing and encouragement during my study, and who accompanied me on this journey, in its bitter-sweet moments.





To my beloved parents,  
**Dr. Dawoud Ahmed Elmezayen**  
**Somaia Abdulkmaksoud Bass**

To my darling wife,  
**Nesrine Mohamed Abdelwahed**

To my precious son,  
**Yamin Ammar Elmezayen**



# 1. INTRODUCTION

## 1.1. CANCER: AN OVERVIEW

The cell cycle in mammals enables organisms to survive and to reproduce their own kind and is extremely regulated and organized process, which drives the cell division and the genetic material duplication. The rate and the time of the cell division are critical. Thus, cell division regulation consists of proteins and growth-regulatory signals that check for any genetic abnormalities and control the integrity of the genetic material (Otto & Sicinski, 2017). Unregulated growth of abnormal cells and the ability of these cells to spread to different parts of the body is defined as cancer. Cancer cell divides excessively where it does not respond to the growth-regulatory signals and fails to go through apoptosis or programmed cell death (G. H. Williams & Stoeber, 2012). Cancer or tumor can be classified as malignant or benign, where benign tumors do not have the ability to spread to other parts of the body (metastasis) and they retain control of differentiation (Schäfer & Werner, 2008). Commonly, malignant cells display major features: invade distant or adjacent tissues, development of a combination of unrelated differentiated cell types, increasing of the proliferation rate, cellular organization disruption, and developing of secondary tumors or metastases (Baba & Cătoi, 2007). In 2000, Hanahan and Weinberg proposed that for tissues to be described as cancer there are six fundamental changes that must occur to alter the normal cell physiology. Despite how these changes arise, they are essential and adequate to trigger malignant development. These alterations include immunity to apoptosis (programmed cell death), infinite duplication ability, metastasis and spread to different parts of the body, constant angiogenesis, self-sufficiency in growth signals and resistance to antigrowth signals (Hanahan & Weinberg, 2000).

Cancer treatment has been developed during latest decades and various treatment options are available nowadays. Cancer treatment depends on its location, type, and progression stage. More than two thirds of all current treatment trials in the world are focusing on treating cancer (Wu et al., 2006). Surgery is considered as conventional cancer treatment

and it is believed to be one of the most favorable treatment for several malignant and benign tumors where it removes the affected tissues with minimum harm to other adjacent tissues (A. Wagner et al., 1995). Radiation-based surgery, also known as radiosurgery, is a surgery which uses radiation for cancer treatment where no blade is involved in the treatment process. However, radiosurgery is described as a surgery because the result of the treatment is quite similar to the conventional operations results. In radiosurgery, the tumor is exposed to high dose of ionizing radiation which destroys cancerous tissues within an organ. Based on the radiation source, there are several types of radiosurgery like stereotactic radiosurgery (SRS), gamma knife systems, linear accelerator (LINAC) systems, and proton beam therapy or cyclotron (Rahman et al., 2009).

Radiation therapy in cancer treatment is used to destroy the cancer cells by applying ionizing radiation. This radiation will electrically charge the small particles in the cell and produce energy that precisely alter the genetic material, which in turn will halt the cell division and causes cells to die. Radiation therapy techniques may include fractionation, 3D conformal radiotherapy (3DCRT), intensity-modulated radiation therapy (IMRT), and image-guided radiotherapy (IGRT) (Goldblum et al., 2013).

Chemotherapy terminates cancer development by stopping their ability to divide or grow and enforcing cell death. Chemotherapeutic drugs are categorized as cytotoxic or cytostatic (biological drugs). More than one hundred chemotherapeutic drugs are approved by the Food and Drug Administration (FDA) and are commercially available. However, chemotherapeutic drugs come with various side effects such as nausea, vomiting, and hair loss as they target normal cells alongside with cancerous cells (Rodgers et al., 2012). Alkylating agents such as Temodar<sup>®</sup> and Cytosan<sup>®</sup> directly damage the deoxyribonucleic acid (DNA) of cancer cells and halt cell division. Various types of tumors are treated with alkylating agents such as multiple myeloma, leukemia, lymphoma, and sarcoma (O'Shaughnessy, 1999). Antimetabolites drugs such as Xeloda<sup>®</sup>, Gemzar<sup>®</sup> and Alimta<sup>®</sup> are DNA and ribonucleic acid (RNA) unit analogs that interfere with the S phase of the cell cycle and stop the cancer cells growth (Peters et al., 2000). Anthracyclines drugs such as Adriamycin<sup>®</sup> and other antitumor antibiotics are used with critical limitations to treat cancer by targeting DNA replication enzymes, thus disrupting the cell cycle in all phases (Minotti et al., 2004). Topoisomerase drugs such as

Mitoxantrone<sup>®</sup>, Teniposide<sup>®</sup>, and Irinotecan<sup>®</sup> have been commonly used as chemotherapeutic agents for cancer treatment. DNA duplication is blocked by topoisomerase inhibitors which prevent the unwinding of DNA and hence stop the cell division (Liang et al., 2019). Mitotic drugs such as Taxotere<sup>®</sup>, Vindesine<sup>®</sup>, and Emcyt<sup>®</sup> are naturally derived products which interfere with cell cycles, specifically the mitotic phase, and inhibit the synthesis of proteins essential for cell division. Mitotic inhibitors are used to treat several cancer types including lymphoma, myelomas, breast cancer, and leukemia (N. Jiang et al., 2006).

In cell biology, hormones play a fundamental role in the control of cell growth and in the regulation of cancerous tissues. More than 30% of cancers are believed to be caused by hormonal imbalances and disturbances. Unlike chemotherapy treatment, hormone therapy is safer and more efficient to treat tumors without cytotoxicity. Drugs such as Prednisone medication group, Solu-Medrol<sup>®</sup>, and Decadron<sup>®</sup> are hormone-based drugs that are used in treatment of many types of cancer like multiple myeloma and lymphoma (Early Breast Cancer Trialists' Collaborative Group (EBCTCG)), 2005; Picot et al., 2011).

In spite remarkable developments have been made in cancer therapy, cancer is still one of the most substantial challenges for the public health globally. There is still an urgent need and serious efforts to search for better ways to detect, treat and prevent cancer (Baselga et al., 2015).

## **1.2. EPIGENETIC REGULATION**

DNA is the heritable genetic unit which is present almost in all living cells. Epigenetics in biology describes the variations in gene expression and differences in the inherited phenotypes, which are not coded in the DNA itself (Klein & Hainer, 2020). DNA is found in the nucleus of human cells and packed with the help of histone proteins, which is biologically known as 'beads in a string.' DNA-histone complex forms what so-called chromatin, and the essential and basic structure of the chromatin is the nucleosome. Nearly 146 base pairs (BP) of double-stranded DNA wrapped around eight histone proteins (two H2A-H2B dimers attached to two H3-H4 dimers) to form a single

nucleosome. Moreover, H1 histone protein (linker histone) links two adjacent nucleosomes together to form the chromatosome (Aguilar & Craighead, 2013; Campos & Reinberg, 2009; Schones et al., 2011). Chromatosomes undergo further folding and compressed into the chromatid (Figure 1.1).

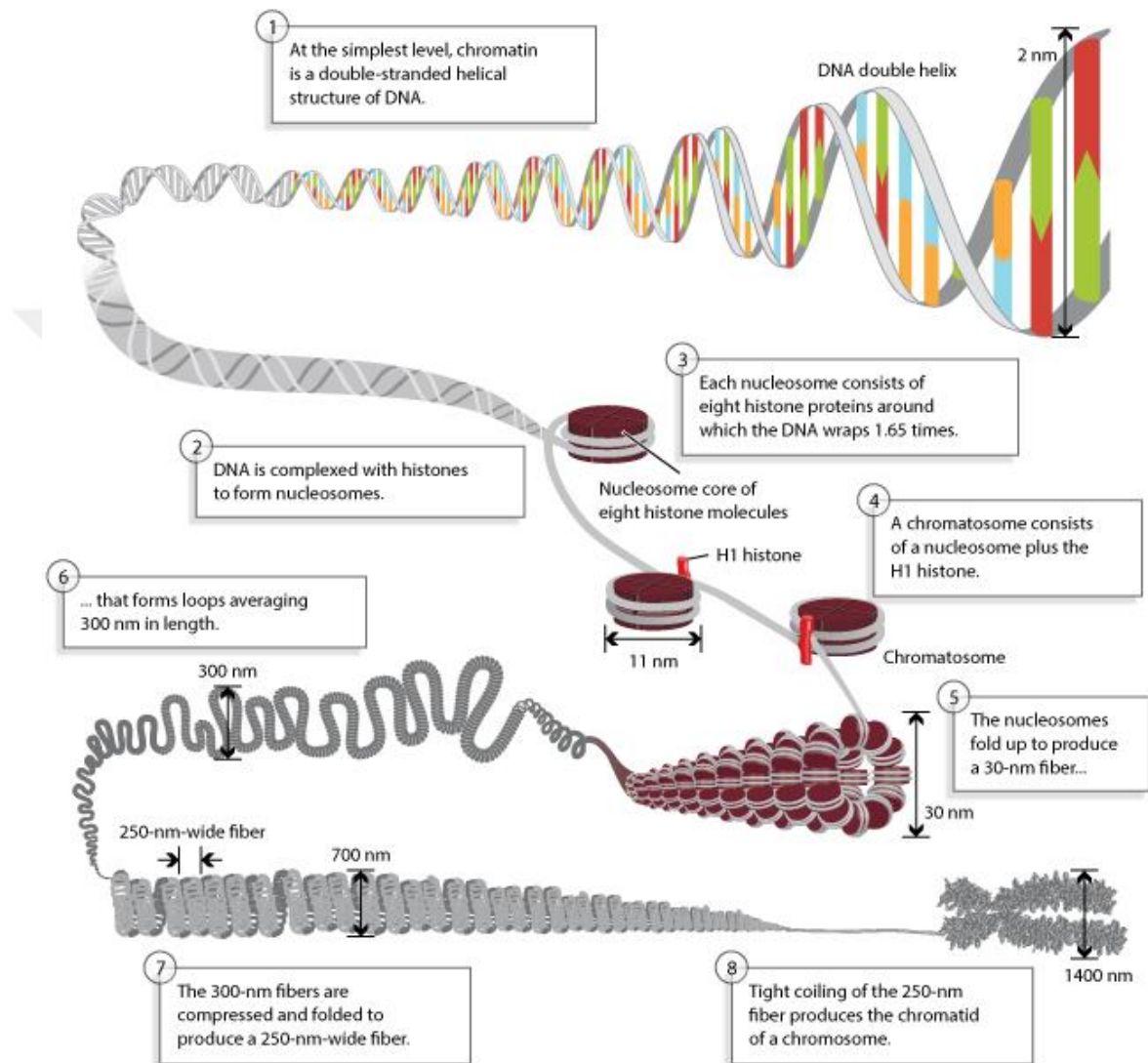


**Figure 1.1.** Chromatin Organization. Double-stranded DNA coiled around octameric core of histone proteins to produce the nucleosomes. Nucleosomes go through multiple levels of folding to produce the chromatin (Annunziato, 2008).

Based on the functional state of chromatin in the cell cycle, chromatin is present in two forms, an open state in which the gene expression is active, and it is called euchromatin, and a closed state where it is transcriptionally inactive and is known as heterochromatin. There are different epigenetic modifications that control and regulate these two states, which have biological influences on the gene expression, thus display variations in the

phenotype. Epigenetic organization is responsible for the cell differentiation and the phenotype conservation in living cells (Goldberg et al., 2007; Kouzarides, 2007).

Epigenetic modifications can be classified into three types: DNA methylation, RNA-associated silencing, and histone modifications. DNA methylation suppresses the gene expression in two ways. The first mechanism is derived by DNA methyltransferases (DNMTs), which insert a methyl group (-CH<sub>3</sub>) to DNA at 5-carbon position of the cytosine ring producing the 5-methylcytosine (5-mC). This modification occurs strictly on the cytosine guanine dinucleotides clusters (CpG) which are found primarily in the gene regulatory regions of the somatic cells in humans, thus repress the gene expression. In contrast, the removal of the methyl group from DNA, a mechanism known as demethylation, is catalyzed by the ten-eleven translocation methylcytosine dioxygenase (TET) and thymine DNA glycosylase (TDG) enzymes (Jin et al., 2011; Neri et al., 2015). The second mechanism is catalyzed by the methyl-CpG-binding protein family (MBPs) such as the methyl-CpG binding protein 2 (MeCP2) enzyme that binds to methylated cytosine (FAN & HUTNICK, 2005).

RNA sequences play a significant role in epigenetic regulation. RNA interference (RNAi) and long non-coding RNAs (lncRNAs) have been associated in many studies with the gene expression regulation and are believed to have their effect on the cell differentiation. These RNA sequences participate in the formation of the heterochromatin and gene silencing. Some studies have shown that interrupting with the RNAi machinery has damaged the DNA and blocked histone modifications at specific locations (Holoch & Moazed, 2015; J.-W. Wei et al., 2017).

Histone modifications are another epigenetic mechanism that involved in the regulation of the transcription. These modifications are posttranscriptional modifications (PTMs) that occur at the n-terminal of histones and involve acetylation, ubiquitylation, methylation, phosphorylation, and others (Table 1.1).

**Table 1.1.** Type of histone modifications (Kouzarides, 2007).

<b>Chromatin Modifications</b>	<b>Residues Modified</b>	<b>Functions Regulated</b>
Acetylation	<b>K-ac</b>	Transcription, Repair, Replication, Condensation
Methylation (lysines)	<b>K-me1 K-me2 K-me3</b>	Transcription, Repair
Methylation (arginines)	<b>R-me1 R-me2a R-me2s</b>	Transcription
Phosphorylation	<b>S-ph T-ph</b>	Transcription, Repair, Condensation
Ubiquitylation	<b>K-ub</b>	Transcription, Repair
Sumoylation	<b>K-su</b>	Transcription
ADP ribosylation	<b>E-ar</b>	Transcription
Deimination	<b>R &gt; Cit</b>	Transcription
Proline Isomerization	<b>P-cis &gt; P-trans</b>	Transcription

As previously mentioned, histone proteins are the foremost components of chromatin that pack the DNA into nucleosomes and play a crucial role in gene expression. Histone proteins are rich in arginine and lysine, that undergo different post-translational modifications. In absence of histones, DNA would be unwound in living cells and as very long form. Histones are classified as core histones, which involve H2A, H2B, H3 and H4, and linker histones, which include H1 and H5. Based on the location of histones expression, they are divided into canonical histones that are expressed during the S phase of the cell cycle and encoded by replication-dependent genes, and histone variants that are encoded by replication-independent genes and expressed during the entire cell cycle (Boyle, 2005; Jang et al., 2015; Redon et al., 2002; Youngson, 2006). The n-terminal of histones, which is also known as histone tail, plays a central role in gene regulation and chromatin constancy, and is subjected to several epigenetic modifications. The best known and studied modifications involve acetylation/deacetylation, methylation/demethylation and phosphorylation/dephosphorylation, and there are specific enzymes responsible for catalyzing and reversing these modifications (Egger et al., 2004; K. Zhang & Dent, 2005).

Histone methylation is catalyzed by histone methyltransferases (HMTs) that add a methyl group (-CH<sub>3</sub>) to lysine and arginine residues on histone tails. This mechanism influences the hydrophobic and basic characteristic of histone tails, thus confer with the chromatin activation and inactivation. For example, methylation of histone lysine residue number 9 at histone H3 (H3K9) represses the gene transcription, while methylation of histone 3 at

lysine 4 (H3K4) is a signal for transcriptional activation (Greer & Shi, 2012; S. Gupta et al., 2010). Histone methylation mechanism can be reversed by the action of histone demethylases that remove the methyl group. This way, the transcription can be turned on or off during the cell cycle. This mechanism is highly regulated, and numerous cancer types occur due to methylation/demethylation dysregulation (Albert & Helin, 2010).

In humans, histone phosphorylation plays an essential role in DNA damage repair. This epigenetic modification occurs on serine residue number 193 of the variant histone H2AX (Celeste et al., 2003; Rossetto et al., 2010). This mechanism is carried out by protein kinases during the entire cell cycle in response to the DNA damage response pathways (DDR). As soon as the DNA has been correctly restored, H2AX phosphatases derive the dephosphorylation mechanism to stop the action of the DNA repair pathway and to complete the cell cycle (Downs et al., 2000; Papamichos-Chronakis et al., 2006). Another mechanism of histone phosphorylation is associated with the gene expression in many ways. For example, epidermal growth factor (EGF) gene transcription is regulated by the action of the phosphorylation of histone H3 at serine residues number 10 and 28, and serine residue number 10 of H2B (H. S. Choi et al., 2005; Lau et al., 2011). Moreover, histone phosphorylation was notably linked to chromosome condensation and regulation of gene expression. Phosphorylation of serine residue number 10 of histone H3 is known to be involved in DNA compaction and relaxation during meiosis and mitosis (Y. Wei et al., 1999).

Histone acetylation and deacetylation mechanisms are essential parts of gene regulation. Histone acetylation is linked to transcriptionally active chromatin while deacetylation is involved in the formation of the transcriptionally inactive heterochromatin (Berg, 1989). Histone acetylation process is regulated by histone acetyltransferases (HATs) that add an acetyl group ( $-C_2H_3O$ ) to the positively charged  $\epsilon$ -amine of conserved lysine residues on histone tails (Figure 1.2). This will block the interaction of lysine side chain to the negatively charged DNA, thus reduces the histone-DNA affinity and relaxes the condensed chromatin structure to allow the transcription factors to reach the promoter regions of genes (Struhl, 1998). The acetylation state is reversed by the action of histone deacetylases (HDACs) that remove the acetyl group from lysine residues on histone tails.

This mechanism or post-transcriptional modification will help in the formation of the heterochromatin and inactivate the gene transcription (Kurdistani & Grunstein, 2003).

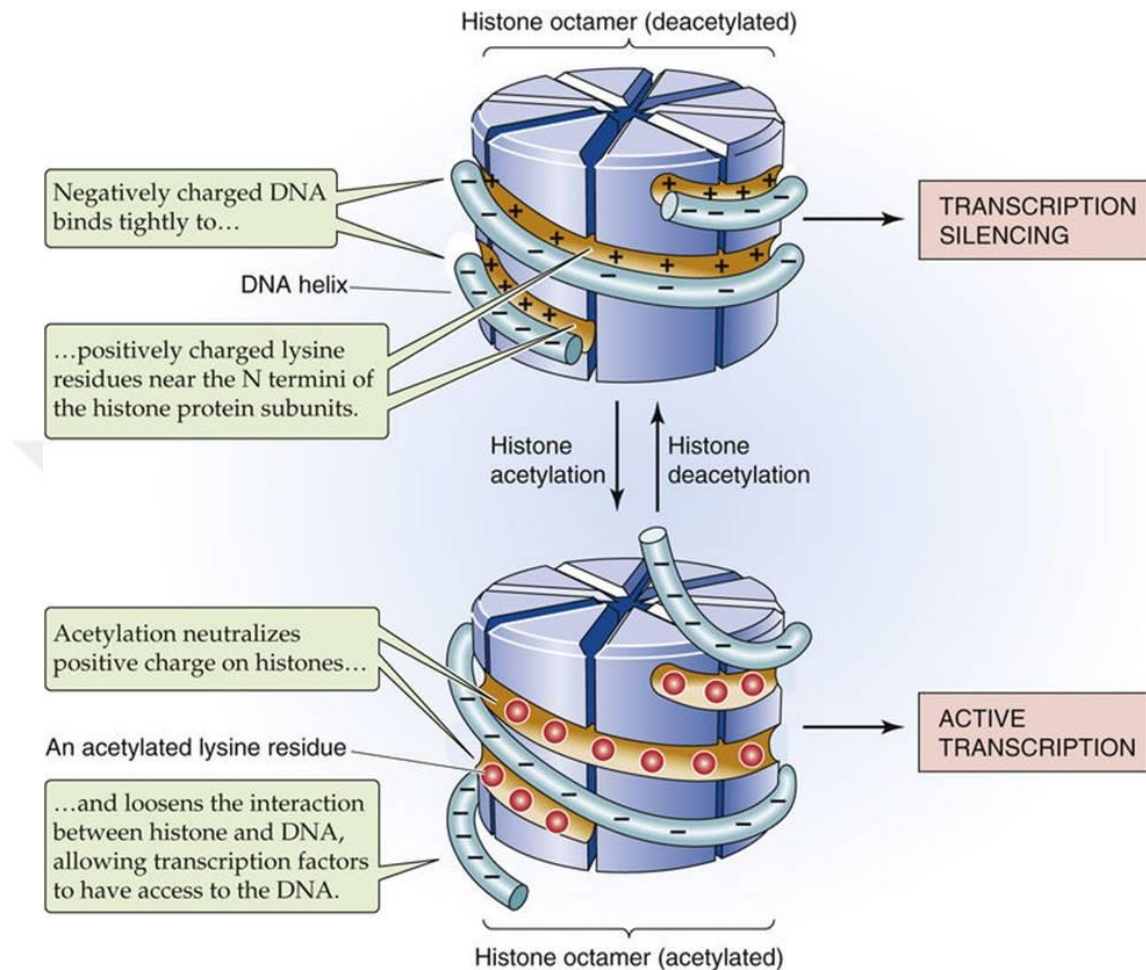


**Figure 1.2.** Histone acetylation and deacetylation epigenetic modifications. HDACs positively charge the deacetylated histone tails so that the DNA strands strongly wrapped around histone proteins (*top*). HATs neutralize the positively charged histones in order to loosen the double-stranded DNA (Boron & Boulpaep, 2016).

Choudhary and his colleagues identified more than three thousand acetylation sites in nearly 1,700 proteins in humans, which shows the importance of lysine acetylation in epigenetic regulation in many cellular processes (Choudhary et al., 2009). In addition to histone proteins, HDACs “referred as lysine deacetylases” also catalyze deacetylation modification on many non-histone proteins such as DNA subunit repair protein (Ku70), heat shock proteins (HSPs),  $\alpha$ -tubulin, transcription factors, hypoxia-inducible factor 1 alpha (HIF-1 $\alpha$ ), myoblast determination protein 1 (MyoD), and many others (Narita et al., 2019; B. N. Singh et al., 2010).



### 1.3. HISTONE DEACETYLASES

Histone deacetylases are crucial enzymes that control several cellular processes. In general, HDACs functioning within bulky multiprotein complexes, which remove the acetyl group from lysine residues on histone tails. Histone deacetylation by HDACs control cell differentiation and organize the gene expression. Now, it is evident that the effect of protein acetylation goes far beyond the epigenetic modifications as well as the better understanding of HDAC biology (Choudhary et al., 2009; Grozinger & Schreiber, 2002). In human, 18 different HDACs have been found and categorized into four classes according to their cellular localization and sequence identity (Figure 1.3). These enzymes are either zinc-dependent enzymes namely HDAC, or nicotinamide adenine dinucleotide (NADH) dependent enzymes called sirtuin proteins (Dokmanovic et al., 2007). Zinc-dependent HDACs are 11 enzymes and further grouped into several subclasses according to their homology to two types of yeast proteins: HDACs 1, 2, 3 and 8 (class I) are mainly close to the reduced potassium dependency-3 transcriptional factor (Rpd3) of *Saccharomyces cerevisiae*, while HDACs 4, 5, 6, 7, 9 and 10 (class II) are mostly related to yeast deacetylase Hda1. HDAC class IV contains only one member (HDAC11) which is not so related to either Rpd3 or Hda1, and does not share enough sequence similarity to be classified as class I or II (X. J. Yang & Seto, 2008). Unlike class I and II HDACs, class III members are NADH-dependent proteins and consist of seven sirtuin enzymes (Sirt1–Sirt7) (Frye, 2000).

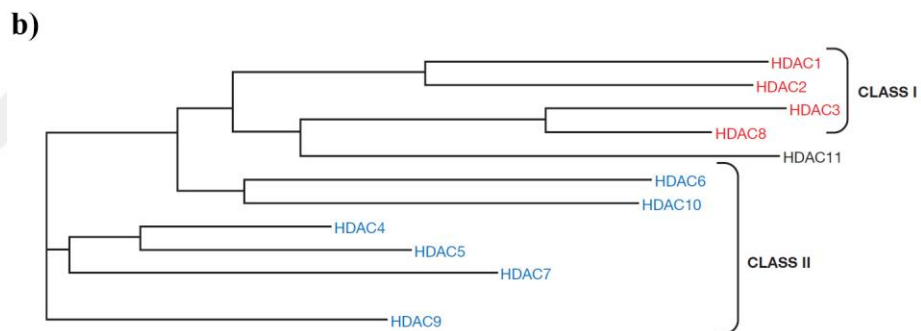
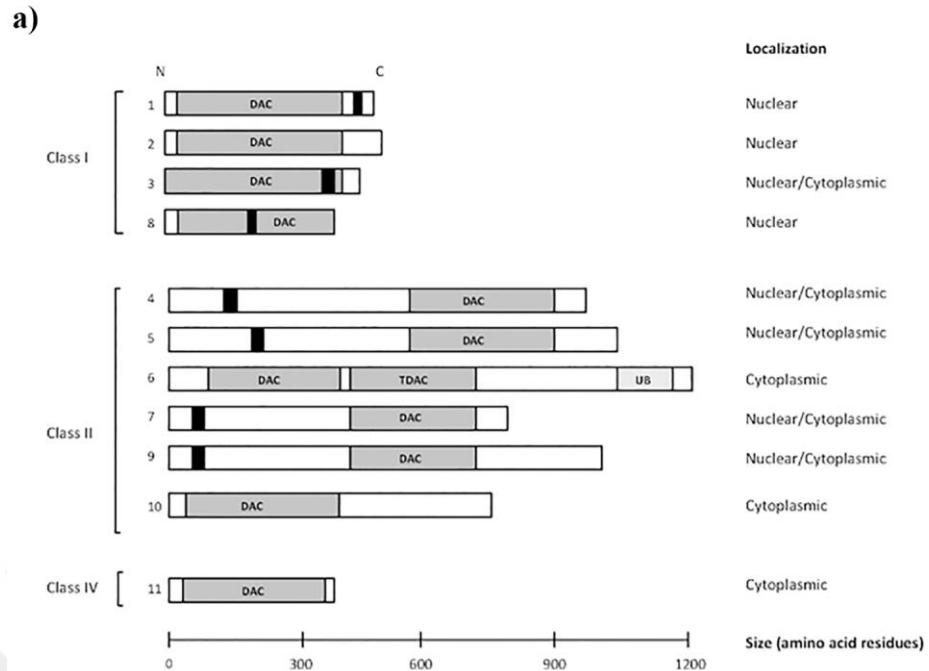


**Figure 1.3.** (a) Different classes of HDAC enzymes based on their cellular localization and similarity. Length of bar represents the number of amino acids in a protein from N- to C-terminal; DAC: is the deacetylase domain location; black bars are the nuclear localization domain; UB: ubiquitin binding; TDAC: tubulin deacetylase domain (Khan & La Thangue, 2012). (b) Phylogenetic tree of human HDACs (De Ruijter et al., 2003).

In comparison to class I HDACs, class II HDACs are larger in size and further subdivided into two classes based on the number of the catalytic domains; class IIa HDACs (HDAC4, HDAC5, HDAC7 and HDAC9) have a single catalytic domain, while class IIb enzymes (HDAC6 and HDAC10) have two catalytic domains (Haggarty et al., 2003).

Interestingly, the earliest X-ray crystal structure reported among HDACs proteins was the HDAC8 bound to a hydroxamic acid inhibitor in 2004 (Somoza et al., 2004; Vannini et al., 2004). Thereafter, several crystal structures of different HDAC isoforms have been

resolved and published at the Protein Data Bank (PDB) website including HDAC1, 2, 3, 4, 6, 7, 8, and 10. This broadens the opportunity of employing different computational approaches to design and find new HDAC inhibitors (HDACi).

### 1.3.1. Action Mechanisms of Histone Deacetylase

Zinc-dependent HDACs share a substantially conserved active site where a Zn ion is submerged in a narrow tunnel (~5 Å diameter) for about 7 to 8 Å depth. This tunnel is covered with aromatic and hydrophobic residues. The buried Zn atom is linked to the carboxylate groups (COO<sup>-</sup>) of two conserved aspartic acid residues, and at the same time, to a conserved histidine residue. Furthermore, throughout the catalytic mechanisms of HDACs, the zinc ion is believed to be coordinated by a water molecule and the carbonyl group (C=O) of the acetyl lysine (Figure 1.4). HDACs binding pocket is characterized by its “charge-relay” system, which consists of two aspartic acids (D183 and D176) hydrogen bonded to two histidine residues (H143 and H142), respectively. This charge-relay system facilitates the polarization of the imidazole rings of the histidine residues and increases their basicity, increases the electrophilicity of the carbonyl group of the acetyllysine, and makes the water molecule more nucleophilic (Somoza et al., 2004).

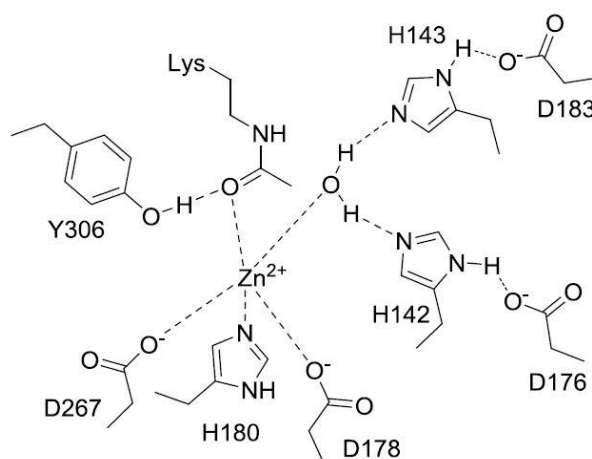


**Figure 1.4.** Proposed mechanism for charge-relay system and the interactions among the active residues within the active sites of the HDACs (Somoza et al., 2004).

In 2011, Lombardi and his colleagues proposed the action mechanism of metal dependent HDACs according to their findings with reference to HDAC8 (Figure 1.5). The catalytic Zn<sup>2+</sup> ion with the participation of histidine residue 143 boost the nucleophilic attack of

the water molecule, that is bound to the zinc atom, at the carbonyl group of the acetyl-L-lysine substrate. The nucleophilic lone pair on the zinc-water molecule becomes available as a result of the proton abstraction. The zinc atom coordination and hydrogen bonds interactions found in histidine 142 and 143 and tyrosine 306 promote and stabilize the oxyanion mechanism of the tetrahedral intermediate and its flanking transition states. Histidine 143 residue functions as a general acid catalyst, that drives the tetrahedral intermediate breakdown to produce acetate and L-lysine following the proton transfer process (Lombardi et al., 2011). Based on what has been observed in similar proteins, it was thought that the side chain of tyrosine 306 residue can undergo a change in the conformation between an “out” and “in” conformations to accommodate substrate binding and catalysis (Bottomley et al., 2008).

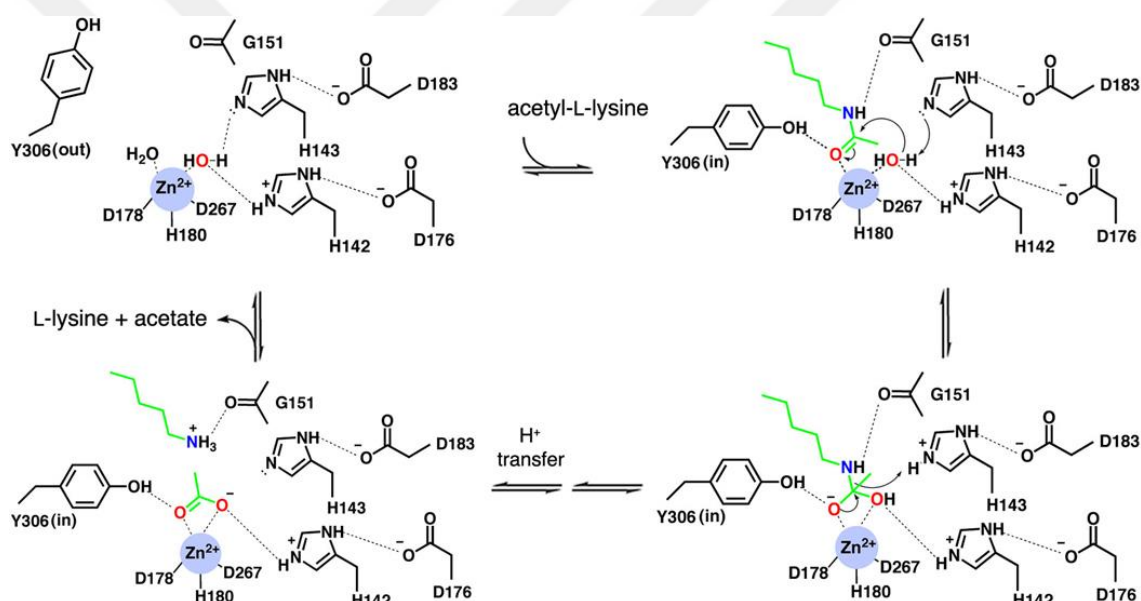


**Figure 1.5.** Schematic diagram of the proposed mechanism of HDACs (Lombardi et al., 2011).

### 1.3.2. Class IIa HDACs

This class of histone deacetylases (HDAC4, 5, 7, and 9) are exclusively expressed in particular cell types (Table 1.2). HDAC4 expression is extremely seen in the epiphyseal plate and brain cells; HDAC5 and HDAC9 are highly expressed in the brain, heart, and muscle tissues; HDAC7 expression is highly notable in thymocytes and endothelial cells. Class IIa HDACs are characterized by a large noncatalytic N-terminal domain, which is responsible for assigning of class IIa HDACs to certain promoters and known for its

regulatory role of the transportation of the enzymes between the cytoplasm and nucleus. This process is facilitated by the phosphorylation modification of the two conserved serine residues on the histone tail (Grozinger & Schreiber, 2000; Haberland et al., 2009). Genetic alterations to those conserved serine residues will lead to a nuclear delocalization of the class IIa HDACs and signal-refractory suppression of their target genes (Kasler & Verdin, 2006). HDAC class IIa enzymes exhibit a relatively low enzymatic activity among histone deacetylases family. Although, they show efficient and potent repression activity towards transcription process by interacting with other protein complexes that help in recruiting different co-repressor transcription proteins (Fischle et al., 2002; Lahm et al., 2007; X. J. Yang & Seto, 2008).

**Table 1.2.** Class IIa HDACs expression level and tissue distribution (Kasler & Verdin, 2006).

<b>Tissue</b>	<b>HDAC4</b>	<b>HDAC5</b>	<b>HDAC7</b>	<b>HDAC9</b>
Brain	+++	++	–	+++
Colon	++	ND	+	+
Gall bladder	ND	ND	ND	+
Heart	++	+++	+++	+++
Kidney	+	+	–	+
Liver	+/-	++	+	+
Lung	+/-	+	++	-/+
Ovary	+++	ND	+	ND
Pancreas	+	+	+	+
PBL	+	ND	+	ND
Placenta	+/-	+	+	+
Prostate	+	ND	+	ND
Skeletal muscle	+++	++	+	++/-
Small intestine	++	ND	+	+
Spleen	+	–	-/+	+
Testis	+	+	–	ND
Thymus	++	ND	+++	ND

PBL: peripheral blood lymphocytes; “+++” and “++” highly expressed; “+” detectable expressed; “–” not detected; “ND” no data. Conflicting findings are separated by slashes (e.g., +/-).

Class IIa HDACs are found in complex with the nuclear receptor co-repressor (N-CoR) and silencing mediator for retinoic acid and thyroid hormone receptors (SMRT) and HDAC3 (SMRT-N-CoR-HDAC3) complex. In absence of SMRT-N-CoR-HDAC3 complex, class IIa HDACs show no catalytic activity, which proposes that these enzymes may act as a network to recruit HDAC3-containing complexes. This may suggest that

class IIa HDACs are not activated unless HDAC3 is present. This is well explained and supported by the presence of other HDAC-HDAC protein interactions such as HDAC1 and HDAC2 that are observed in a single complex at the same time (Fischle et al., 2002; Verdin et al., 2003). Class IIa HDACs are also found to be interacted with the myocyte enhancer factor 2 (MEF2), that acts as a DNA transcription factor with a substantial role in the muscle differentiation. This association stops the function of MEF2 and prevent the muscle cell differentiation.  $\text{Ca}^{2+}$ /calmodulin-dependent kinase (CaMK) reverses the previous mechanism by phosphorylating the HDACs and detaching the MEF2-HDAC complex (McKinsey et al., 2001). Class IIa HDACs are transported between the cytoplasm and nucleus during muscle differentiation, which proves a precise role that each HDAC enzyme plays throughout the cell differentiation (De Ruijter et al., 2003).

One of the characteristics of class IIa is the substitution of the tyrosine residue at the entrance to the lysine channel into histidine, as seen in HDAC4, 5, and 7, where this change affects the activity about a thousand degrees less compared to the rest of other HDACs. Unlike the side chain of tyrosine that is directed directly towards the active site and has an active role in the catalytic mechanism, the histidine side chain is directed away from the active site towards the solvent (Lahm et al., 2007; Schuetz et al., 2008).

In addition to the catalytic zinc ion ( $\text{Zn}^{2+}$ ) found in the active site of class I, II, and III HDACs, class IIa HDACs have a unique conserved structural zinc-binding subdomain. Remarkably, this zinc ion-binding subdomain has shown to play a critical role in the structural conformation of the catalytic domain of the protein. Two different conformations have been adopted by the zinc-binding subdomain: the inhibitor-free protein (apo-structure) namely “closed” conformation that might offer a path for the substrate to catalytic  $\text{Zn}^{2+}$  in the binding pocket; the inhibitor-bound protein namely “open” conformation (Bottomley et al., 2008; Bürli et al., 2013; Schuetz et al., 2008). Furthermore, structural  $\text{Zn}^{2+}$ -binding subdomain has been linked to the recruitment of HDAC3/N-CoR and blocking the active site of class IIa HDACs may disrupt this recruitment and deterring the catalytic activity that results from HDAC3-class IIa HDACs interaction (Bottomley et al., 2008; Fischle et al., 2002).

Structural analysis of class IIa HDACs revealed two important loops that play a critical role in the enzyme activity. Large and short insertions in loops L2 and L1 were found

exclusively in class IIa HDACs. One cysteine residue from L2, and two cysteine and one histidine residue from L1 control the binding pockets of these enzymes as they coordinate the catalytic  $Zn^{2+}$  ion and stabilize the long flexible loops (Figure 1.4). These cysteine residues can undergo two different chemical modifications in cell: reduction and oxidation reactions that result in change of the nuclear localization of class IIa HDACs, which might be associated to the enlargement of heart muscles (cardiac hypertrophy) in vivo (Ago et al., 2008).

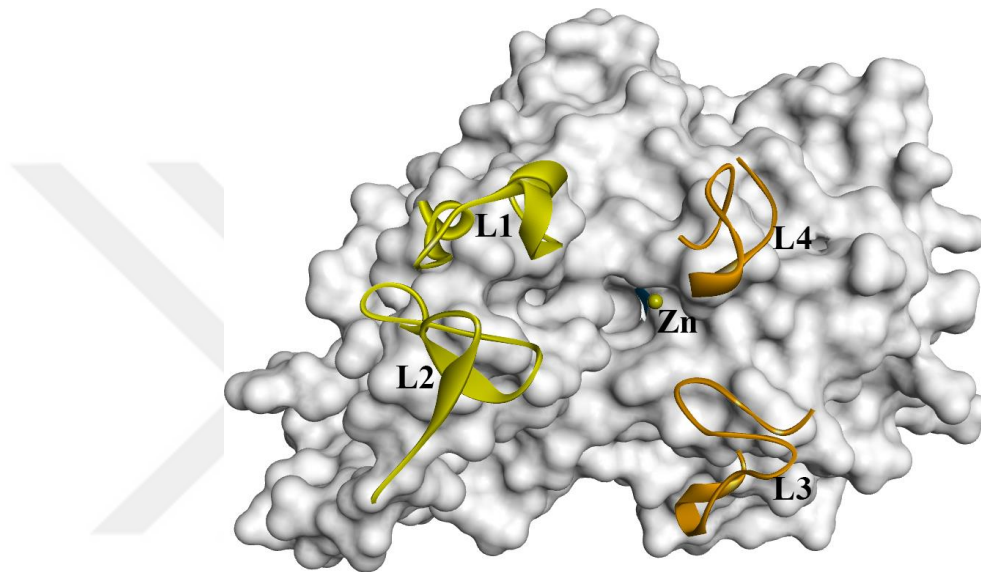


**Figure 1.6.** Representative crystal structure of the catalytic domain of HDAC7. Four loops are surrounding the active site of HDAC7: L1 and L2 loops are shown in yellow; L3 and L4 loops are shown in orange. Catalytic zinc ion is shown as yellow sphere.

#### 1.4. THE ROLE OF CLASS IIA HDACS IN HUMAN DISEASES

Understanding the massive PTMs and class IIa HDACs localization, proves that these enzymes play a critical role in regulation of many cellular processes significant to human health. Class IIa HDAC enzymes are described to control cellular mechanisms in a tissue-specific way and are profoundly expressed in the brain, heart, and skeletal muscle tissues. Deregulation of these enzymes at any cellular level has been associated to important health issues. Several studies in recent decades have shown the impact of class IIa HDACs in disease development in different organs and tissues, such as cancer, diabetes, muscle degenerative disorders, neurological and immunological disorders (McGee et al., 2008; Moresi et al., 2015). Glucose transporter type 4 (GLUT4) is known for its role in

insulin resistance and its expression is regulated by the action of HDAC5 (McGee et al., 2008). Muscle atrophy is identified by degeneration of motor neurons and muscle fibers or as a result of changes in neuromuscular junctions, which is regulated by the transcription factor myogenin where HDACs 4 and 5 are associated to the execution process (Moresi et al., 2010). In the following section, the involvement of class IIa HDAC enzymes will be further discussed.

#### **1.4.1. Nervous System and Neurological Disorders**

Class IIa HDACs are well identified in the physiological and pathological perspective of nervous system function and development. HDAC4 is extremely expressed in neuron cells and profoundly located in the cytoplasm where it is associated with the memory development and the plasticity of synapses (Darcy et al., 2010; Fitzsimons, 2015). In many studies, brachydactyly mental retardation syndrome (BDMR) has been linked to point mutations and microdeletions in HDAC4 gene, where patients are reported with learning disabilities, delayed development, anomalous behavior, aberrant skeletal, and craniofacial features (B. Morris et al., 2012; Villavicencio-Lorini et al., 2013; S. R. Williams et al., 2010). Morris et al. correlated the low expression level of HDAC4 mRNA to the high severity of BDMR syndrome (B. Morris et al., 2012). Haploinsufficiency of HDAC4 was also clinically reported in BDMR patients (Villavicencio-Lorini et al., 2013). Huntington's disease is another neurodegenerative disorder that was associated with HDAC4. Excessive number of "CAG" repeats within Huntingtin (HTT) gene at exon 1 is responsible for Huntington's disease. This will lead to the generation of polyglutamine (polyQ) expanses in the produced protein which will result in protein aggregation of the misfolded protein and eventually to neurological abnormalities and apoptosis (Mielcarek et al., 2013). According to Mielcarek et al., HDAC4 showed the tendency to associate with the mutant HTT. The study confirmed that a reduction in HDAC4 enzyme was combined with the declination of the HTT accumulation, which led to the restoration of the essential function of neural synapses and an improvement in the vital signs in the knockout mice models (Mielcarek et al., 2013). During diffuse axonal injury, HDAC5 has been providing a crucial role in the axonal regeneration process by tubulin deacetylation mechanism. Tubulin deacetylation is promoted by the activation of



HDAC5 upon the protein kinase C (PKC) attachment (Cho & Cavalli, 2012). Moreover, PKC and calcium have been involved in the nuclear export of class IIa HDAC5, which leads to restoration of the transcription of pro-regenerative genes by the elevation of histone acetylation mechanism (Cho et al., 2013). A study by Dietrich et al. has reported that cocaine can promote the HDAC5 nuclear export and myocyte enhancer factor 2C protein (MEF2C) activation by the phosphorylation of the salt-inducible kinase 1 (SIK1) (Dietrich et al., 2012). Remarkably, another study has revealed that cocaine may instead provoke HDAC5 nuclear aggregation via cyclic adenosine monophosphate (cAMP) signaling and dephosphorylation of HDAC5 through protein phosphatase 2A (PP2A) protein (Taniguchi et al., 2012). Cerebellar granule neurons (CGNs) protection against cell death has been related to the cellular function of class IIa HDAC7. This neuroprotective role is a deacetylase-dependent activity and participates in the inhibition of the oncogenic transcription factor c-Jun protein (Ma & D'Mello, 2011). Hemizygotously deletion in HDAC9 gene was involved in a minor ration of schizophrenia patients. HDAC9 has been reported to be profoundly expressed in mice brains exactly where the schizophrenia affected area was observed (Lang et al., 2011).

#### **1.4.2. Immune System and Immunological Disease**

In recent decades, the study of the association of HDACs with the immune system has become the focus of many researchers. For an instance, HDAC7 is excessively expressed through the generation of a cluster of differentiation 4 and 8 (CD4+ and CD8+) thymocytes. HDAC7 has been related to inhibition and repression of the orphan steroid nuclear receptor Nur77 in the cell nucleus through MEF2. Nur77 is known for its pro-apoptotic activity and its correlation to the T cell apoptosis. T cell activation induces protein kinase D1-mediated HDAC7 phosphorylation and exportation to the cytoplasm, which will lead to the removal of the Nur77 repression and initiation of cell death (Dequiedt et al., 2003; Parra et al., 2005). A study by Kasler et al. in 2011 demonstrated a positive selection of CD4+ lymphocytes or lower survival rate in knockout mice because of HDAC7 deletion in double positive thymocytes as well as nuclear export of HDAC7 (Kasler et al., 2011). In addition, Kasler et al. in 2012 studied the effect of nuclear export of phosphorylation deficient mutant-HDAC7 in thymocytes. They noted

that the negative thymic selection was blocked. However, transgenic thymocytes were still able to endure positive selection and the autoreactive T cell was able to escape to the periphery. Consequently, this blockage may lead to the development of lethal autoimmune syndrome (Kasler et al., 2012). Recent study has conducted an analysis of HDAC7 and its effect on the natural killer T cells (NKT). The study reported that the NKT generation was reduced in phosphorylation deficient mutant-HDAC7 thymocytes, and instead, naïve-like T cells development was induced. Accordingly, a correlation between these observations and tissue-specific autoimmunity was confirmed (Kasler et al., 2018). HDAC7 deletion has shown a serious impact on B lymphocyte development and differentiation in conditional knockout mice models. Thus, B cell development was suppressed in peripheral organs and led to lymphopenia (Azagra et al., 2016). Lobera et al. identified an association between class IIa HDACs and monocyte differentiation by application of TMP195 as a selective class IIa HDACs inhibitor (HDACi). In their study, they treated four different cells by using TMP195: monocytes (CD14+), T cells (CD3+), stimulated peripheral blood mononuclear cells (PBMC) and B cells (CD19+). Significantly, monocytes (CD14+) were more sensitive to the HDAC7 inhibition than other examined cells (Lobera et al., 2013). Guerriero et al. in 2017 were first to report that repressing class IIa HDACs can prompt an anticancer response by manipulating the immune system. They found that anticancer macrophages have been promoted and recruited in mice models of breast cancer by using TMP195 (Guerriero et al., 2017).

#### **1.4.3. Cardiovascular System and Related Diseases**

Class IIa HDACs and their influence on the cardiovascular system in humans are well studied, especially their role in cardiac hypertrophy onset. Cardiac hypertrophy, which is described as cardiac tissue enlargement, can arise from a continuous response of the cardiac cells to the physiological and immunological stimuli. High stress caused by several pathophysiological conditions such as valve disease, hypertension, myocardial infarction, and cardiac injury can lead to hypertrophy that increases the cardiac wall rigidity. Nevertheless, heart failure, fibrosis, and cardiomyopathy can arise from persistent hypertrophy (Chien, 1999; Heineke & Molkenin, 2006; McKinsey & Olson, 2005). Cardiac cells regeneration is promoted by the activation of the “fetal gene

program” which regulates proteins responsible for calcium absorption and muscle contraction (N Frey & Olson, 2003). “Fetal gene program” is inhibited by MEF2-HDCAs protein-protein interaction when no injury is found (Black & Olson, 1998; McKinsey et al., 2002). MEF2-HDCAs repression is reversed via phosphorylation-dependent nuclear export by hypertrophic stimuli that triggers the cardiac kinase. Unlike HDAC9 knockout mice, that exhibited a remarkable increase in the response to hypertrophic stimuli, mutated HDACs that lacks phosphorylation sites were hypertrophic-stimuli resistant (C. L. Zhang et al., 2002).

Calcium signaling alterations have been associated to cardiac remodeling as a result of stress conditions and HDAC4 phosphorylation through CaMK-I and CaMK-II (Backs et al., 2006; Norbert Frey et al., 2000). HDACs phosphorylation level is localization-dependent and numerous kinases can only modify particular HDAC enzymes. In CaMKII $\delta$  deficient mice models, kinase activity was not affected in HDAC5, while diminished in HDAC4 (Fielitz et al., 2008; Little et al., 2007). In addition, kinase specificity is affected by alternate splicing of CaMKII $\delta$ , that leads to HDAC4 localization-dependent phosphorylation via activation of nuclear  $\delta$ B and  $\delta$ C isoforms of phenylephrine and caffeine, respectively (McKinsey, Zhang, Lu, et al., 2000). HDAC4 can be phosphorylated by CaMKII $\delta$  B and C isoforms and can offer comparable MEF2 gene expression. Also, calcium regulatory proteins can be phosphorylated by CaMKII $\delta$ C to control Ca<sup>2+</sup> concentrations (T. Zhang et al., 2007). Moreover, several studies have reported that various HDAC modification enzymes can provoke cardiac hypertrophy through Ca<sup>2+</sup>-independent signaling pathway. Downstream effect of protein kinase D (PKD) can specifically initiate HDAC5 nuclear export upon its phosphorylation (Fielitz et al., 2008; Vega, Harrison, et al., 2004). In hypertensive conditions, G protein-coupled receptor kinase-5 (GRK5) can induce MEF2 activation and nuclear export of HDAC5 which may lead to ventricular hypertrophy (Akhter et al., 1998; I. et al., 2012). Recently, HDAC5 was shown to be related to left ventricle hypertrophy and elevated salt intake. HDAC5 phosphorylation is induced by SIK1 activation upon elevated sodium concentrations, and consequently improves the transcriptional activity of MEF2 and nuclear factor of activated T-cells (NFAT) (Frohlich et al., 1993; Popov et al., 2012; Schmieder et al., 1988). Haworth et al. studied HDAC enzymes phosphorylation by neurohormones stimuli in human myocardiocyte cells. In addition to the substantial role

of PKD in promoting the HDAC5 nuclear export and MEF2 activation, later mechanisms were also mediated via independent phosphorylation of  $\beta$ 1-adrenergic receptor ( $\beta$ 1-AR) (Haworth et al., 2012). In the same context, more focused studies are needed to understand how these mechanisms are put together to deliver a conjoint endpoint as in “fetal gene program” activation. It is of a great challenge to fully understand how HDAC enzymes are controlled in cardiovascular diseases and how MEF2 inhibition and HDACs retention contribute to cardiac hypertrophy prevention. Such knowledge can potentially be used for therapeutic purposes. Signaling pathway for phenylephrine was proved to induce nuclear export of HDAC4 and the formation of disulfide bonds between cysteine 667 and cysteine 669 residues in HDAC4. Crucially, cardiac hypertrophy has been reduced as a result of breaking down these disulfide bonds by thioredoxin 1 enzymes (Ago et al., 2008). Other specific phosphorylation modifications are also known to block nuclear export of HDAC enzymes. 14-3-3 binding (a conserved regulatory protein that is expressed in human cells) is shown to be interrupted as a result of PKA-mediated phosphorylation of serine 279 residue in HDAC5, which can lead to cardiac hypertrophy inhibition and MEF2 repression (Ha et al., 2010). Importantly, PKA has a crucial cardioprotective function that is associated with the HDAC4 proteolytic cleavage, in which MEF2 is repressed by the cleaved N-terminal fragment upon its translocation to the nucleus (Bucks et al., 2011).

In addition to cardiac hypertrophy, comparable molecular mechanisms can also lead to vascular smooth muscle cells (VSMCs) hypertrophy under certain pathological conditions. Class IIa HDAC enzymes modifications were also seen to be regulated under certain vascular hypertrophy conditions. HDACs 4 and 5 phosphorylation mechanism in VSMCs is mediated by PKD1 and CaMKII (Jinjiang et al., 2008; Xiangbin et al., 2007). Mature endothelial cells (ECs) and VSMCs are known to be involved in new blood vessels generation namely angiogenesis (Risau, 1997). Through angiogenesis, HDACs 5 and 7 nuclear export and 14-3-3 binding sites undergo PKD-mediated phosphorylation mechanism that is promoted by vascular endothelial growth factor (VEGF). These modifications are known to enhance VEGF-responsive genes expression, that are involved in micro-vessel growth, tube generation, and cell proliferation and migration (Chang, Bong, et al., 2008; Chang, Wang, et al., 2008; S. Wang et al., 2008). During atherosclerosis, localization and phosphorylation of HDAC5 are mediated by CaMK,

thus endothelial nitric oxide synthase (eNOS) and Kruppel-like factor 2 expression level is improved in ECs (W. Wang et al., 2010). Interestingly, nitric oxide, that is a product of nitric oxide synthase, was shown to promote HDAC4 PP2A-mediated dephosphorylation (Illi et al., 2008). Delehanty et al. proposed that class IIa HDAC enzymes are not only involved in the formation of blood vessels and development of cardiovascular cells. They reported that HDAC5 undergo PKD-dependent phosphorylation as is involved in the regulation of red blood cells production, also known as erythropoiesis (Delehanty et al., 2012).

#### **1.4.4. Musculoskeletal System and Related Diseases**

Histone deacetylases class IIa are known to undergo phosphorylation modifications that play substantial roles in gene expression related to the differentiation of bone and muscle tissues and associate them with the pathophysiological conditions of the musculoskeletal system, such as osteoarthritis and myopathies.

Muscular tissue formation in embryonic life stage, also known as myogenesis, involves myoblast cells differentiation to form myotubes. During myogenesis, large number of muscle-related genes undergo molecular activation mechanisms combined with suppression of cell proliferation genes (Maud Martin et al., 2009). In case of undifferentiated cells, HDACs 4 and 5 are found to be interacted with the inactivated form of the transcriptional factor MEF2. Upon myogenesis, MEF2-HDAC4/5 complex go through nuclear export as a result of the CaMK- and GIT1-mediated phosphorylation process of 14-3-3 binding sites (J. Lu et al., 2000; McKinsey, Zhang, & Olson, 2000; McKinsey, Zhang, Lu, et al., 2000). Class II HDAC proteins are known for their ability to relocalize themselves during different biological and cellular mechanisms. Thus, HDACs class IIa isoforms display diverse cellular localization forms during the differentiation of myoblast cells. Upon myoblast fusion, HDAC4 undergo cellular relocalization from the cytoplasm to the nucleus, but this transition can be inhibited by the calcium/calmodulin-dependent protein kinase IV (CaMKIV) (Miska et al., 2001). Remarkably, class II HDAC7 isoform is utterly located in the cytoplasm during myotubes differentiation (Gao et al., 2010). During skeletal muscle differentiation, MEF2-interacting transcription repressor (MITR), which is a HDAC9-splice variant, can

undergo CaMK-dependent phosphorylation as well as Mirk/dyrk1B-dependent phosphorylation (Minibrain-related kinase/dual-specificity tyrosine-regulated kinase 1B) (Deng et al., 2005; C. L. Zhang et al., 2001).

Bones growth and formation including chondrocytes and osteoblast cells differentiation is known to be modulated by bone morphogenic proteins family (BMP) which is also regulated by class IIa HDACs functions (Cao & Chen, 2005; Wan & Cao, 2005). Jensen et al. demonstrated that HDAC7 (but not HDACs 4, 5, or 6) can be subjected to nuclear export by BMP2 through PKD-dependent phosphorylation (Jensen et al., 2009). This mechanism ensures the derepression of the runt-related transcription factor 2 (Runx2) via HDAC7, which is considered to be the most important transcriptional factor in the musculoskeletal system (Jensen et al., 2009). Enhanced levels of Runx2 and HDAC4 nuclear transition by CaMKIV, together play a prominent role in chondrocytes differentiation into pre-hypertrophic chondrocytes. Premature bone ossification condition was observed in knockout mice models lacking HDAC4, suggesting that these regulatory systems are of critical importance in osteoarthritis onset (Guan et al., 2012; Vega, Matsuda, et al., 2004). It is thought that this prematuration mechanism can be avoided by the parathyroid hormone-related peptide (PTHrP) expression, which with the help of dephosphorylated-HDAC4, is involved in Runx2 suppression. Hence, regulation of HDACs phosphorylation may be considered as a potential treatment for orthopedic disorders such as calcification disorders and osteoporosis (Kozhemyakina et al., 2009).

#### **1.4.5. Cancer**

Whilst HDACs class IIa post-transcriptional modifications have been ascertained to influence and interfere with the pathophysiological conditions as previously discussed; many other studies have shown that their effects are far to count. HDACs family has been well known for their association with the development of cancer. Vorinostat, one of the most famous pan-HDACs inhibitors, has been FDA-approved since 2006 for T-cell lymphoma treatment, signifying the importance of HDACs as targets for preventing cancer progression. Class I HDAC proteins have drawn the foremost attention of cancer research so far, because their impaired function is related to the development of cancer

(Ropero & Esteller, 2007). Nevertheless, HDACs class IIa have shown significant functional roles in tumorigenesis development and progression in several disorders.

In stomach cancer cells (also known as gastric cancer), due to nuclear accumulation of PKD2, PKD-dependent phosphorylation of HDAC7 is utterly increased which ultimately leads to HDAC7 nuclear export and downstream targets expression involving Nur77 (Von Blume et al., 2007). On the contrary, in colon cancer cells, HDAC4 is located in the nucleus and interacts with the transcription factor Sp1 named as specificity protein 1 and suppress p21 transcription, thus induces growth of cancer cells (Wilson et al., 2008). Kao et al. demonstrated that RNAi induces repression of HDAC4 expression which results in reduction of HeLa cells viability. In addition, they reported that after double-stranded DNA break, the p53 tumor suppressor protein and HDAC4 are colocalized. This colocalization was observed via immunoprecipitation assay (Kao et al., 2003). In other pathological conditions, Kaletsch et al. reported that HDAC4 demonstrated the contrary effect as the expression of HDAC4 in urothelial cancer cells rather blocks the cancer cells proliferation (Kaletsch et al., 2018). In a different study by Geng et al., they showed that HDAC4 in H23 and H460 cell lines of the non-small cell lung cancer (NSCLC) have been exported from the cytoplasm into the nucleus upon irradiation exposure. They further reported that uses of the Panobinostat (pan-HDACi antitumor agent) have promoted the HDAC4 relocalization into nucleus and reversed the irradiation effect.  $\gamma$ -H2AX is a special phosphorylated form of H2A histone family, which is involved DNA repair. Geng et al. also found that Panobinostat administration before the exposure to an irradiation extends the duration of  $\gamma$ -H2AX foci (Geng et al., 2006). It is captivating to postulate whether cytoplasmic relocalization can be induced by HDAC4 inhibition, which may help in the DNA repair process. It is more likely to conduct such study due to the availability of HDACs inhibitors to draw more attention on the potential association of HDAC4 with designated effects of Panobinostat. Blocking of HDAC4 nuclear interaction with other partners such as HDAC3 may provide an explanation of HDAC4 nuclear export via Panobinostat. Another study by Stronach et al. demonstrated the association between HDAC4 expression and the platinum-based DNA damaging drugs resistance (Stronach et al., 2011). Sixteen matching tumor biopsies of ovarian cancer were taken and tested in advance and after platinum resistance occurrence. An enhanced expression of HDAC4 was observed in 44% in platinum-resistant biopsies. Moreover,

they established a molecular connection between the expression rate of HDAC4 and the acetylation level of signal transducer and activator of transcription 1 (STAT1), which plays a crucial role in tumor suppression. They found that when Cisplatin (a chemotherapeutic agent) was introduced to platinum-resistant cells, tyrosine 701 residue of STAT1 was phosphorylated and hence activated and transported into the nucleus. In ovarian cancer tissues, STAT1 acetylation was enhanced upon HDAC4 inhibition, which led to neutralizing its platinum-induced activation and increased the STAT1 sensitivity towards Cisplatin (Stronach et al., 2011). Cadot et al shed some light on knockdown (partial loss of function) and knockout (complete loss of function) of HDAC4 in normal and tumor cells and its impact on the progression of the cell cycle. Mitotic arrest was seen in HeLa cell line of the knockdown HDAC4 and consequently led to apoptosis. Deficiencies in chromosome segregation were just reported in p53-lacking cells (Cadot et al., 2009). p53-independent mechanisms may also explain how HDACs class IIa can promote cancer progression via the cyclin-dependent kinase inhibitor 1 (p21<sup>WAF1/CIP1</sup>). Expression of p21<sup>WAF1/CIP1</sup> may increase in different types of cancer cells through HDAC4 suppression via small interfering RNA (siRNA). Down regulation of p21<sup>WAF1/CIP1</sup> via HDAC4 was seen after the interaction with the transcription factor Sp1, which resulted in the binding of HDAC4-Sp1 to the Sp1/Sp3 binding site of the p21<sup>WAF1/CIP1</sup> promoter region (Mottet et al., 2009). Mathias and colleagues proposed that other interacting proteins may participate in the suppression of the p21<sup>WAF1/CIP1</sup> expression, since HDAC4 alone is enzymatically inactive. This could be achieved by the recruitment of other transcriptional co-repressor proteins such as SMRT-N-Cor-HDAC3 (Fischle et al., 2002). In the same context, Wilson et al. in 2008 proved that SMRT-N-Cor-HDAC3 interaction with HDAC4 resulted in the repression of the p21<sup>WAF1/CIP1</sup> expression in colon cancer cells (Wilson et al., 2008). Class IIa HDAC4 was shown to have a caspase cleavage site at aspartic acid 289 residue, where cysteine-aspartic proteases (caspase) enzymes play prominent roles apoptosis (F. Liu et al., 2004; Paroni et al., 2004). When HDAC4 undergoes caspases cleavage, the N-terminal fragments of HDAC4 accumulate in the nucleus and subsequently induce the release of cytochrome C and promote the programmed cell death via caspase-9 (Paroni et al., 2004). MEF2 binding site (HDAC4/1-165) was missing in the N-terminal part of HDAC4 signified that MEF2 suppression is required for the apoptosis. MEF2-HDAC4 interaction is essential to



promote cancer development and cell differentiation. Mutational experiments have demonstrated that integral and undamaged MRF2 binding site alongside with nuclear localization are critical for the HDAC4 transitional activity (Di Giorgio et al., 2013). In 2018, a study has related HDAC4 to the tumor suppressor p53-dependent senescence in fibroblasts and promoting cell transformation (Paluvai et al., 2018). Similar to HDAC4, HDAC7 is a potential tumorigenic and exhibits transforming ability (Di Giorgio et al., 2013). In lung cancer, HDAC7 is highly expressed and associated with low survival rate. In addition, HDAC7 is also related to cancer development by STAT3 deacetylation which blocks the activation of STAT3 (Lei et al., 2017). Similar to the caspase cleavage site seen in HDAC4, HDAC7 as well has this feature, a caspase cleavage site at aspartic acid 375 residue, which is a target for caspase8. The HDAC7 proteolytic cleavage was associated with the change in subcellular localization of the two cleaved parts and MEF2 suppression (Scott et al., 2008). However, unlike HDAC4, the apoptotic impact of HDAC7 in cancer cells has not been established yet. Zhong et al. reported the correlation of HDAC5 to tumor-related development such as angiogenesis. They proposed that extreme expression of HDAC5 in lung cancer was related to the invasion ability, proliferation and survival of cancerous cells (Zhong et al., 2018). Earlier study demonstrated the contrary effect of HDAC5 overexpression in breast carcinoma cells, osteogenic sarcoma cells, and neuroblastoma cells, which resulted in the repression of cancer development and subsequently apoptosis that was related to the activation of death receptors signaling of tumor necrosis factor (TNF) (Y. Huang et al., 2002). Another publication by Huang et al. have reported an overexpression of HDACs 2 and 5 in the estrogen receptor positive (ER<sup>+</sup>) tamoxifen-resistant MCF7-TamC3 breast cancer cell line. On the other hand, decreased expression of HDACs 2 and 5 was observed in the MCF7 tamoxifen-sensitive cells. Additionally, overexpression of HDAC5 was linked to the decreased regulation of tumor suppressor microRNA-125a-5p as well as to the increased regulation of anti-apoptotic protein surviving. Interestingly, decreased expression of microRNA-125a-5p was associated with the low survival rate in patients with tamoxifen-treated ER<sup>+</sup> breast cancer (W. T. Huang et al., 2017). It is possible that the increased or decreased expression of HDAC5 effect on the cellular responses differs according to the origin of the cells because of the tissue-specificity expression manner of class IIa HDACs. Moreover, HDACs class IIa 7 and 9 have been correlated to the cancer

development. Similar to HDAC5, angiogenesis has been associated with HDAC7. Upregulated expression of the platelet-derived growth factor receptor beta (PDGFR $\beta$ ) and platelet-derived growth factor B (PDGF-B) has been seen in endothelial cells upon HDAC7 knockdown, which in turn altered the migration process and thus altered angiogenesis (Denis et al., 2007). In pancreatic cancer cells, high level of HDAC7 expression was seen in the cytoplasm (Ouaïssi et al., 2008). Moreno and colleagues have demonstrated a correlation between the overexpression level of HDACs 7 and 9 and the poor prognosis in childhood acute lymphoblastic leukemia (ALL) (Moreno et al., 2010). Another study has shown that HDAC7 inhibition caused cellular senescence and cell cycle halt. HDAC7 has a direct influence on cancer cell development in a variety of cancer cell lines through decreased regulation of the cell cycle regulatory proteins p21 and p27 and, at the same time, by increased regulation of the proto-oncogenic transcriptional factor c-Myc (C. Zhu et al., 2011). On the other hand, HDAC7 expression was reduced tragically in B-cell malignancies such as chronic lymphocytic leukemia (CLL). However, enhanced expression of HDAC7 in B-cell malignancies has led to apoptosis and decreased regulation of the c-Myc (Barneda-Zahonero et al., 2015). Several studies showed that the increased protein level of HDAC9 and its overexpression have been associated to different cancer cells including osteosarcoma, lymphoma and breast cancer (Clocchiatti et al., 2013; Lapierre et al., 2016; Moreno et al., 2010; Zhao et al., 2015). Improved proliferation and reduced apoptosis rates were reported in the breast cancer cells and correlated to the increased level of HDAC9 expression. This was also linked to the downregulation of cyclin dependent kinase inhibitor 1a (CDKN1A), bcl-2 associated x-protein (BAX), and TNF receptor superfamily member 10a (TNFRSF10A) genes. HDAC inhibitors effectiveness to lower the cell proliferation rate and the expression of CDKN1A have been decreased in lymphoma. Gil et al. demonstrated that lymphoproliferative disorders and splenic marginal zone lymphoma have been reported in genetically modified mice models where HDAC9 was continuously expressed during the cell cycle. Additional investigation showed that altering survival and growth signaling pathways by manipulating the activity of p53 and B-cell lymphoma 6 (BCL6) might explain the HDAC9 contribution to lymphomagenesis (Gil et al., 2016).

#### 1.4.6. Diabetes

Class IIa HDACs function was also related to the diabetes pathological process and linked to the insulin resistance in several tissues like skeletal muscle tissues. Class IIa HDACs 4, 5, and 7 nuclear preservation and dephosphorylation in mammalian cells are promoted by the fasting hormone glucagon (Mihaylova et al., 2011). Interestingly, HDACs class IIa are necessitated to the deacetylation modification and activation of the forkhead box protein O (FOXO) transcriptional factors that are involved in the expression of gluconeogenic genes, e.g., catalytic subunit of glucose 6-phosphatase (G6Pase) (Mihaylova et al., 2011). In this case, HDACs class IIa have shown the ability to regulate the blood glucose level through hormones production regulation. Moreover, GLUT4 expression, which is a principal modifier of insulin resistance, is modulated by HDAC5 suppression and phosphorylation-mediated nuclear export (McGee et al., 2008). Remarkably, upon aerobic exercises, phosphorylation of HDAC5 rate has been reported to be increased, which may suggest that HDACs are subjected to alterations in blood oxygen levels (Vissing et al., 2008). HDACs family is well known to act in response to alterations in cellular metabolic environs. Class III HDACs (SIRT6) activity is controlled by NAD<sup>+</sup> and their catalytic activity is regulated by the accessibility to glutamine and glucose (Mathias et al., 2014; Pirinen et al., 2012; Poulsen et al., 2014; Y. Zhu et al., 2013). Additionally, HDACs class I (HDAC1 and HDAC2) have been reported to allosterically activated via nicotinamide adenine dinucleotide phosphate (NADPH) along with acetyl-CoA and other CoA-derived molecules (Vogelauer et al., 2012). It is now evident that other metabolic regulators can affect HDACs activity such as short chain fatty acids including butyrate, which is considered as the base unit for the development of antitumor agents (Rajendran et al., 2011). High consumption of butyrate along with short chain fatty acids have been suggested to provide an anti-diabetic and cardioprotective function of whole-grain nutrition. It is thought that tempering of HDACs catalytic activity in diabetic patients might be linked to the changes in butyrate levels (Nilsson et al., 2010).

## 1.5. HISTONE DEACETYLASE KNOWN INHIBITORS

Several human disorders such as sickle cell disease (SCD), cystic fibrosis (CF), inflammatory disorders, acquired immunodeficiency syndrome (AIDS), muscular dystrophies, and neurodegenerative have been linked to HDAC proteins as epigenetic targets (Tang et al., 2013; Wiech et al., 2009). With a closer look at the large number of scientific publications in recent years, HDACs have proven to be vital targets for anticancer drugs. The biological effect of inactivating HDACs in various types of cancers has shown their importance in treating cancer and reversing the pathological implications. HDACis are well established to control several molecular processes through regulating histone and non-histone proteins, including immune system response, cell cycle control, programmed cell death, and angiogenesis (Eckschlager et al., 2017; Hull et al., 2016). Nevertheless, their exact molecular mechanisms are still ambiguous (Kim & Bae, 2011).

The first pharmacophore model of HDACi was established in 1997 by Jung et al., which led to the revolution of HDACis rational design. The mostly common and currently recognized HDACi pharmacophore features obey three main components: a zinc-binding group (ZBG) also known as chelator which can interact with catalytic zinc ion in the active site; a linker that normally mimics the acetyl-lysine and span through the substrate binding channel; and a cap group that is important for the isoform selectivity and also known as surface recognition domain (Figure 1.7) (Finnin et al., 1999; Jung, 2012; Jung et al., 1999).

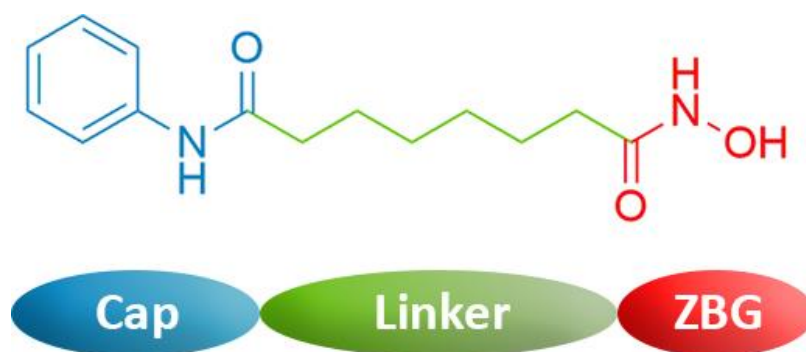


**Figure 1.7.** HDACs inhibitors pharmacophore model features (M. A. Choi et al., 2019). Also, this model represents the chemical structure of suberanilohydroxamic acid (SAHA), the HDAC inhibitor.

Nonetheless, the above pharmacophore model is not entirely applied for HDACi that targets other pockets besides the main active site like lower pocket, foot pocket and side

pocket. Hence, another pharmacophore model was proposed by Melesine et al. in 2018 which contains six components instead of three: surface cap S-cap, side pocket cap SP-cap, lower pocket LP-group, foot pocket FP-group, ZBG, and linker (Melesina et al., 2018). HDACi can either display an isoform selectivity or can be pan inhibitors and non-selective.

So far, only four HDAC inhibitors have been approved for treatment of cancer by the Food and Drug Administration (FDA) including the pan-inhibitor suberoylanilide hydroxamic acid (SAHA/Vorinostat) which is used for the treatment of patients with cutaneous T-cell lymphoma (CTCL), Belinostat (PXD101) and Romidepsin (FK228) are used for the treatment of patients with peripheral T-cell lymphoma (PTCL) and Panobinostat (LBH589) for the treatment of multiple myeloma. Tsuji et al. extracted one of the first HDACi in 1976 from *Streptomyces hygroscopicus*, which showed an antifungal activity against *Trichophyton* (Tsuji et al., 1976). Later in 1990, Yoshida et al. proved the high potency of Trichostatin A (TSA) against HDACs as it blocks the cell cycle of normal fibroblasts in both the G1 and G2 phases (Yoshida, 2007). Vorinostat was the first HDACs inhibitor to be approved by FDA in 2006, which is a non-selective broad-spectrum HDAC inhibitor with  $IC_{50}$  of ~10 nM in cell-free assays and is used in treatment of patients with CTCL (Mann et al., 2007; Schölz et al., 2015). Romidepsin (FK228) was the second HDACi to be approved by FDA in 2009, which shows a potent selectivity against HDACs 1 and 2 with  $IC_{50}$  of 36 nM and 47 nM in cell-free assays and is used in treating patients with CTCL and PTCL (Bantscheff et al., 2011; Ellis & Pili, 2010). Belinostat (PXD101) was also approved in 2014 by FDA that is a broad-spectrum HDAC inhibitor with  $IC_{50}$  of 27 nM in a cell-free assay and is used in treating patients with PTCL (Bantscheff et al., 2011; H. Z. Lee et al., 2015). Lastly, Panobinostat (LBH589) got approved by FDA in 2015, which shows an  $IC_{50}$  activity of 5 nM in a cell-free assay in HDACs and is used in treating patients with multiple myeloma (Laubach et al., 2015; Schölz et al., 2015).

Based on the chemical structure of HDACs inhibitors, they are generally classified into five classes: carboxylates, hydroxamic acids, benzamides, electrophilic ketones, and cyclic peptide inhibitors (Table 1.3).

**Table 1.3.** Structural classification of HDACs inhibitors.

HDAC inhibitor	Classification	Clinical trials	Class selectivity
Valproic acid	Carboxylic acid	FDA app.	I
Butyrate	Carboxylic acid	Phase II	I and II
Vorinostat (SAHA)	Hydroxamic acid	FDA app.	Broad-spectrum
Belinostat	Hydroxamic acid	FDA app.	I
Panobinostat	Hydroxamic acid	FDA app.	Broad-spectrum
Abexinostat	Hydroxamic acid	Phase III	I and II
Pracinostat	Hydroxamic acid	Phase III	Broad-spectrum
Resminostat	Hydroxamic acid	Phase II	I and II
Givinostat	Hydroxamic acid	Phase III	I and II
Quisinostat	Hydroxamic acid	Phase II	Broad-spectrum
Ricolinostat	Hydroxamic acid	Phase II	HDAC6
Citarinostat	Hydroxamic acid	Phase I	HDAC6
Dacinostat	Hydroxamic acid	N/A	Broad-spectrum
Droxinostat	Hydroxamic acid	N/A	HDACs 3, 6, 8
Trichostatin A	Hydroxamic acid	Phase I	Broad-spectrum
CUDC-101	Hydroxamic acid	Phase I	I and II
Tacedinaline	Benzamide	Phase III	I
Chidamide	Benzamide	Phase III	I and IIb
Mocetinostat	Benzamide	Phase II	I and IV
Entinostat	Benzamide	Phase III	I
Tubastatin A	Benzamide	N/A	HDAC6
KD5170	electrophilic ketones	N/A	I and II
Romidepsin	Cyclic Peptide	FDA app.	I
Apicidin	Cyclic Peptide	N/A	I

FDA app.: FDA approval. N/A: Not in clinical trials. Broad-spectrum: applied when the inhibitor covers more than two HDAC classes. Valproic acid was approved by FDA for other several disorders but not for cancer treatment.

**Carboxylates (short-fatty acid) derivative HDACi:** Boffa et al. described butyric acid namely phenyl butyrate as one of the first HDACs inhibitors in 1978 to be investigated in proteins (Figure 1.8) (Boffa et al., 1978). Phiel et al. in 2001 recognized the anticonvulsant valproic acid as an HDAC inhibitor (Phiel et al., 2001). Carboxylic acid HDACs inhibitors have shown less activity in comparison to the hydroxamic acid inhibitors because of the low coordination level with catalytic zinc ion in the active site of HDAC enzymes. Regardless the less catalytic activity of carboxylic acid HDACs inhibitors, phenyl butyrate and valproic acid are globally well-studied histone deacetylase inhibitors. Phenyl butyrate and valproic acid have been broadly endorsed for the treatment of several cancer types and epilepsy. Interestingly, valproic acid plays a critical

role in several cellular pathways in the cell (Blaheta et al., 2002). Valproic acid is undergoing clinical trials phase I, while phenyl butyrate is undergoing clinical trials phase II.

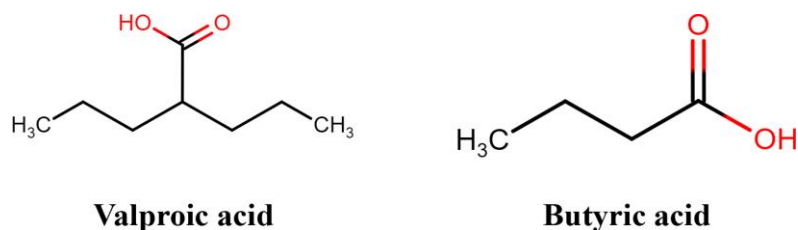


**Figure 1.8.** Carboxylic acid based HDAC inhibitors.

**Hydroxamic acids derivative HDACi:** Hydroxamic acid HDAC inhibitors represent the largest category of HDACi as they are well-studied molecules targeting the HDAC's active site. The common structural feature of these inhibitors contains a hydroxamic group that helps the chelation process between the zinc ion in the binding pocket and the hydroxamic acid moiety of the inhibitor; an aromatic ring namely cap group and acts as a surface recognition group; and a linear linker (saturated or unsaturated) between the hydroxamic group and cap group (Figure 1.7) (Breslow et al., 2000). The natural product TSA, and the designed SAHA (Vorinostat), are the most well-known examples of hydroxamic acid HDAC inhibitors (Breslow et al., 2000; Richon et al., 1996). TSA and SAHA are broad-spectrum HDAC inhibitors that target classes I, II and IV and are effective at nanomolar concentrations. TSA is undergoing clinical trials phase I, while SAHA has been approved by FDA in 2006 for the treatment of CTCL (Mann et al., 2007; E. K. Singh et al., 2010). Enormous number of hydroxamic acid derived HDACi have been developed and designed mimicking TSA structure.

**Benzamides derivative HDACi:** In 1999, Suzuki et al. synthesized the first benzamide-derivative HDAC inhibitors (Saito et al., 1999; Suzuki et al., 1999). These inhibitors share no similarity with the previous designed HDAC inhibitors. Their benzamide moiety ligate the catalytic zinc ion in the active site, thus impeding the histone deacetylases. Like carboxylates (short-fatty acid) HDACi, benzamide HDACi are mostly less potent than those of hydroxamic HDACi. Entinostat (MS-275) is one of the most well-studied and highest potent benzamide HDACi, that promotes the overexpression of p21 protein and increases the acetylation of nuclear histones in several cancer cells. Entinostat shows an inhibition activity of 5  $\mu$ M and displayed effective cancer fighting in vivo (Jaboin et al.,

2002; Saito et al., 1999). Entinostat is undergoing clinical trials phase III and is a class I HDACs selective inhibitor. Another benzamide derivative HDAC inhibitor is Tacedinaline (CI-994), which is highly potent against human and rodent tumor cells and is used for the treatment of patients with acute myelocytic leukemia (AML) and colon cancer and others. Tacedinaline is undergoing clinical trials phase III (El-Beltagi et al., 1993; Graziano et al., 2001; Seelig & Berger, 1996).

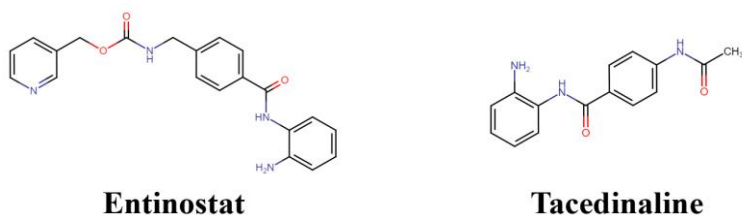


**Figure 1.9.** Benzamide derivative HDAC inhibitors.

**Electrophilic ketones derivative HDACi:** Electrophilic ketones-based inhibitors are proven to be instantly hydrated and have been identified as significantly effective inhibitors against HDAC enzymes, which chelate the catalytic zinc ion at the bottom of HDAC active site (Christianson & Lipscomb, 1986; Walter et al., 1996). Trifluoromethyl ketones are the most well-known electrophilic ketones based HDACi. Frey et al. reported in 2002 a SAHA derivative linear chain trifluoromethyl ketones as a histone deacetylase inhibitor (R. R. Frey et al., 2002). In the following year, Wada et al. designed  $\alpha$ -ketoamides and  $\alpha$ -ketoesters as histone deacetylase inhibitor (Wada et al., 2003). Various electrophilic ketones compounds show inhibition activity at micromolar concentrations in cancer cells of fibrosarcoma and breast cell lines (R. R. Frey et al., 2002).

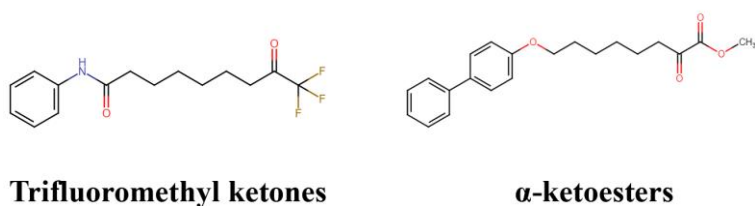


**Figure 1.10.** Electrophilic ketones derivative HDAC inhibitors.

**Cyclic peptide HDACi:** Cyclic peptide derivative histone deacetylase inhibitors are described as highly complicated molecules among HDACi. Cyclic peptide-based HDAC inhibitors consist of main macrocycle moiety including four hydrophobic amino acid residues in the surface recognition group; a ZBG with a functional group; and a linker



group that has an alkyl chain (Figure 1.11). This class of HDAC inhibitors binds to the binding pocket of HDAC enzymes in a similar way to TSA. The alkyl (aliphatic) linker of these inhibitors sprawls down the protein's tunnel placing the binding domain close to the catalytic zinc ion in the binding pocket, whilst the macrocycle moiety interacts with the rest of the active site.

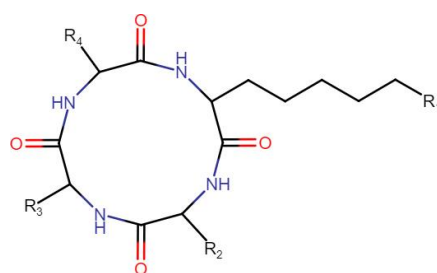


**Figure 1.11.** Main pharmacophore model of cyclic peptide derivative HDAC inhibitors.

The macrocycle moiety of the cyclic peptide includes cyclic tetrapeptide that is assembled with an imino acid and D-amino acid neighboring the linker domain, which creates a 12 restricted membered cyclic structure with massive intramolecular hydrogen bonds. The D-confirmation of the amino acids is believed to be crucial for close-fitting of the inhibitor with the rim of the binding pocket, thus facilitate the insertion of the linker domain into the enzyme's tunnel (Komatsu et al., 2001). Cyclic peptide HDAC inhibitors are divided into several structural classes based on the functional group of the zinc binding group which may include: ~epoxyketone (e.g., Chlamydocin), ~hydroxamic acids (e.g., Trapoxins), ~ketone (e.g., Apicidin), ~hydroxymethyl ketone (e.g., FR-225497), ~electrophilic ketones (e.g., cyclic peptide with pentafluoroethyl ketone), ~sulfur (e.g., FK228 and Largazole), ~carboxylic or amide group (e.g., Azumamide), and many others.

### 1.5.1. Class IIa HDAC Inhibitors

Mainly, three different characteristics of HDACs class IIa aided in developing and designing of selective inhibitors, including the enzyme's active site involving the zinc atom, the cytoplasmic-nuclear localizing, and the N-terminal region. As previously discussed, a standard histone deacetylase inhibitor consists of three groups; a zinc-binding group ZBG (also referred as metal binding group) with the ability of chelating the catalytic  $Zn^{2+}$  in the active site, a hydrophobic linker which mimics the acetyl-lysine,

and a cap group which acts as a surface recognition domain. Chemical alterations of these groups may affect both the potency and the selectivity of the compound. Theoretically, designing of isoform selective HDACi may need just minor modification to the linker group property to match the specific active site of HDACs class IIa. Henkes et al. in 2012 reported that few changes in the linker group of the HDACi SAHA improved the inhibitor selectivity towards classes IIa and IIb HDACs (Henkes et al., 2012). Nonetheless, the accomplished outcomes were not as satisfied as those achieved after changes in both the linker and the cap group of SAHA (Marek et al., 2013), which turned to be the best approach to design SAHA-based isoform selective class IIa HDAC inhibitor.

***Class IIa HDACi intended for the zinc binding domain:*** Tasquinimod was proposed to be a potential HDACi that is used for treatment of patients with castration-resistant prostate cancer (CRPC) (Dalrymple et al., 2012; Olsson et al., 2010). Unlike many HDACis, Tasquinimod was not rationally identified or screened particularly for HDACs. Although, it showed the ability to bind to the catalytic zinc ion in the active site of HDAC4, thus inactivating the enzyme catalysis. Displacement of the protein-protein N-CoR-SMRT-HDAC3 complex is caused by structural modifications of Tasquinimod (Isaacs et al., 2013). Remarkably, unlike all other SAHA-based molecules, previous observation emphasizes the steric hindrance property of the inhibitor. Nonetheless, by considering its specificity towards the structural zinc atom (which is one of the unique features of class IIa), SAHA can be replaced by Tasquinimod structural backbone as a pharmacophore model for the designing of isoform selective inhibitors. Isaacs and colleagues suggested Tasquinimod for the treatment of patients with angiogenesis disorders, where its cancer-fighting efficiency is still evaluated and is undergoing clinical trials phase III with  $IC_{50}$  of  $\sim 1 \mu\text{M}$  (Isaacs et al., 2013). Two aroyl-pyrrolyl-hydroxyamides (APHAs) derivative inhibitors, MC1568 and MC1575, were designed specifically to target HDAC4 and HDAC6 (Fleming et al., 2014). Originally, APHAs are class I HDACs inhibitors. However, modifications to the linker group of APHAs resulted in increased selectivity towards class IIa HDACs. MC1568 was found to inhibit class IIa HDACs with  $IC_{50}$  of  $0.22 \mu\text{M}$ , while MC1575 inhibits HDAC4 with  $IC_{50}$  of  $5 \mu\text{M}$  (Duong et al., 2008; Mai et al., 2005; Nebbioso et al., 2010; Venza et al., 2013). MC1568 and MC1575 showed significantly lowered cytotoxic effect in comparison to classical class I HDAC inhibitors (Mai et al., 2005). Although, both compounds showed some

cytotoxicity in ER<sup>+</sup> breast cancer cells and in melanoma cells (Duong et al., 2008; Venza et al., 2013). Interestingly, MC1568 facilitates the HDAC4-MEF2D complex stabilization in developed C2C12 myoblasts, which resulted in impairing myogenesis rather than of promoting it (Nebbio et al., 2009). A structural hybridization between the hydroxamic acids and the benzamides of class I HDAC inhibitors resulted in a new class IIa selective inhibitor, N-((6-(hydroxyamino)-6-oxohexyl)oxy)-3,5-dimethylbenzamide namely LMK235. The hydrophobic dimethyl of the cap group in LMK235 fits better in the active site of class IIa than class I and led to increase in the selectivity towards HDAC4 and HDAC5. In comparison to class I HDACs inhibitors, LMK235 shows less cytotoxicity and better outcomes for the treatment of many cancer cells due to the structural hybridization between different inhibitor classes. Moreover, LMK235 increased the cancer cell sensitivity to cisplatin, more than SAHA does (Marek et al., 2013). In 2013, Lobera et al. designed TMP269 and TMP195, two class IIa HDACis in which the classical hydroxamic acid group was replaced by a trifluoromethyloxadiazolyl group (TFMO) (Lobera et al., 2013) that mimics the trifluoromethylketone (TFMK) developed by Bottomley et al. in 2008 (Bottomley et al., 2008). Unlike the instability of the TFMK series of inhibitors, TFMO inhibitors show improved stability due to the presence of the ring group in the TFMO structure (Ontoria et al., 2009). TMP269 was found to inhibit class IIa HDACs with IC<sub>50</sub> of 0.023~0.157 μM, while TMP195 was found to inhibit class IIa HDACs with IC<sub>50</sub> of 0.009~0.111 μM (Lobera et al., 2013). Furthermore, unlike the hydroxamates, the TFMO group interacts with the catalytic zinc ion by a weak electrostatic interaction where it acts as a non-chelating metal binding domain. As a result, the TFMO inhibitors target a smaller number of enzymes compared to the hydroxamic acid inhibitors. Intriguingly, SAHA showed the ability to regulate about 4,500 genes expression in the human PBMC, whereas TMP195 modulates about 76 genes. This specificity is indirectly supported through gene expression profile studies in phytohemagglutinin (PHA)-activated human PBMC (Lobera et al., 2013). Besterman and colleagues designed two diphenylmethylene hydroxamic acid inhibitors, N-hydroxy-9H-xanthene-9-carboxamide and N-hydroxy-2,2-diphenylacetamide, that are class IIa HDACs selective inhibitors with IC<sub>50</sub> of 0.05~0.75 μM. The two inhibitors show a close structural symmetry, involving N-hydroxy-9H-xanthene-9-carboxamide that may be counted for the fixation of the diphenyl group of N-

hydroxy-2,2-diphenylacetamide. This structural change led to increase in the potency of the compound towards HDAC7 (Tessier et al., 2009). In 2011, and in the middle of screening of a commercially available library of small molecules, Haus et al. identified a new class IIa HDAC inhibitor. The study reported N-lauroyl-(l)-phenylalanine that inhibits class IIa with IC<sub>50</sub> of 21 μM (Haus et al., 2011). This compound proved cancer fighting potency towards ER<sup>+</sup> breast cancer cells, and showed the ability to modulate the gene expression of several MEF2 (Di Giorgio et al., 2013). Class IIa selectivity was assessed by standard activity measurements in addition to fluorescence assay that utilizes the antagonism properties between the known HDAC inhibitor and a fluorescent substrate (Haus et al., 2011). 2-trifluoroacetylthiophenes is a class II HDAC inhibitor that was developed from ethyl 5-(trifluoroacetyl)thiophene-2-carboxylate with increased specificity towards class IIa and HDAC6 (P. Jones et al., 2008). Originally, this compound was obtained during the screening of a commercially available library of small molecules targeting both the wild-type and the mutant HDAC4 which showed a half-maximal inhibitory concentration of 0.22 μM. The enhanced specificity of this inhibitor can be justified by its multi-domain structure that consists of a trifluoromethyl ketone domain, which strongly induces the chelation of the catalytic zinc ion in the HDACs active site; a thiophene ring in the middle that precisely matches the active site; and an amide domain that binds to the adjacent active residues in the binding pocket (Bottomley et al., 2008). In 2019, Luckhurst and colleagues identified CHDI-390576 as a new class IIa selective HDAC inhibitor, as a result of the structural modification in the cap region of the benzhydryl hydroxamic acids. In their study, CHDI-390576 interacted in a bidentate manner with the catalytic zinc ion in the active site. CHDI-390576 was found to inhibit class IIa with a half-maximal inhibitory concentration of 0.031~0.051 μM (Luckhurst et al., 2019). In 2016, Boskovic et al. developed a series of HDACis and measured their inhibition potency towards zinc-dependent HDACs. The authors reported BRD4354 (Compound 64 in the original study) as one of the most potent compounds that contain hydroxyquinoline as the zinc-triggered electrophile. BRD4354 lacks the zinc binding group and showed preferably inhibition towards HDAC5 and HDAC9 with IC<sub>50</sub> of 0.85 and 1.88 μM, respectively (Boskovic et al., 2016). Despite the absence of the ZBG, BRD4354 goes through zinc-catalyzed decomposition into an orthoquinone

methide that covalently moderates the nucleophilic cysteine residue inside the histone deacetylase enzymes, and eventually inactivating their activities (Boskovic et al., 2016).

***Class IIa HDACi targeting the cytoplasmic-nuclear localizing:*** The earliest effort to stop class IIa HDACs enzymatic activity in the cytoplasm was made by Kong et al. in 2011 through designing several SAHA derivatives and changing the amino-phenyl moiety into a fluorescent dansyl moiety (Kong et al., 2011). Despite the weak catalytic activity of these compounds towards class I HDACs, previous structural modification increased the compounds selectivity for the class IIa. Compound 2 from that study provided the highest efficacy and led to the accumulation of HDAC4 in the cytoplasm of prostate cancer cells. Accumulation of class IIa HDACs in the nucleus seems to be a fascinating approach, since many studies reported that class IIa nuclear accumulation can possibly exhibit oncogenic functions (Clocchiatti et al., 2013; Di Giorgio et al., 2013). However, this strategy may also display few disadvantages. Class IIa HDACs have cytoplasmic catalytic functions as well and might be increased upon their nuclear localization inhibition. In addition, blocking of class I HDACs may show indirect influence on class IIa cytoplasmic accumulation, such as Panobinostat (class I and II inhibitors), that has the ability to restrict HDAC4 in the cytoplasm in non-radiated non-small lung cancer cells. Taking into account these disadvantages, cytoplasmic-nuclear localizing inhibitors show less favorable feature of these enzymes (Geng et al., 2006).

***Class IIa HDACi targeting the N-terminal region:*** As previously discussed, the N-terminal region of class IIa is unique where it consists of poly-glutamine domain and is known for its regulation of the protein-protein interaction. The N-terminal also allows hetero- and homodimerization between class IIa HDAC enzymes except for HDAC7 (Clocchiatti et al., 2011). MEF2 proteins are the most perfect mates for class IIa HDACs (Grégoire et al., 2006; Miska et al., 1999), where various class IIa HDACs biological functions are recognized as a result of the transcriptional suppression of MEF2 (Clocchiatti et al., 2013; Di Giorgio et al., 2013; M. Martin et al., 2007). Designing of an inhibitor that able to interfere with the interaction of class IIa HDACs and MEF2 may sound promising approach to achieve isoform selectivity. However, this strategy can block a particular amino acid sequence of class IIa (e.g., 166-184 amino acid residues of HDAC4) and prevent some necessary protein-protein interactions. For example, this

amino acid sequence is essential for class IIa HDACs interaction with the demethylase JARID1B (Barrett et al., 2007) and the nucleoporin Nup155 (Kehat et al., 2011). Instead, Jayathilaka et al. identified a new inhibitor that can target a particular region in MEF2 (amino acids 66-69 residues) and is able to displace the class IIa HDACs. BML-210 is a weak benzamide derivative class I HDACs inhibitor, that can bind to the hydrophobic moiety of MEF2 by its aminophenyl group (Jayathilaka et al., 2012).

Though, previous mentioned HDACs inhibitors have shown a variety of undesired effects that comes with their inhibition influence against numerous HDACs through numerous classes. Hence, current research has aimed is to identify novel isoform selective HDAC compound to avoid side effects and keep the cancer-fighting action of broad-spectrum HDACs inhibitors.

## **1.6. COMPUTER-AIDED DRUG DESIGN TECHNIQUES**

The latest advances in the recent decade of computer technologies and new computational modeling tools provided a robust boost to the area of computer-aided drug design (CADD). Additionally, X-ray crystallography, nuclear magnetic resonance (NMR), and mass spectrometry-based assay offer abundance of information about properties of molecules such as their molecular structure, electron density distributions, bonds, angles, and many others. The profound availability of three-dimensional (3D) structure of biological molecules like proteins and other molecules was necessary for the development of the computational drug design. In the next section, several computational drug discovery approaches will be briefly discussed such as virtual screening, molecular docking, homology modeling, pharmacophore modeling, molecular dynamics simulations and ligand-protein free binding energy calculation (Figure 1.12).

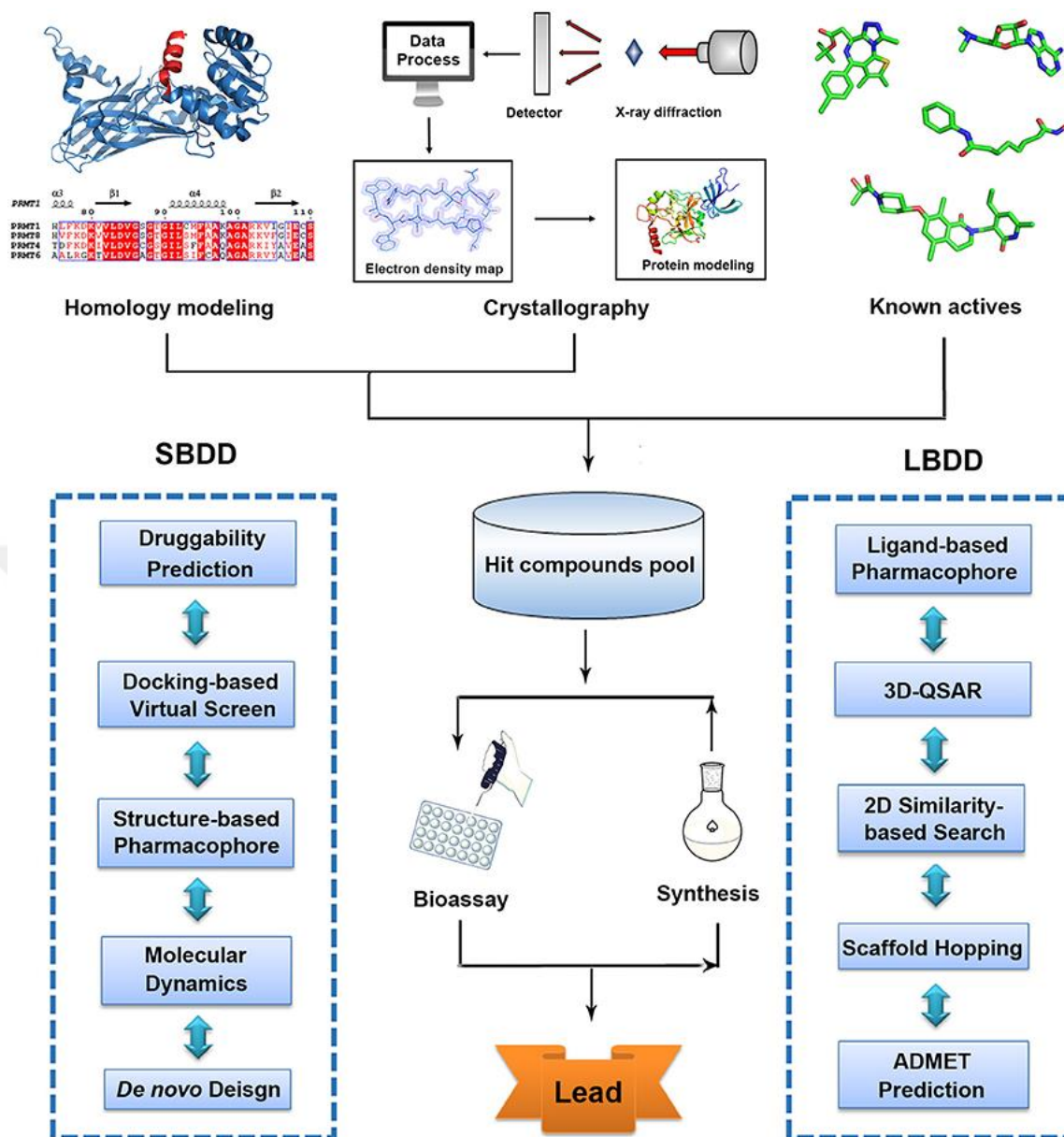


Figure 1.12. Classical workflow of drug design techniques (W. Lu et al., 2018).

### 1.6.1. Virtual Screening

High-throughput screening (HTS) and virtual screening (VS) are widely approaches applied for in silico drug discovery in order to efficiently by screen any enormous number of small molecules against a particular target molecule (e.g., protein) via computational experiments. This approach differs from the theoretical approach, which was mainly established to screen large compound library and choose candidates for in vitro experiments (Miller, 2002; Walters et al., 1998; Waszkowycz et al., 2001). VS techniques

have become more and more popular in the last decade in which large number of compounds will be reduced to be examined by HTS (Kontoyianni, 2017). David E. Clark stated that the term “virtual screening” was probably first used by Dragos Horvath in his research study searching for trypanothione reductase inhibitors in 1997 (Clark, 2008). A number of similarity screening methods can be applied in virtual screening including 3D or two-dimensional (2D) structural inquiries, pharmacophore and quantitative structure-activity relationship (QSAR) models, 2D and 3D fingerprints (Azimi et al., 2019; Gu et al., 2019; Pirhadi & Ghasemi, 2013). There are several successful applications of virtual screening in class IIa HDAC drug design. In 2017, Hsu and colleagues demonstrated six novel non-hydroxamate inhibitors that preferentially target class IIa HDACs (Hsu et al., 2017). Sinha et al. in 2017 found a hydroxamic based class IIa inhibitor for the treatment of ataxia Type-2 using 3D-QSAR and pharmacophore modeling approach (Sinha et al., 2017). Various filtering approaches can be utilized to exclude small molecules with undesired chemical properties. One of the important approaches is to eliminate compounds that contain toxic, reactive, or any other unwanted properties. Drug-likeness is one of the crucial steps in virtual screening that evaluates the safety of oral drugs, such as the well-known Lipinski’s rule of five applications (Lipinski et al., 1997).

### **1.6.2. Molecular Docking**

Structure-based drug design (SBDD) is a common virtual screening approach that is widely used in docking active small molecules to larger targets as proteins, simultaneously with the application of the molecular dynamics simulation (MD) of biological systems as protein-ligand complexes. With the help of molecular docking methods, it is easy and efficient to predict the favored conformation and orientation of a particular compound, and to calculate molecular interactions between the target and the compound such as hydrophobic interactions, hydrogen bonds, van der Waals, and ionic interactions in order to create a stable complex system with the least free energy (Meng et al., 2011). The calculated binding free energy ( $\Delta G_{\text{bind}}$ ) is obtained from a combination between different energy factors involving total internal energy ( $\Delta G_{\text{total}}$ ), dispersion and repulsion ( $\Delta G_{\text{vdw}}$ ), hydrogen bond ( $\Delta G_{\text{hbond}}$ ), desolvation ( $\Delta G_{\text{desolv}}$ ), electrostatic contributions ( $\Delta G_{\text{elec}}$ ), unbound system’s energy ( $\Delta G_{\text{unb}}$ ), and torsional free energy



( $\Delta G_{\text{tor}}$ ) (Murcko, 1995). A decent knowledge about the theoretical context of molecular docking can consequently deliver significant perceptions on elemental interactions between ligand and protein. Molecular docking is based on two main phases: prediction of the compound orientation and conformation within the binding pocket, and approximate calculation of the binding free energy. Molecular docking methods include several important steps from ligands and target preparations to analysis of the outcomes. Generally, each compound is docked individually into a particular target with a computed binding affinity and given a rank consequently. The top and finest ranked conformation are then further assessed in either in silico studies or in vitro. Molecular docking can be completed by two diverse methods, the shape complementarity or simulation. In the shape complementarity method, both the small molecule and the target are recognized, and the matching between them helps identifying the compound's best fitting in the target. This method is very efficient and fast and can be utilized in the HTS of compound databases (Lamb & Jorgensen, 1997; Shoichet et al., 2002). The simulation method is more sophisticated and computationally high-priced. The physical distance of the target and the compound are parted, and the compound tests the conformational space awaiting the favored orientation in the binding pocket of the target. This method involves experimenting rotations, torsional angle rotations and translations (Meng et al., 2011). Upon each individually new created conformation, the total free energy of the complex is being predicted. The foremost benefit of this approach is the straightforward integration of the compound flexibility into the free energy calculation. Though, this method is also more expensive and time-consuming. The simulation method has been made more efficient by the application of grid-based approaches and fast optimization method (Lamb & Jorgensen, 1997). Nowadays, there are plenty of molecular docking tools available commercially or as free including AutoDock, Dock, GOLD, Glide, FlexX, rDock, AutoDock Vina, Fred, LigandFit, and many others. These tools generally use a variety of search algorithms like Monte Carlo, genetic algorithms, molecular dynamics algorithms, and fragment-based algorithms. In general, molecular docking can be accomplished through three different approaches including flexible ligand docking (flexible ligand and a rigid target), rigid body docking (both ligand and protein are rigid), or flexible docking (both ligand and protein are flexible) (Gschwend et al., 1996; Lamb & Jorgensen, 1997). Even though ligand flexibility has been more considered in several available molecular

docking tools, due to the relatively large size of most targets with many degrees of freedom, processing the protein flexibility is still challenging and very limited. To overcome such dilemma, other several tactics have been carried out such as side-chain flexibility, molecular relaxation, and soft docking (Totrov & Abagyan, 2008). Soft docking is considered as the easiest strategy, in which a little ratio of overlap between ligand and protein is permitted and included in the scoring function as a van der Waals interatomic energy (Ferrari et al., 2004; F. Jiang & Kim, 1991). Side-chain flexibility strategy applies rotational isomer (or rotamer) datasets to experiment the conformational space of the binding pocket side chains (Leach, 1994). On the other hand, molecular relaxation strategy performs a dock-and-relax technique through docking rigid ligand into rigid target and later relaxing the side chains and the protein's backbone around the ligand (Davis & Baker, 2009). The latter approach allows some degree of backbone flexibility but at the same time is considerably time-consuming. Other more sophisticated approaches may be needed such as MD simulation to deal with major conformational alterations and structural rearrangements in order to consider different structural conformation and produce a complete protein structure.

### **1.6.3. Homology Modeling**

Homology modeling, also referred as comparative or template-based modeling, is a computational method that is applied to create an unidentified macromolecule structures such as proteins, DNA, or others (target) from a proportionally similar (homologous) known 3D structures (template) that have been experimentally resolved by either X-ray crystallography or NMR techniques (András Fiser, 2004). The theory behind this approach relies on the belief that similar templates with a defined sequence identity and a comparable 3D structure, or variations among them, are directly accounted for the range of changes in the structure. Therefore, the success in generating the structure of a target is guaranteed by the range of sequence similarity or identity (Chothia & Lesk, 1986). It is important to take into consideration that certain protein families, for instance the G protein-coupled receptors (GPCRs), share conserved 3D structure rather than conserved amino acid sequences (Cavasotto & Phatak, 2009). In general, Protein Data Bank (PDB) website offers 3D structures that can be used as templates for the homology modeling,

and by October 2020 it contains about 170,172 experimentally resolved structures (Berman et al., 2002). Although PDB offers a huge number of experimentally resolved structures, there is even a larger number of amino acid sequences for unknown protein structures available on UniProt website, that is still needed to be experimentally identified (Bateman, 2019). Therefore, in spite of its limitations, homology modeling proved to be a promising approach with several applications in SBDD. Homology modeling method has shown its liability to generate structures with site-directed mutation, and even higher quality models in comparison to some experimentally solved proteins (Ohlendorf, 1994; Šali & Blundell, 1993; Vernal et al., 2002).

In homology modeling, there are main consecutive stages that are followed to generate the desired model: (i) identification of amino acid sequence of the target; (ii) selection of a template (that shares a homologous sequence with the target) which has an experimentally resolved structure; (iii) alignment of sequence between the template and the target; (iv) build the model (e.g., target) to match the template structure; (v) refinement of the constructed model; and (vi) validation of the generated homology model. Every one of these previous stages may require a variety of technical operations, and could be reproduced to fully generate a reliable model (Martí-Renom et al., 2000).

#### **1.6.4. Pharmacophore Modeling**

The pharmacophore concept was established to better understand the nature of the interactions between a ligand and its target based on Ehrlich's perspective of functional chemical groups that are accountable for binding (haptophores) and functional chemical groups that are accountable for the toxicity (toxophores). In 1909, Ehrlich P. suggested that the catalytic activity of a drug compound is determined by a particular functional chemical groups (Ehrlich, 1909). In 1961, Schueler defined the earliest innovative description of pharmacophore. Conversely, he postulated the catalytic activity is determined by the abstract features of the drug molecule rather than its functional chemical group (Schueler, 1961). In 1967, Kier presented the earliest computational pharmacophore model of muscarinic receptor inhibitors (KIER, 1967), which was originally inspired by Beckett and colleagues work in 1963 (Beckett et al., 1963). The most recent description of the 3D pharmacophore was based on Schueler's definition by

the International Union of Pure and Applied Chemistry (IUPAC), which states the following: pharmacophore is “an ensemble of steric and electronic features that are necessary to ensure the optimal supramolecular interactions with a specific biological target and to trigger (or block) its biological response” (Wermuth et al., 1998). Guner and Bowen demonstrated a complete revision on the advancements in the concept of pharmacophore (Güner & Bowen, 2014). The main concept of pharmacophore centers on the common features shared by a series of compounds that recognize and bind to related sites of particular targets (e.g., active compounds) (Leach et al., 2010). Consequently, pharmacophore model defines the spatial arrangement, electrical and chemical characteristics that are needed for a ligand to perfectly bind and fit into a biological macromolecule such as protein. A pharmacophore model consists of a group of physicochemical properties that reflect the molecular interactions, where different functional groups may be embodied by the same property (Leach et al., 2010).

Despite the differences in the fundamental algorithms in various pharmacophore modeling software, all of them produce similar pharmacophore features that illustrate hydrogen bond acceptor (HBA) groups, hydrogen bond donor (HBD) groups, aromatic rings, metal–ion interactions, +ve/-ve ionizable/charged groups, and hydrophobic groups. In certain cases, some modifications in the common features are needed to meet the requirements of the program (Steindl et al., 2005). A successful pharmacophore model requires several main steps: (i) pharmacophore model generation based on either the knowledge of the protein-ligand interaction (which is called structure/receptor-based pharmacophore modeling) or by superimposing a series of active compounds with shared bioactivity features (which is known as ligand-based pharmacophore modeling); (ii) dataset designing, in which it contains several active compounds for the pharmacophore model generation; and (iii) assessment and theoretical validation of the generated pharmacophore models (Langer et al., 2006).

### **1.6.5. ADMET Prediction in CADD**

A drug compound undergoes several complicated evaluation steps including bioactivity measurements, cytotoxicity, chemical assessment, metabolic stability, and many other measurements before being described as a safe treatment. Several chemical molecules

are filtered out and excluded from the acceptable normal range of properties that have been acknowledged in drug compounds. The process of excluding those molecules that lack the normal range of bioactivity assisted in the creation of a variety of drug-like compounds libraries. The concept of drug-like has been emphasis the physicochemical properties that the majority of oral drugs share in common. Lipinski's rule of 5 is among the most widely applied standards for evaluating the drug-likeness of compounds with a simple extent of physicochemical properties (Lipinski et al., 2001). Lipinski's rule of 5 has four measurements that ought to be met with the permeability and solubility of oral drugs: (i) molecular weight (MW) is 500 Dalton (Da) or less; (ii) octanol-water partition coefficient (LogP) must be between -5 and 5 (or MLogP  $\leq$  4.15); (iii) the total number of hydrogen bond donors should not exceed 5 hydrogen, which is simply the summation of attached hydrogen to all oxygen and nitrogen; and lastly (iv) no more than 10 hydrogen bond acceptors. There are several aspects that must be taken into account when applying these standards. First of all, these parameters are used for searching for oral drugs, while there are some considerable distinctions between oral and other different drug categories, which means that the rule of 5 is tested for oral administration rather than tests the compounds drug-likeness (Vieth et al., 2004). Secondly, the rule of 5 criteria were developed from commercially available drugs, whereas the screening of chemical compound libraries is intended for finding lead compounds as a start point for drug design. In addition to Lipinski's rule of 5, several other physicochemical properties have been proved to be of significance to the drug discovery including total polar surface area (TPSA) (that should be  $\leq$  140 Å<sup>2</sup>) and total number of rotatable bonds (ought to remain  $\leq$  10) (Veber et al., 2002). For the past decade, pharmacokinetic properties prediction, such as blood-brain barrier permeability and water solubility prediction, have been measured using a variety of virtual screening approaches (Y. Wang et al., 2015).

#### **1.6.6. Molecular Dynamics (MD) Simulation**

Conventional molecular dynamics simulation assists SBDD to entirely describe the structural flexibility of the studied systems, and is also vital to evaluate the system's kinetic and thermodynamic properties (De Vivo et al., 2016). MD methods benefit efficiently in motion and interaction prediction of macromolecules such as protein by

applying Newton's equations of motion to each individual atom (Adcock & McCammon, 2006). Throughout MD simulation, Newton's second law of motion is incorporated in order to create sequential frames of the system through application of a certain force field to approximate the functioning forces on each atom. As a result, a phase space trajectory is allocated over time for velocities and positions for each element in the studied system (G. M. Wang et al., 2002). In molecular dynamics simulation, the molecular component is primarily ascertained by nucleus attitude and electron motions are averaged out. To put it in another way, molecular mechanics (MM) energy expression can describe the system according to the following formula (Equation 1.1):

$$\begin{aligned}
 V(r) = & \sum_{bonds} k_b(b - b_0)^2 + \sum_{angles} k_\theta(\theta - \theta_0)^2 \\
 & + \sum_{torsions} k_\phi [\cos(n\phi + \delta) + 1] \\
 & + \sum_{nonbond\ pairs} \left[ \frac{q_i q_j}{r_{ij}} + \frac{A_{ij}}{r_{ij}^{12}} - \frac{C_{ij}}{r_{ij}^6} \right]
 \end{aligned} \tag{1.1}$$

As shown in Figure 1.13, the first three summations represent bonds which are denoted as  $b$  (1-2 interactions), angles (1-3 interactions), and torsions (1-4 interactions) (Figure 1.13). Torsions may also include what so-called improper torsions, as the four atoms surrounding the angle are not all linked by covalent bonds. The final summation including atoms  $i$  and  $j$  (except for 1-2 and 1-3 interactions) usually applies different parameters for 1-4 interactions in comparison to those applied for atoms parted by more than three covalent bonds. MM energy defines electrostatic forces that apply partial charges  $q_i$  on each atom that functions according to Coulomb's law. The main aspect of protein energy models can be generated by the simple potential energy function as in Equation 1.1 at an atomic level of detail. Equation 1.1 was also developed to give deep insight into a significantly wide range of properties. The summation of potential energy function as shown in Equation 1.1 and all other components like  $k_b$   $b_0$   $k_\theta$   $\theta_0$  represent the force field (Ponder & Case, 2003).

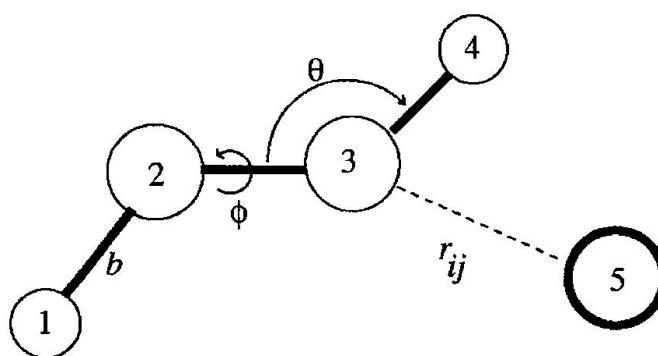


**Figure 1.13.** Graphical representation of the force field interactions. Dark lines display covalent bonds. Dash line represents nonbonded interaction (Ponder & Case, 2003).

Generally, any force field must be able to transfer rigorously from one atom to another related atom in a way that the computed geometry of a new one is obtained from the first atom. Therefore, a large molecule is basically the summation of known properties of all small atoms combined. Basically, different force field is grounded on comparable operational formulas, however, each force field has its own advantages and disadvantages according to the parameter set (Arinaminpathy et al., 2002). Molecular dynamics simulation should be preferentially operated on supercomputers or cluster of computers because of the excessive complexity and large quantity of computations necessary to create a space trajectory. Several MD software packages are available, and the majority are consistent with the Message Passing Interface (MPI), which is a transmission system that is able to communicate between computers and accelerate the performance of multi-simulation jobs. Each MD software package applies its own force field settings that defines bonded and nonbonded interactions, energy utilization, force restraints and water type. In addition, due to the infeasibility of performing MD simulations for a countless number of atoms, periodic boundary conditions (PBC) are utilized by the simulation algorithm to create a large system, which necessitates a unit cell with a particular figure to act as a 3D crystal structure. Throughout the MD simulations, the properties of only a single unit cell are logged and then replicated to other frames (Yeh & Hummer, 2004).

Even though various improvements have been made for molecular docking studies over the last decades, docking scores still experience many limitations and need to be enhanced. Molecular dynamics simulation proved to be vital post-production method to refine and evaluate docked complexes and also precisely compute binding free energy. In addition, MD simulations can deliver deep perceptions on induced-fit conformational

variations, protein-ligand interactions affinity level, and the effect of water molecules of the ligand interaction with the binding pocket (de Beer et al., 2010). MD simulations can provide many eminent measurements from the generated trajectory such as heat variability, pressure consistency and internal energy (Frenkel et al., 1997). The protein-ligand binding free energy is described as one of the most significant measurements in the field of drug discovery, which is expressed as the association constant  $K_a$  and can be obtained by Equation 1.2 as follows:

$$K_a = \frac{[PL]_{eq}}{[P]_{eq}[L]_{eq}} \quad (1.2)$$

Where  $L$  represents the ligand concentration,  $P$  refers to the protein concentration, and  $PL$  signifies the protein-ligand complex concentration. On the other hand, the dissociation constant  $K_d$ , which is a reciprocal of  $K_a$ , is applied in the pharmaceutical studies more than  $K_a$ . Moreover, the dissociation constant  $K_d$  is replaced by the inhibitory constant  $K_i$  when referred to enzyme inhibitor analyses. The relationship between the thermodynamic measurements obtained from the MD simulations and the analytical equilibrium constants can be computed through the classical free-energy change at constant temperature and pressure as given in Equation 1.3.

$$\Delta G^0 = -kT \ln(K_a C^0) = kT \ln\left(\frac{K_d}{C^0}\right) \quad (1.3)$$

Where  $k$  signifies the Boltzmann constant and  $C^0$  refers to the standard concentration constant in 1 molar (M). Upon the equilibrium status of the system, Equation 1.3 can be made simpler as in Equation 1.4, where  $K_{eq}$  represents the equilibrium constant of the reaction.

$$\Delta G^0 = -kT \ln(K_{eq}) \quad (1.4)$$

### 1.6.7. MM-PBSA Binding Free Energy

Binding free energy of a complex system (ligand-protein) can be obtained and computed through a variety of MD-based methods including the free energy perturbation (FEP) and



thermodynamic integration (TI). On the other hand, these previous methods are excessively high-priced, and their appliance is limited to very few relatively related compounds due to the extensive conformational preparation process (Beveridge & DiCapua, 1989). The molecular mechanics Poisson-Boltzmann surface area (MM-PBSA) and linear interactions energy (LIE) are two approaches which are commonly used to overpass the previous drawbacks (Hansson et al., 1998; Swanson et al., 2004). MM-PBSA approach utilizes both the continuum solvent methods and the molecular mechanics to approximate the binding free energy of a ligand (Kollman et al., 2000; Massova & Kollman, 2000). Following MD simulations performed in explicit solvent, multiple frames are obtained and treated in order to exclude ions and water molecules, and consequently the binding free energy can be calculated using Equation 1.5 as follows:

$$\Delta G_{bind} = G_{complex} - [G_{protein} - G_{ligand}] \quad (1.5)$$

Where  $G$  is the average free energy of the systems and can be obtained based on the following formulas (Equation 1.6):

$$G = E_{MM} - G_{solvation} - TS$$

$$E_{MM} = E_{internal} + E_{electrostatic} + E_{vdw} \quad (1.6)$$

$$G_{solvation} = G_{polar} - G_{nonpolar}$$

Where  $E_{MM}$  symbolizes the average molecular mechanic energy in the gas phase,  $G_{solvation}$  describes the solvation free energy designed by the Poisson-Boltzmann electrostatic component  $G_{polar}$  and a solvent accessible surface area model  $G_{nonpolar}$  (Sitkoff et al., 1994). The entropic  $TS$  involvement can be neglected in case that the approximate binding energies of a group of molecules are needed. However, in case the molecules are considerably dissimilar, entropy contribution is necessary as the absolute binding energies are required.

MM-PBSA approach has been used by several studies to calculate the binding energy, although, in some cases this method was not able to produce comparable energies for certain systems. For an instance, von Langen et al. reported five human glucocorticoid receptor selective inhibitors using molecular docking approach, MD simulations, and

MM-PBSA binding energy calculation for all complexes. The ligands pose ranking after docking study did not agree with the calculated MM-PBSA binding energies (Von Langen et al., 2005). High affinity complexes were perfectly detected using this method in the study, but low affinity complexes could not be identified using the same method. Conversely, similar method was applied by Wang and colleagues to calculate the binding affinity of HIV-1 reverse transcriptase inhibitors, and correctly predicted the absolute and relative binding free energies, and the experimental value was in agreement with the top-ranked molecule (J. Wang et al., 2001).

## **AIM AND OBJECTIVES**

The aim of the current studies is to discover isoform selective class IIa HDACs inhibitors that may serve as epigenetic targeting drugs for the treatment of cancer. The discovered compounds may serve as a starting point for lead design and may require more experimental optimization. Therefore, the following distinct objects were followed:

- A. Comparative homology modeling of class IIa HDAC5 and HDAC9 and the design of dual-acting inhibitors.
- B. Isoform selective class IIa HDACs inhibitors by structure-based drug design.
- C. Isoform selective class IIa HDAC5 and HDAC9 inhibitors by ligand-based pharmacophore modeling approach.

## 2. MATERIALS AND METHODS

In order to fulfill the objectives of the current studies, different computer-aided drug design approaches were employed. In this chapter, those methods will be discussed and categorized into three main sections including comparative homology modeling of class IIa HDAC5 and HDAC9 and the design of dual-acting inhibitor; isoform selective class IIa HDACs inhibitors by structure-based drug design; and isoform selective class IIa HDAC5 and HDAC9 inhibitors by ligand-based pharmacophore modeling approach.

### 2.1. HOMOLOGY MODELING OF CLASS IIA HDAC5 AND HDAC9, AND THE DESIGN OF DUAL ACTING INHIBITOR

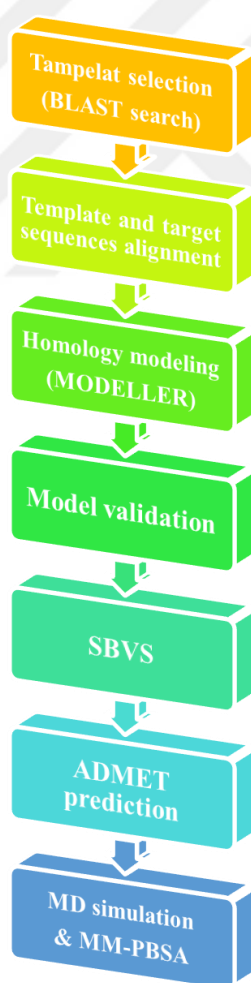


**Figure 2.1.** Flowchart of the homology modeling and the search for HDACs 5 and 9 dual-acting inhibitors.

### **2.1.1. Selection of The Template**

The whole amino acid sequences of HDAC5 and HDAC9 were obtained from the UniProt website as “FASTA” files (<https://www.uniprot.org/>) (Bateman, 2019) with UniProt accession number “Q9UQL6” for HDAC5 and “Q9UKV0” for HDAC9. Selection of the best matching template is achieved by searching for structures or amino acid sequences of homologous proteins with sophisticated tools such as the web-based Basic Local Alignment Search Tool (BLAST) which can be accessed from the following link (<https://blast.ncbi.nlm.nih.gov/Blast.cgi>) (Altschul et al., 1990; Johnson et al., 2008). Herein, BLAST search was carried out with 100 E-value cutoff and 100 as the maximum number of hits. The best matching template retrieved from the BLAST search was the X-ray crystallography structure of human catalytic domain of HDAC4 (PDB accession no. 2VQM) (Bottomley et al., 2008) and exhibited the highest amino acid sequence identity of 75% for HDAC5 and 72% for HDAC9.

### **2.1.2. Template and Target Sequences Alignment**

In homology modeling, created structures are believed to reveal similar structural properties when there is at least 30% amino acid sequence identity shared between the template and the target. Furthermore, 50% amino acid sequence identity or more is expected to generate a model with reliable and excellent quality (Andras Fiser, 2010). The sequence alignment was carried out using “Align Sequences” protocol in BIOVIA Discovery Studio 4.5 (DS 4.5) (Dassault Systèmes, 2016). Human HDAC4 (2VQM) was downloaded as the catalytic domain of HDAC4 and the protein had one chain.

### **2.1.3. Homology Model Building**

There are various homology modeling tools available for creating 3D structures from a scratch. These tools use different approaches such as comparative homology modeling, segment matching, rigid-body assembly, and homology modeling by satisfaction of spatial restraints. Modeling by satisfaction of spatial restraints is a commonly used approach which uses sequence alignments and interprets the extracted information to

distance and chirality constraints that can be considered as the initial basis for the calculations of the distance geometry. For this purpose, MODELLER tool is widely utilized to generate and optimize the model depending on conjugate gradients and molecular dynamics (Šali & Blundell, 1993; Webb & Sali, 2016). The concept of homology modeling relies on the fact that the process begins with the calculation of the contact points and the secondary structure prediction for the aligned and unaligned points to search for the conformational space according to the distance clustering and geometry to surpass alignment miscalculations (Kolinski et al., 2001). Herein, “Homology Modeling” tool from BIOVIA DS 4.5 was applied to generate 20 models. Before proceeding with the creation of the homology models, HDAC4 (2VQM) was prepared to add any missing loops using the “Prepare Protein” protocol in BIOVIA DS 4.5. The ligand, water molecules, and salt ions were removed. After the sequence alignments between the template and the targets were performed from the previous section, the sequence of the catalytic domains of HDAC5 and HDAC9 were extracted so they match the sequence of HDAC4 catalytic domain, while other sequences were excluded from the homology modeling procedure. “Build Homology Models” was then applied with high levels of optimization following the default protocol of DS 4.5. Later, the new 20 generated models were verified with MODELLER tool, and the best created models were chosen based on their discrete optimized potential energy (DOPE) scores. “Clean Geometry” toolkit in BIOVIA DS 4.5 is applied to minimize the model’s energy applying CHARMM (Chemistry at Harvard Macromolecular Mechanics) force field to relax and overcome any steric hindrances of amino acid side chains. Lastly, “Prepare Protein” protocol was utilized to prepare the built models and properly protonate the protein at physiological pH 7.4.

#### **2.1.4. Homology Model Validation**

One of the most important steps after building the desired model is to evaluate and validate its 3D structure relying on previous acquired information from experimentally resolved structures or successful homology models such as chemical bonds, angle, length of bonds, hydrophilic and hydrophobic residues, and many others (Pevsner, 2009). Herein, to assess the model quality, ProSA-web, the online version of Protein Structure

Analysis tools (ProSA) (<https://prosa.services.came.sbg.ac.at/prosa.php>), was used to detect any potential errors within a given structure based on previous structural errors gathered from available experimentally resolved structures or homology models (Sippl, 1993; Wiederstein & Sippl, 2007). In addition, the stereochemical quality of the homology models were further validated using ERRAT website (<https://servicesn.mbi.ucla.edu/ERRAT/>) (Colovos & Yeates, 1993) and Ramachandran plot analysis form PROCHECK website (<https://servicesn.mbi.ucla.edu/PROCHECK/>) (Laskowski et al., 1996).

### **2.1.5. Molecular Docking with Known Inhibitors**

Further homology model validation was performed to evaluate the quality of enzyme's active site by docking a series of HDACs known inhibitors using the well-known molecular docking software AutoDock 4.2 (G. M. Morris et al., 2009). Molecular docking studies are commonly used to calculate and predict the best possibly conformational pose of a compound and its interaction with a certain target. The created homology models were prepared by the "Prepare Protein" protocol in BIOVIA DS 4.5 and protonated at pH, 7.4. Datasets of HDAC5 and HDAC9 known inhibitors with calculated biological activity ( $K_i$  or  $IC_{50}$ ) were retrieved from the ChEMBL website (<https://www.ebi.ac.uk/chembl/>) (Gaulton et al., 2017) and prepared using the "Prepare Ligands" toolkit at pH 7.4 according to BIOVIA protocol. Both HDAC5 and HDAC9 generated models were prepared using AutoDockTools (G. M. Morris et al., 2009) and saved as PDBQT (Protein Data Bank, Partial Charge (Q) & Atom Type (T)) files after assigning Gasteiger partial charges to all atoms of the proteins. Also, grid parameter file GPF and docking parameter file DPF were subsequently generated for the docking study. The size of the grid boxes was set for each protein and centered close to the catalytic zinc ion in the active site ( $x=19.199$ ,  $y=-10.083$ ,  $z=-1.089$ ), and made sure to cover the whole active sites as 50, 50, 50 Å dimensions with 0.375 spacing point. Lamarckian genetic algorithm was used to generate the docking input files and the docking energy evaluations were set to 25,000,000 for each ligand conformational search. Independently, for each compound in the known inhibitors' series, 20 runs were performed.

### 2.1.6. Dataset Preparation

In order to start searching for dual inhibiting leads, about 100,000 small molecules were retrieved from ChEMBL website. ChEMBL website offers a large chemical libraries and drug-like datasets that are ready-to-use in different virtual screening approaches. The studied dataset was prepared by the “Prepare Ligands” protocol in DS 4.5 and protonated at pH 7.4.

### 2.1.7. Molecular Docking and Structure-Based Virtual Screening

As previously discussed, virtual screening is a computational approach that is increasingly used in the field of drug discovery. In the present study, AutoDock Vina (Trott & Olson, 2009) was utilized to decrease the large number of the dataset and rule out compounds with least binding affinity towards HDAC5 and HDAC9. AutoDock Vina was proved to offer a quick and precise docking result in which an empirical and knowledge-based scoring functions are both combined in one tool (Trott & Olson, 2009). The energy grid box size and the XYZ coordinates were set as follows: 20, 20, 20 Å and 19.199, -10.083, -1.089, respectively. Out of the 100,000 compounds, 1,027 showed the highest binding affinity towards HDAC5, and 1,925 compounds towards HDAC9 with binding energy scores equal to or less than -8.5 kcal/mol. Subsequently, top 9 compounds were selected from each set for further molecular docking study. The 18 compounds were cross-docked against the catalytic sites of both HDAC5 and HDAC9 using AutoDock 4.2 applying the same docking parameters used in the previous section.

### 2.1.8. Physicochemical Properties Description

It is substantially prominent to predict the physicochemical properties of chemical compounds to exclude those with undesired toxic effect. These parameters include absorption, distribution, metabolism, excretion, and toxicity (ADMET). In addition, the most commonly used Lipinski’s rule of 5 is essential to assess the compound’s drug-likeness, which molecular weight  $\leq 500$  Da,  $\text{LogP} \leq 5$ , total number of hydrogen-bond donors  $\leq 5$ , and total number of hydrogen-bond acceptors  $\leq 10$ , where one violation is

tolerated (Lipinski et al., 2001). These criteria were predicted using admetSAR 2.0 web server (<http://lmmd.ecust.edu.cn/admetSar2/>) (H. Yang et al., 2019) and SwissADME website (<http://www.swissadme.ch/>) (Daina et al., 2017).

#### **2.1.9. Pan-Assay Interference Compounds (PAINS) Filtration**

Pan-assay interference compounds (PAINS) were first described in 2010 by Baell and Holloway as specific substructural features that at certain cases might result in false positive effect in the virtual screening study (Baell & Holloway, 2010). These substructural groups can interact to several proteins in unspecific manner instead of affecting specific protein. Such compounds should be excluded by PAINS remover tools to avoid false positive effects. “PAINS Remover” web server was used in the present study (<https://www.cbligand.org/PAINS/>) (Baell & Holloway, 2010).

#### **2.1.10. Molecular Dynamics MD Simulation**

MD simulation studies were performed by the Nanoscale Molecular Dynamics software 2.11 (NAMD) (Phillips et al., 2020) for better understanding of proteins stability. Herein, four systems were subjected to MD simulations: free form of HDAC5 “M0014,” HDAC5-Rac26 complex, free form of HDAC9 and, HDAC9-TMP269 complex. Furthermore, the top-ranked hits retrieved from the structure-based virtual screening were also subjected to MD simulations. CHARMM-GUI web service (<http://www.charmm-gui.org/>) (J. Lee et al., 2016) was utilized to generate input files for MD simulations to be run under NAMD environment applying CHARMM36m force field. All small molecules used in this study were parameterized using CHARMM General Force Field server (CGenFF), where charges assigning and atom typing for small molecules are entirely automated (Vanommeslaeghe et al., 2010). For all systems, water box was assembled using TIP3 module and salt atoms (Na<sup>+</sup> and Cl<sup>-</sup>) were added to neutralize the system at a 0.15 M concentration. At the beginning of MD simulations, systems energy was minimized applying the steepest descent method for 20,000 steps. Then, each system was equilibrated and heated to 310 K for 10 ns in NVT ensemble (constant number of atoms, volume, and temperature). Finally, all systems were simulated for 100 ns



production in NPT ensemble (constant number of atoms, pressure, and temperature). MD simulations were performed with 2 fs time step, where the coordinates were recorded every 5000 steps to the MD trajectory file.

### 2.1.11. Binding Free Energy (MM-PBSA) Calculations

Binding free energy demonstrates the thermodynamic feature of the interaction between a ligand and a protein, which precisely indicates the binding affinity of the complex upon equilibrium state (Kollman et al., 2000). For all studied systems, the binding free energy was computed applying the MM-PBSA method using CaFE tools developed by Liu and Hou in 2016 (H. Liu & Hou, 2016). As formerly discussed in the previous chapter, MM-PBSA approach integrates continuum solvent models and molecular mechanics (Kollman et al., 2000). CaFE tool is the first method that allows binding free energy using DCD and PSF files that were generated by NAMD and CHARMM programs, respectively. Theoretically, binding energy calculation of a protein-ligand is divided into two phases: solvation in the aqueous phase and association in the gas phase (H. Liu & Hou, 2016).

The energetic elements that were calculated in the MM-PBSA method include the gas-phase energy variations among the ligand, the protein, and the ligand-protein complex. The free energy of the polar solvation was computed according to the PB formula APBS (N. A. Baker et al., 2001). Then, the nonpolar solvation free energy and the variations in the solvent-accessible surface area (SASA) were calculated. The following equation was applied to calculate the binding free energy (Equation 2.1):

$$\Delta G_{bind} = \Delta H - T\Delta S = [\Delta E_{gas} + \Delta G_{sol}^{polar} + \Delta G_{sol}^{nonpolar} - T\Delta S] \quad (2.1)$$

From each studied system, a total of 200 snapshots were extracted from the last 10 ns of each MD trajectory file using the Visual Molecular Dynamics (VMD) software (Humphrey et al., 1996). PSF file, DCD file, and all related parameter files including the ligand and the protein, were all collected in one directory. CaFE tool can be accessed and downloaded from the following link: ([https://github.com/huiliu/code/cafe\\_plugin](https://github.com/huiliu/code/cafe_plugin)). A value of 1.0 Å was set for the reciprocal of grid spacing, a value of 80.0 was set for the external dielectric constant, and a value of 4 Å was set for the internal dielectric constant.

## 2.2. STRUCTURE-BASED DRUG DESIGNING OF ISOFORM SELECTIVE CLASS IIA HDACS INHIBITORS

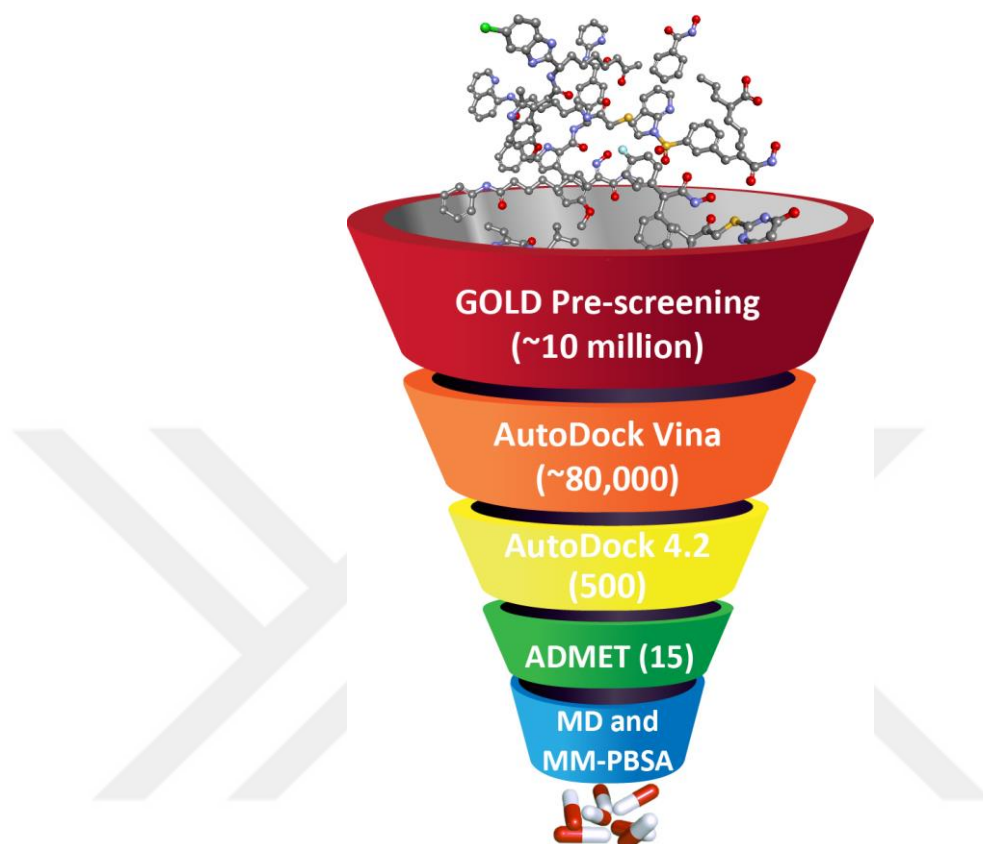


Figure 2.2. Structure-based virtual screening workflow.

### 2.2.1. Class IIa Proteins Preparation

The 3D structures of HDAC5 (M0014) and HDAC9 (M0020) were generated by homology model method as discussed in the previous section. In addition, the next X-ray crystallography structures of human HDAC were downloaded from the PDB website (<http://www.rcsb.org/>) (Berman et al., 2002): (i) HDAC4 (2VQM) “the structure of human HDAC4 catalytic domain bound to a hydroxamic acid inhibitor, resolution: 1.80 Å” (Bottomley et al., 2008); (ii) HDAC7 (3C10) “the crystal structure of catalytic domain of human HDAC7 in complex with Trichostatin A (TSA), resolution: 2.00 Å” (Schuetz et al., 2008). Native ligands (the co-X-ray crystallography resolved ligands), water molecules, and salt ions were next removed from each structure using BIOVIA DS 4.5 (Dassault Systèmes, 2016). Native ligands were next re-docked again into their relevant enzymes to evaluate the protocol used in the molecular docking studies where their

RMSD values were found to be less than 2.0 Å in reference to the native poses. Using the “Prepare Protein” protocol in BIOVIA DS 4.5, hydrogen atoms were added to the proteins at physiological pH 7.4, and missing loops were added if necessary. Moreover, a dataset of class IIa HDAC known inhibitors were retrieved from the ChEMBL web site and were docked into their respective proteins to define the selection criteria of novel compounds using GOLD software (G. Jones et al., 1997). Further details are given the molecular docking subsection.

### **2.2.2. Class IIa HDACs Structural and Sequence Alignment**

The 3D structures of class IIa HDACs were aligned using BIOVIA DS 4.5 program (Figure 2.3). Also, their respective amino acid sequences were aligned (Figure 2.4). Table 2.1 shows class IIa HDACs conserved active amino acids in the enzyme’s catalytic site (Table 2.1). Figure 2.5 displays the phylogenetic tree of class IIa enzymes that was generated utilizing BLAST web-based tool, which is available on the National Center for Biotechnology Information (NCBI) website (Figure 2.3)

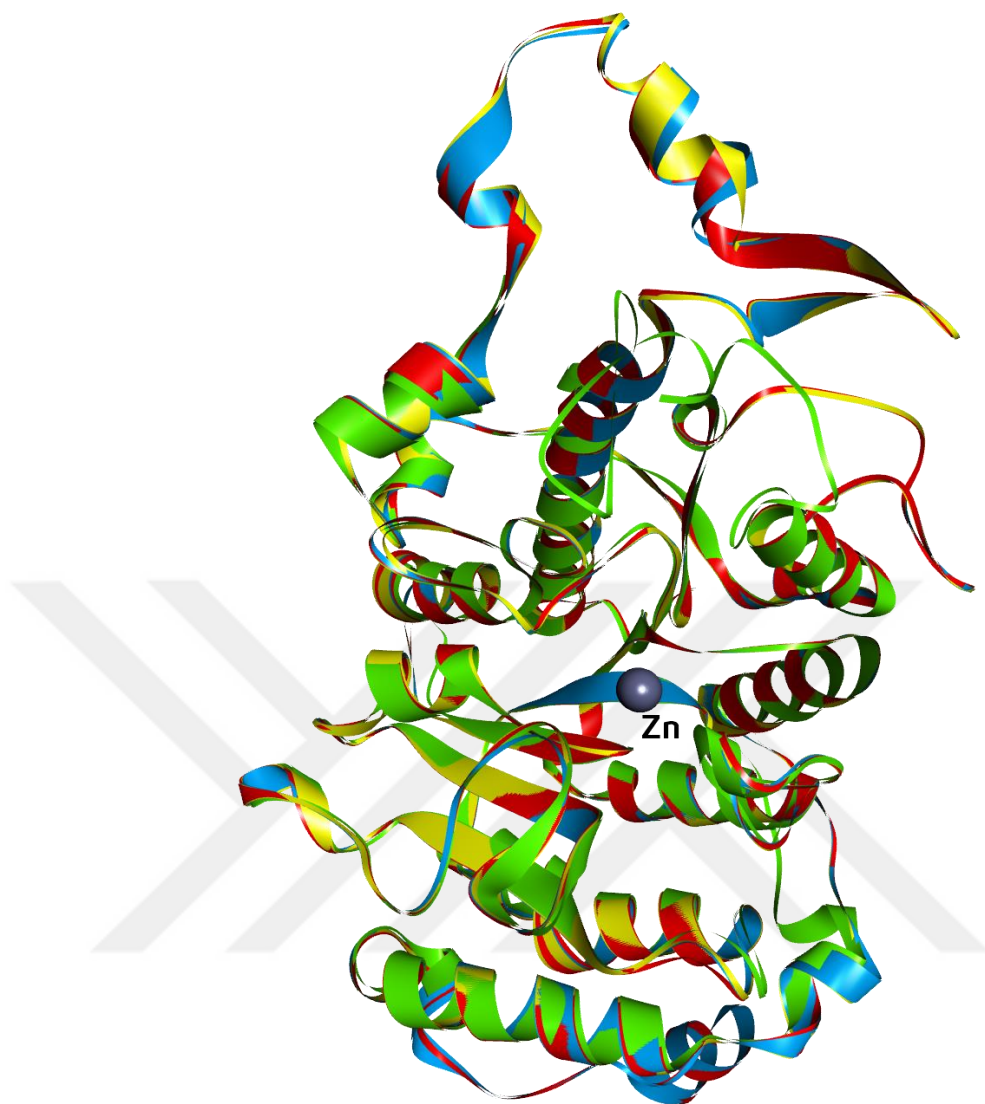


**Figure 2.3.** Structural alignment of class IIa HDAC enzymes. HDAC4: red, HDAC5: blue, HDAC7: green, HDAC9: yellow.

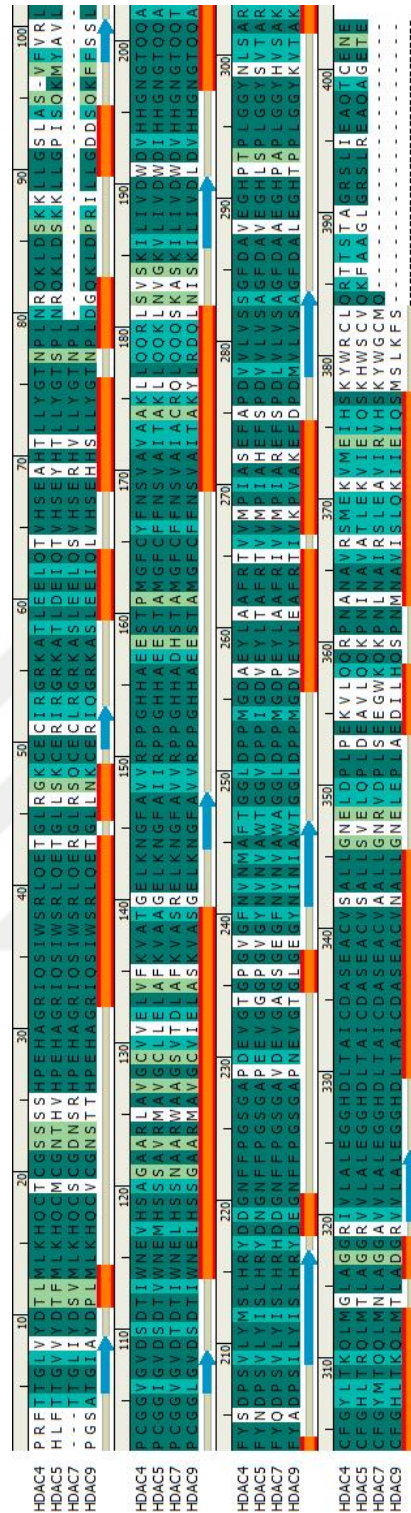


**Figure 2.4.** Amino acid sequence alignment of class IIa HDAC proteins. Amino acids identity is shown as dark green, similarity is represented as light green and no similarity is shown in white. Overall sequence identity among this class of HDACs is 55.6% and sequences similarity is 71.5%. [→  $\beta$ -sheet, ■  $\alpha$ -helix].

**Table 2.1.** Conserved amino acid residues in class IIa HDACs' catalytic domains.

HDAC4	HDAC5	HDAC7	HDAC9
His158	His159	His166	His159
His159	His160	His167	His160
Gly167	Gly168	Gly175	Gly168
Phe168	Phe169	Phe176	Phe169
Asp196	Asp197	Asp204	Asp197
His198	His199	His206	His199
Asp290	Asp291	Asp235	Asp291
Gly330	Gly331	Gly297	Gly331

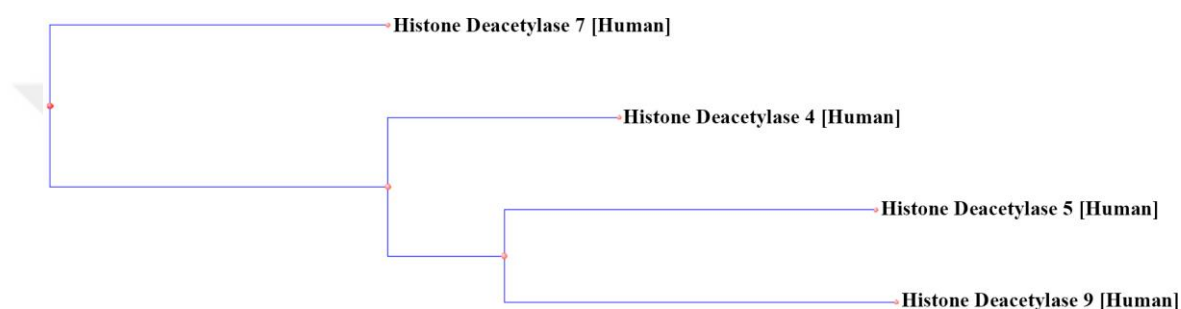


**Figure 2.5.** Phylogenetic tree of human class IIa HDAC enzymes. The tree shows that HDAC5 and HDAC9 are related as they share one node with their ancestral origin HDAC4, whereas they share two nodes and with HDAC7.

### 2.2.3. Dataset Preparation

A total of 10,154,992 compounds were downloaded from several databases including ZINC15 database (<https://zinc15.docking.org/>) (Sterling & Irwin, 2015), ChEMBL (<https://www.ebi.ac.uk/chembl/>) (Gaulton et al., 2017), and the National Cancer Institute (NCI) (<https://cactus.nci.nih.gov/index.html>) (Milne et al., 1994). The ZINC15 dataset contains 3D tranches drug-like compounds which have a variety of molecular weight ranging from 200 to 500 MW, and octanol-water partition coefficient (LogP) ranging from -1 to 5. The advantage of this ZINC15 compounds library is that the compounds are ready for screening where they are previously protonated, all hydrogen atoms are included, and their 3D structures were optimized (Sterling & Irwin, 2015). The dataset was retrieved in SDF file format. The dataset was organized in tranches for easy management, each tranche had 100,000 compounds.

## 2.2.4. Structure-Based Virtual Screening Approach

Structure-based virtual screening is a computational method that has proved its liability and efficiency in searching for novel lead, lead-like, and drug-like compounds and is most widely applied in in-silico lab (Walters et al., 1998). In silico SBVS screening has boosted up the modern drug-like discovery and optimization, that saves money and time (Rester, 2008). In the current study, the SBVS method has been divided into three stages, where each stage used different molecular docking software in order to reduce the large number of the dataset and to filter out compounds with the least binding affinity, by taking advantage of each software's capabilities. The first SBVS stage used GOLD docking software, the second SBVS used QuickVina 2.0, and the third SBVS used AutoDock 4.2.

### 2.2.4.1. First stage of SBVS

GOLD docking software was used for its high speed and efficiency in HTS of large compounds dataset (G. Jones et al., 1997). GOLD software provides four different scoring functions: ChemPLP, ChemScore, GoldScore, and ASP (the Astex Statistical Potential), where ChemPLP is an empirical fitness function which is considered as the most accurate scoring function for general docking studies and it is optimized for pose prediction (G. Jones et al., 1997). It is applied for sampling the steric harmonizing between the ligand and its respective target, and also examining the angle and distance dependency in terms of hydrogen bonding (G. Jones et al., 1995). The ChemPLP scoring function that is applied to rank various binding poses obeys the following formulas (Equation 2.2):

$$\begin{aligned} fitness_{PLP} = & (W_{PLP} \cdot f_{PLP} + W_{lig-clash} \cdot f_{lig-clash} + W_{lig-tors} \cdot f_{lig-tors} \\ & + f_{chem-cov} + W_{prot} \cdot f_{chem-prot} + W_{cons} \cdot f_{cons}) \end{aligned} \quad (2.2)$$

$$fitness_{ChemPLP} = fitness_{PLP} - (f_{chem-hb} + f_{chem-cho} + f_{chem-met})$$

Where  $f_{lig-clash}$  is the internal score of the ligand which contains the heavy-atom clash potential;  $f_{lig-tors}$  is the torsional potential;  $W_{PLP}$  is the weight of PLP contributions;

$W_{lig-clash}$  is the weight of ligand clashes potential;  $W_{lig-tors}$  is the weight of ligand torsion potential;  $W_{prot}$  is the weight of ChemScore protein potential; and  $W_{cons}$  is the weight of constraint contributions.

Herein, the docking experiments were performed using the ChemPLP scoring function, and the 10,154,992 compounds were screened against HDAC4, HDAC5, HDAC7 and HDAC9. HDACs proteins were uploaded to GOLD software as PDB files and all hydrogen atoms were added to protonate the proteins, and each protein was saved as mol2 file. The binding site for each protein was centered close to the catalytic zinc atom and the box size was set to 10 Å, where the XYZ coordinates were set as follows; HDAC7 = 7.8, 49.864, -18.724; HDACs 4, 5 and 9 = 19.199, -10.083, -1.089. The dataset (ligands) was uploaded as SDF file format. GOLD performed 10 genetic algorithms runs for each ligand. HDACs class IIa known inhibitors were retrieved from the ChEMBL website (<https://www.ebi.ac.uk/chembl/>) (Gaulton et al., 2017) and were docked against their respective HDAC. Preliminary investigations of the docking results showed that the highest fit values were as follows: HDAC4 = 88, HDAC5 = 70, HDAC7 = 95, and HDAC9 = 80. The criteria of selection after the GOLD docking study was made according to the previous fit values. Thus, the large dataset was reduced to a total of 89,632 molecules (HDAC4 = 26,709; HDAC5 = 24,173; HDAC7 = 18,702, and HDAC9 = 20,048).

#### **2.2.4.2. Second stage of SBVS**

In the second stage of the virtual screening, QuickVina 2.0 was used due to its comparable fast screening. QuickVina 2.0 is an AutoDock Vina-based tool that was designed for faster and more accurate results, where it automatically determines the grid maps and ranks the outputs for simple interpretation. (Alhossary et al., 2015). QuickVina 2.0 can be downloaded from the following link: (<https://qvina.github.io/>). The scoring function of QuickVina 2.0 relies on the same scoring function of classical AutoDock Vina where the method combines between the knowledge-based and empirical approach and obeys the following formula (Equation 2.3):



$$\Delta G_{binding} = \Delta G_{gauss} + \Delta G_{repulsion} + \Delta G_{hbond} + \Delta G_{hydrophobic} + \Delta G_{tors} \quad (2.3)$$

Due to the highly conserved amino acid sequence and the great resemblance among class IIa HDAC enzymes (Bottomley et al., 2008; Schuetz et al., 2008), the 89,632 ligands that displayed highest affinity towards their corresponding targets at the first SBVS stage, were additionally docked into each protein of the class (e.g., cross-docking). All SDF files were first converted to PDB files using the following command by OpenBabel program (O'Boyle et al., 2011):

```
$ openbabel.obabel *.sdf -opdb -m
```

Then, all PDB files were converted to PDBQT files to be readable by QuickVina 2.0 using the following script file:

```
#!/bin/bash
#
# use the 'prepare_ligand4.py' python script to create pdbqt files
VSTROOT=`pwd`

cd $VSTROOT/VirtualScreening/Ligands
for f in `ls *pdb`; do
  echo $f
  ~/MGLTools-1.5.6/bin/python2.5 ../../prepare_ligand4.py -l $f -o "$f"qt -d
  ../etc/ligand_dict.py -F -B amide
done

# The `examine_ligand_dict.py` scripts reads the `ligand_dict.py`
# and writes a summary describing the set of ligands to stdout.

cd $VSTROOT/VirtualScreening/etc
cp ../etc/examine_ligand_dict.py .
~/MGLTools-1.5.6/bin/python2.5 examine_ligand_dict.py > summary.txt
```

All individual members of class IIa HDACs were prepared and correctly protonated and saved as PDBQT using AutoDockTools (G. M. Morris et al., 2009). The configuration files for each protein were prepared and the exhaustiveness was set to 8, while the energy grid box size and the coordinates were specified as shown in Table 2.2.

**Table 2.2.** Coordinate parameters and grid box size used for QuickVina 2.0.

	<b>HDAC4</b>	<b>HDAC5</b>	<b>HDAC7</b>	<b>HDAC9</b>
<b>Centre</b>				
X	19.199	19.199	7.8	19.199
Y	-10.083	-10.083	49.864	-10.083
Z	1.089	1.089	-18.724	1.089
<b>Dimension (Å)</b>				
X	22.5	22.5	20	22.5
Y	22.5	22.5	20	22.5
Z	22.5	22.5	20	22.5

Lastly, to screen this large number of compounds (89,632) against each individual member of class IIa HDACs, a specific script code was used for this purpose, that assisted in running QuickVina 2.0 in one step for each protein. The script source code was given as follows:

```
vinapath={QuickVina 2.0 Path}

workingdir={WORKING DIRECTORY}

cd $workingdir
mkdir docking_results

outputdirectory=$workingdir/docking_results

for f in $workingdir/Ligands/*.pdbqt
do
b=`basename $f .pdbqt`
echo Processing ligand $b
${vinapath} --config vina_conf.txt --cpu 3 --ligand $f --out ${outputdirectory}/${b}_out.pdbqt --
log ${outputdirectory}/${b}_log.txt
done
```

For each ligand, the output was given as a text file, which then all outputs were combined and converted into a single Excel file for simple analysis using the following bash file:

```
#!/bin/bash
for f in *.txt; do
  b=`basename $f .txt`
  echo ${b} >> Vina_result_${b}.txt
  grep "0.000" ${b}.txt | awk '{print $2}' >> Vina_result_${b}.txt
  paste -s Vina_result_${b}.txt >> Vina_result_ALL.xls
done
```

Upon results analyses, the ligands were filtered according to their binding affinity, and, in order to end up with the highest binding affinity for the third stage of SBVS, all compounds with a binding energy ( $\Delta G$ ) of -10 kcal/mol or less were selected for the third SBVS stage, thus a total of 6,325 compounds fulfilled this condition.

### 2.2.4.3. Third stage of SBVS

The final virtual screening was conducted using AutoDock 4.2 (G. M. Morris et al., 2009) in order to identify the highest binding affinity among the tested dataset and assess the selectivity among them towards each class IIa isoform. Therefore, based on the binding affinity, the top 500 compounds retrieved from previous stage were cross-docked against each individual member of class IIa HDACs. At first, grid map files and GPF file were prepared for one of the 500 compounds using AutoDockTools4 and AutoGrid4 with the docking parameters given in Table 2.3.

**Table 2.3.** Coordinate parameters and grid box size used for AutoDock 4.2.

	<b>HDAC4</b>	<b>HDAC5</b>	<b>HDAC7</b>	<b>HDAC9</b>
Centre				
X	19.199	19.199	7.8	19.199
Y	-10.083	-10.083	49.864	-10.083
Z	1.089	1.089	-18.724	1.089
Dimension (Å)				
X	55	55	50	55
Y	55	55	50	55
Z	55	55	50	55

Then, with the help of the next source codes, grid map files, GPF and DPF for all the compounds were sorted and separated into folders according to the ligands names in few simple steps. The first bash file created a separate folder for each of the 500 compounds

and copied all necessary docking parameter files into the newly created folder, including the grid map files, ligand PDBQT file, protein PDBQT file, GPF, and DPF files.

```
#!/bin/bash
#
# Create the ``Dockings`` directory::

VSTROOT=`pwd`

mkdir -p $VSTROOT/VirtualScreening/Dockings
cd $VSTROOT/VirtualScreening/Dockings

# Create a subdirectory named ``<ligand>_protein`` and populate it
# with the docking input files: a) the ``pdbqt`` from the ``Ligands``
# directory will be copied directly; b) the maps will be lined to
# the ``Receptor`` directory; and, c) the ``dpf`` file will be created
# using ``prepare_dpf.py``

for f in `ls ../Ligands/*.pdbqt`; do
    name=`basename $f .pdbqt`
    echo $name
    mkdir "$name"_{RECEPTOR NAME}
    cd "$name"_{RECEPTOR NAME}
    cp ../"$f" .
    ln -s ../../Receptor/{RECEPTOR NAME}.pdbqt .
    ln -s ../../Receptor/{RECEPTOR NAME}*map* .
    ~/MGLTools-1.5.6/bin/python2.5 /{DIRECTORY PATH}/prepare_dpf4.py -l `basename $f` -r
    {RECEPTOR NAME}.pdbqt \
    -p ga_num_evals=25000000 \
    -p ga_pop_size=150 \
    -p ga_run=20 \
    -p rmstol=2.0
    cd ..
done
```

The second bash file started the docking process of the 500 compounds one-by-one and generated the output as DLG file.

```

#!/bin/bash
#
# Create a file with a list of the dockings to run::

VSTROOT=`pwd`

mkdir -p $VSTROOT/Results/dlg

cd $VSTROOT/VirtualScreening/Docking

for d in `ls` ; do
  echo $d
  cd $d
  autodock4 -p "$d".dpf -l $d.dlg
  cp "$d".dlg $VSTROOT/Results/dlg/
  cd ../
done

```

In the present study, the search for the ligand conformation in AutoDock 4.2 was calculated by the Lamarckian genetic algorithm, and twenty independent runs were allowed for each ligand using 25,000,000 energy evaluation.

Herein, the selection criteria of the isoform-selective compounds were directed by Bieliauskas and Pflum (Bieliauskas & Pflum, 2008). The authors demonstrated a thorough insight into the HDAC inhibitors selectivity. For example, compound 24 in their study displayed 15-fold specificity towards HDAC4 over HDAC6, and thus they considered compound 24 as HDAC4 selective inhibitor (Bieliauskas & Pflum, 2008). Their work guided the selection process in our study, which was performed by calculating the ratio of the inhibitory constant ( $K_i$ ) of one compound obtained from one individual member of class IIa HDACs, to the  $K_i$  of the same compound obtained from the other isoforms. For example, the selectivity index of inhibitor “A” for HDAC4 over HDAC5 can be calculated as follows (Equation 2.4):

$$\text{Selectivity of "A" for HDAC4} = \frac{K_i \text{ of other HDACs isoform}}{K_i \text{ of HDAC4}} \quad (2.4)$$

Based on the calculated binding energy and the predicted  $K_i$  value that was obtained from the AutoDock 4.2, a total of 15 compounds showed a wide range of selectivity for their respective proteins (HDAC4: 5, HDAC5: 3, HDAC7: 6, HDAC9: 1).

### **2.2.5. ADMET Profile Description**

ADMET descriptors including absorption, distribution, metabolism, elimination, and toxicity properties are significant in the computational drug discovery and design. There are several computational tools that combine in vivo and in vitro prediction of ADMET profile. In addition, ADMET profile has been successfully predicted in silico over the last decade (Cheng et al., 2013). In the current study, all 15 compounds were saved and uploaded as SMILES files, where the ADMET properties and drug-likeness were predicted using admetSAR 2.0 web server (<http://lmmd.ecust.edu.cn/admetsar2>) (H. Yang et al., 2019) and SwissADME website (<http://www.swissadme.ch/>) (Daina et al., 2017). These properties include: Lipinski's rule of 5 that calculates the molecular weight (MW), octanol-water partition coefficients (LogP), total number of hydrogen bond acceptors, and hydrogen bond donors (Lipinski et al., 2001); topological polar surface area (TPSA); Caco-2 cell permeability; and the water solubility.

### **2.2.6. Pan-Assay Interference Compounds (PAINS) Filter**

In addition, pan-assay interference compounds (PAINS) filter was applied for all the 15 compounds using the PAINS Remover website (<https://www.cbiligand.org/PAINS/>) (Baell & Holloway, 2010). PAINS are identified as special structural properties that can lead to false positive effects at certain cases during the virtual screening and can nonspecifically interact to random targets rather than a particular target (Baell & Holloway, 2010). Consequently, it is important to eliminate compounds with PAINS features to avoid false positive outcomes.

### **2.2.7. Molecular Dynamics (MD) Simulation**

Molecular dynamics (MD) simulation has proved its importance in examining the structural stability of the proteins and in extracting important details about the major conformational modifications in the protein-ligand binding. MD simulation is a computational simulation approach that allows the investigation of the physical movement and orientation of all atoms in the system, and thus, explores the dynamics

and structures in detail. Detailed information about the concept of MD simulation is given under the “2.1.10” section. In the present study, seven isoform-selective complexes were subjected to MD simulation using NAMD package (Phillips et al., 2020), including HDAC4-CHEMBL2177655, HDAC4-CHEMBL3126309, HDAC5-ZINC000033260361, HDAC5-CHEMBL2426361, HDAC7-CHEMBL1968496, HDAC7-ZINC000009640741, and HDAC9-CHEMBL1761559. The web server of CHARMM-GUI (<http://www.charmm-gui.org/>) (J. Lee et al., 2016) was used to generate all the necessary input files for the MD simulation study. The web server of the CHARMM General Force Field (CGenFF) server (<https://cgenff.umaryland.edu/>) was utilized for the parameterization of all the seven ligands, in which the charges assignment and atoms typing were carried out (Vanommeslaeghe et al., 2010). The seven systems were water solvated applying the transferable intermolecular potential with 3 points model (TIP3) and NaCl salt ions were added to neutralize the systems at 0.15 M concentrations. The first step of the MD simulation consisted of energy minimization for 20,000 steps by means of steepest descent method. The second step included restrained equilibration run for 10 ns at 310 K in constant number of atoms, volume, and temperature ensemble (NVT). Finally, all seven systems were subjected to unrestrained 100 ns run in constant number of atoms, pressure, and temperature ensemble (NPT) with 2 fs of collection period, while the system’s coordinates were recorded into the trajectory files every 5,000 steps. The MD simulation trajectory files were analyzed using VMD software (Humphrey et al., 1996) and the analyses included the root mean square deviation (RMSD), root mean square fluctuation (RMSF), radius of gyration (Rg), potential energy, and number of hydrogen bonds.

### **2.2.8. Binding Free Energy Calculations**

The Molecular Mechanics-Poisson-Boltzmann Surface Area (MM-PBSA) (Massova & Kollman, 2000) is widely used approach for the prediction of the binding free energy, which provides more accurate calculations than the majority of molecular docking scoring functions and requires less computational processing than classic alchemical free energy approaches (E. Wang et al., 2019). Herein, this method was used to calculate the

binding free energy for all the seven systems after MD simulations. The binding free energy of any given complex (protein-ligand) can be expressed as given in Equation 1.5.

Where  $G_{com}$  describes the total free energy of the complex.  $G_{pro}$  and  $G_{lig}$  refers to their free energies in their unbound conditions. In general, the free energy can be expressed as shown in Equation 1.6.  $E_{MM}$  denotes the average potential energy of the molecular mechanics in a vacuum.  $G_{sol}$  refers to the free energy of solvation. Therefore, the average potential energy of the molecular mechanics in vacuum can be calculated following the same formula (Equation 1.6). The solvation free energy is a combination of electrostatic  $G_{polar}$  and nonpolar  $G_{nonpolar}$  energies and can be expressed as in Equation 1.6.  $G_{polar}$  can be obtained from the Poisson-Boltzmann (PB) equation, whereas  $G_{nonpolar}$  can be obtained from the solvent-accessible surface area (SASA) as follows (Equation 2.5):

$$G_{nonpolar} = \gamma SASA + b \quad (2.5)$$

Where  $\gamma$  denotes the coefficient of solvent surface tension with 0.0072 kcal/mol/Å, and  $b$  represents its fitting parameter that is 0 kcal/mol.

In this study, CaFE tools (H. Liu & Hou, 2016) was used to calculate the binding free energy for all studied complexes. The last 10 ns was extracted from all trajectory files after performing the MD simulations, in which each DCD file contains 200 snapshots generated by VMD software (Humphrey et al., 1996). All necessary files including DCD, PSF and toppar files were prepared to be used by CaFE tools. The configuration file was created and the reciprocal size of the grid spacing was defined as 1.0 Å, while the internal and external dielectric constants were defined as 4.0 Å and 80.0 Å, respectively.

### **2.3. LIGAND-BASED PHARMACOPHORE MODELING FOR DESIGNING OF ISOFORM SELECTIVE HDAC5 AND HDAC9 INHIBITORS**

Chemically, only certain portion of the drug is included in the interactions with proper target and is responsible for the biological activity. This portion is called “pharmacophore” (S. Y. Yang, 2010). Pharmacophore defines the chemical features of a drug that are vital for its biological effect (Wermuth et al., 1998).



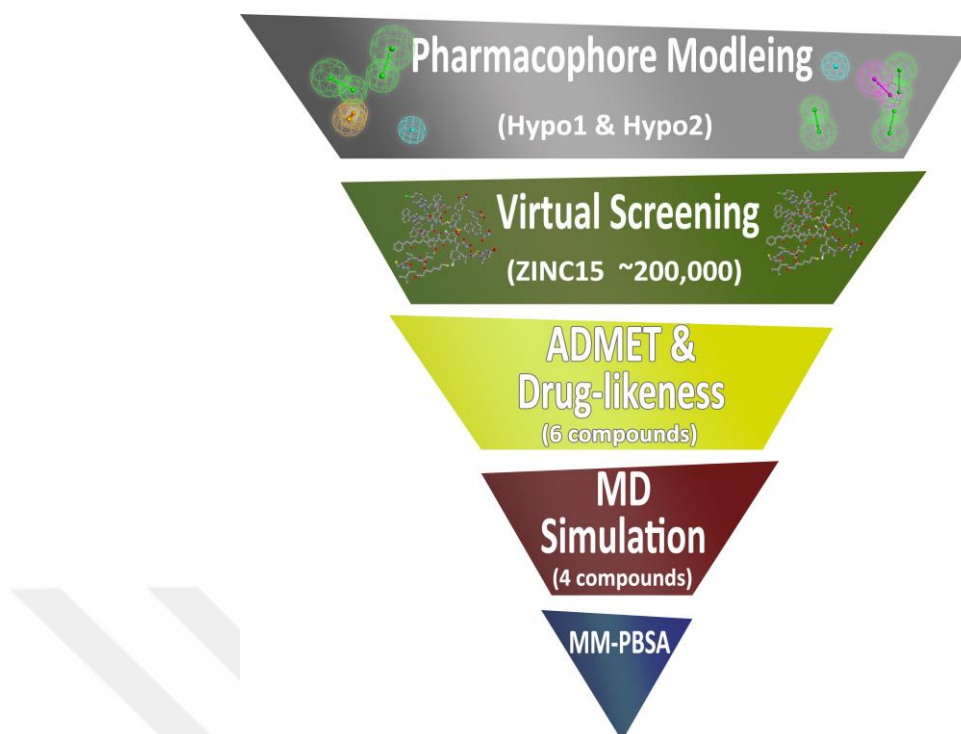


**Figure 2.6.** Pharmacophore modeling and virtual screening workflow.

### 2.3.1. Training Set Compounds Selection

In order to create pharmacophore models, a total of 21 HDAC5 and 21 HDAC9 known inhibitors were selected for the training sets, which contain a variety of experimental half maximal inhibitory concentration ( $IC_{50}$ ) varying between 1 and 11,700 nM and with a diverse structural component, were retrieved from the ChEMBL website (<https://www.ebi.ac.uk/chembl/>) (Gaulton et al., 2017) and from several literatures (Alan Kozikowski, Jay H. Kalin, Kyle V. Butler, Joel Bergman, 2016; Angibaud et al., 2010; Auzzas et al., 2010; Bergman et al., 2012; Boskovic et al., 2016; Botta et al., 2011; Cai et al., 2010; Y. Chen et al., 2016; De Vreese & D'hooghe, 2017; Giannini, Marzi, Pezzi, et al., 2009; Giannini, Marzi, Marzo, et al., 2009; Hutt et al., 2010; Kalin & Bergman, 2013; Kao et al., 2003; H. Y. Lee et al., 2017; Marek et al., 2013; Olson et al., 2013; Paris et al., 2008; Pescatore et al., 2008; Raepfel et al., 2009; Sekizawa et al., 2014; Stephen Joseph Shuttleworth, 2014; F. F. Wagner et al., 2013; T. Wang et al., 2013; Yao et al., 2015; Ziwei YUN, 2012). These known inhibitors included: T009, Trichostatin, Cudc-101, LMK235, R306465, Dacinostat, Vorinostat, Tubastatin A, Chimera 4, Marbostat, ST2987, Entinostat, ST3049, Tubacin, Largazole, Azumamide E, Mocetinostat, HPB,

redFK228, ST3710, Nexturastat A, BDBM119696, IYS-15, IYS-1, TMP269, IYS-14, BRD4354, BDBM218159, Fimepinostat, BDBM119709, Scriptaid, BDBM191641, BDBM124205, ST2741, and BDBM191640 (Figures 2.7 and 2.8). In addition, these known inhibitors involve a various structural components and are well studied against class IIa HDAC enzymes; thus, they were used to design the training data sets in order to create the pharmacophore models.

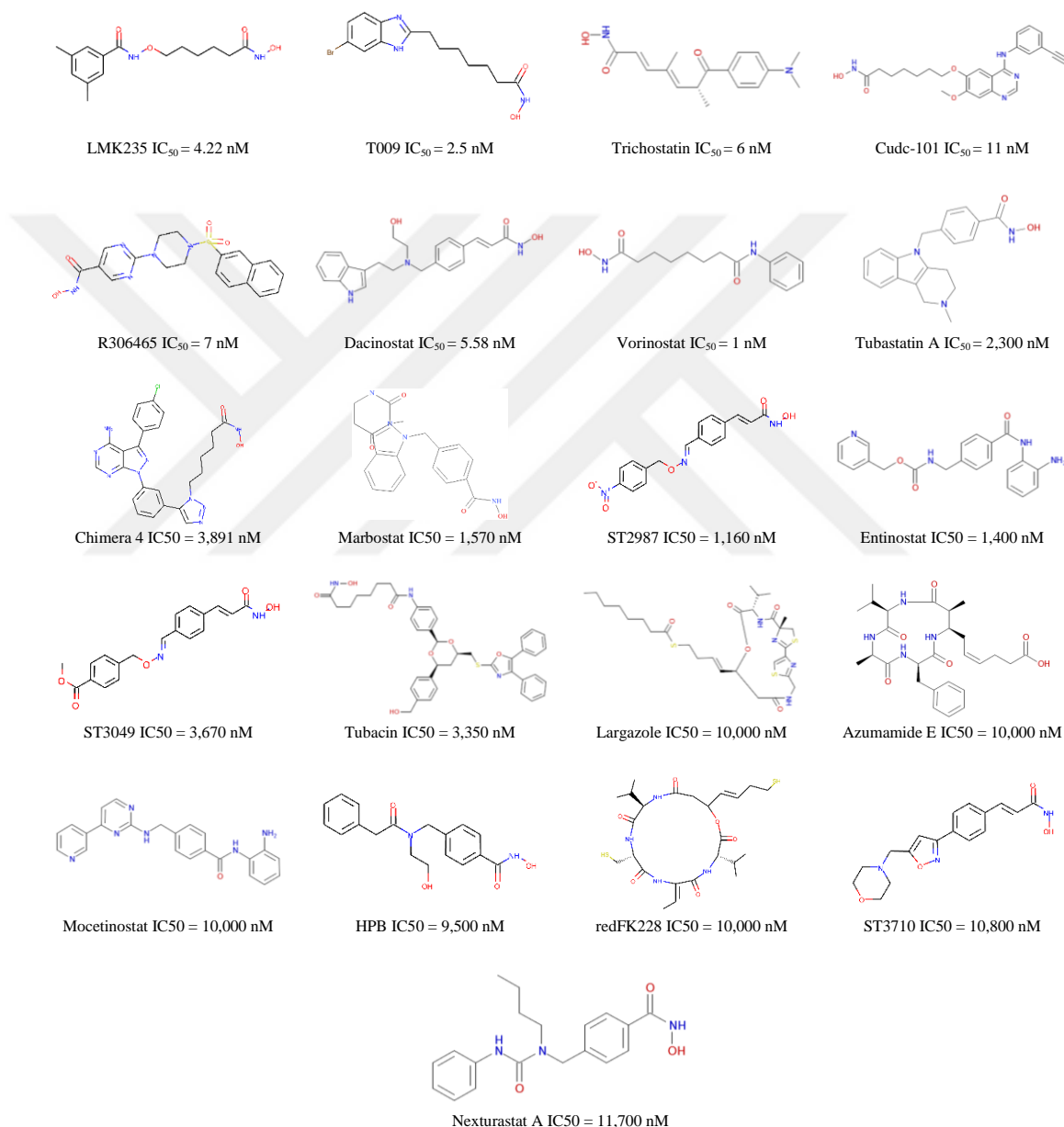


**Figure 2.7.** 2D structures of HDAC5 known inhibitors collected for the training set along with their  $IC_{50}$  values in nM.

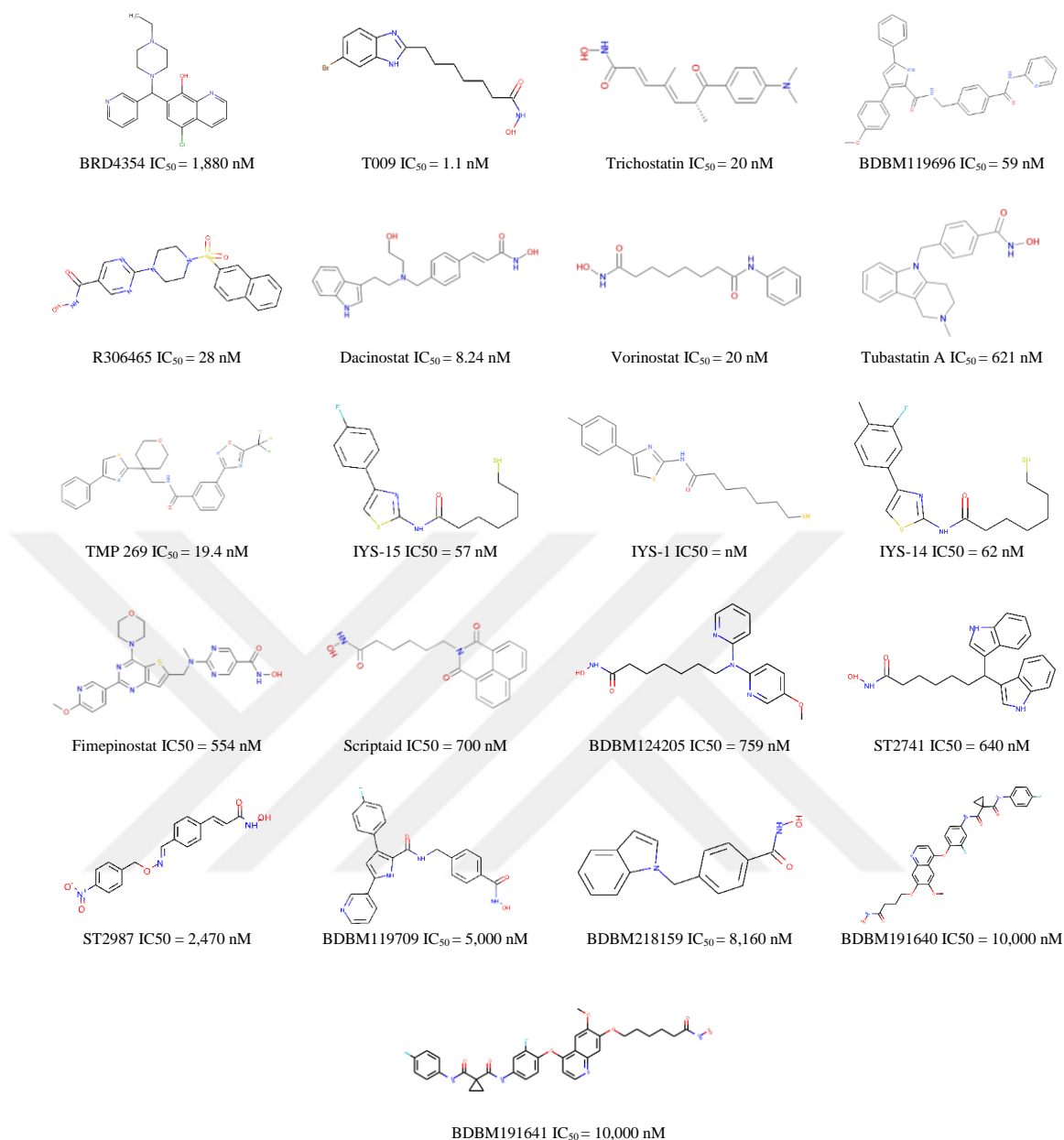


**Figure 2.8.** 2D structures of HDAC9 known inhibitors collected for the training set along with their IC<sub>50</sub> values in nM.

### 2.3.2. Pharmacophore Hypothesis Generation

To generate the pharmacophore hypotheses in the current study, the Catalyst package in BIOVIA DS 4.5 (Dassault Systèmes, 2016) was utilized by following the “Common Feature Pharmacophore Generation” protocol. The Catalyst package relies on the HipHop method, which recognizes the common structural features based on the alignment of a group of active molecules rather than their biological activity (Barnum et al., 1996). The

algorithm of the HipHop module creates a qualitative hypothesis that allows the differentiation of active from inactive compounds and the pharmacophore hypotheses are ranked according to the fitting of the training set compounds (Barnum et al., 1996). Matching a compound with the pharmacophore configuration is only achievable if the compound holds structural properties that can be aligned in a specific tolerance from the hypothesized positions (Clement & Mehl, 2000). LMK235 and BRD4354 are two class IIa HDAC inhibitors that preferentially target HDAC5 and HDAC9 rather than the rest of HDACs, respectively, with some selectivity. Therefore, LMK235 was defined as a reference compound in the training set which was used for the HDAC5-pharmacophore hypothesis generation, while BRD4354 was defined as a reference compound in the training set which was used for the HDAC9-pharmacophore hypothesis generation. The “Principal” parameter was set to 2 for LMK235 and BRD4354, whereas the “Principal” value was set to 1 for the rest of the compounds in the training sets. In addition, the “MaxOmitFeat” value was set to 0 for the reference compounds and 2 for the remaining molecules (Luo et al., 2016). The pharmacophore conformational generation was performed in “BEST” module at energy threshold of 20 kcal/mol. The maximum number of conformations was set to 225 for each compound. To guarantee the generation of the pharmacophore features with a close proximity, the minimum interfeature distance was set to 1. In addition, the minimum feature point was set to 1, with at least 1 minimum feature and maximum 10 features. All other parameters were left at default values.

### **2.3.3. Pharmacophore Hypotheses Validation**

Pharmacophore model/hypothesis validation is an essential step in which it confirms the quality of the generated model by its ability of recognizing active from inactive compounds towards specific target. The quality of the pharmacophore model depends on its reliability to distinguish active compounds (different from those in the training set) from a set contains both inactive and active compounds (namely decoy set) (Vuorinen et al., 2014). In order to validate the generated pharmacophore models, another two different datasets of known inhibitors respectively to HDAC5 and HDAC9, each set contains 21 compounds, were collected from ChEMBL database (<https://www.ebi.ac.uk/chembl/>) (Gaulton et al., 2017) and from several literatures

including Cudc-101, Romidepsin, Tubacin, Largazole, PBHA, BRD-2577, ST5732, BRD73594, BRD9757, HPT-6-carboxylic acid, NCH-31, IYS-10, BDBM124206, BDBM124207, BDBM119703, rac-15, HPB, BDBM119704, and BDBM124203 (Bürli et al., 2013; Cai et al., 2010; Y. Chen et al., 2016; De Vreese & D’hooghe, 2017; Di Pompo et al., 2015; Fass et al., 2011; Giannini, Marzi, Marzo, et al., 2009; Giannini, Marzi, Pezzi, et al., 2009; Kalin & Bergman, 2013; Kemp et al., 2011; H. Y. Lee et al., 2018; Li et al., 2013; Muthyala et al., 2015; Olson et al., 2013; Sekizawa et al., 2014; Stephen Joseph Shuttleworth, 2014; F. F. Wagner et al., 2013, 2016; Z. Yang et al., 2016; Yao et al., 2015; Ziwei YUN, 2012) (Figures 2.9 and 2.10). These known inhibitors have an experimental IC<sub>50</sub> values ranging from 0.05 to 35 µM and were used as active compounds in the test datasets. To obtain inactive compounds from the test set in the current work, DecoyFinder software (Cereto-Massagué et al., 2012) was used. Each set of the HDACs 5 and 9 known inhibitors were uploaded to the DecoyFinder software, and for each compound in the set, 10 inactive compounds were generated. So totally, the decoy set of HDAC5 contained 231 compounds (21 active + 210 inactive), as well as another 231 compounds in the decoy set of HDAC9. Consequently, both of the decoy sets were used to evaluate the quality of the generated pharmacophore hypotheses via testing each pharmacophore model against the decoy set and use the output information to calculate the goodness of hit (GH) through applying the following formulas (Kurogi & Guner, 2001) (Equation 2.6):

$$\begin{aligned}
 Y\% &= \frac{H_a}{H_t} \times 100\% \\
 A\% &= \frac{H_a}{A} \times 100\% \\
 E &= \frac{H_a \times D}{H_t \times A} \\
 GH &= \frac{H_a(3A + H_t)}{4H_t \times A} \times \left(1 - \frac{H_t - H_a}{A - D}\right)
 \end{aligned}
 \tag{2.6}$$

Where “Y%” denotes the ratio of active compounds identified by the pharmacophore model from the decoy set; “H<sub>a</sub>” represent the total number of the active compounds shown in the hit list; “H<sub>t</sub>” defines the total number of the hits within the decoy set; “A%” denotes the ratio of active compounds within the hits list; “A” expresses the sum of the

active compounds in the decoy set; “*E*” is the enrichment factor, “*D*” is the sum of the compounds presents in the decoy set; and “*GH*” is the goodness of hit that defines the reliability of the generated pharmacophore models, and according to Kurogi & Guner study, “*GH*” is expected to obtain a score ranging between 0.6 and 1.0 for a reliable pharmacophore model (Guner et al., 2004; Kurogi & Guner, 2001).

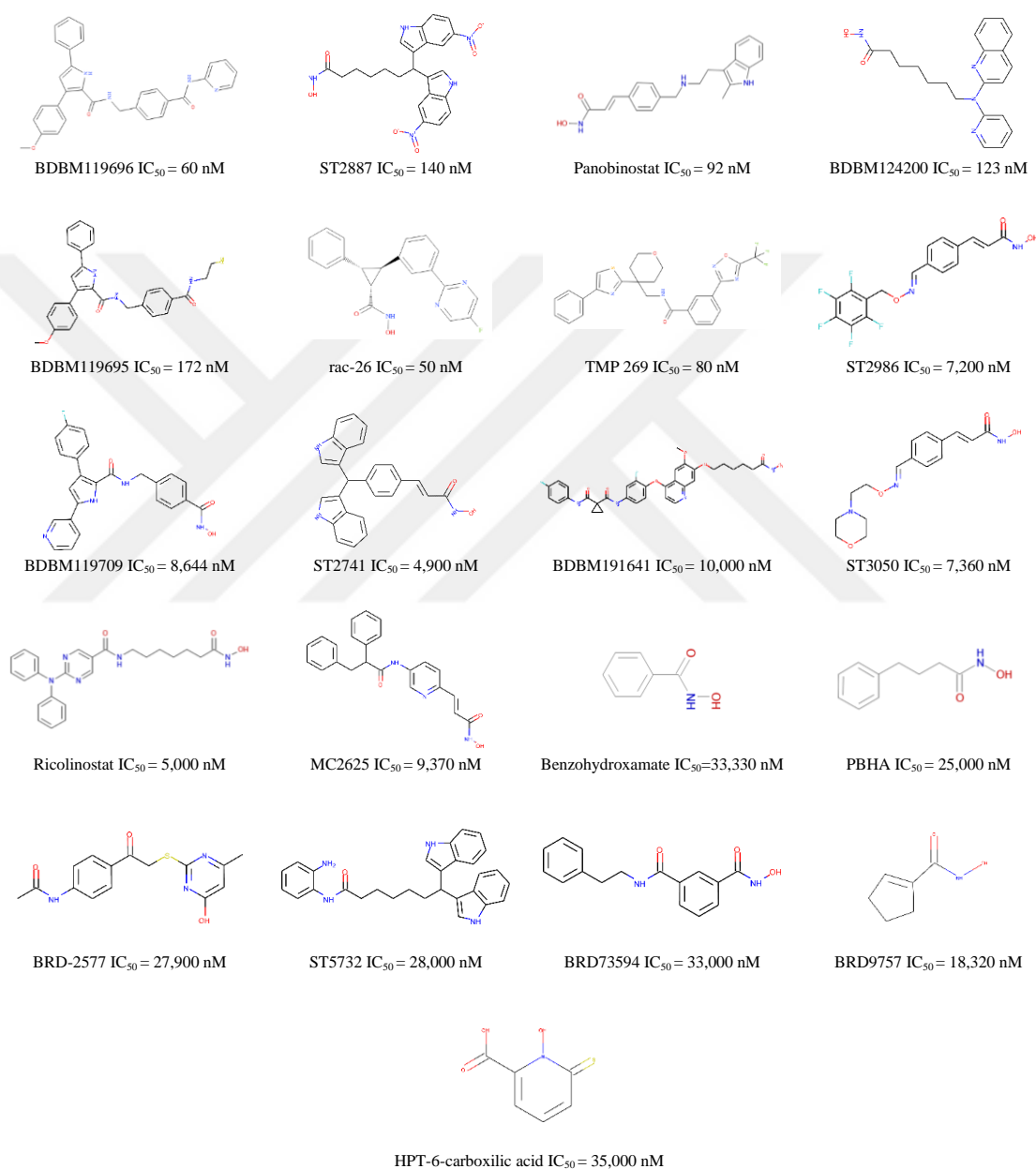


**Figure 2.9.** 2D structures of HDAC5 known inhibitors collected for the test set used in pharmacophore hypothesis validation.

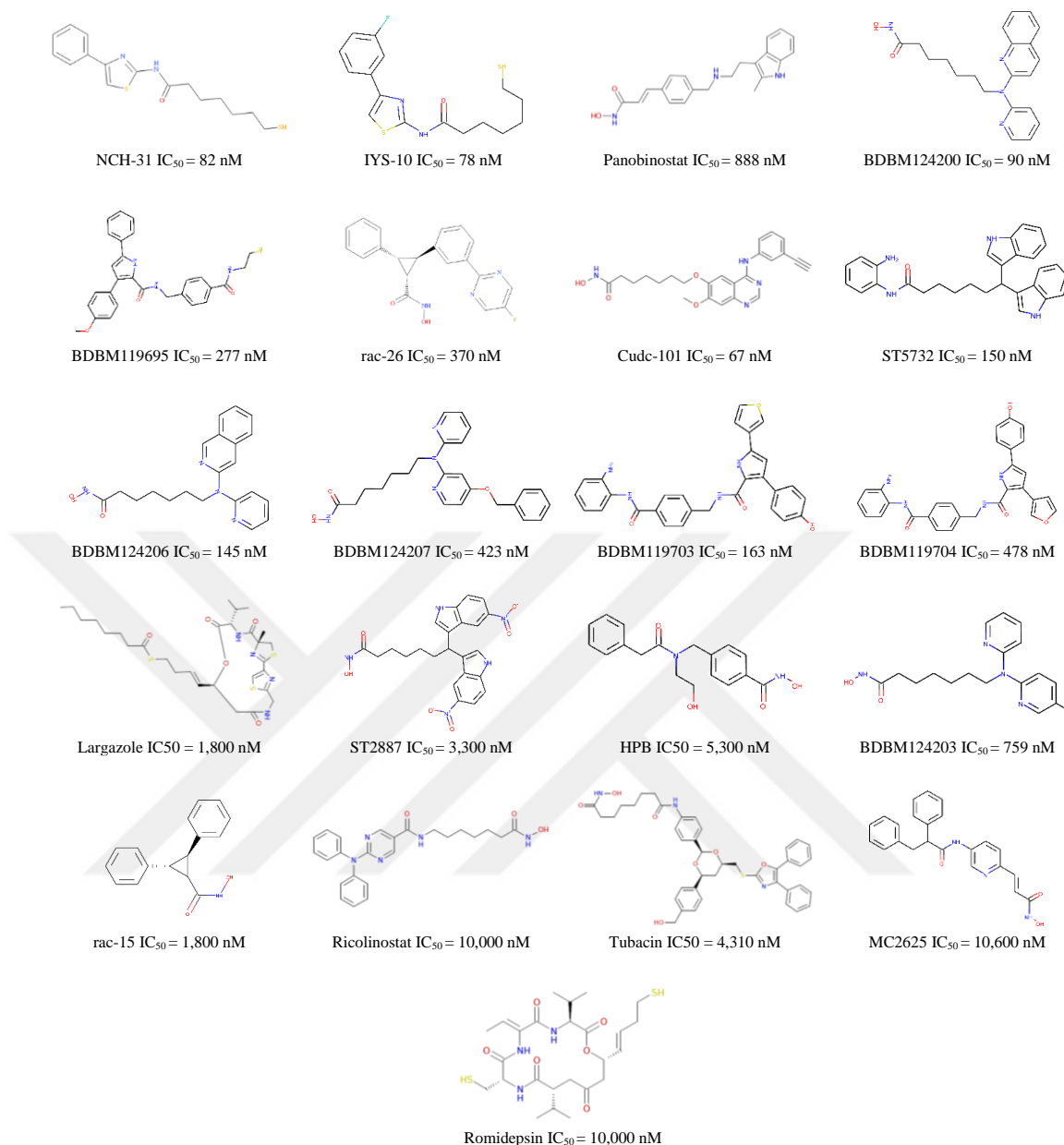


**Figure 2.10.** 2D structures of HDAC9 known inhibitors collected for the test set used in pharmacophore hypothesis validation.

### 2.3.4. 3D Database Search for New Hits

After validating the quality of the pharmacophore models and selecting the models based on their goodness of fit, 3D database search was conducted for identifying new lead molecules as HDAC5 and HDAC9 inhibitors. Thus, “Search 3D Database” protocol in BIOVIA DS 4.5 software was used to search the database against HDAC5-pharmacophore Hypo1 and HDAC9-pharmacophore Hypo2. HDAC5-pharmacophore

Hypo1 and HDAC9-pharmacophore Hypo2 were selected according to their goodness of hit from the previous step. The 3D database contained of ~200,000 compounds from the ZINC15 website (<http://zinc15.docking.org/>) (Sterling & Irwin, 2015).

### **2.3.5. Molecular Docking Study**

In order to evaluate the hit compounds obtained from the 3D database search and examine their interactions and binding poses within their respective targets, molecular docking method was conducted using QuickVina 2.0 (Alhossary et al., 2015). QuickVina 2.0 is an enhanced molecular docking tool, which was developed from classic AutoDock Vina program (Trott & Olson, 2009). According to the 3D database search results, HDAC5-pharmacophore Hypo1 retrieved 7,966 hit compounds and HDAC9-pharmacophore Hypo2 retrieved 21,422 hit compounds, where these compounds showed fit values of 3.00 or more. Proteins and all small molecules were prepared and saved as PDBQT files using AutoDockTools (G. M. Morris et al., 2009). AutoDockTools assisted in assigning Gasteiger charges and adding polar hydrogen atoms to both the proteins and the compounds. The size of the energy grid boxes for HDAC5 and HDAC9 was modified to include all active residues in the active site and was centered around the Zn<sup>2+</sup> ion. XYZ coordinates and the energy grid boxes were set as follows: 19.199, -10.083, -1.089 and 22.5, 22.5, 22.5 Å, respectively.

### **2.3.6. ADMET Description and Drug-Likeness**

Important ADMET properties such as Caco-2 cell membrane permeability, water solubility, and LogP for all lead compounds were predicted using the admetSAR 2.0 website (<http://lmmd.ecust.edu.cn/admetsar2>) (H. Yang et al., 2019) in order to examine their physicochemical properties. In addition, the Lipinski's rule of five was also predicted for the hit compounds using the SwissADME web service (<http://www.swissadme.ch/>) (Daina et al., 2017) to evaluate their drug-likeness. All input files were uploaded to these web servers as SMILES files.



### 2.3.7. Pan-Assay Interference Compounds (PAINS) Filter

The advances in high-throughput screening in computer-aided drug design have accelerated the drug discovery process and the identification of new compounds as active leads, however, many of these leads are eliminated due to their false positive impacts. These leads may contain certain sub-structures that were demonstrated by Baell and Holloway as pan assay interference compounds (PAINS) (Baell & Holloway, 2010). These substructure features have the ability to interact and bind to random targets with unspecific manner which results in false positives. To guarantee that the studied hit compounds are free of PAINS, the PAINS Remover website (<https://www.cbligand.org/PAINS/>) (Baell & Holloway, 2010) was used in the present study.

### 2.3.8. Molecular Dynamics Simulation

MD simulations were conducted for all complexes employing NAMD package (Phillips et al., 2020) to evaluate and study structural stability of both the protein and the ligand's binding mode. The subjected complexes included: HDAC5-LMK235, HDAC5-ZINC000257282664, HDAC5-ZINC000008918470, HDAC9-BRD4354, HDAC9-ZINC000016012342, and HDAC9-ZINC000020942817. The CHARMM-GUI web-based tools (<http://www.charmm-gui.org/>) (J. Lee et al., 2016) were used to generate all NAMD input files for all complexes. The CHARMM36m force field was assigned to all systems in the present study (J. Huang et al., 2016). All compounds were parameterized according to the CHARMM General Force Field (CGenFF), and all topology files were generated using the CGenFF web-based tool (<https://cgenff.umaryland.edu/>) (Vanommeslaeghe et al., 2010). Water box for all studied systems were generated using the transferable intermolecular potential 3 (TIP3) modules and several salt ions (NaCl) were added to neutralize the systems. The first step of the MD simulation included energy minimization applying the steepest descent method for 20,000 steps. Then, the systems were equilibrated for 10 ns at a temperature of 310 K in NVT ensemble. Finally, unrestrained MD simulations were run in NPT ensemble for 100 ns production phase at a temperature of 310 K. VMD software (Humphrey et al., 1996) was used to analyze all

of the generated trajectory files by examining the RMSD, RMSF, Rg, potential energy, and the total number of the intermolecular hydrogen bonds throughout the MD simulation.

### 2.3.9. Binding Free Energy Calculations

The Poisson-Boltzmann Surface Area (MM-PBSA) method (Massova & Kollman, 2000) was used to compute the binding free energy of the compounds after the MD simulations via CaFE tools (H. Liu & Hou, 2016). The free binding energy  $\Delta G_{bind}$  is composed of three main components: free energy of the gas phase  $\Delta G_{MM}$ ; free energy of the solvation  $\Delta G_{sol}$ ; and the change in the entropy of the system  $T\Delta S$  (Kollman et al., 2000) (Equation 2.7).

$$\Delta G_{bind} = \Delta E_{vdw} + \Delta E_{elec} + \Delta G_{polar} + \Delta G_{nonpolarc} - T\Delta S \quad (2.7)$$

For each system, the energy elements were calculated using 200 snapshots extracted from the last 10 ns of MD trajectory files. The internal dielectric constant was set to 4.0, the external dielectric constant was 80 and the reciprocal of grid spacing was set to 1 Å. All other parameters were used as default.

### 3. RESULTS

#### 3.1. HOMOLOGY MODELING OF CLASS IIA HDAC5 AND HDAC9, AND THE DESIGN OF DUAL ACTING INHIBITOR

##### 3.1.1. Sequence Alignment of The Template with The Targets

Entire amino acid sequences of both HDAC5 and HDAC9, including the catalytic domains, consist of 1,122 and 1,011 amino acid residues, respectively. The whole amino acid sequences of both HDAC5 and HDAC9 were individually aligned to amino acid sequence of HDAC4 catalytic domain. Consequently, 403 and 383 amino acid residues were obtained from HDAC5 and HDAC9, respectively, which represent the catalytic domains of the enzymes. Sequence alignment resulted in 76.2% sequence identity and 89.6% sequence similarity between human HDACs 5 and 4, whereas 73.4% sequence identity and 87.2% sequence similarity between human HDACs 9 and 4 (Figure 3.1).

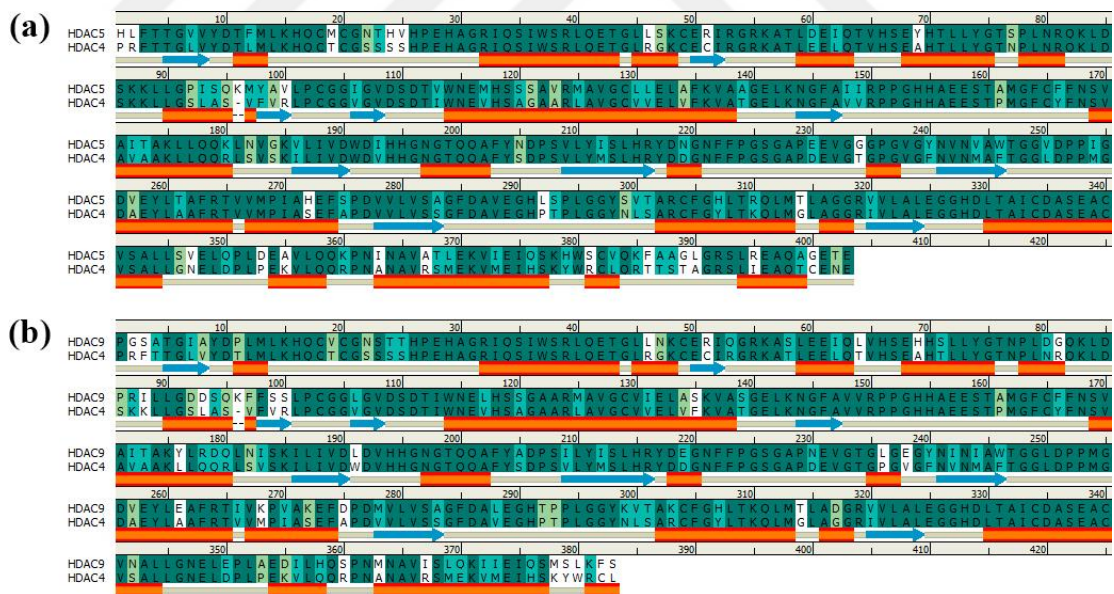


**Figure 3.1.** Sequences alignment of human (a) HDACs 4 and 5; and (b) HDACs 4 and 9. ■ Identical  
 identity ■ Strong ■ Weak □ Non-matching → β-sheet → α-helix.

### 3.1.2. Generated Homology Models

The generated homology models of HDAC5 and HDAC9 were performed based on the X-ray crystallography structure of the catalytic domain of human HDAC4 (PDB accession no. 2VQM\_A). In the present study, the amino acid sequence of the catalytic domains of HDACs 5 and 9 were only subjected to homology modeling, and other regions were excluded from the FASTA files, because those regions have no matches within the 3D structure of HDAC4 and won't be correctly modeled. Twenty models were generated for each of the HDACs (HDAC5 and HDAC9) (Figure 3.2). Loop regions were diverged in a very minor way in comparison to the rest of the structure, which might be caused by their higher internal energy. All built models were verified using MODELLER tools (Šali & Blundell, 1993; Webb & Sali, 2016) in order to select the best generated structure. Consequently, model M0014 of HDAC5 showed DOPE and Normalized DOPE scores of -47397.77344 and -1.206321, respectively. While model M0020 of HDAC9 showed DOPE and Normalized DOPE scores of -43881.875 and -1.210314, respectively (Table 3.1). Models M0015 and M0020 were chosen based on their lowest Normalized DOPE scores. Both built models were structurally superimposed to the HDAC4 structure, and the RMSD values were 0.53 Å and 0.34 Å for M0014 and M0020, respectively (Figure 3.3). These exquisitely aligned structures with their low RMSD values were anticipated due to the high amino acid sequence identity among HDACs 4, 5, and 9.

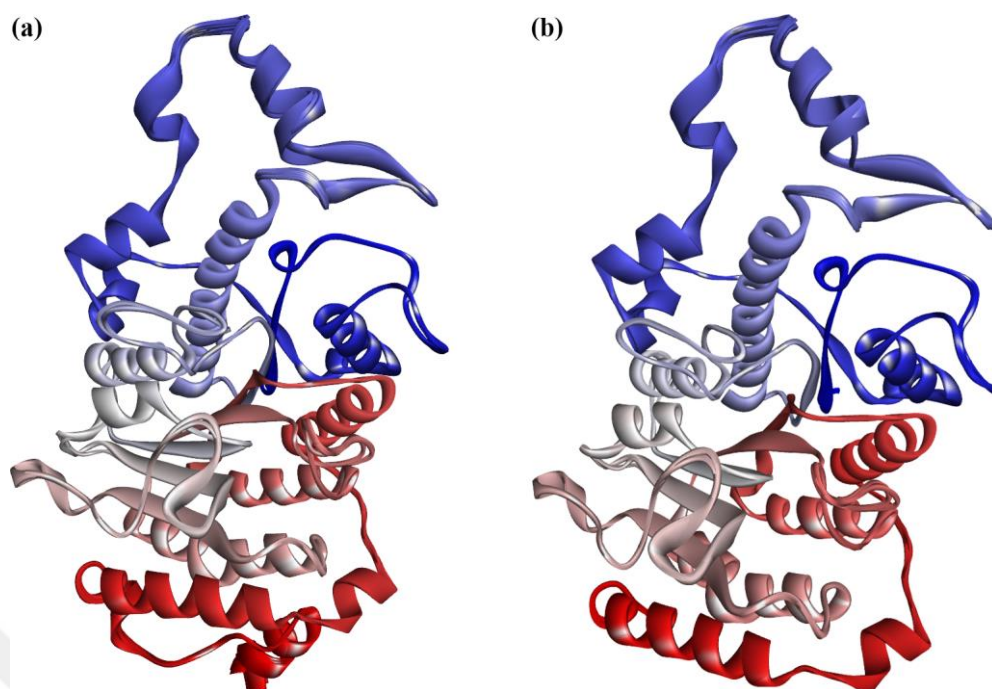


**Figure 3.2.** The 20 generated homology models of (a) HDAC5:M0014; and (b) HDAC9:M0020 based on the X-ray crystallography structure of human HDAC4 (PDB ID: 2VQM\_A).

**Table 3.1.** DOPE and Normalized DOPE scores for generated HDACs 5 and 9 models.

HDAC5			HDAC9		
Model	DOPE Score	Normalized DOPE Score	Model	DOPE Score	Normalized DOPE Score
M.0001	-46719.71875	-1.087162	M.0001	-43604.05078	-1.158941
M.0002	-46956.49219	-1.128772	M.0002	-43881.27734	-1.210204
M.0003	-46882.48438	-1.115766	M.0003	-43484.63281	-1.136859
M.0004	-46950.22266	-1.12767	M.0004	-43643.51563	-1.166239
M.0005	-46895.67188	-1.118083	M.0005	-43696.78125	-1.176088
M.0006	-46655.94531	-1.075955	M.0006	-43661.30859	-1.169529
M.0007	-47089.32031	-1.152114	M.0007	-43733.95703	-1.182962
M.0008	-47064.72266	-1.147792	M.0008	-43669.16406	-1.170981
M.0009	-46788.92578	-1.099324	M.0009	-43576.26953	-1.153804
M.0010	-47094.14453	-1.152962	M.0010	-43625.00391	-1.162816
M.0011	-47116.92188	-1.156965	M.0011	-43771.51172	-1.189907
M.0012	-46887.25391	-1.116604	M.0012	-43671.1875	-1.171355
M.0013	-47299.375	-1.189028	M.0013	-43610.08984	-1.160058
<b>M.0014</b>	<b>-47397.77344</b>	<b>-1.206321</b>	M.0014	-43405.6875	-1.122261
M.0015	-46102.95313	-0.978774	M.0015	-43610.94141	-1.160215
M.0016	-47212.98438	-1.173846	M.0016	-43863.78125	-1.206968
M.0017	-46935.68359	-1.125115	M.0017	-43462.08984	-1.132691
M.0018	-47064.32422	-1.147722	M.0018	-43740.91016	-1.184248
M.0019	-46656.07031	-1.075977	M.0019	-43744.10547	-1.184839
M.0020	-47153.78516	-1.163443	<b>M.0020</b>	<b>-43881.875</b>	<b>-1.210314</b>

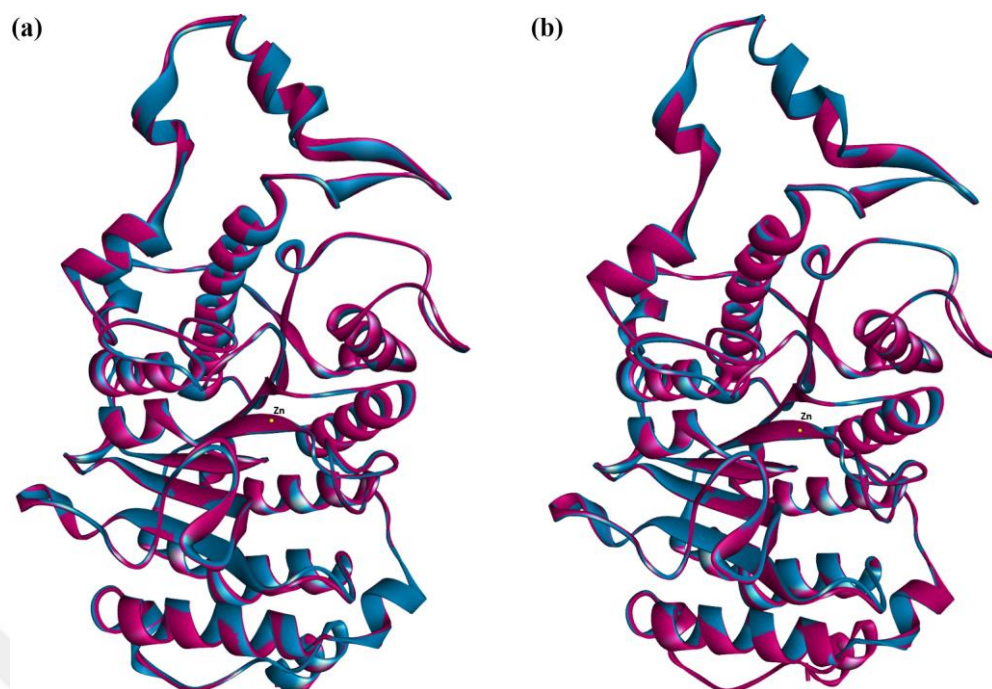


**Figure 3.3.** HDAC4 structural superimpose with (a) HDAC5:M0014 with RMSD value of 0.53 Å; and (b) HDAC9:M0020 with RMSD of 0.34 Å RMSD.  
■ HDAC4 ■ HDAC5:M0014 and HDAC9:M0020.

### 3.1.3. Homology Model Validation

ProSA-web tools depends on the scores of all X-ray crystal structures and NMR structures provided by the PDB database to evaluate and examine the quality of the generated homology models (Wiederstein & Sippl, 2007). Models M0014 and M0020 were found to have Z-scores of -8.12 and -8.04, respectively, which indicate that the conformations of these structures fit within the extent of native conformations of all NMR/X-ray resolved structures (Figure 3.4 (a) and (b)). The energy scheme describes the quality of local model and demonstrated inclusive negative values for the created models with errors (Figure 3.4 (c) and (d)). Furthermore, additional models' validation was performed by PROCHECK tool (Laskowski et al., 1996). The generated Ramachandran plot defines the psi ( $\Psi$ ) and Phi ( $\Phi$ ) distribution to demonstrate the energetically allowed areas of the protein structure (Figure 3.4 (e) and (f)). Model M0014 had 90.4% amino acids in the best preferred regions; 7.9% in the further allowed regions; 1.5% amino acids within the generally allowed regions; and 0.3% in disfavored regions. Model M0020 had 90.7% amino acids in the best preferred regions; 7.4% in the further allowed regions; 1.2% amino acids within the generally allowed regions; and 0.6% in



disfavored regions. Ramachandran plots for both M0014 and M0020 models were found to be satisfied. Furthermore, the built models stereochemical overall qualities were additionally evaluated by EERAT web server (<https://servicesn.mbi.ucla.edu/ERRAT/>) (Colovos & Yeates, 1993). ERRAT predicted the overall quality factor (OQF) for non-bonded atomic interactions in both M0014 and M0020 models, where 50 OQF or more for a structure is considered as a good quality (Colovos & Yeates, 1993). Herein, the homology models were found to be of high quality according to ERRAT results, where M0014 model showed 87.34 OQF and M0020 had an OQF of 86.4 (Figure 3.5).



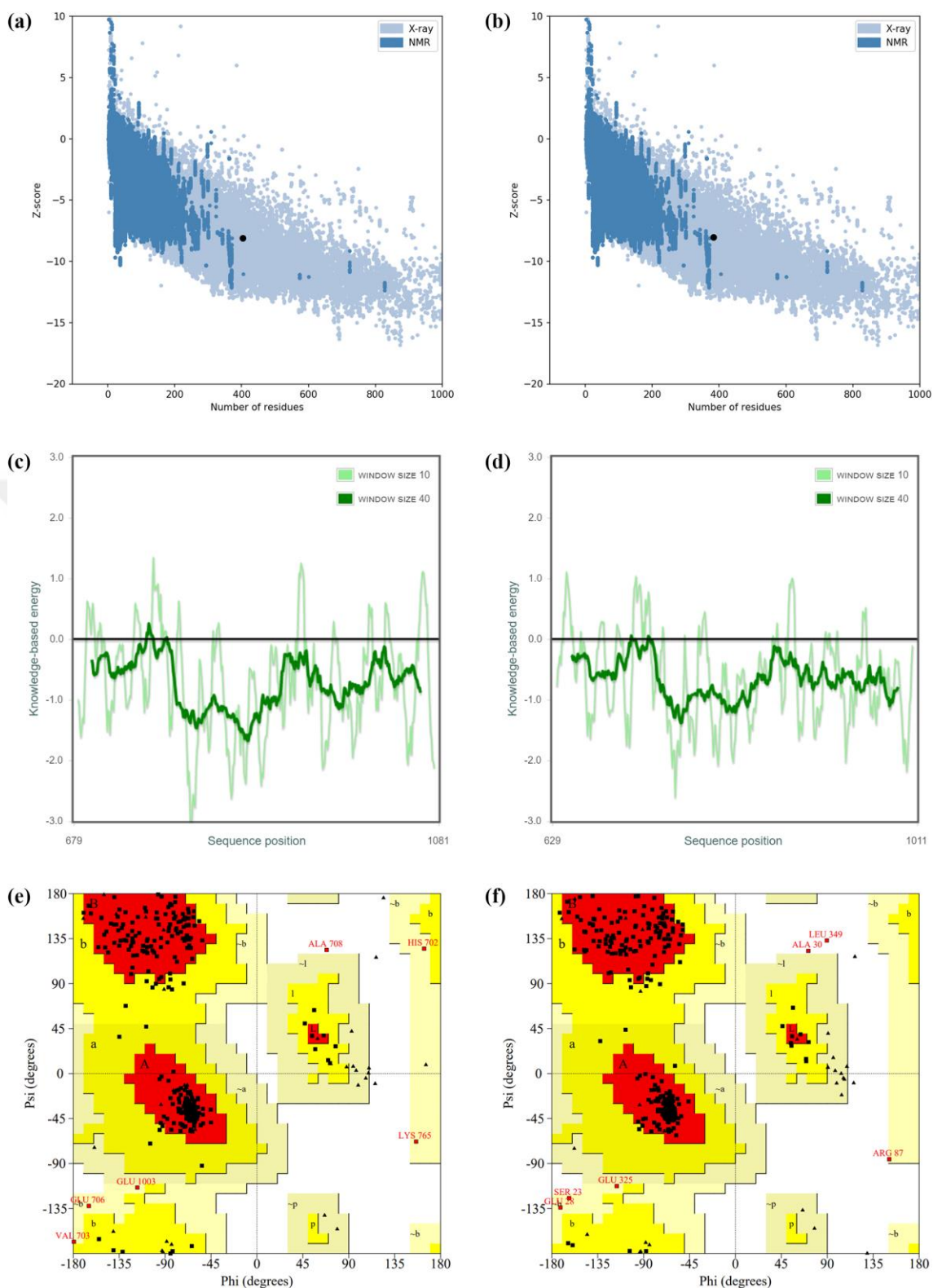


**Figure 3.4.** Validation of the homology models. Black dots describe the generated models among native conformations of all PDB database, where (a) M0014 has a Z-score of -8.12; and (b) M0020 has a Z-score of -8.04. ProSA's energy plots of (c) M0014 model; and (d) M0020 model. Ramachandran plots displays allowed and favored regions for (e) M0014 model; and (f) M0020 model.





**Figure 3.5.** ERRAT plots for the generated homology models (a) HDAC5:M0014 (b) HDAC9:M0020. Green bars describe the perfectly folded regions in the protein; Yellow bars refer to the 95% confidence misfolded regions; Red bars are 99% confidence of misfolded regions.

### 3.1.4. Molecular Docking with Known Inhibitors

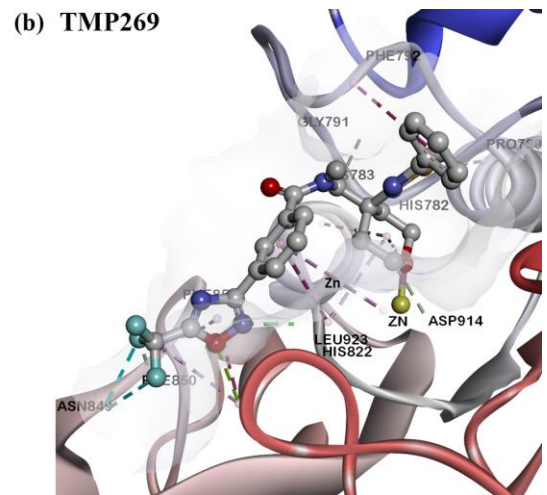
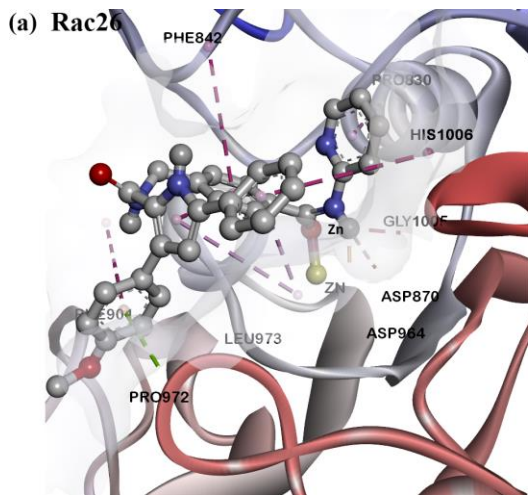
The quality of the built homology models was further evaluated by their capability to interact with their respective known inhibitors and produce a reasonable binding pose within the active sites. The experimental catalytic activities ( $IC_{50}$  or  $K_i$ ) of those selected HDACs of HDACs 5 and 9 were compared to the predicted  $K_i$  values calculated by AutoDock 4.2 (Tables 3.2 and 3.3). Clustered column graphs are given in the ANNEX A to compare the experimental catalytic activities ( $K_i$  or  $IC_{50}$ ) of HDACs 5 and 9 known inhibitors with their corresponding in silico calculated  $K_i$  values. Despite the fact that those experimental  $IC_{50}$  and  $K_i$  were not produced in silico, the in silico calculations of inhibitory constant  $K_i$  of the docked inhibitors proved rationally comparable results. Among all studied HDAC5 known inhibitors, Rac26 displayed the topmost affinity towards the protein with the lowest binding energy, -10.5 kcal/mol (Figure 3.6 a). Whereas TMP269 showed the topmost binding affinity towards HDAC9 compared to all other HDAC9 known inhibitors, with a binding energy of -10.66 kcal/mol (Figure 3.6 b). Compounds TMP269 and Rac26 are two class IIa HDAC inhibitors that were first identified in 2013 by Bürli (Bürli et al., 2013). The 2D chemical structure of all selected HDACs is shown in Figure 3.7, while their 3D presentations and interactions with their respective proteins are shown in Figures 3.8 and 3.9.

**Table 3.2** A comparative study between the experimental catalytic activities ( $K_i$  or  $IC_{50}$ ) (Exp.) of the HDAC5 known inhibitors and their corresponding in silico calculated  $K_i$  values.

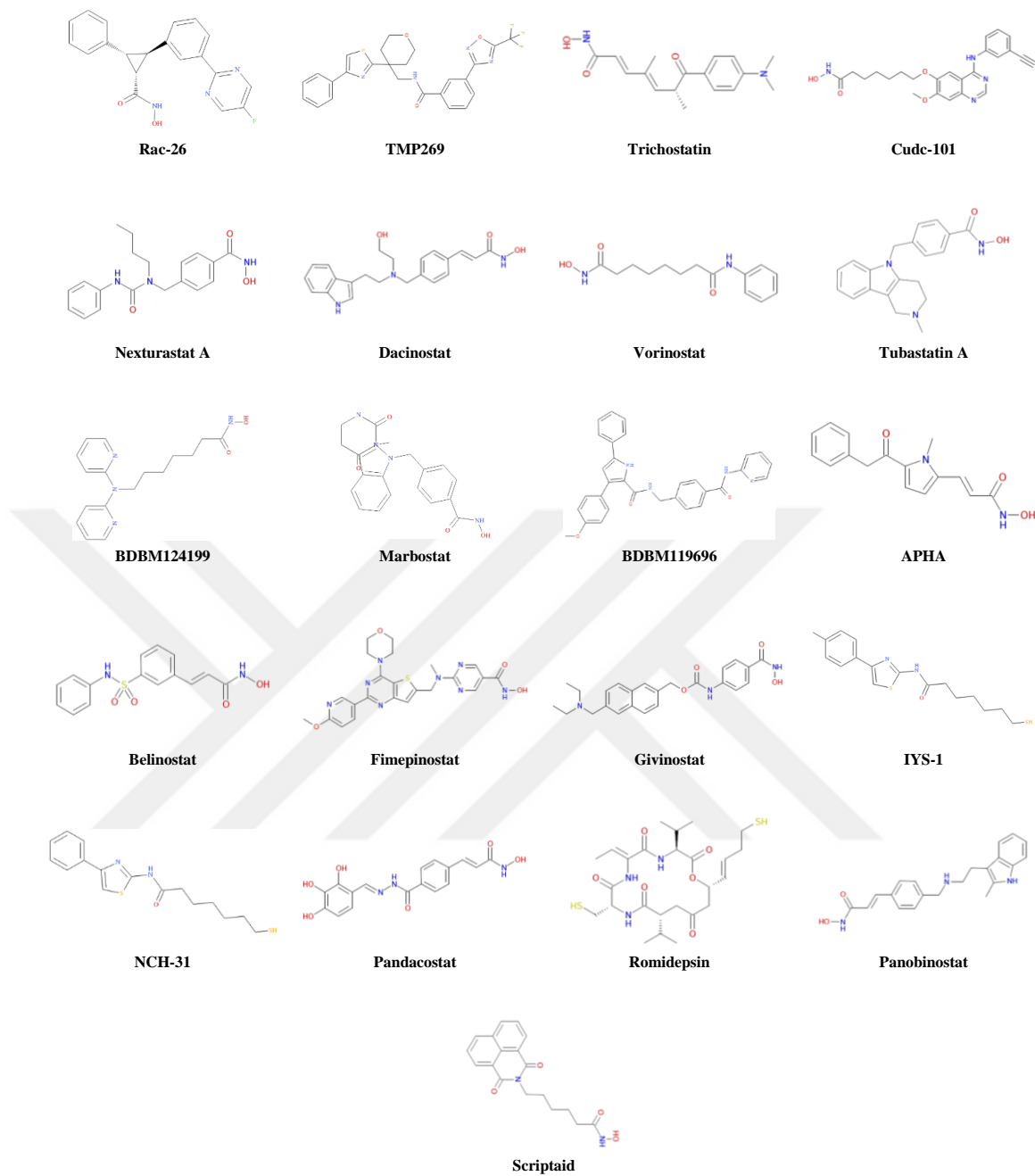
Compound	Exp. $K_i$ ( $\mu\text{M}$ )	Exp. $IC_{50}$ ( $\mu\text{M}$ )	Predicted $K_i$ ( $\mu\text{M}$ )	Calculated Binding Energy $\Delta G$ (kcal/mol)	Ref.
Rac26	–	0.050	0.020	-10.5	Bürli et al., 2013
TMP269	0.086	–	0.028	-10.29	Bürli et al., 2013
BDBM119696	–	0.060	0.024	-10.39	Pedro et al., 2011
Pandacostat	0.180	–	0.116	-9.46	Bradner et al., 2010
Romidepsin	0.550	–	0.915	-8.27	Bradner et al., 2010
Scriptaid	1.000	–	1.750	-7.86	Bradner et al., 2010
Fimepinostat	–	0.674	0.128	-9.4	Chen et al., 2016
Dacinostat	0.420	–	0.817	-8.31	Carrillo et al., 2015
Givinostat	0.600	–	0.264	-8.97	Carrillo et al., 2015
Belinostat	0.175	–	0.445	-8.66	Carrillo et al., 2015
BDBM124199	–	0.548	0.949	-8.22	Shuttleworth et al., 2014
Marbostat	0.701	–	0.960	-8.21	Sellmer et al., 2018
Tubastatin	–	2.300	1.390	-7.99	Wagner et al., 2013
Trichostatin	–	1.400	2.400	-7.65	Muthyala et al., 2015

**Table 3.3** A comparative study between the experimental catalytic activities ( $K_i$  or  $IC_{50}$ ) (Exp.) of the HDAC5 known inhibitors and their corresponding in silico calculated  $K_i$  values.

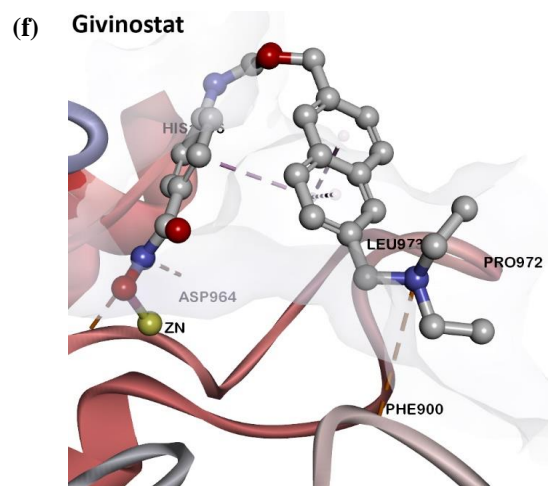
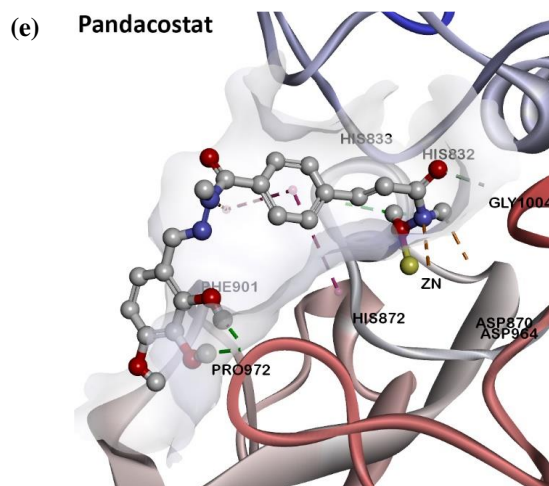
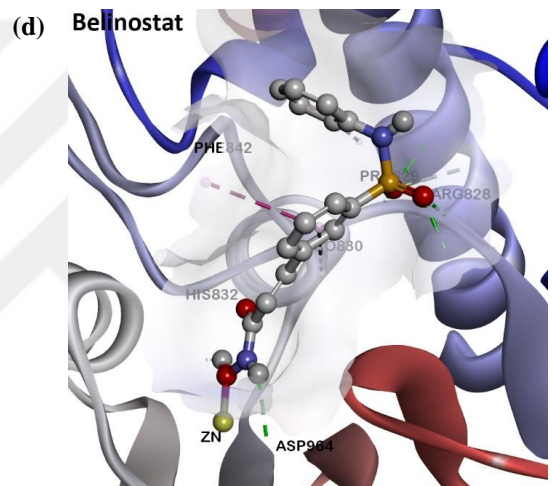
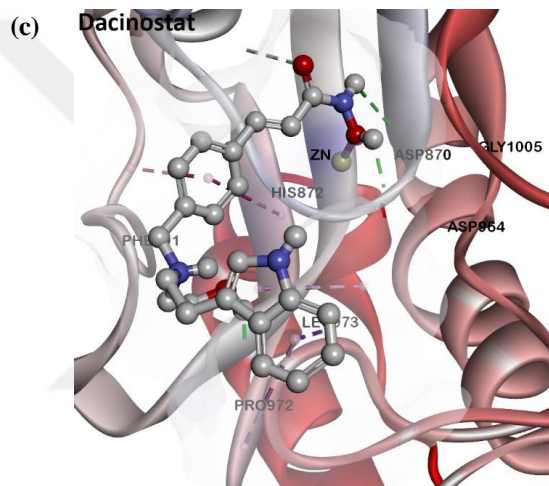
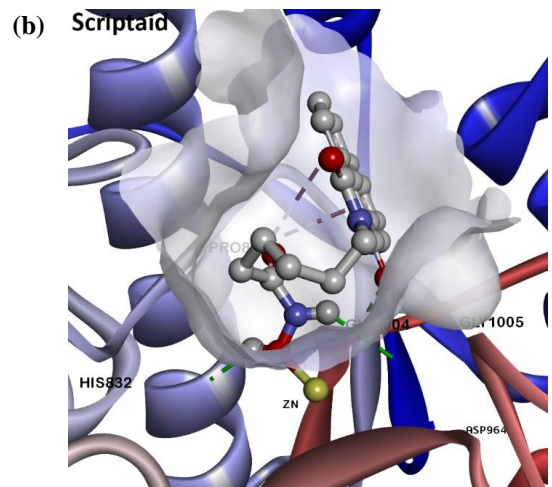
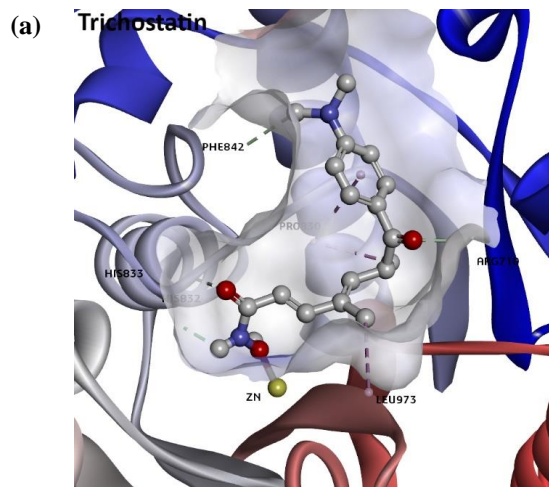
Compound	Exp. $K_i$ ( $\mu\text{M}$ )	Exp. $IC_{50}$ ( $\mu\text{M}$ )	Predicted $K_i$ ( $\mu\text{M}$ )	Calculated Binding Energy $\Delta G$ (kcal/mol)	Ref.
TMP269	–	0.019	0.015	-10.66	H. Y. Lee et al., 2017
IYS-1	–	0.042	0.015	-10.64	Sekizawa et al., 2014
NCH-31	–	0.082	0.017	-10.58	Sekizawa et al., 2014
BDBM119696	–	0.059	0.029	-10.27	Pedro et al., 2011
Givinostat	0.390	–	0.169	-9.24	Bradner et al., 2010
Pandacostat	1.400	–	0.375	-8.77	Bradner et al., 2010
Romidepsin	1.100	–	1.080	-8.14	Bradner et al., 2010
CUDC-101	–	0.067	0.393	-8.74	Cai et al., 2010
Belinostat	0.250	–	0.469	-8.63	Carrillo et al., 2015
Trichostatin	0.800	–	2.820	-7.57	Carrillo et al., 2015
Fimepinostat	–	0.554	0.490	-8.61	Chen et al., 2016
Panobinostat	0.888	–	0.680	-8.41	Yang et al., 2016
Scriptaid	–	0.700	1.510	-7.94	Hutt et al., 2010
Vorinostat	2.000	–	2.260	-7.7	Estiu et al., 2008
Nexturastat	–	6.720	3.150	-7.51	Bergman et al., 2012



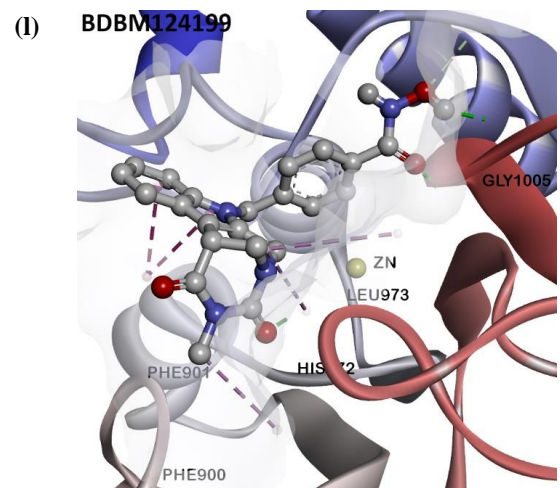
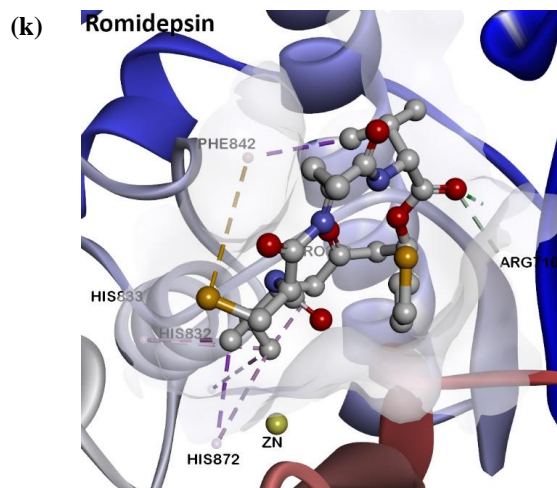
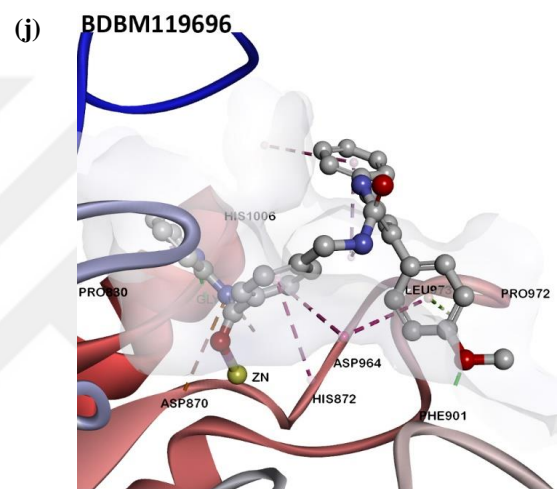
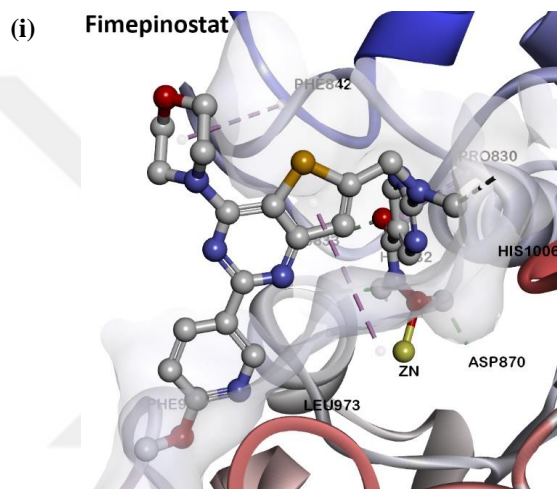
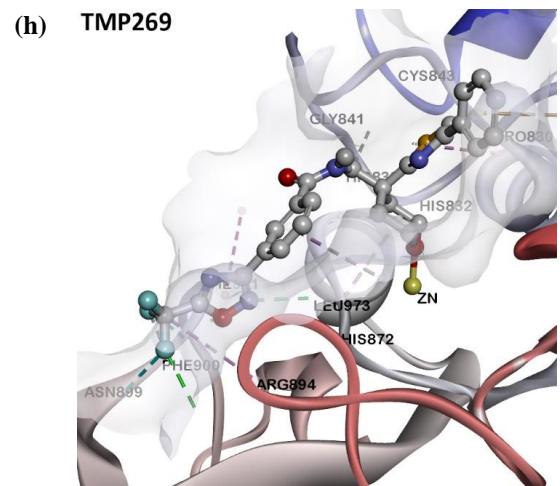
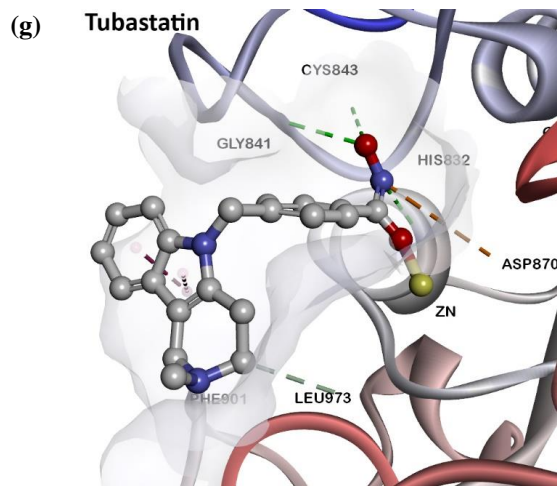
**Figure 3.6.** 3D presentations of the binding pose of (a) HDAC5-Rac26; and (b) HDAC9-TMP269.



**Figure 3.7.** The 2D Structures of the selected HDACs 5 and 9 known inhibitors







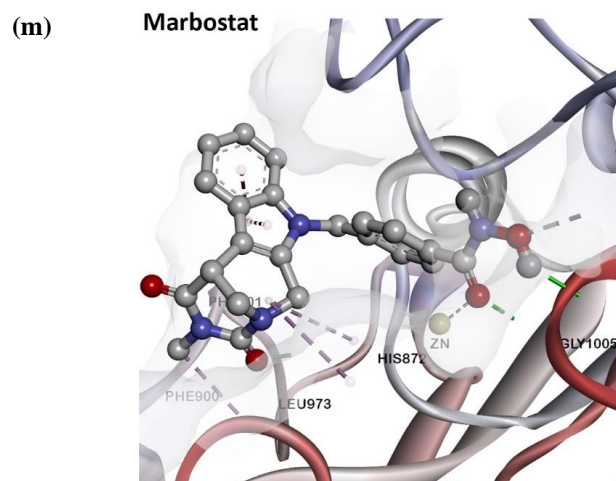
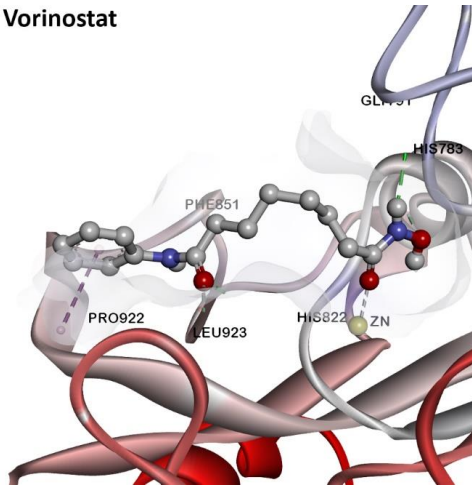
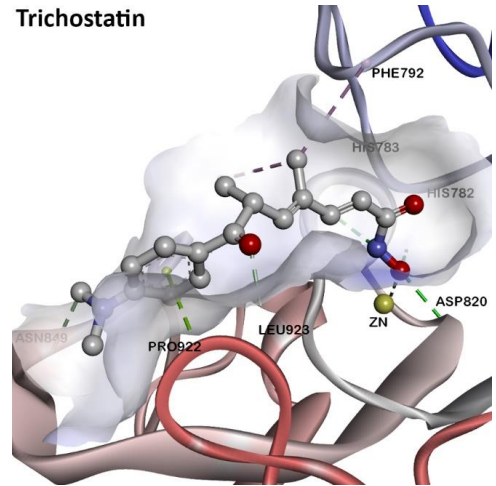


**Figure 3.8.** (“a” to “m”) The 3D schemes of the binding pose of the selected HDAC5 known inhibitors and their interactions to the active site of M0014 model.

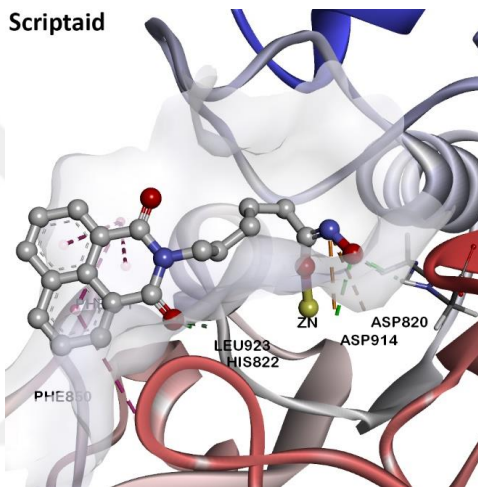
(a) Vorinostat



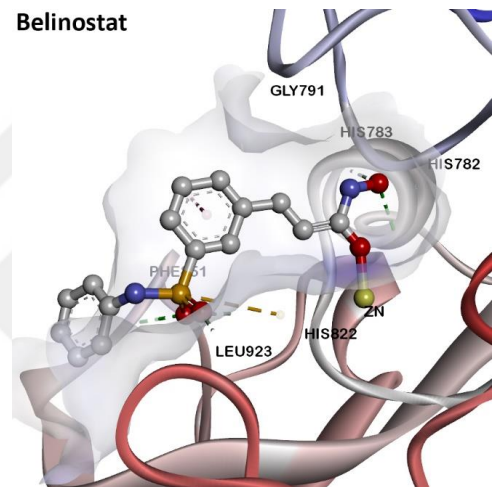
(b) Trichostatin



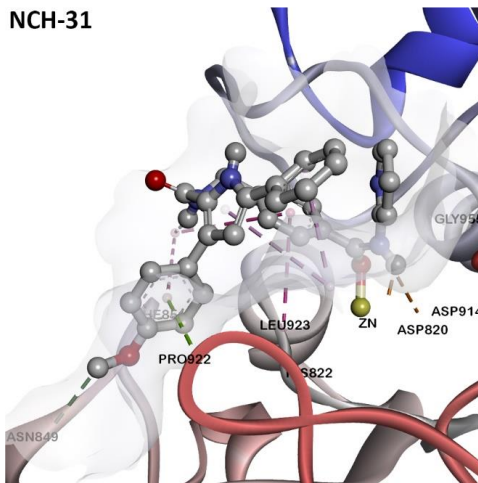
(c) Scriptaid



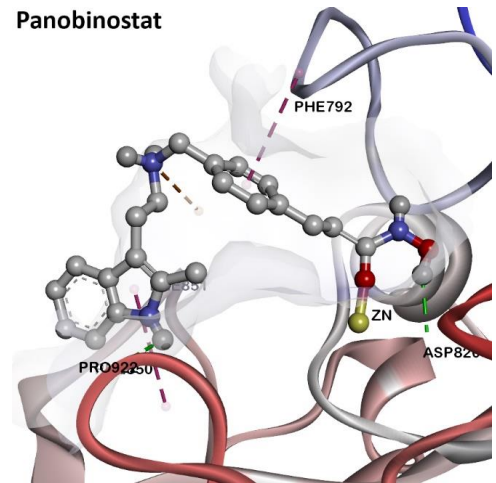
(d) Belinostat



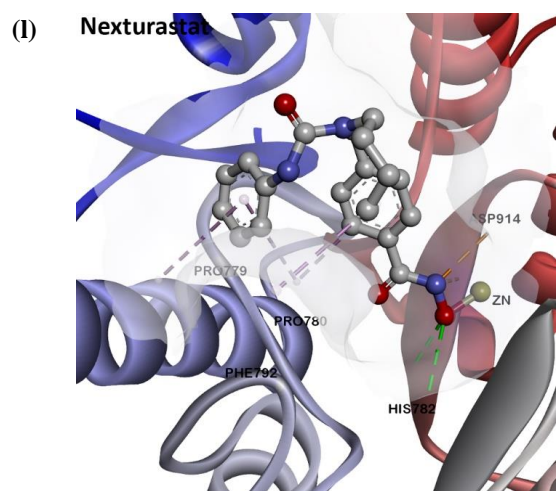
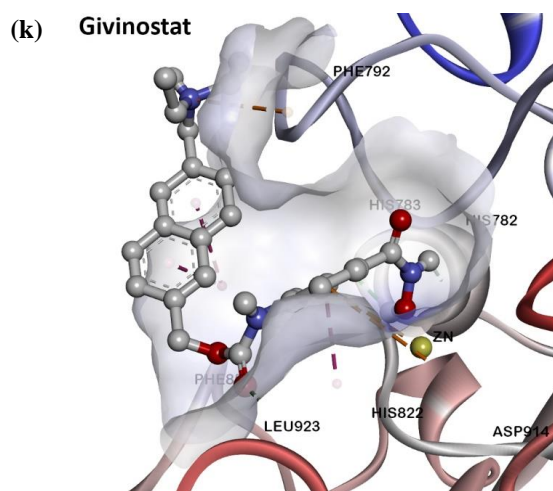
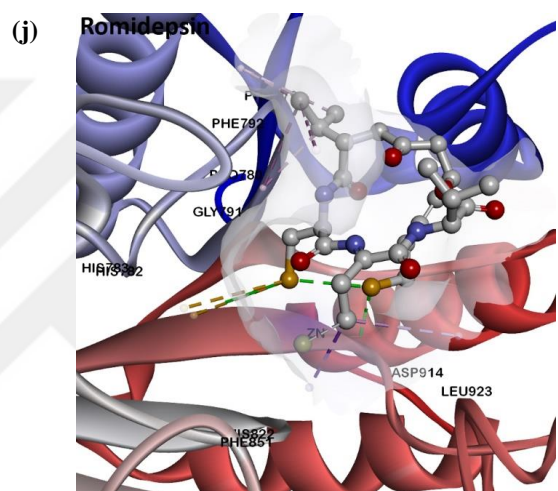
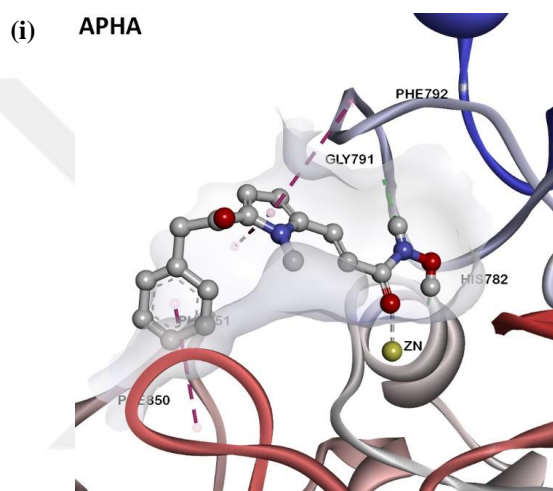
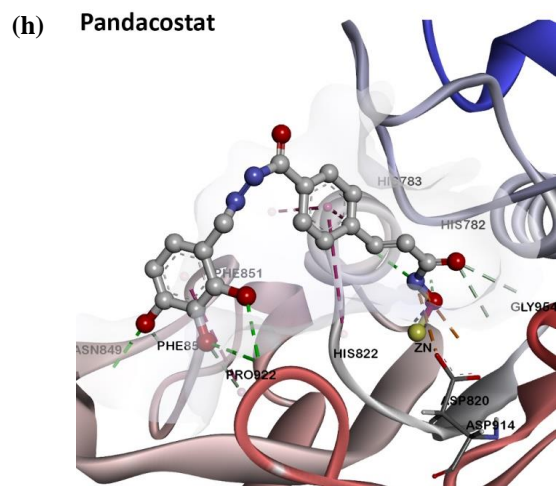
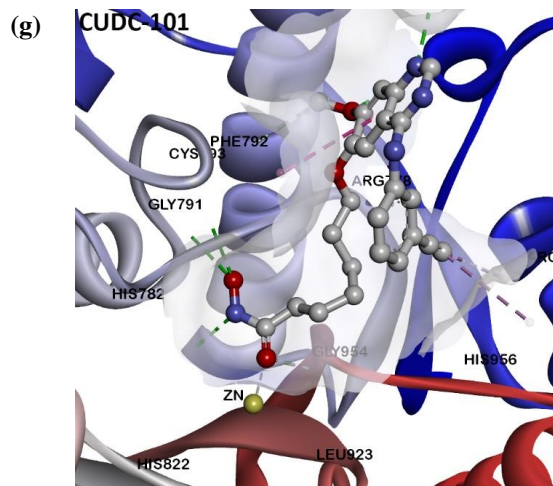
(e) NCH-31



(f) Panobinostat







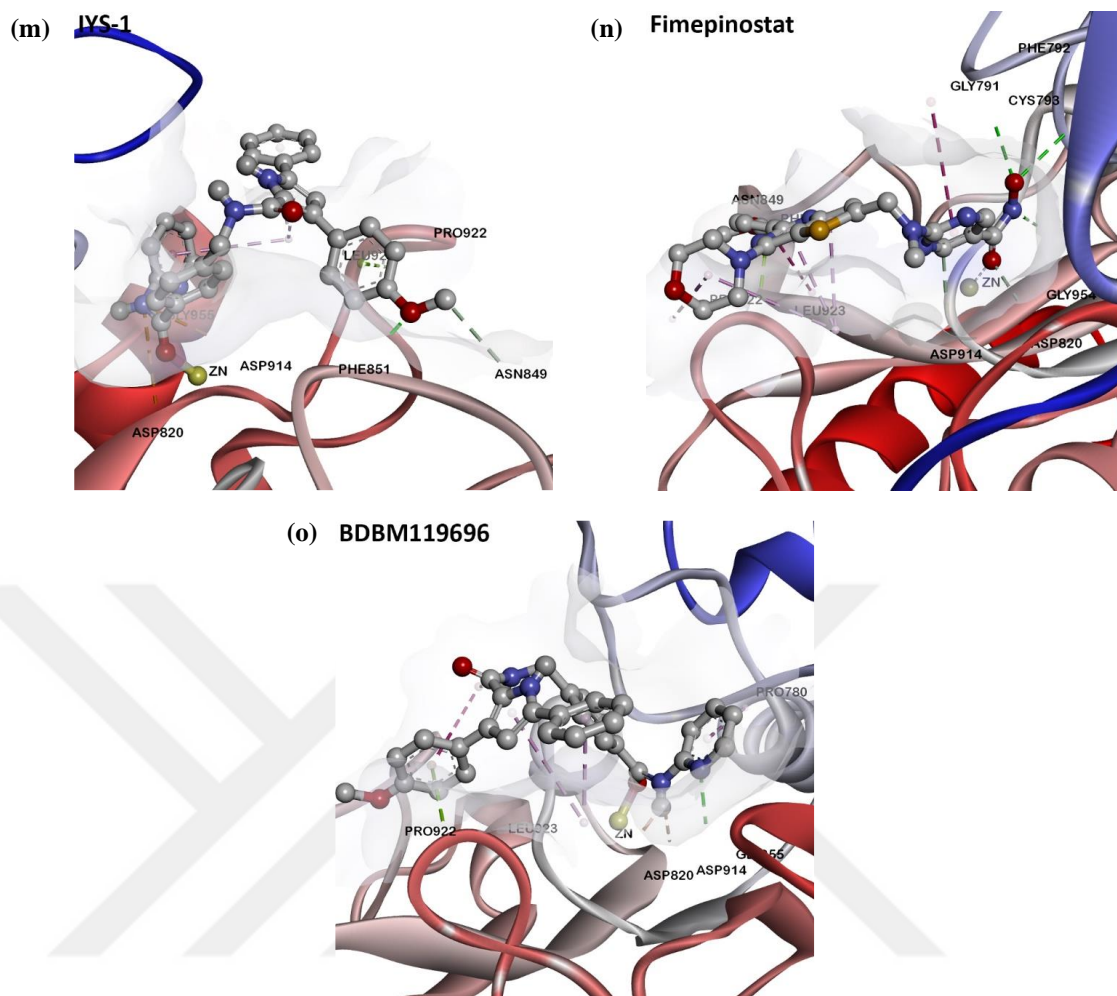


**Figure 3.9.** (“a” to “o”) The 3D schemes of the binding pose of the selected HDAC9 known inhibitors and their interactions to the active site of M0020 model.

### 3.1.5. Molecular Docking and Structure-Based Virtual Screening

Interestingly, based on the molecular docking study, two out of the 18 compounds showed comparatively close binding affinity towards both HDAC5 and HDAC9, compound CHEMBL2114980 and compound CHEMBL217223. This could mean that these two compounds can potentially display a dual action effect towards both proteins, inhibiting their catalytic actions at the same time. Predicted binding energy of the studied 18 compounds with their estimated inhibitory constant  $K_i$  is given in Table 3.4. CHEMBL2114980 was found to have binding energy scores of -11.63 and -11.66 kcal/mol for HDAC5 and HDAC9, respectively. While compound CHEMBL217223 had binding energy scores of -11.44 and -11.48 kcal/mol for HDAC5 and HDAC9,

respectively. Compound CHEMBL2114980 was found to have the lowest inhibitory constant with a value of 2.99 nM against HDAC5 and 2.85 nM against HDAC9, respectively, with a percentage difference of only 4%. On the other hand, Compound CHEMBL217223 had the second low inhibitory constant with a value of 4.12 nM against HDAC5 and 3.83 nM against HDAC9, respectively, with a percentage difference of 7%. Compound CHEMBL2114980 bound to both HDAC5 and HDAC9 in a very similar binding mode and interacted with the catalytic Zn<sup>2+</sup> atom and with other key amino acid residues in the active sites (Figure 3.10; Figure 3.11). The chemical interactions included several types of bonds; hydrogen bonds, salt-bridge interaction,  $\pi$ -alkyl or alkyl interactions, van der Waals, and charged interactions. Furthermore, compound CHEMBL217223 was also found to have a similar binding pose within the active sites of both HDAC5 and HDAC9 (Figures 3.10; 3.11). In addition to the covalent bond between compound CHEMBL217223 and the catalytic Zn<sup>2+</sup> ion, several other essential interactions formed including hydrogen bond, van der Waals,  $\pi$ - $\pi$  stacked,  $\pi$ -cation and  $\pi$ - $\pi$  T-shaped interaction.

**Table 3.4.** In silico calculations of the binding energy and the inhibitory constant  $K_i$  of the 18 molecules.

Compound	ChEMBL ID	HDAC5		HDAC9	
		$\Delta G$ (kcal/mol)	$K_i$ (nM)	$\Delta G$ (kcal/mol)	$K_i$ (nM)
1	CHEMBL2114980	-11.63	2.99	-11.66	2.85
2	CHEMBL217223	-11.44	4.12	-11.48	3.83
3	CHEMBL391373	-11.26	5.58	-10.5	20.21
4	CHEMBL3290141	-11.05	7.99	-10.45	21.7
5	CHEMBL280713	-10.94	9.57	-11.37	4.62
6	CHEMBL437407	-10.43	22.69	-11.07	7.69
7	CHEMBL3952453	-10.42	23.16	-10.47	21.21
8	CHEMBL1183361	-9.75	71.38	-10.42	23.12
9	CHEMBL286733	-9.99	47.33	-10.39	24.1
10	CHEMBL3186912	-9.74	72.17	-10.19	33.78
11	CHEMBL2170731	-10.49	20.55	-9.77	69.39
12	CHEMBL1940821	-10.27	29.61	-9.31	150.92
13	CHEMBL3088181	-10.23	31.59	-9.92	53.21
14	CHEMBL2170648	-10.23	31.7	-9.6	92.58
15	CHEMBL3114783	-9.94	52.02	-9.21	178.68
16	CHEMBL3114762	-9.8	65.66	-8.86	320.74
17	CHEMBL1440899	-8.84	332.73	-9.24	169.63
18	CHEMBL1897391	-8.75	384.92	-9.03	240.81

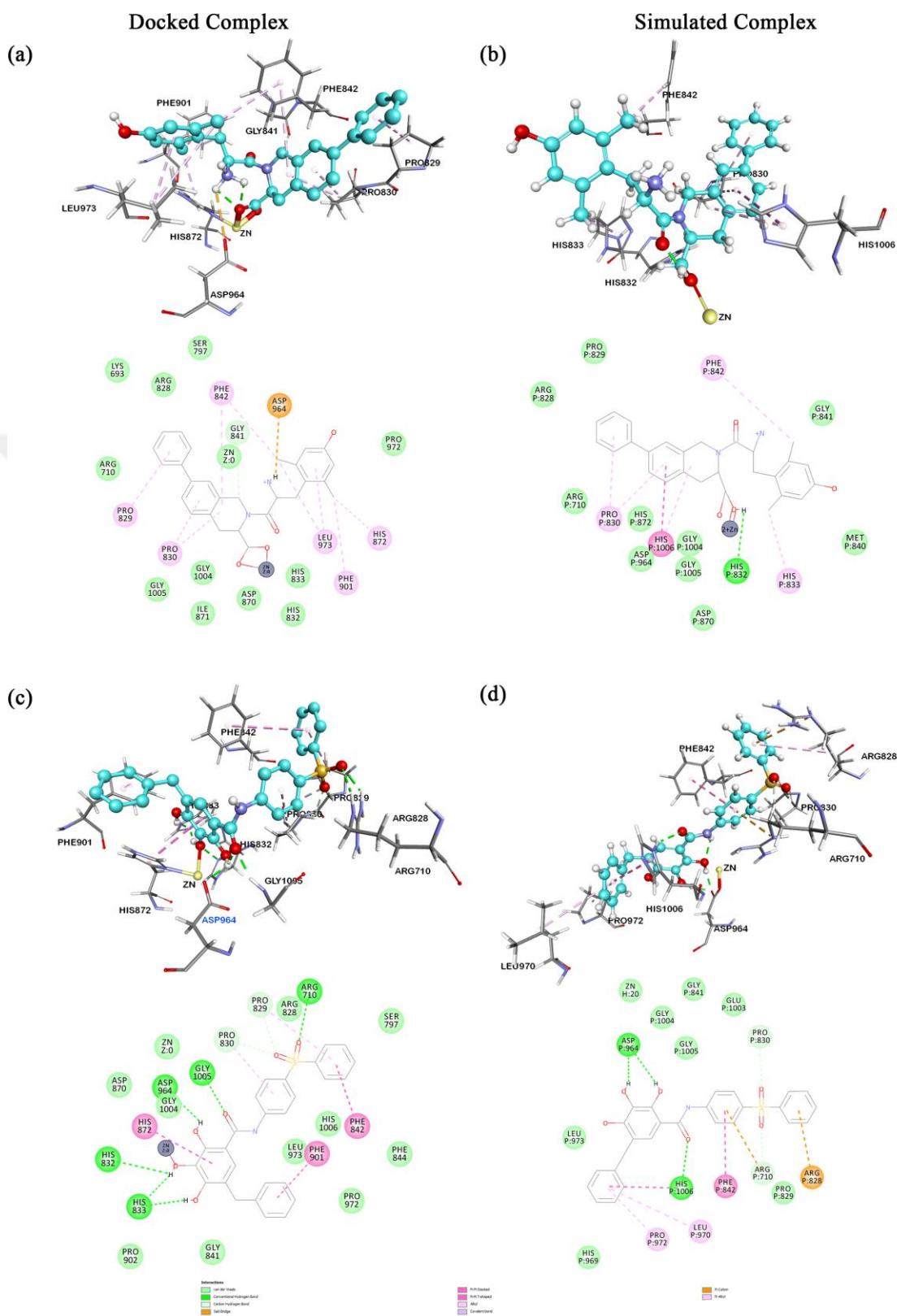


**Figure 3.10.** 3D presentations of the binding modes and 2D schemes of the chemical interactions of HDAC5 complexes: (a) docked pose of CHEMBL2114980 and (b) MD simulation snapshot (c) docked pose of CHEMBL217223 and (d) MD simulation snapshot.



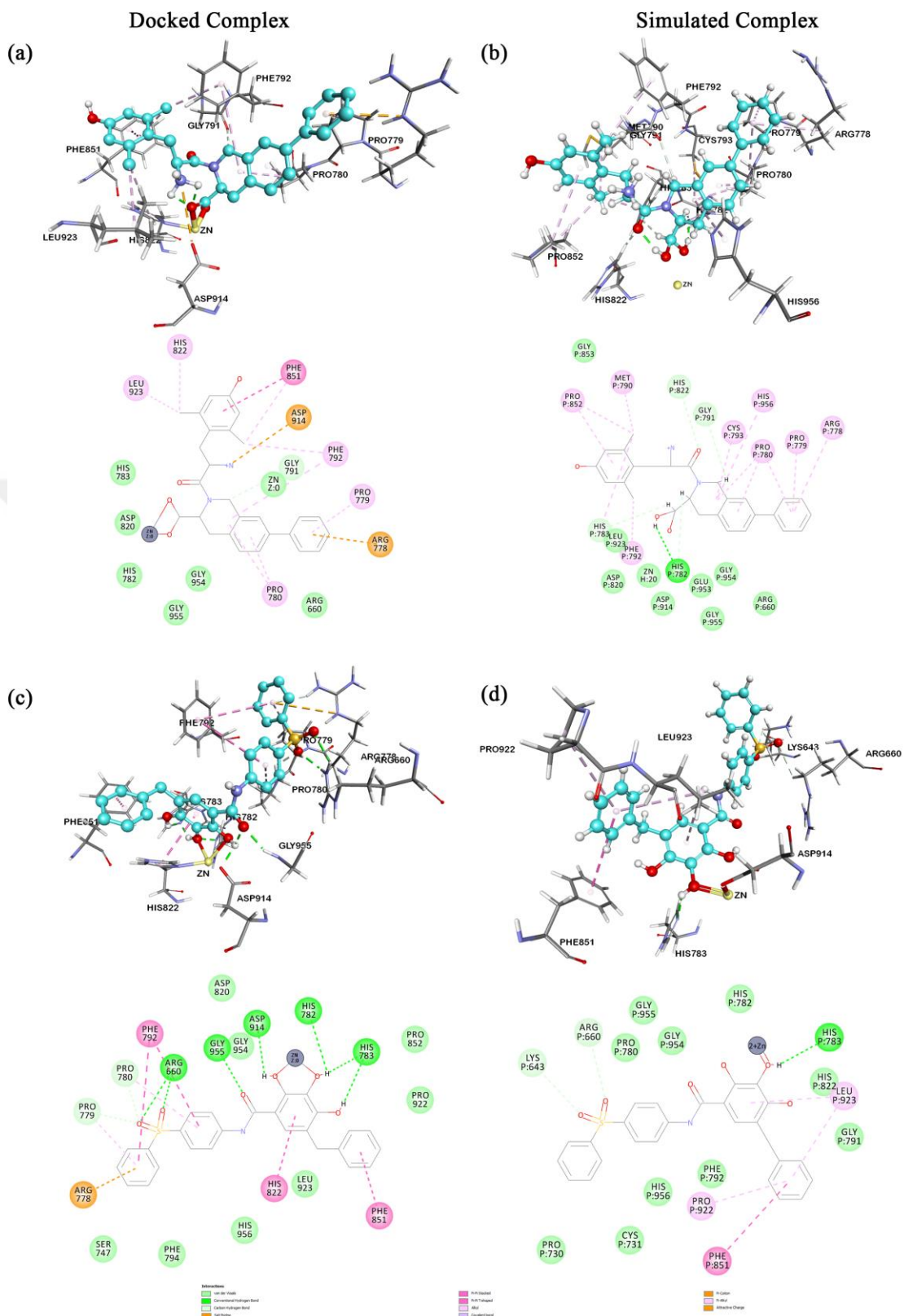


**Figure 3.11.** 3D presentations of the binding modes and 2D schemes of the chemical interactions of HDAC9 complexes: (a) docked pose of CHEMBL2114980 and (b) MD simulation snapshot (c) docked pose of CHEMBL217223 and (d) MD simulation snapshot.

### 3.1.6. Physicochemical Properties Description

Based on the admetSAR and SwissADME results, all the studied 18 compounds were found to obey Lipinski's rule of 5 and were described as drug-like leads (Table 3.5). In drug discovery field, one violation of Lipinski's rule of five is tolerated (Lipinski et al., 2001). The capability of a drug to across the cell membranes of living body tissues (e.g., intestine) is described by the topological polar surface (TPSA) area, and is commonly used in the field of CADD (Pajouhesh & Lenz, 2005). The Moriguchi's octanol water partition coefficients (MLogP) defines the hydrophilicity/hydrophobicity proportion of small molecules in an octanol/water solution which ought to be less than 4.15 (Moriguchi et al., 1992). Another important ADMET property is the measurement of the gastrointestinal permeability level of a given drug in human epithelial colorectal adenocarcinoma (Caco-2) (Shah et al., 2006). Caco-2 gastrointestinal permeability speed should be faster than 22 nm/s, and the aqueous solubility (LogS) level has to be  $> -5$  (Bergström & Larsson, 2018; Di & Kerns, 2016).

**Table 3.5.** In silico AMDET properties prediction of the novel 18 compounds.

#	ChEMBL ID	Lipinski #violations	MW $\leq 500$	HA $\leq 10$	HD $\leq 5$	MLogP $\leq 4.15$	TPSA $\leq 140$	Caco-2 (cm/s)	LogS $> -5$
1	CHEMBL2114980	0	444.52	5	3	2.68	103.86	0.665	-3.60
2	CHEMBL217223	0	475.51	6	4	3.4	132.31	0.910	-2.97
3	CHEMBL391373	0	492.67	4	0	3.77	66.07	0.782	-3.79
4	CHEMBL3290141	0	488.54	4	4	3.12	122.03	0.837	-3.56
5	CHEMBL280713	0	437.45	7	1	2.84	103.02	0.792	-2.75
6	CHEMBL437407	0	490.59	5	3	2.71	105.48	0.853	-3.45
7	CHEMBL3952453	0	457.56	5	1	2.41	65.9	0.769	-2.86
8	CHEMBL1183361	0	497.65	3	1	0.23	47.56	0.726	-3.73
9	CHEMBL286733	0	486.63	5	2	3.31	75.81	0.777	-3.64
10	CHEMBL3186912	1	473.58	4	2	4.33	55.81	0.728	-4.08
11	CHEMBL2170731	0	431.52	5	2	3.39	71.7	0.491	-3.84
12	CHEMBL1940821	1	440.51	6	6	2.23	104.98	0.882	-3.03
13	CHEMBL3088181	0	473.48	7	3	1.13	135.26	0.897	-3.12
14	CHEMBL2170648	1	494.51	6	3	4.25	99.28	0.856	-3.89
15	CHEMBL3114783	0	497.52	5	3	2.25	99.35	0.822	-3.37
16	CHEMBL3114762	0	483.49	5	3	2.06	99.35	0.799	-3.31
17	CHEMBL1440899	0	491.53	5	0	3.01	59.99	0.678	-3.58
18	CHEMBL1897391	0	416.5	5	0	3.17	76.47	0.568	-3.30

### 3.1.7. Pan-Assay Interference Compounds (PAINS) Filtration

PAINS filtration showed that all of the top ranked 18 studied compounds have passed the filtration and were described as PAINS-free.

### 3.1.8. Molecular Dynamics MD Simulation

MD simulations were performed for the generated models M0014 and M0020 as well as their complexes with their corresponding known HDACis, DAC5-Rac26 and HDAC9-TMP269. Moreover, the top ranked compounds, CHEMBL2114980 and CHEMBL217223 were also subjected to MD simulations in complexes with HDAC5 and HDAC9. Root mean square deviation (RMSD) was calculated for all systems to shed a light on the structural alterations during the MD simulations (Figure 3.12). HDAC5 and HDAC5-Rac26 reached their equilibrium stability around 20 ns of the MD run. HDAC5's RMSD rose to 3.8 Å at 6 ns, and the protein showed sustained stability till the end with minor fluctuations between 2.6 Å and 3.9 Å. HDAC5-Rac26 complex's RMSD also rose to 4.5 Å around 5 ns then decreased to 3.4 Å around 10 ns and continued its stability with small fluctuations between 4 Å and 5.3 Å. The RMSD of the HDAC9 structure steadily increased until 5.2 Å at 37 ns, and later decreased at 53 ns to 3.4 Å to remain stable with minor fluctuations from 57 ns to the end of the run (ranging between 3.4 Å and 4.6 Å). HDAC9-TMP269 system's RMSD gradually increased until 34 ns to 5.2 Å, but then decreased at 43 ns to 4.6 Å and remained that way until the end of the run. These previous observations suggested that both the free modeled proteins and their HDACis complexes had achieved their equilibrium state and showed good structural stability. HDAC5-CHEMBL2114980 and HDAC5-CHEMBL217223 complexes demonstrated rational structural stability throughout the MD simulations and, remarkably, they both displayed quite similar behavior from 60 ns till the end. HDAC9-CHEMBL217223 complex displayed a rise in the RMSD from 2 Å to 6 Å, but then decreased under 5 Å. Whereas the RMSD of the HDAC9-CHEMBL2114980 complex achieved its structural stability around the 50 ns and remained at 5.5 Å till the end of the MD run.

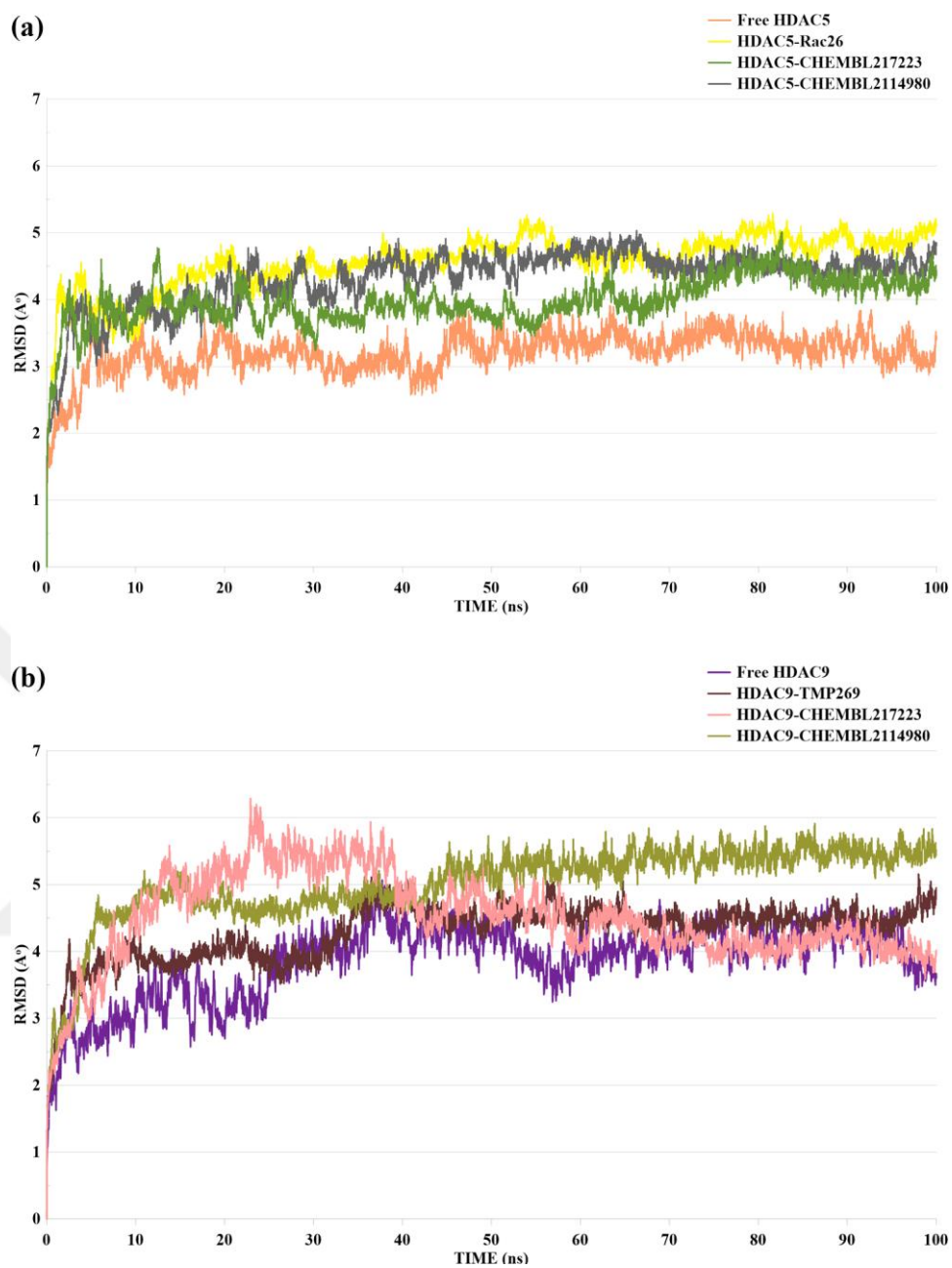


**Figure 3.12.** RMSD plots of (a) free HDAC5 and HDAC5 complex with the Rac26 known inhibitor, CHEMBL2114980, CHEMBL217223; (b) free HDAC9 and HDAC9 complex with the TMP269 known inhibitor, CHEMBL2114980, CHEMBL217223.



Root mean square fluctuation (RMSF) was calculated to investigate the flexibility of the amino acids in the active site and their interactions with the ligand during the MD simulation (Figure 3.13). Examining the RMSF plot deliver a great insight on the flexible parts of the protein. RMSF analysis of all studied systems showed slightly minor fluctuations over time. Increased fluctuated points in all systems reflect loop regions, which are known with their high flexibility. These loops are found to be far from the active sites, except for two points, Gly841 within HDAC5 and Gly791 in HDAC9, they are located near the entrance of the active site of the proteins. Both residues demonstrated moderate fluctuation manner.

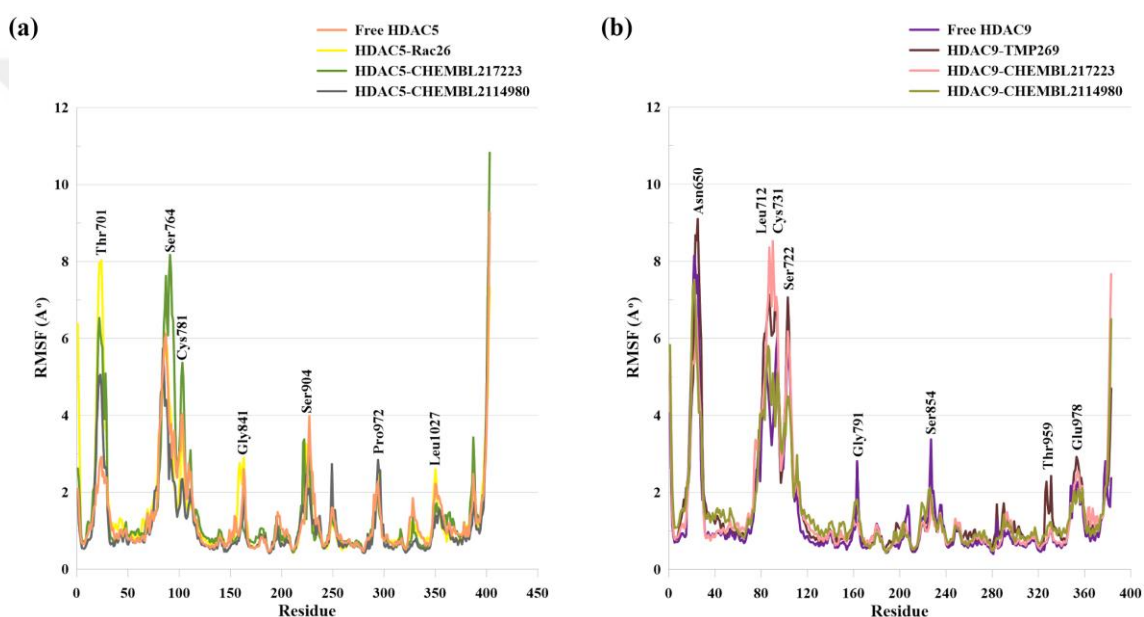


**Figure 3.13.** RMSF plots of (a) free HDAC5 and HDAC5 complex with the Rac26 known inhibitor, CHEMBL2114980, CHEMBL217223; (b) free HDAC9 and HDAC9 complex with the TMP269 known inhibitor, CHEMBL2114980, CHEMBL217223.

Radius of gyration ( $R_g$ ) is another measurement that assesses the 3D structure compactness.  $R_g$  refers to the calculation of the mass-weighted root mean square distance of systems atoms from their center of mass (Davoudmanesh & Mosaabadi, 2018).  $R_g$  calculations of all systems were found to be consistent over time, which is harmonious with the observations from the RMSD and RMSF analysis (Figure 3.14). The  $R_g$  average score of the HDAC5-Rac26 and HDAC9-TMP269 systems was found to be 1.42 Å. While the  $R_g$  average scores of all other studied systems were found to be 1.26 Å.

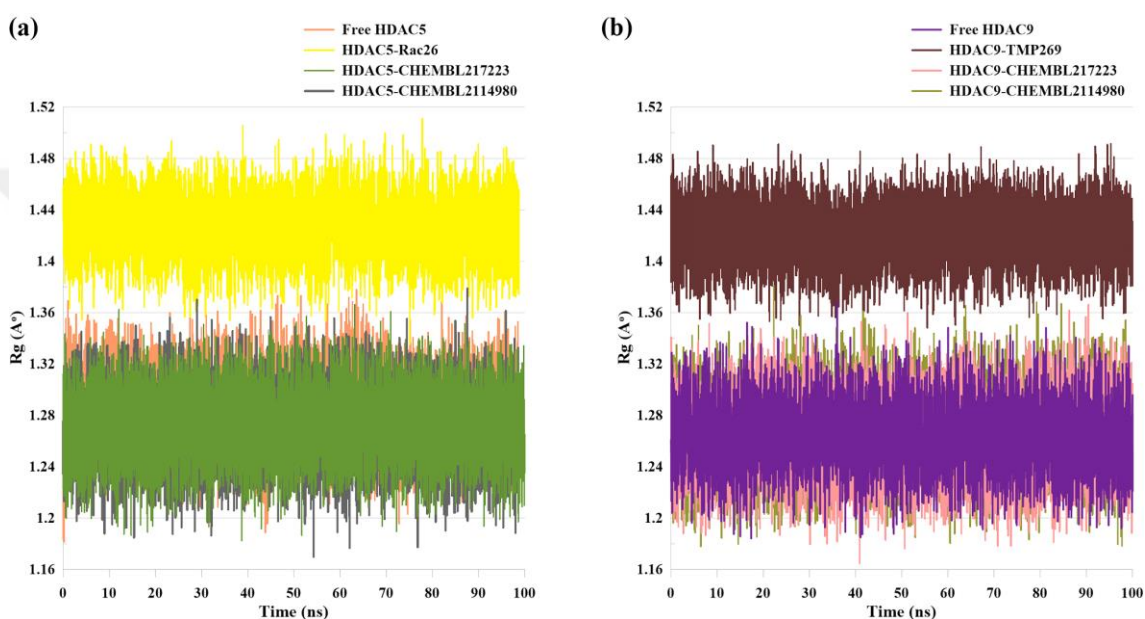


**Figure 3.14.** Radius of gyration ( $R_g$ ) plots of (a) free HDAC5 and HDAC5 complex with the Rac26 known inhibitor, CHEMBL2114980, CHEMBL217223; (b) free HDAC9 and HDAC9 complex with the TMP269 known inhibitor, CHEMBL2114980, CHEMBL217223.

Potential energy calculation is a valuable measurement to understand the system energy over time. The potential energy graphs proved that all the complexes were balanced and remained in their equilibrium state the whole time (Figure 3.15). The calculated average potential energy scores were as follows: free HDAC5 (-279857 kcal/mol); HDAC5-Rac26 (-277260 kcal/mol); HDAC5-CHEMBL2114980 (-277260 kcal/mol); HDAC5-CHEMBL217223 (-269160 kcal/mol); free HDAC9 (-210607 kcal/mol); HDAC9-TMP269 (-201857 kcal/mol); HDAC9-CHEMBL2114980 (-201857 kcal/mol); and HDAC9-CHEMBL217223 (-201857 kcal/mol).

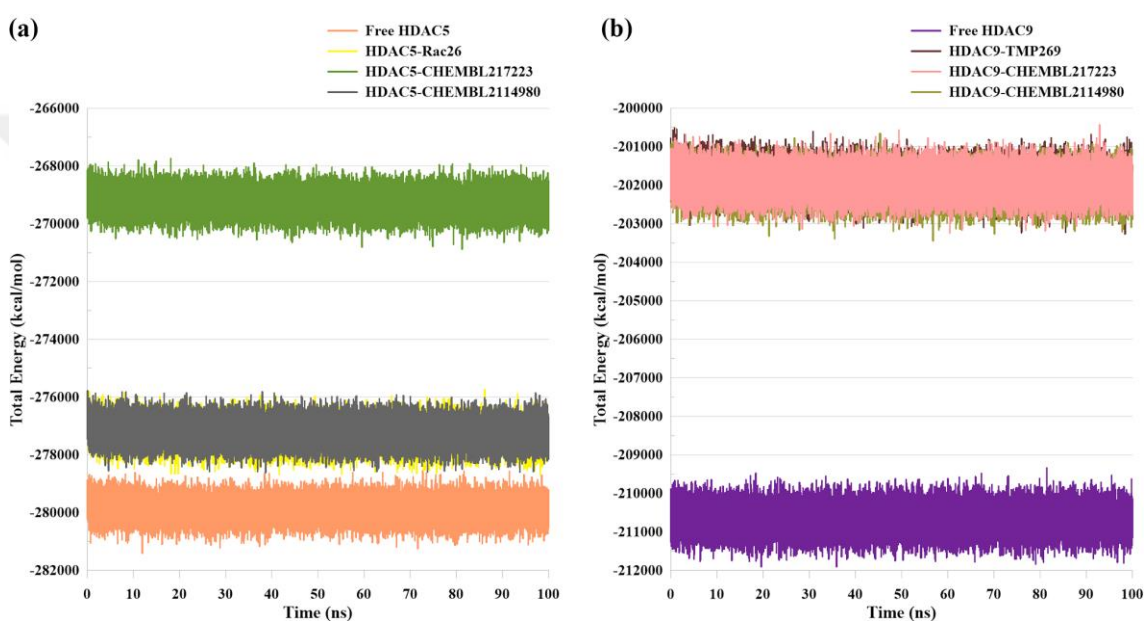


**Figure 3.15.** Potential energy graphs of (a) free HDAC5 and HDAC5 complex with the Rac26 known inhibitor, CHEMBL2114980, CHEMBL217223; (b) free HDAC9 and HDAC9 complex with the TMP269 known inhibitor, CHEMBL2114980, CHEMBL217223.

Even though hydrogen bonds are relatively weak noncovalent bonds, they play an important role in the molecules structure stability of nearly all living systems (E. N. Baker, 2006). In the present study, hydrogen bonds number profiles were estimated over time for all studied systems (Figure 3.16). Including all complexes, at least a single H-bond was formed and sustained throughout the MD simulation run. Relatively speaking, similar H-bond number profile was observed in the HDAC5/HDAC9-CHEMBL2114980 complexes. HDAC5-CHEMBL217223 complex displayed less H-bond number profile compared to HDAC9-CHEMBL217223 complex. These observations suggest that neither the complex stability nor the ligand quality are influenced by the H-bond number profile throughout the MD simulation run.

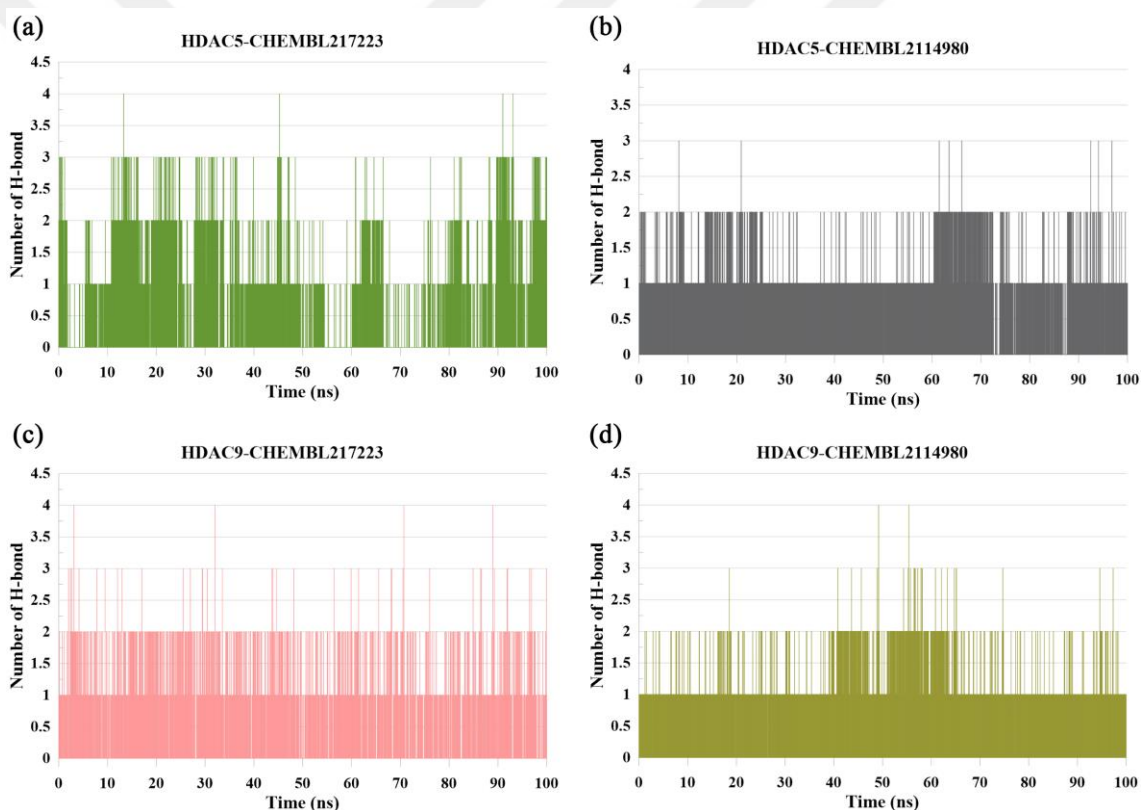


**Figure 3.16.** Plots of the number of hydrogen bonds in ligand-protein complexes: (a) HDAC5-CHEMBL217223, (b) HDAC5-CHEMBL2114980, (c) HDAC9-CHEMBL217223, (d) HDAC9-CHEMBL2114980.

### 3.1.9. Binding Free Energy (MM-PBSA) Calculations

Binding free energy (MM-PBSA) calculations were carried out in order to additionally assess the systematics of the compounds binding to HDAC5 and HDAC9 proteins throughout the MD simulation (Table 3.6). Compound CHEMBL2114980 showed the highest binding energy value of -60.78 kcal/mol when it was calculated in complex with HDAC9, while it showed a binding energy value of -48.00 kcal/mol with HDAC5. On the other hand, compound CHEMBL217223 showed a higher binding energy value with HDAC5 (-48.97 kcal/mol) compared to HDAC9 (-16.20 kcal/mol).

**Table 3.6.** Calculated binding free energy (MM-PBSA) of HDAC5 and HDAC9 complexes.

Complex	Binding Energy (kcal/mol)
HDAC5-CHEMBL217223	-48.9711 ± 8.4823
HDAC5-CHEMBL2114980	-48.0030 ± 8.8650
HDAC9-CHEMBL217223	-16.2084 ± 11.821
HDAC9-CHEMBL2114980	-60.7874 ± 9.3262

## 3.2. STRUCTURE-BASED DRUG DESIGNING OF ISOFORM SELECTIVE CLASS IIA HDACS INHIBITORS

### 3.2.1. Class Iia HDACs Structural and Sequence Alignment

Analysis of the entire amino acid sequence of all individual members of class Iia HDACs showed that these residues are similar within the active sites of this family class (Figure 2.2). Collectively, the overall sequence identity among this class of HDACs is 55.6% and sequences similarity is 71.5%. The catalytic sites among class Iia HDACs are highly conserved (Table 3.7). The highest conservation was seen between HDAC4 and HDAC5 with sequence similarity and identity of 89.6% and 76.2% respectively. While the least conservation was observed between HDAC7 and HDAC9 with sequence similarity and identity of 79.9% and 67.1% respectively. Analysis of the structural alignment of class Iia HDACs revealed that lowest RMSD value was between HDAC5 and HDAC9 with 0.311 Å. While the highest RMSD value was observed between HDAC5 and HDAC7 with 0.79 Å (Table 3.8). Analysis of the phylogenetic tree of human class Iia HDACs showed that HDAC4 and HDAC7 descendant from the same ancestor. Also, HDAC4

represents the same ancestor for both HDAC5 and HDAC9 (Figure 2.3). This information might be helpful in the discovery of isoform selective inhibitors due to the minor variation among the enzymes' active sites.

**Table 3.7.** Comparative analysis of sequence similarity (SIM) and identity (IDN) among class IIa HDACs in percentage %.

	HDAC4		HDAC5		HDAC7		HDAC9	
	<i>SIM</i>	<i>IDN</i>	<i>SIM</i>	<i>IDN</i>	<i>SIM</i>	<i>IDN</i>	<i>SIM</i>	<i>IDN</i>
<b>HDAC4</b>			89.6	76.2	83.6	71.8	87.2	73.4
<b>HDAC5</b>	89.6	76.2			81.5	67.2	88.0	74.9
<b>HDAC7</b>	83.6	71.8	81.5	67.2			79.9	67.1
<b>HDAC9</b>	87.2	73.4	88.0	74.9	79.9	67.1		

**Table 3.8.** Comparative analysis of the structural superimpose of class IIa HDACs. RMSD (Å) calculations are shown in Blue cells. Overlapping amino acid residues are shown in GREEN.

	HDAC4	HDAC5	HDAC7	HDAC9
<b>HDAC4</b>		402	319	381
<b>HDAC5</b>	0.53800		319	381
<b>HDAC7</b>	0.77900	0.79000		319
<b>HDAC9</b>	0.55100	0.31100	0.76700	

Hydrophobic surface illustrations of the active sites of class IIa HDAC proteins are contrasted in Figure 3.17. All individual members of class IIa HDACs have in common a relatively deep catalytic cavity, which is lined with hydrophilic amino acid residues close to the catalytic Zn<sup>2+</sup> ion, and hydrophobic amino acid residues at the entrance of the binding pocket. Additionally, they share relatively more H-bond donor residues than H-bond acceptor residues covering in the catalytic pocket (Figure 3.18).



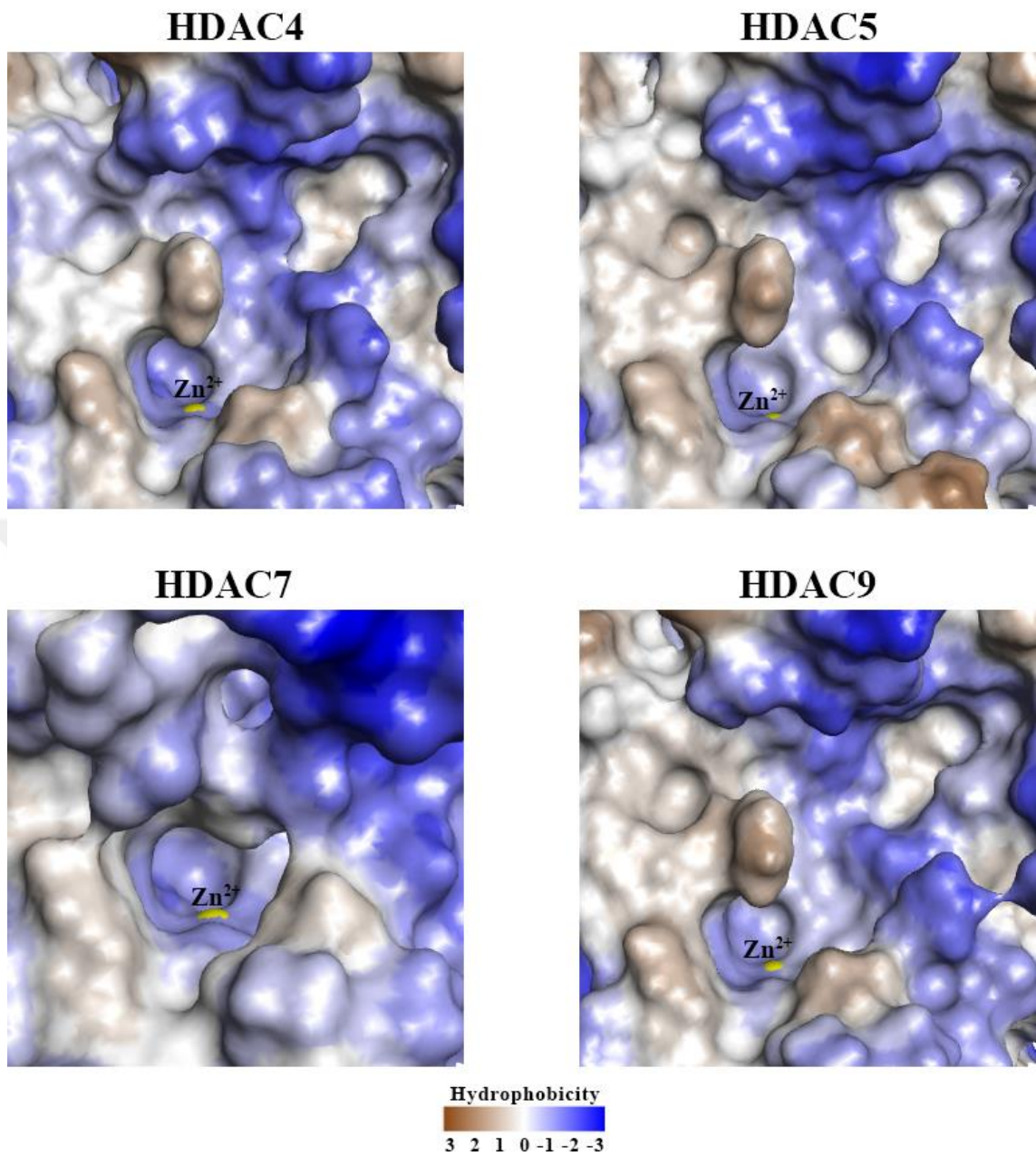


**Figure 3.17.** Hydrophobic surface illustrations of the active sites of class IIa HDAC proteins. The hydrophobicity degree varies from complete hydrophilicity (BLUE) to entirely hydrophobic (BROWN).

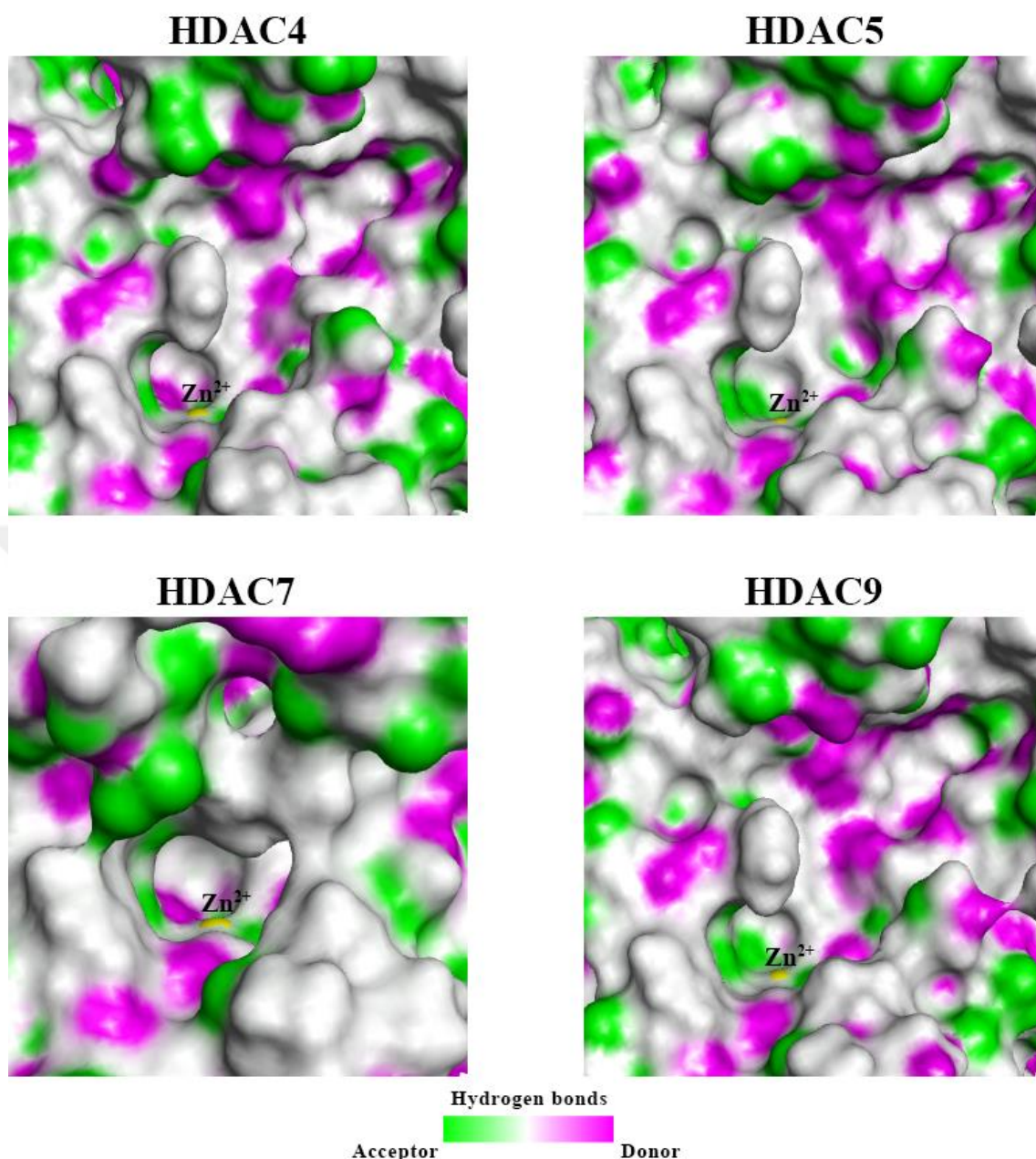


**Figure 3.18.** Hydrogen bonds surface illustrations of the active sites of class IIa HDAC proteins. H-bond acceptor residues are represented in GREEN, while H-bond donor residues are in PINK.

### 3.2.2. Virtual Screening Results

A total of fifteen compounds displayed potential selectivity towards their corresponding targets according to their calculated binding energy and estimated inhibitory constant ( $K_i$ ) (Table 3.9). Five compounds were selective for HDAC4 over the rest of class IIa HDACs; Three compounds were found to be selective for HDAC5; Six compounds selective for HDAC7; and one selective compound for HDAC9. The compounds selectivity indices



are given in Table 3.10. To obtain the selectivity of a certain compound for specific HDAC member of the class IIa, the  $K_i$  of the same compound for the four members of the HDAC is sorted from the lowest to the largest, and the second-lowest  $K_i$  is divided by the first lowest one. For example, compound CHEMBL2177655 has shown a variety of  $K_i$  values among class IIa HDACs, HDAC4 = 0.00805 nM, HDAC5 = 35.73 nM, HDAC7 = 0.864 nM, and HDAC9 = 19.88 nM. In that case,  $K_i$  of HDAC7 was divided by the  $K_i$  of HDAC4,  $0.864 \div 0.00805 = 107.32$ , which indicates that compound CHEMBL2177655 is preferentially selective for HDAC4 by 107~fold over HDAC7. Table 3.10 shows a detailed data about each compound  $K_i$  value and its selectivity for each member of the class IIa HDACs.

**Table 3.9.** Calculated binding energy by AutoDock 4.2 of the hit compounds against each member of class IIa HDACs. HDAC4 selective compounds are in green color, HDAC5 selective compounds are in blue color, HDAC7 selective compounds are in orange color, and HDAC9 selective compound is in yellow color.

#	Compound ID	HDAC4	HDAC5	HDAC7	HDAC9
		$\Delta G$ (kcal/mol)	$\Delta G$ (kcal/mol)	$\Delta G$ (kcal/mol)	$\Delta G$ (kcal/mol)
1	CHEMBL2177655	-15.14	-10.16	-12.36	-10.51
2	CHEMBL3126309	-15.04	-12.74	-12.64	-11.94
3	CHEMBL236510	-13.18	-11.93	-8.52	-11.7
4	ZINC000095945790	-11.44	-10.49	-10.06	-10.31
5	ZINC000001058982	-9.81	-8.98	-8.82	-8.93
6	ZINC000033260361	-10.61	-11.81	-10.37	-9.83
7	CHEMBL2426361	-10.01	-11.27	-9.63	-10.16
8	CHEMBL529211	-8.6	-9.6	-7.85	-8.68
9	CHEMBL1968496	-11.25	-9.59	-14.25	-9.91
10	ZINC000009640741	-11.97	-11.07	-14.67	-11.17
11	NSC 23217	-8.69	-7.42	-11.16	-8.22
12	ZINC000019704978	-11.37	-10.76	-13.35	-10.91
13	ZINC000514563218	-9.52	-9.75	-11.8	-9.81
14	ZINC000674197814	-9.08	-9.61	-11.49	-9.78
15	CHEMBL1761559	-7.16	-7.49	-5.93	-8.09

**Table 3.10.** Selectivity index of class IIa HDACs.  $K_i$  of specific HDAC is compared to the nearest  $K_i$  of others for the same compound.

Compounds	HDAC4			HDAC5			HDAC7			HDAC9			Selectivity Index			Selectivity
	$K_i^4$ (nM)	$K_i^5$ (nM)	$K_i^7$ (nM)	$K_i^9$ (nM)	$K_i^4/K_i^5$	$K_i^4/K_i^7$	$K_i^4/K_i^9$	$K_i^5/K_i^7$	$K_i^5/K_i^9$	$K_i^7/K_i^9$	$K_i^5/K_i^4$	$K_i^7/K_i^4$	$K_i^9/K_i^4$			
CHEMBL2177655	0.0080	35.73	0.8640	19.88	4438	107	2469	HDAC4/HDAC7								
CHEMBL3126309	0.0094	0.458	0.5460	1.780	48	58	189	HDAC4/HDAC5								
CHEMBL236510	0.2190	1.790	568.00	2.680	8	2593	12	HDAC4/HDAC5								
ZINC000095945790	4.0900	20.00	42.050	27.00	5	10	7	HDAC4/HDAC5								
ZINC000001058982	64.650	261.0	342.00	282.0	4	5	5	HDAC4/HDAC5								
ZINC000033260361	16.590	2.200	25.020	62.48	$K_i^4/K_i^5$	$K_i^7/K_i^5$	$K_i^9/K_i^5$	HDAC5/HDAC4								
CHEMBL2426361	45.920	5.460	86.690	35.60	8	16	7	HDAC5/HDAC9								
CHEMBL529211	492.00	91.00	1750.0	433.0	5	19	5	HDAC5/HDAC4								
CHEMBL1968496	5.6200	94.20	0.0360	54.68	$K_i^4/K_i^7$	$K_i^5/K_i^7$	$K_i^9/K_i^7$	HDAC7/HDAC4								
ZINC000009640741	1.6700	7.680	0.0175	6.540	156	2616	1518	HDAC7/HDAC4								
NSC 23217	426.00	3610	6.6300	938.0	95	438	373	HDAC7/HDAC4								
ZINC000019704978	4.6500	12.99	0.1650	9.990	64	544	141	HDAC7/HDAC4								
ZINC000514563218	104.80	71.18	2.2400	64.11	28	78	60	HDAC7/HDAC4								
ZINC000674197814	219.53	89.90	3.7700	67.91	46	31	28	HDAC7/HDAC9								
CHEMBL1761559	5670.0	3230	44950	1160	58	23	18	HDAC7/HDAC9								
					$K_i^4/K_i^9$	$K_i^5/K_i^9$	$K_i^7/K_i^9$									
					5	3	38	HDAC9/HDAC5								

The top two ranked compounds that showed potential selectivity for HDAC4 over other HDACs are CHEMBL2177655 and CHEMBL3126309 (Figure 3.19). Compound CHEMBL2177655 was found to have the highest binding affinity among all studied compounds, with a binding energy of -15.14 kcal/mol and an inhibitory constant of 8.0 pM (0.0080 nM). Compound CHEMBL2177655 revealed a potential selectivity for HDAC4 ranging from ~ 107 to 4400-fold compared to HDACs 5, 7 and 9. The second top-ranked compound, CHEMBL3126309 showed the second-highest affinity and selectivity for HDAC4, with a binding energy of -15.04 kcal/mol and an inhibitory constant of 9.4 pM (0.0094 nM). Compound CHEMBL3126309 displayed a promising selectivity for HDAC4 ranging from ~ 48 to 189-fold compared to HDACs 5, 7 and 9.

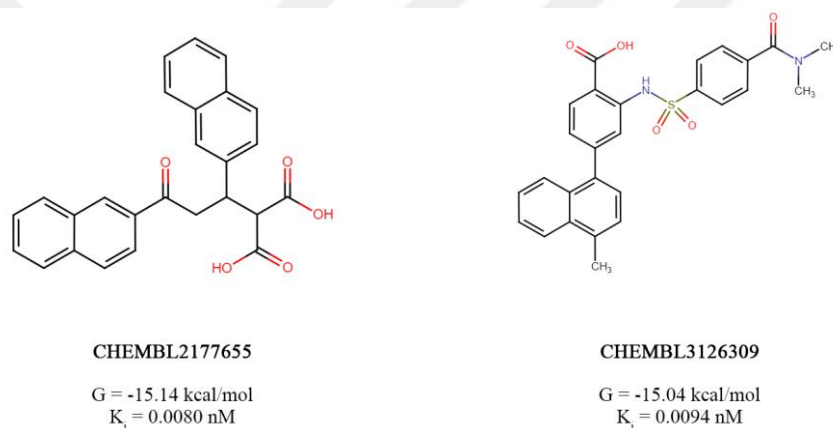


**Figure 3.19.** Top two-ranked selective compounds for HDAC4.

CHEMBL2177655 and CHEMBL3126309 compounds spanned the HDAC4 active site in very similar ways. They both interacted with the key amino acid residues in the catalytic site by several types of chemical interactions including hydrogen bonds, van der Waals interactions, attractive charge,  $\pi$ - $\pi$  stacked,  $\pi$ - $\pi$  T-shaped,  $\pi$ -alkyl, alkyl,  $\pi$ -cation. Both compounds interacted with the catalytic Zn<sup>2+</sup> metal atom through their carboxyl groups by covalent bonds (Figure 3.20 and Figure 3.21).

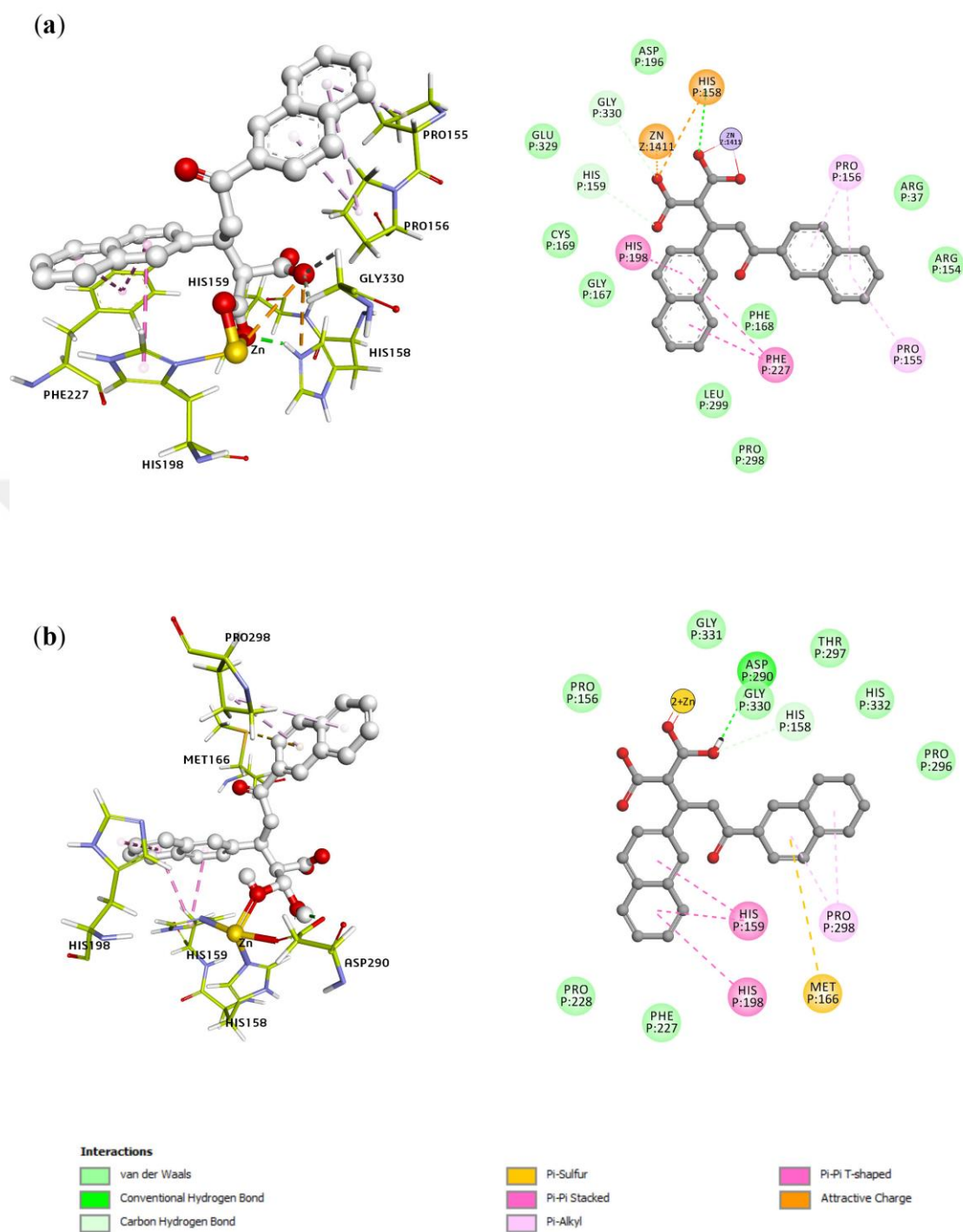


**Figure 3.20.** 2D and 3D illustrations of CHEMBL2177655 bound to HDAC4 (a) after molecular docking study; (b) after MD simulation.

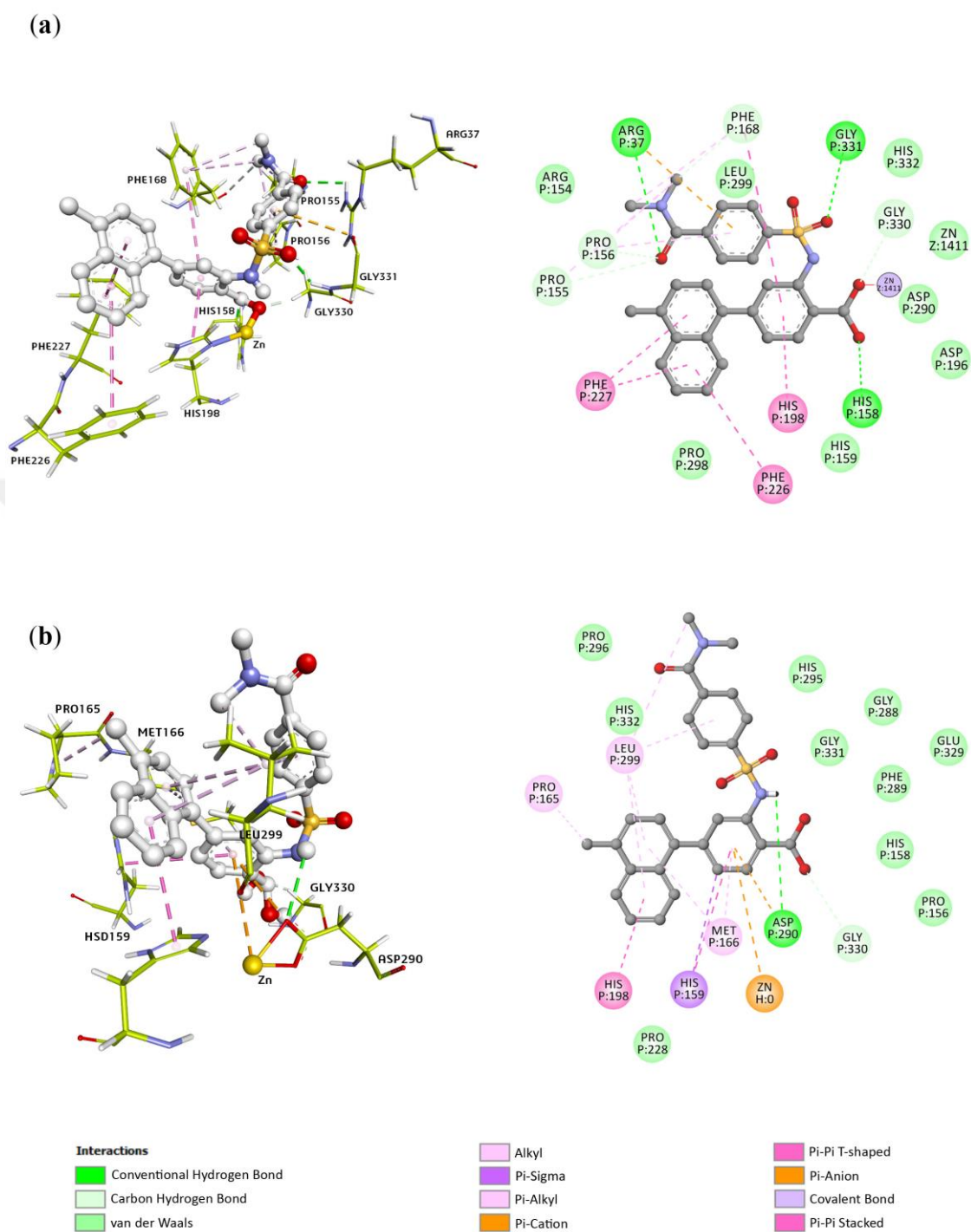


**Figure 3.21.** 2D and 3D illustrations of CHEMBL3126309 bound to HDAC4 **(a)** after molecular docking study; **(b)** after MD simulation.

Thorough molecular docking study identified three moderate HDAC5 isoform selective compounds, and the top two-ranked compounds are ZINC000033260361 and CHEMBL2426361 (Figure 3.22). Compound ZINC000033260361 bonded to HDAC5 with a binding energy of -10.61 kcal/mol and an inhibitory constant ( $K_i$ ) of 16.59 nM. In comparison to all class IIa HDACs, the ZINC000033260361 compound revealed a moderate selectivity for HDAC5 ranging between  $\sim 8$  to 28-fold. On the other hand, compound CHEMBL2426361 was the second HDAC5 isoform selective compound which showed a binding energy of -10.01 kcal/mol and an inhibitory constant ( $K_i$ ) of 45.92 nM. Compound CHEMBL2426361 exhibited a moderate isoform selectivity for HDAC5 ranging from 7 to 16-fold over the rest of class IIa HDACs family.

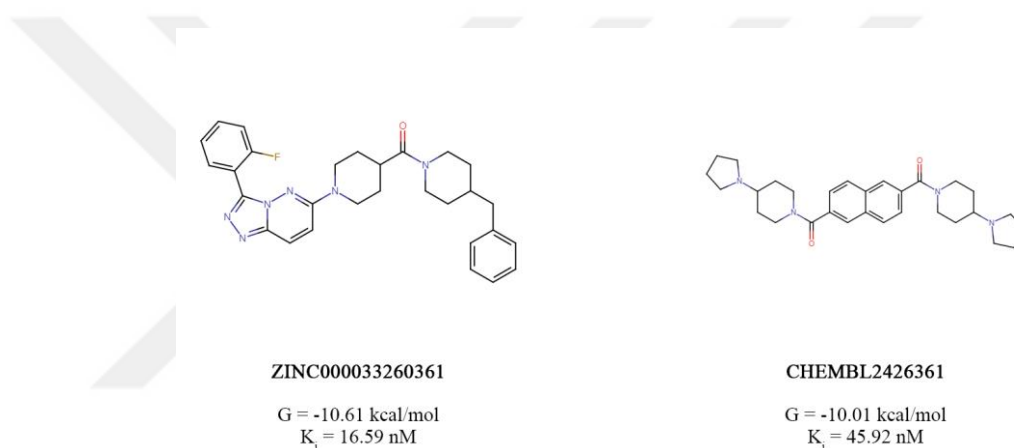


**Figure 3.22.** The top two-ranked selective compounds for HDAC5.

Both compounds, ZINC000033260361 and CHEMBL2426361, extend over the catalytic channel of HDAC5 relatively in the same binding mode (Figure 3.23 and Figure 3.24). Both compounds interacted with the active amino acid residues within the binding pocket through different chemical interactions including salt bridge interaction, van der Waals interactions, hydrogen bonds,  $\pi$ -cation,  $\pi$ -sulfur interaction, alkyl,  $\pi$ -alkyl, amide- $\pi$  stacked interactions. In addition, ZINC000033260361 compound had two distinctive interactions through its fluorobenzene group, a covalent bond with the catalytic  $Zn^{2+}$  ion, and a halogen interaction with Asp291 residue of HDAC5.

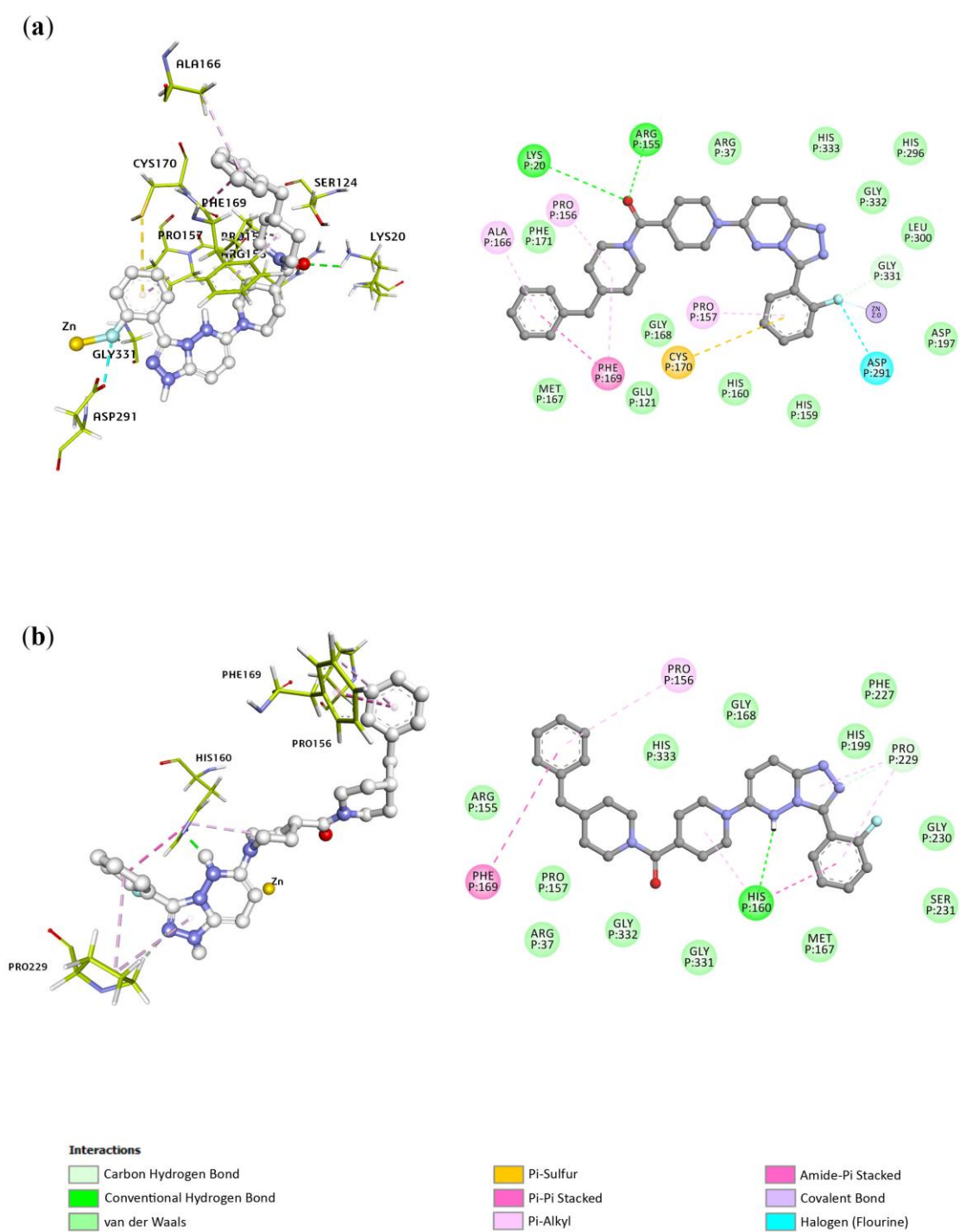


**Figure 3.23.** 2D and 3D schemes of ZINC000033260361 bound to HDAC5 **(a)** after molecular docking study; **(b)** after MD simulation.



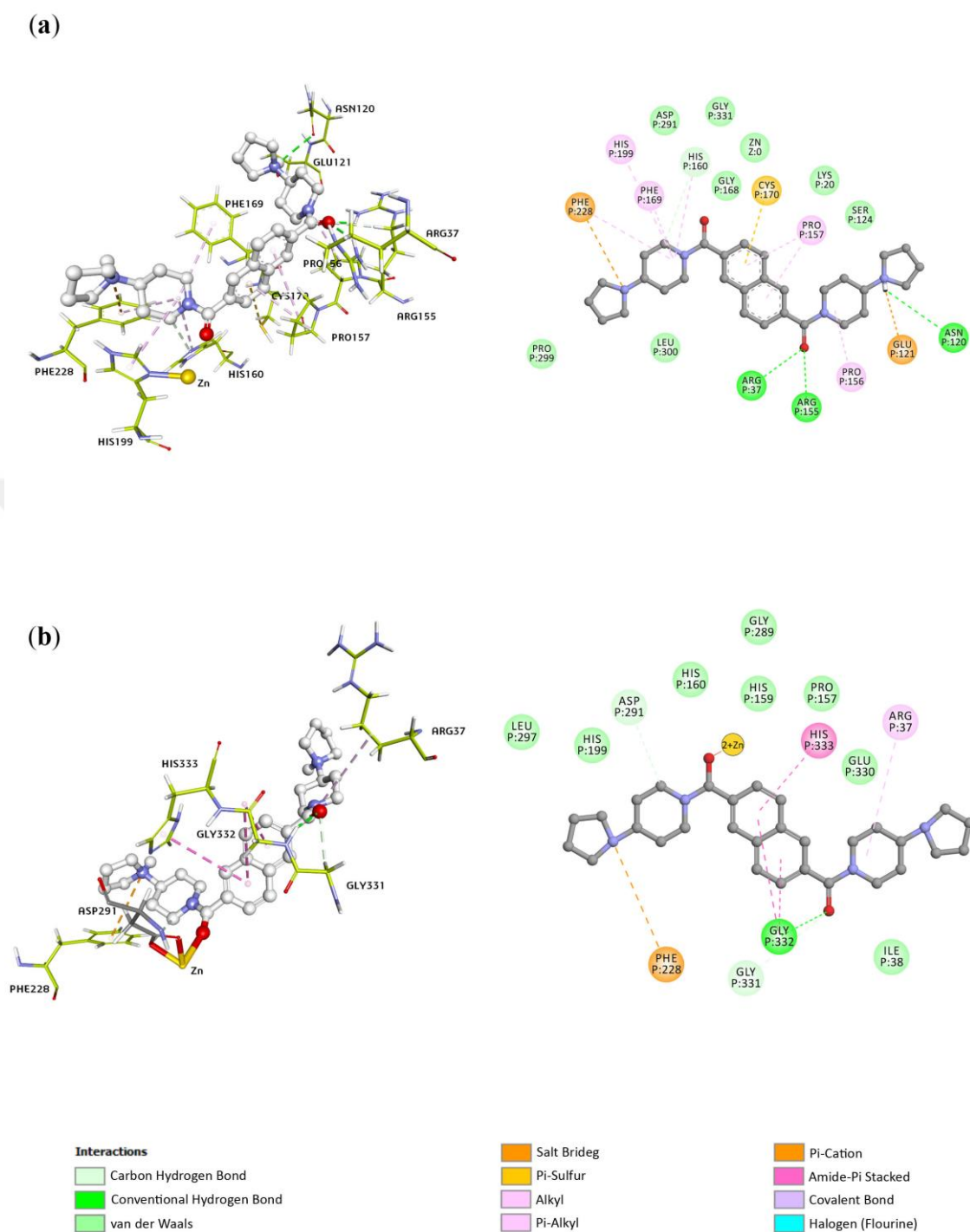


**Figure 3.24.** 2D and 3D illustrations of CHEMBL2426361 bound to HDAC5 (a) after molecular docking study; (b) after MD simulation.

The structure-based virtual screening identified six promising HDAC7 enzyme selective drug-like compounds that showed a diversity in the binding affinity level. According to the binding affinity, the top two compounds are ZINC000009640741 and CHEMBL1968496 (Figure 3.25). The first top-ranked molecule, ZINC000009640741,



demonstrated the highest binding affinity towards HDAC7 with the lowest binding energy (-14.67 kcal/mol) and has an inhibitory constant of 0.0175 nM (17.5 pM). The second compound, CHEMBL1968496, showed a binding energy with a score of -14.25 kcal/mol and an inhibitory constant  $K_i$  of 0.036 nM (36 pM). Compound ZINC000009640741 favorably bonded to HDAC7 with a selectivity index ranging between ~ 95 to 438-fold compared to the rest of the class IIa HDACs. Whereas compound CHEMBL1968496 preferentially expressed higher selectivity towards HDAC7 compared to HDACs 4, 5, and 9 (about 156 to 2616-fold).

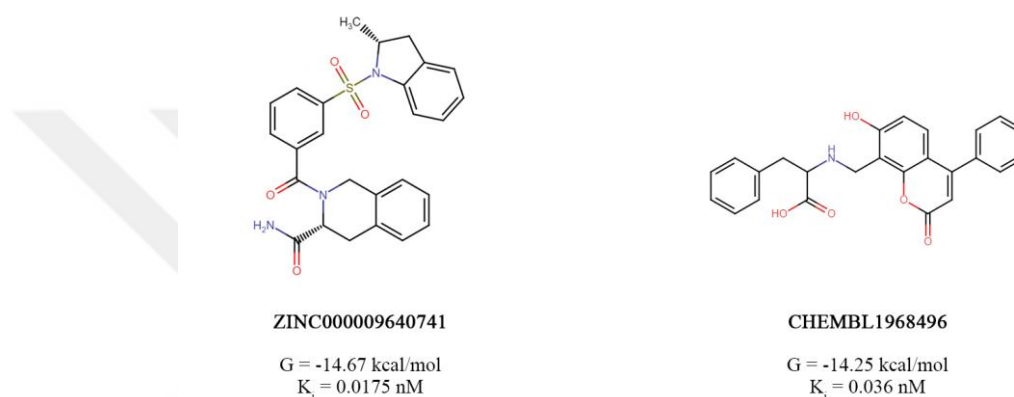


**Figure 3.25.** The top two-ranked HDAC7 selective compounds.

Both compounds, ZINC000009640741 and CHEMBL1968496, spanned the deep catalytic tunnel of the active site of HDAC7, where they interacted with most of the key amino acid residues in the active site. ZINC000009640741 compound was found to be interacted with  $Zn^{2+}$  ion through its hydroxyl group by a covalent bond, while compound CHEMBL1968496 was covalently bonded to the  $Zn^{2+}$  ion through its carboxyl group (Figure 3.26 and Figure 3.27). The common prevalent interactions of these two compounds included hydrogen bonds, van der Waals interactions,  $\pi$ - $\pi$  stacked,  $\pi$ - $\pi$  T-shaped,  $\pi$ -alkyl, alkyl, and amide- $\pi$  stacked interactions.  $\pi$ -donor hydrogen bond was seen specifically in ZINC000009640741 compound with Gly339, and a  $\pi$ -anion interaction was formed between the benzene ring of CHEMBL1968496 and the Asp298 residue.

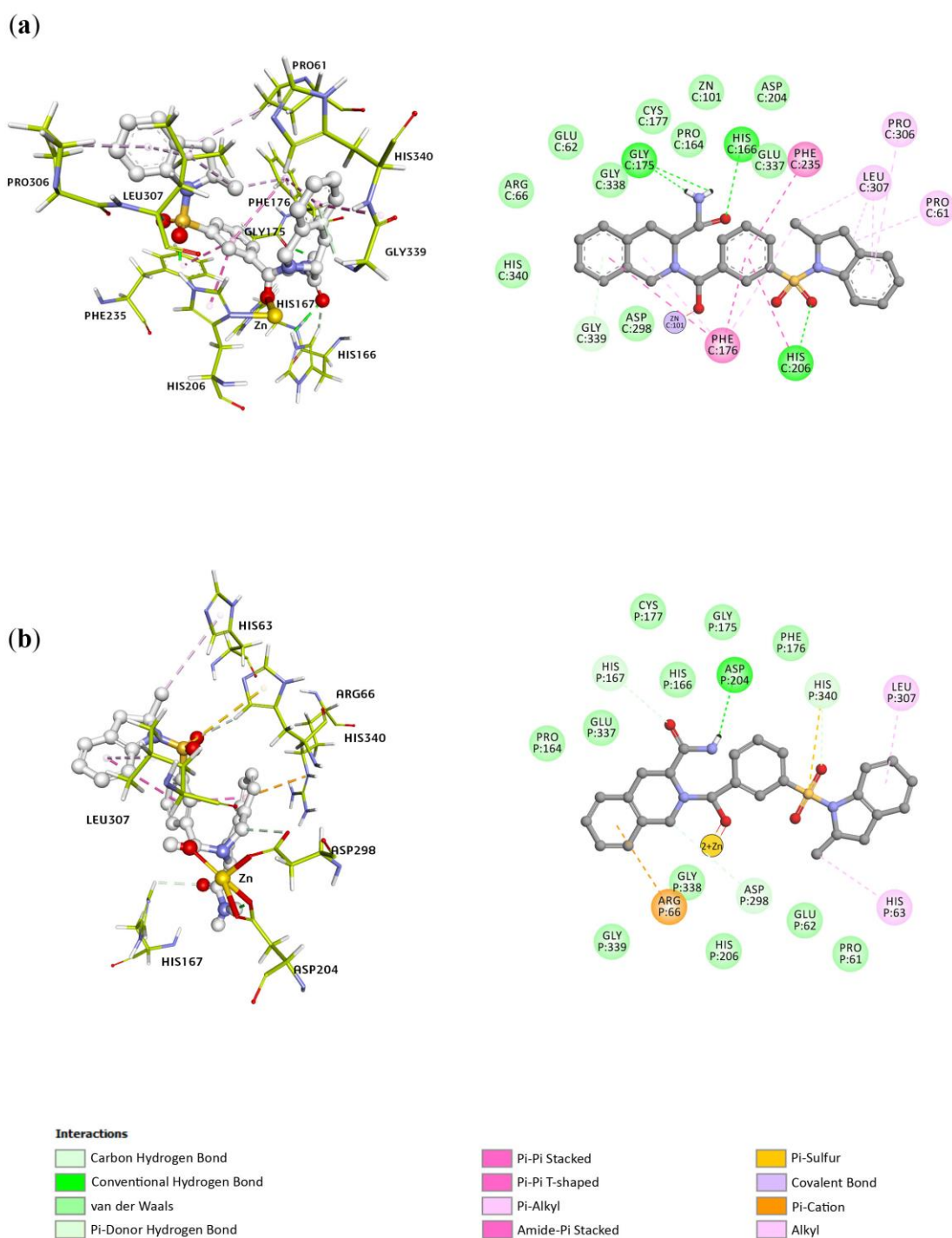


**Figure 3.26.** 2D and 3D presentations of ZINC000009640741 bound to HDAC7 (a) after molecular docking study; (b) after MD simulation.

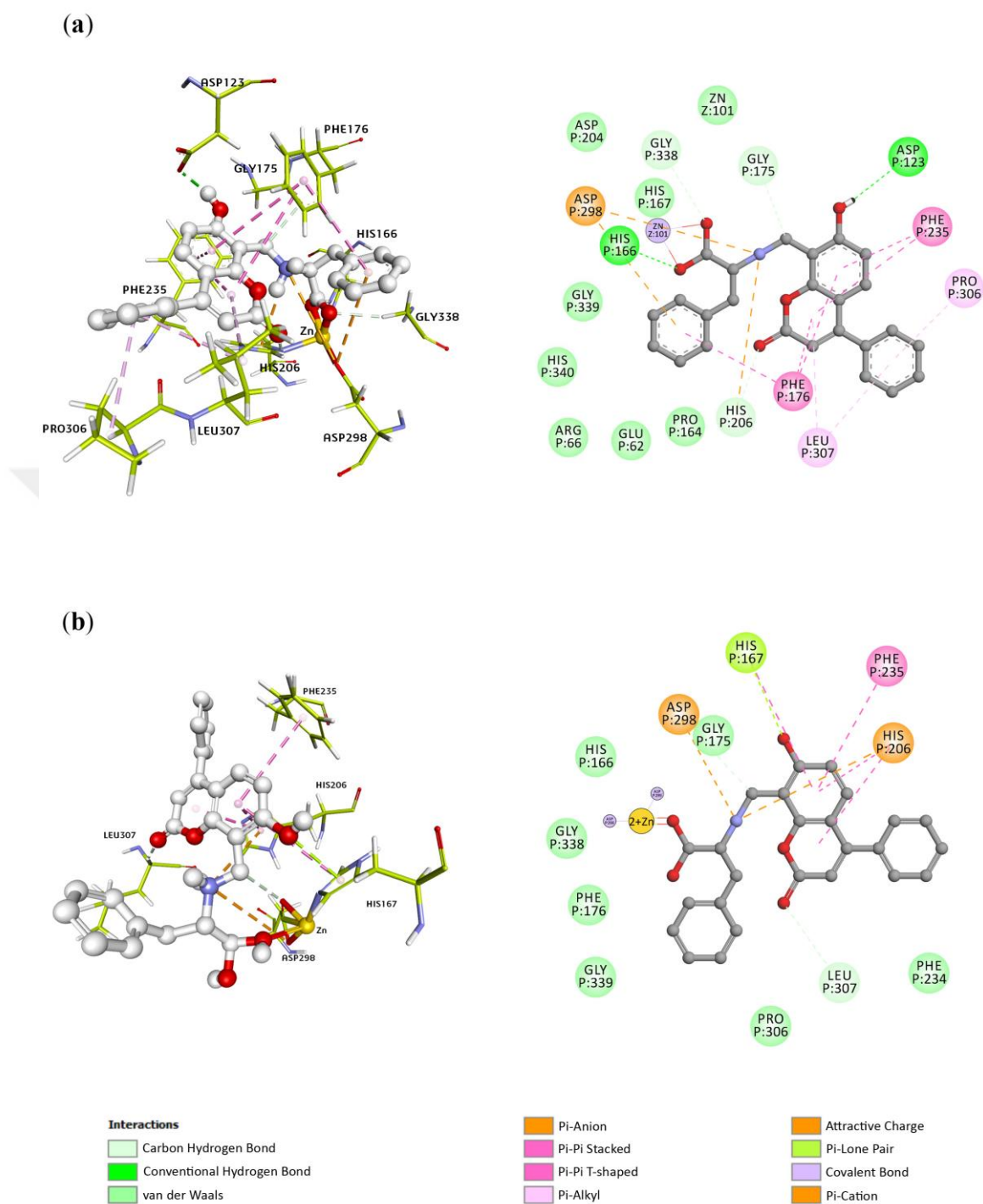
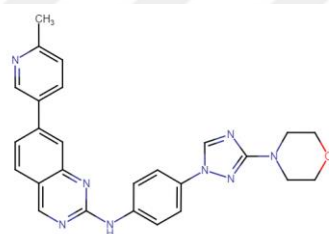


**Figure 3.27.** 2D and 3D illustrations of CHEMBL1968496 bound to HDAC7 (a) after molecular docking study; (b) after MD simulation.

Lastly, VS application identified compound CHEMBL1761559, which displayed a binding energy of -8.09 kcal/mol and an inhibitory constant ( $K_i$ ) of 1160 nM against HDAC9 (Figure 3.28). CHEMBL1761559 covered the binding pocket of HDAC9 and interacted with several active residues within the catalytic pocket such as two hydrogen bonds with His199 and Phe169, and a  $\pi$ - $\pi$  T-shaped interaction with Phe19. A  $\pi$ -cation interaction was seen between the  $Zn^{2+}$  ion and the benzene ring of the compound. Additionally, other significant interactions were observed with several amino acid residues in the active site including hydrogen bonds, van der Waals interactions,  $\pi$ -alkyl, and alkyl interactions (Figure 3.29). CHEMBL1761559 compound exhibited modest selectivity for HDAC9 in comparison to the remaining class IIa members with a selectivity index ranging from ~ 3 to 38-fold.

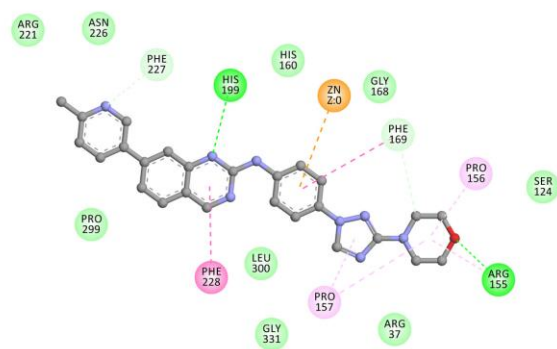
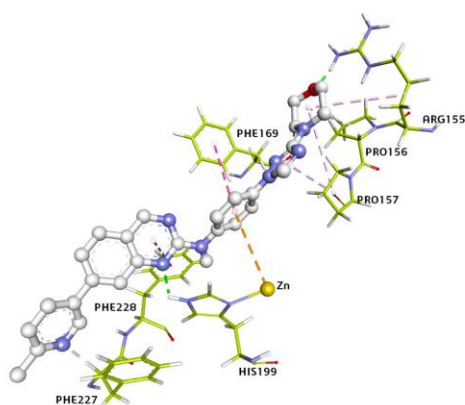


CHEMBL1761559

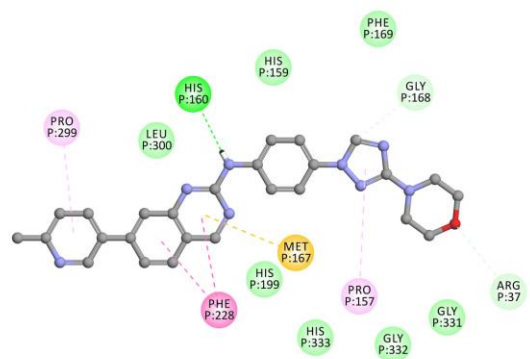
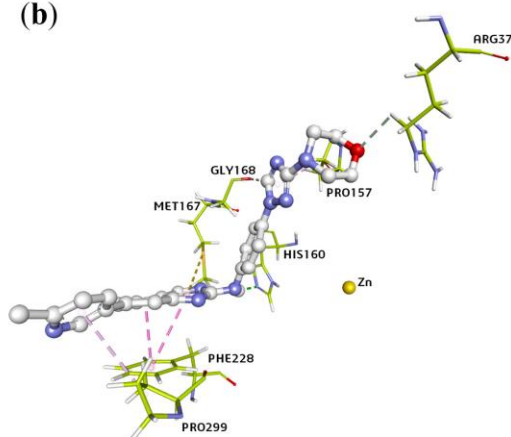
G = -8.09 kcal/mol  
 $K_i$  = 1160 nM

**Figure 3.28.** The 2D structure of compound CHEMBL1761559.

(a)



(b)



**Interactions**

Carbon Hydrogen Bond

Conventional Hydrogen Bond

van der Waals

Pi-Pi Stacked

Pi-Pi T-shaped

Pi-Alkyl

Pi-Sulfur

Pi-Cation

Alkyl

**Figure 3.29.** 2D and 3D illustrations of CHEMBL1761559 bound to HDAC9 (a) after molecular docking study; (b) after MD simulation.

### 3.2.3. ADMET Profile and PAINS Filtration

The predicted ADMET profile of the 15 top-ranked compounds from the virtual screening is given in Table 3.11 along with their drug-likeness properties. These properties were predicted using the admetSAR and SwissADME web servers. According to Lipinski's rule of 5, oral drugs must obey at least three of four properties: the molecular weight should not exceed 500 Dalton; the total number of hydrogen bond acceptors (including oxygen and nitrogen) must not exceed 10; the total number of hydrogen bond donors (including -OH and -NH) should not exceed 5; and the octanol-water partition coefficient (LogP) must not be more than 5 (or 4.15 as in Moriguchi model MLogP) (Lipinski et al., 2001; Moriguchi et al., 1992). In addition, other important ADMET properties including water/aqueous solubility (LogS) should be  $> -5$ ; the topological polar surface area (TPSA) must be less or equal to  $140 \text{ \AA}^2$ ; and human colorectal adenocarcinoma cells (Caco-2) Caco-2 permeability (cm/s) must be faster than  $22 \text{ nm/s}$ . All the 15 compounds obeyed the Lipinski's rule of five except for two compounds ZINC000033260361 and NSC 23217 where they had a MLogP more than 4.15. Even though, it is tolerated to have one violation of the rule of five for oral drugs according to Lipinski's rule (Lipinski et al., 2001). Although compounds ZINC000514563218 and ZINC000674197814 exhibited a slightly increase in the TPSA with a value of  $145.2 \text{ \AA}^2$ , rational intestinal permeability can still be seen in drugs with a TPSA ranging between 140 and  $150 \text{ \AA}^2$  (Lipinski, 2003). The prediction of the Caco-2 permeability and the water solubility for all the 15 compounds were found to be within the normal range. Furthermore, the 15 top-ranked compounds have been proved to be PAINS-free compound.

**Table 3.11.** Physicochemical properties of the 15 hits, including ADMET profiles and Lipinski's rule of five parameters.

	Compound	Lipinski violations	MW	HA	HD	MLogP	TPSA	HIA	Caco-2	WS
1	CHEMBL2177655	0	412.43	5	2	3.61	91.67	0.9943	0.857	-3.008
2	CHEMBL3126309	0	488.55	5	2	2.47	112.16	0.8998	0.7953	-3.63
3	CHEMBL236510	0	485.62	4	2	3.27	76.64	0.9259	0.7631	-3.08
4	ZINC000095945790	0	489.48	5	2	2.73	117.16	0.9196	0.821	-3.271
5	ZINC00001058982	0	492.45	7	1	4.05	86.22	0.9268	0.6646	-3.616
6	ZINC000033260361	1	498.59	5	0	5.4	66.63	0.9845	0.7621	-3.379
7	CHEMBL2426361	0	488.66	4	0	3.39	47.1	0.993	0.798	-3.107
8	CHEMBL529211	0	452.59	2	3	3.35	54.53	0.9846	0.6446	-2.884
9	ZINC000009640741	0	475.56	4	1	2.48	109.16	0.9701	0.7725	-3.5
10	CHEMBL1968496	0	415.44	6	3	0.56	99.77	0.8145	0.9147	-2.998
11	NSC 23217	1	404.53	0	2	5.37	56.15	0.964	0.5672	-4.616
12	ZINC000019704978	0	448.52	4	2	3.52	86.8	0.9904	0.8016	-2.739
13	ZINC000514563218	0	484.47	8	1	2.6	145.2	0.9771	0.8338	-3.376
14	ZINC000674197814	0	470.44	8	1	1.84	145.2	0.9771	0.8404	-3.277
15	CHEMBL1761559	0	464.52	6	1	2.6	93.88	0.9956	0.8111	-2.754

MW: Molecular weight, Da.

HA: Total number of H-bond acceptors, O and N.

HD: Total number of H-bond donors, OH and NH.

TPSA: Topological polar surface area, Å<sup>2</sup>.

HIA: Human intestinal absorption.

WS: Water solubility, LogS

### 3.2.4. Molecular Dynamics MD Simulation

- **RMSD analysis:** The root mean square deviation (RMSD) of the HDAC4 apo-protein (inhibitor-free), HDAC4-hydroxamic acid inhibitor (known inhibitor), HDAC4-CHEMBL2177655, and HDAC4-CHEMBL3126309 profiles have been evaluated throughout the 100 ns MD simulations (Figure 3.30 (a)). HDAC4 apo-protein showed an initial increase till 20 ns around 4 Å, then remained stable between 3 and 3.5 Å till the end of the MD simulation. HDAC4-hydroxamic acid complex exhibited a higher fluctuation compared to the apo-protein, where the RMSD fluctuated between 2 and 5 Å till the 64 ns and thereafter displayed stable trend around 5 Å. The RMSD of the HDAC4-CHEMBL2177655 complex at first rose to 4.7 Å around 17 ns then gradually fell down to 4 Å around 55 ns and thereafter remained stable around 4.1 Å until the end of the MD simulation. Similarly, the RMSD of the HDAC4-CHEMBL3126309 ascended to 4.8 Å till 13 ns and then fell down to 3.7 Å near 62 ns and remained fluctuating between 3.5 and 4.2 Å until the end of the 100 ns run.

RMSD profiles were calculated during the 100 ns MD simulations for the HDAC5 apo-protein (ligand-free), HDAC5-Rac62 (known inhibitor), HDAC5-ZINC000033260361,

and HDAC5-CHEMBL2426361 (Figure 3.30 (b)). HDAC5 apo-protein RMSD was observed to slowly rise up to 3.4 Å around 12 ns and afterward it showed steady stable nature with an average RMSD of 3.2 Å to 100 ns. The average RMSD of HDAC5-CHEMBL3110016 (Rac-26 known inhibitor) was found to be 4.5 Å between the 22 ns and until the end of the MD run. The RMSD of HDAC5-ZINC000033260361 and HDAC5-CHEMBL2426361 complexes were well converged and exhibited relatively comparable stability after the 32 ns with an average of 4.6 Å and 4.4 Å, respectively.

The RMSD of the HDAC7 apo-protein, HDAC7-Trichostatin A, HDAC7-ZINC000009640741, and HDAC7-CHEMBL1968496 were analyzed after the MD run and presented in Figure 3.30 (c). Remarkably, all HDAC7 complexes retained their steady-stable equilibrium below 3.5 Å throughout the MD simulation. The RMSD of the free HDAC7 protein initially increased to 3.2 Å around 25 ns and later kept slowly decreasing through time to reach 2.1 Å around 100 ns. Both HDAC7-ZINC000009640741 and HDAC7-CHEMBL1968496 systems were shown to display similar minor fluctuation and stability state after the 47 ns with an average RMSD of 3.3 Å and 3.1 Å, respectively.

Lastly, the RMSD analysis was performed for the free HDAC9 protein, HDAC9-TMP269 (known inhibitor), and HDAC9-CHEMBL1761559 during the 100 ns MD run (Figure 3.30 (d)). The free HDAC9 RMSD was seen to rise up to 5.2 Å around 37 ns and then fluctuated between 3.4 Å and 4.6 Å during the 53 and 57 ns and thereafter remained in equilibrium state until the end of the MD run. HDAC9-TMP269 RMSD profile was observed to gradually elevated up to 5.2 Å around 34 ns and then decreased to 4.6 Å over 43 ns and remained in its equilibrium state until the end. The RMSD of HDAC9-CHEMBL1761559 preliminary increased to 5.5 Å until 43 ns and then stabilized until the end of the 100 ns with an average RMSD of 5.2 Å.



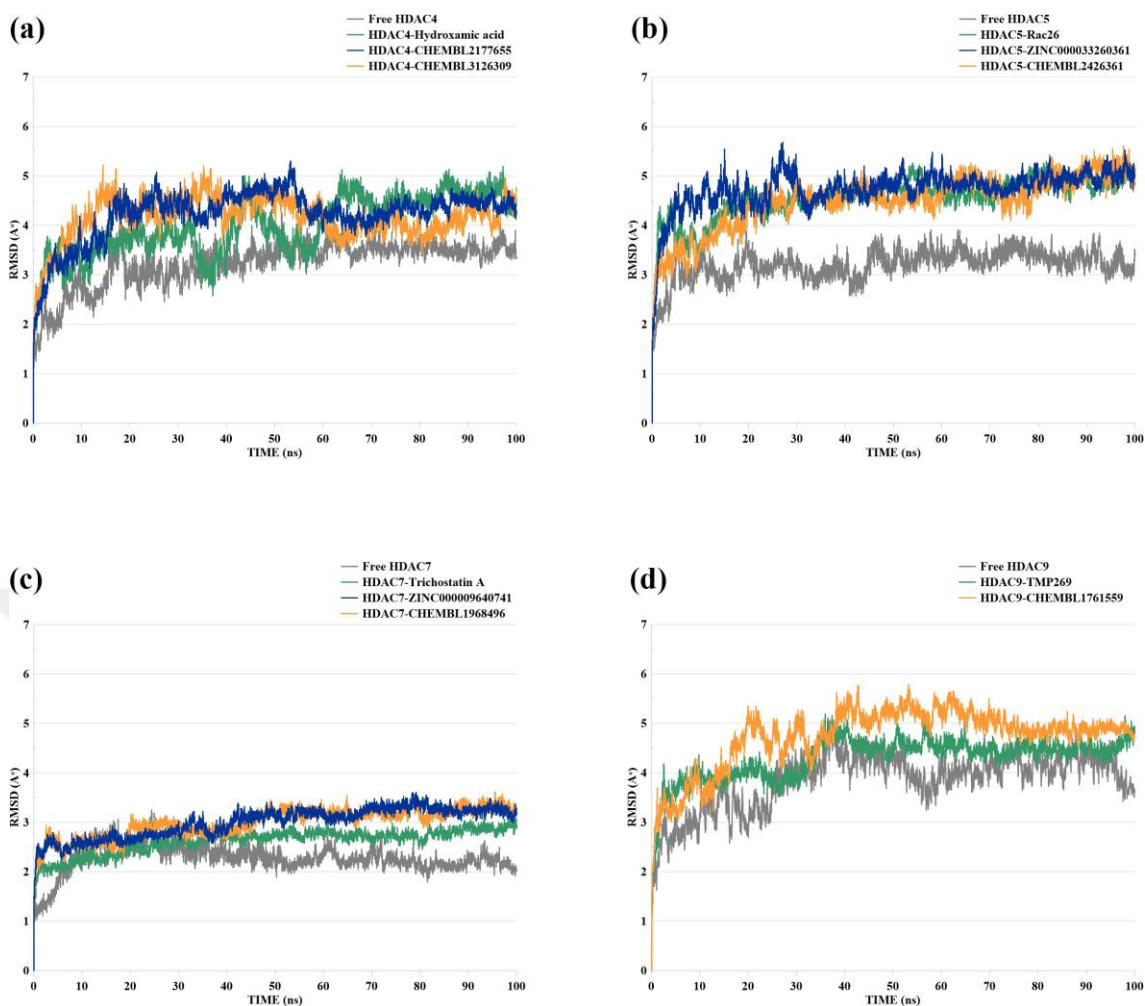


**Figure 3.30.** The root mean squared deviation (RMSD) plots of (a) HDAC4 systems; (b) HDAC5 systems; (c) HDAC7 systems; and (d) HDAC9 systems.

- RMSF analysis:** In order to fully assess the dynamics of the protein's backbone, the root mean square fluctuation (RMSF) profile was analyzed for all amino acids throughout the MD simulation. RMSF helps in describing local variations during the MD run along the protein sequence. During MD simulations, higher RMSF profiles are presented by higher flexible regions within the protein such as loops. High stable regions of the proteins are indicated by the low RMSF values and highly flexible atoms are located within loops regions. RMSF analysis of HDAC4 apo-protein, HDAC4-hydroxamic acid, CHEMBL2177655, and HDAC4-CHEMBL3126309 are shown in Figure 3.31 (a). The RMSF of the HDAC5 apo-protein (ligand-free), HDAC5-Rac62 (known inhibitor), HDAC5-ZINC000033260361, and HDAC5-CHEMBL2426361 are illustrated in Figure 3.31 (b). The RMSF of the HDAC7 apo-protein (free protein), HDAC7-Trichostatin A, HDAC7-ZINC00009640741, and HDAC7-CHEMBL1968496

are shown in Figure 3.31 (c). The RMSF profile of the free HDAC9 protein, HDAC9-TMP269 (known inhibitor), and HDAC9-CHEMBL1761559 during the 100 ns MD runs are presented in Figure 3.31 (d). The highest peaks in the RMSF plots represent the loop regions that are known for their high flexibility. These regions include the following amino acid residues: HDAC4 (Leu17-Gly36, Thr81, Asn82, Gln87-Leu94, and Phe102-Ile117); HDAC5 (Lue19-Gly36, Thr81-Pro83, Lys88-Leu94, and Lys101-Val118); HDAC7 (Leu48-Ala64 and Thr110-Ser131); HDAC9 (Lue19-Gly36, Thr81, Asn82, Lys88-Leu94, and Lys101-Ile118).

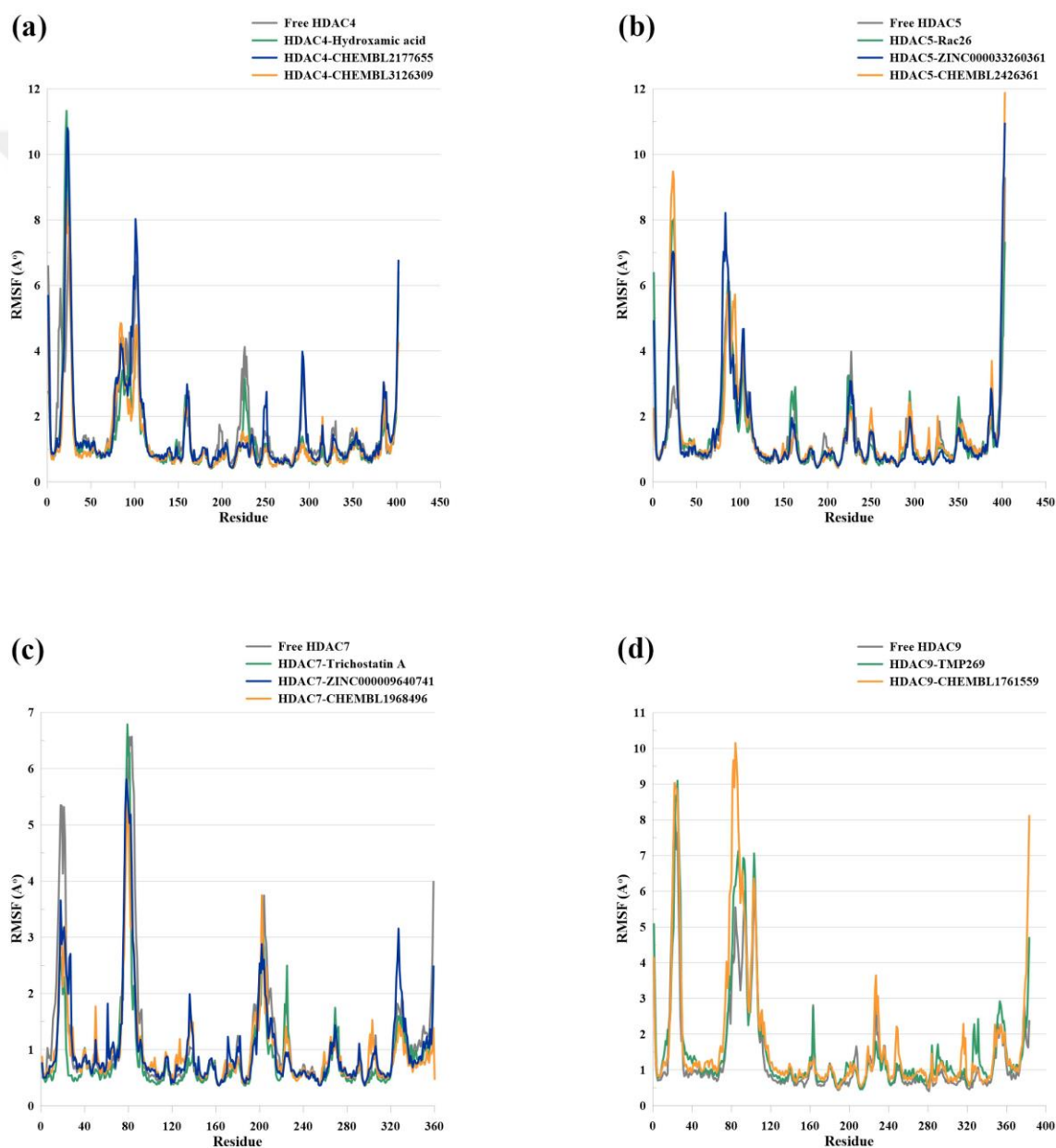


**Figure 3.31.** The root mean squared fluctuation (RMSF) plots of (a) HDAC4 systems; (b) HDAC5 systems; (c) HDAC7 systems; and (d) HDAC9 systems.

- **Radius of gyration (Rg) analysis:** Analysis of the compactness level of a protein is useful to fully understand the protein folding level. This analysis is denoted by the radius of gyration (Rg). Higher degree of Rg describes higher flexibility of the protein, while lower level of Rg implies less flexibility. Furthermore, steady level of Rg indicates firmly folded protein, whereas changes in Rg values refer to alteration in protein folding. The Rg of HDAC4 systems seemed to be stable throughout the MD run with average values of 1.37 Å for both the apo-protein and HDAC4-hydroxamic acid complex, 1.27 Å for HDAC4-CHEMBL2177655, and 1.38 Å for HDAC4-CHEMBL3126309 (Figure 3.32 (a)). The Rg profile of all HDAC5 systems were also remained stable during the 100 ns MD simulations with average Rg of 1.28 Å for the apo-protein, 1.42 Å for the HDAC5-Rac26, HDAC5-ZINC000033260361, and HDAC5-CHEMBL2426361 (Figure 3.32 (b)). All systems of HDAC7 were found to be stable throughout the MD simulations over the 100 ns run time with an average Rg value of 1.37 Å for the apo-protein, HDAC7-Trichostatin A, and HDAC7-ZINC000009640741, whereas the Rg of HDAC7-CHEMBL1968496 complex was found to be 1.43 Å (Figure 3.32 (c)). Lastly, the average Rg value of the apo-protein of HDAC9 was found to be 1.26 Å, while the average Rg value for HDAC9-TMP269 and HDAC9-CHEMBL1761559 was 1.42 Å (Figure 3.32 (d)). All HDAC9 systems remained stable over time.

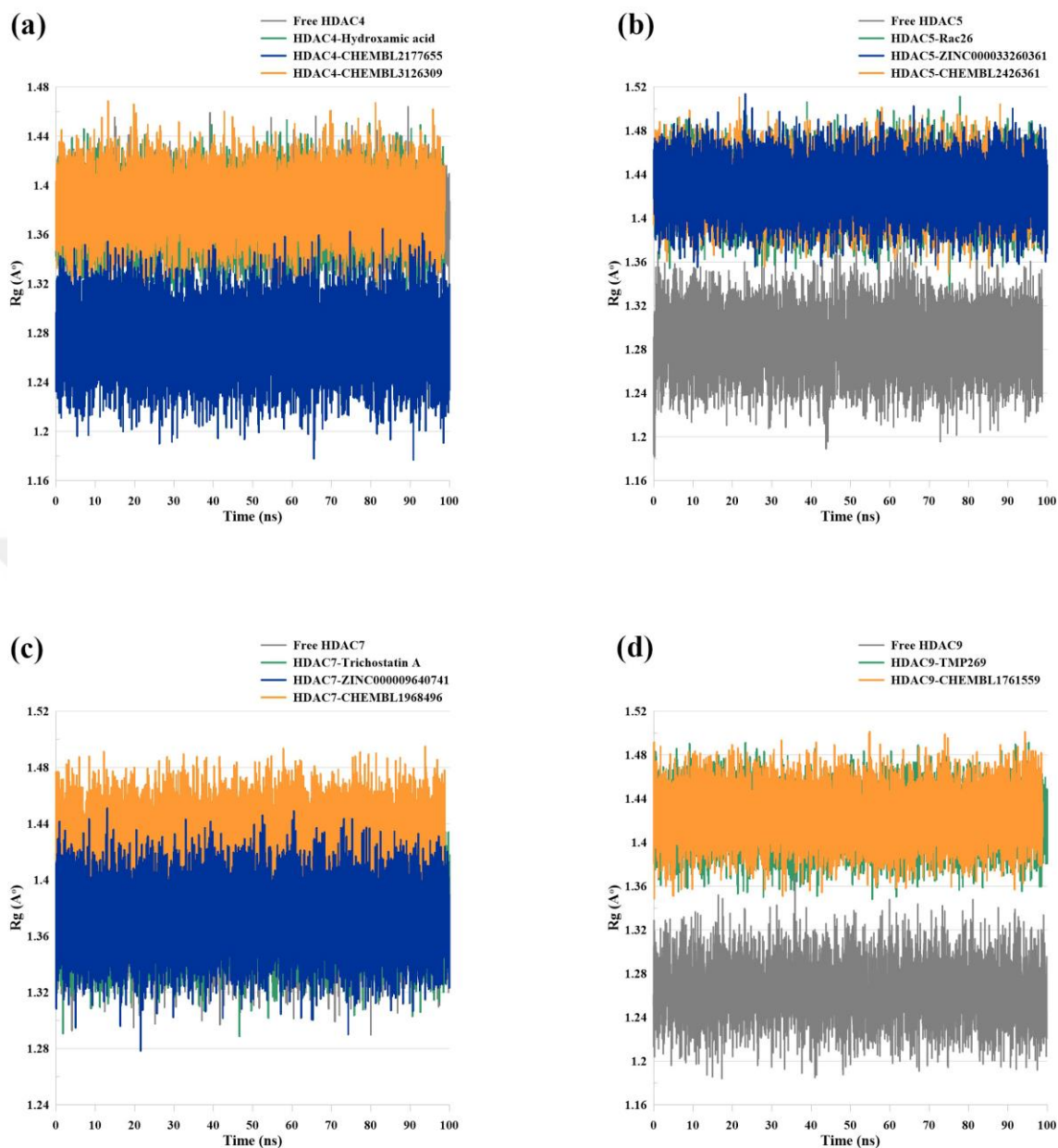


**Figure 3.32.** The radius of gyration ( $R_g$ ) plots of (a) HDAC4 systems; (b) HDAC5 systems; (c) HDAC7 systems; and (d) HDAC9 systems.

- Potential energy profile:** The potential energy measurement is beneficial in validating the energy consistency and stability during the MD simulations. Herein, the total energy is plotted as potential energy versus run time, and all studied systems proved to be energetically stable throughout the MD run (Figure 3.33).

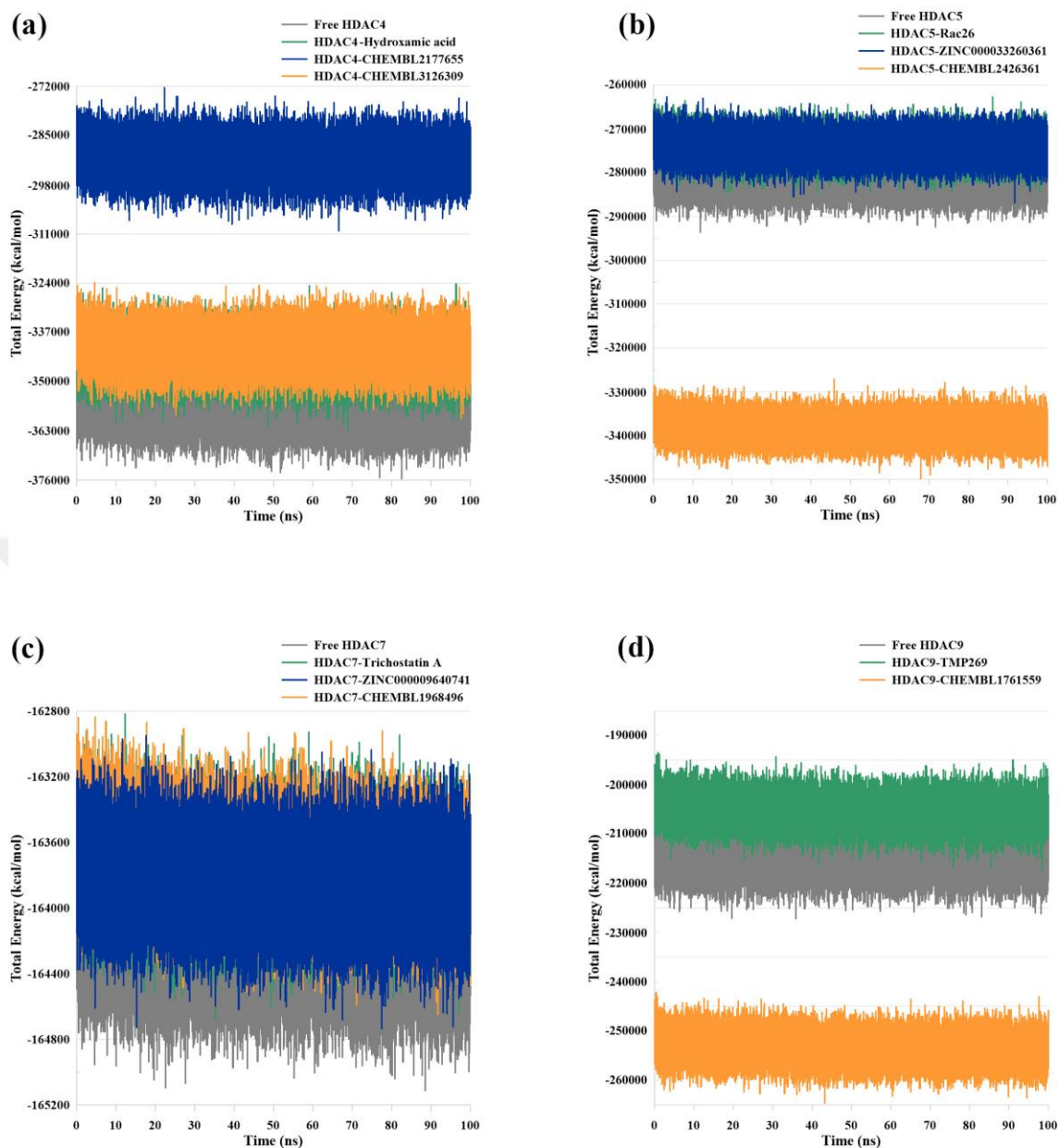


**Figure 3.33.** The potential energy plots of (a) HDAC4 systems; (b) HDAC5 systems; (c) HDAC7 systems; and (d) HDAC9 systems.

- Number of hydrogen bonds:** In all living systems, the molecular interactions are highly influenced by the presence of hydrogen bonds. Hydrogen bonds are crucial in regulating the changes in the secondary structures that in turn influence the protein-ligand interactions. During MD simulation, proteins can be found in different conformations mimicking real biological environments. Each of these conformations may provide a different protein-ligand interaction. Thus, the number of hydrogen bonds formed throughout the MD simulation was calculated for the selected isoform selective compounds (Figure 3.34). In HDAC4-CHEMBL2177655 complex, the maximum

number of H-bonds formed was found to be 5 during the MD simulation. In the first 19 ns, many conformations showed 3 H-bonds, and less showed 4 H-bonds. The majority of the conformations showed two hydrogen bonds (Figure 3.34 (a)). On the other hand, HDAC4-CHEMBL3126309 showed at most 3 H-bonds during the simulation (Figure 3.34 (a)). Most of the conformations showed 1 H-bonds and about 60% showed 2 H-bonds. HDAC5-ZINC000033260361 complex showed at most 4 H-bonds in few conformations and more two H-bonds after the first 6 ns of the simulation. It also had at least 1 H-bond in most of the conformations (Figure 3.34 (b)). The greatest number of conformations in HDAC5-CHEMBL2426361 complex showed 1 H-bonds, and one conformation with 3 H-bonds (Figure 3.34 (b)). The largest number of H-bonds seen in HDAC7-ZINC000009640741 complex was 3 in one conformation and the average number of H-bonds formed was found to be 2 (Figure 3.34 (c)). HDAC7-CHEMBL1968496 complex showed one conformation with 4 H-bonds, and many with 3 H-bonds in the first 53 ns. In addition, most of the conformations formed 2 H-bonds during the first 57 ns of the simulation, and thereafter, the complex retained in average 1 H-bond till the end of the simulation (Figure 3.34 (c)). Lastly, HDAC9-CHEMBL1761559 complex formed up to 3 H-bonds in several conformations during the simulation and consisted of at least 1 H-bond over time (Figure 3.34 (d)).



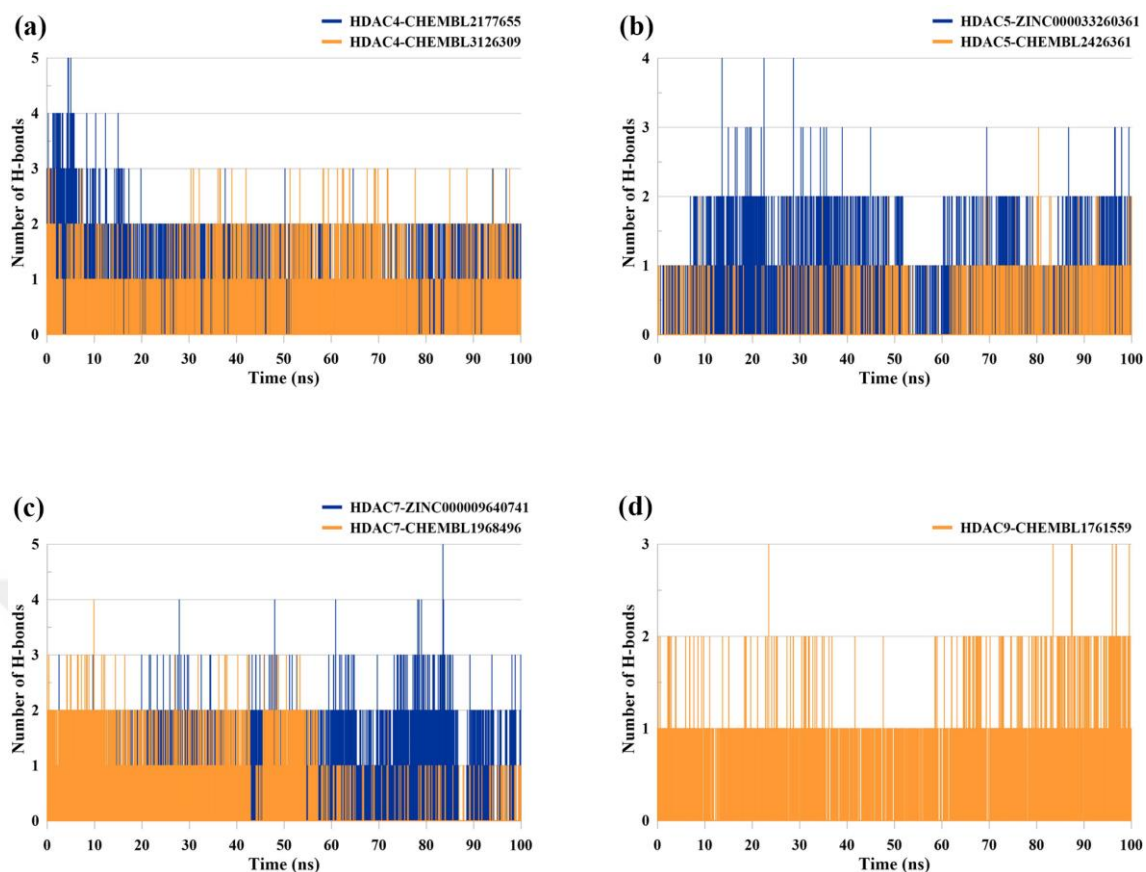


**Figure 3.34.** Number of hydrogen bonds profile of (a) HDAC4 complexes; (b) HDAC5 complexes; (c) HDAC7 complexes; and (d) HDAC9 complex.

### 3.2.5. Binding Free Energy (MM-PBSA) Calculations

CaFE tools were used in the present study to calculate average free binding energy of the studied isoform selective compounds (Table 3.12). The tools calculate the free binding energy average using the MM-PBSA method in addition to the standard deviation/error for each protein-ligand complex. The binding energy represents the interaction between the protein and the ligand (e.g., the released energy throughout the formation of the bonds). Higher binding affinity between the ligand and protein complex is identified by lesser binding energy. The total binding energy is a summation of electrostatic, van der Waals, SASA and polar solvation energy.

**Table 3.12.** Calculated binding free energy (MM-PBSA) of the selected isoform HDACs selective complexes.

Complex	Binding Energy (kcal/mol)
HDAC4-CHEMBL2177655	-31.3569 ± 20.17
HDAC4-CHEMBL3126309	-21.4164 ± 6.996
HDAC5-ZINC000033260361	-21.0986 ± 5.264
HDAC5-CHEMBL2426361	-55.2850 ± 8.694
HDAC7-ZINC000009640741	-17.4562 ± 13.00
HDAC7-CHEMBL1968496	-56.7090 ± 6.336
HDAC9-CHEMBL1761559	-27.2031 ± 3.478

### 3.3. LIGAND-BASED PHARMACOPHORE MODELING FOR DESIGNING OF ISOFORM SELECTIVE HDAC5 AND HDAC9 INHIBITORS

#### 3.3.1. Generated Pharmacophore Hypotheses

The 10 generated pharmacophore models based on HDAD5 known inhibitors comprise the same five features: 1 hydrophobic (aromatic/aliphatic); 1 hydrogen bond donor; and 3 hydrogen bond acceptor groups (Figure 3.35). Among the generated hypotheses, Hypo1 showed the top rank value (Table 3.13) and proved the highest GH score (0.86) and enrichment factor (10.26) (Table 3.14). The five pharmacophore features of Hypo1 were found to be well mapped onto the following HDAC5 known inhibitors that were included in the training set: LMK235, Chimera 4, HPB, R306465, Cudc-101, Dacinostat, Vorinostat, T009, Trichostatin A, Marbostat, Tubastatin A, ST3049, Tubacin, ST3710. The 3D database search against the Hypo1 retrieved a total of 7,996 compounds, that showed fit value of 3 or more and met the geometric constrictions of Hypo1 and well mapped onto the hypothesis with their unique scaffolds.



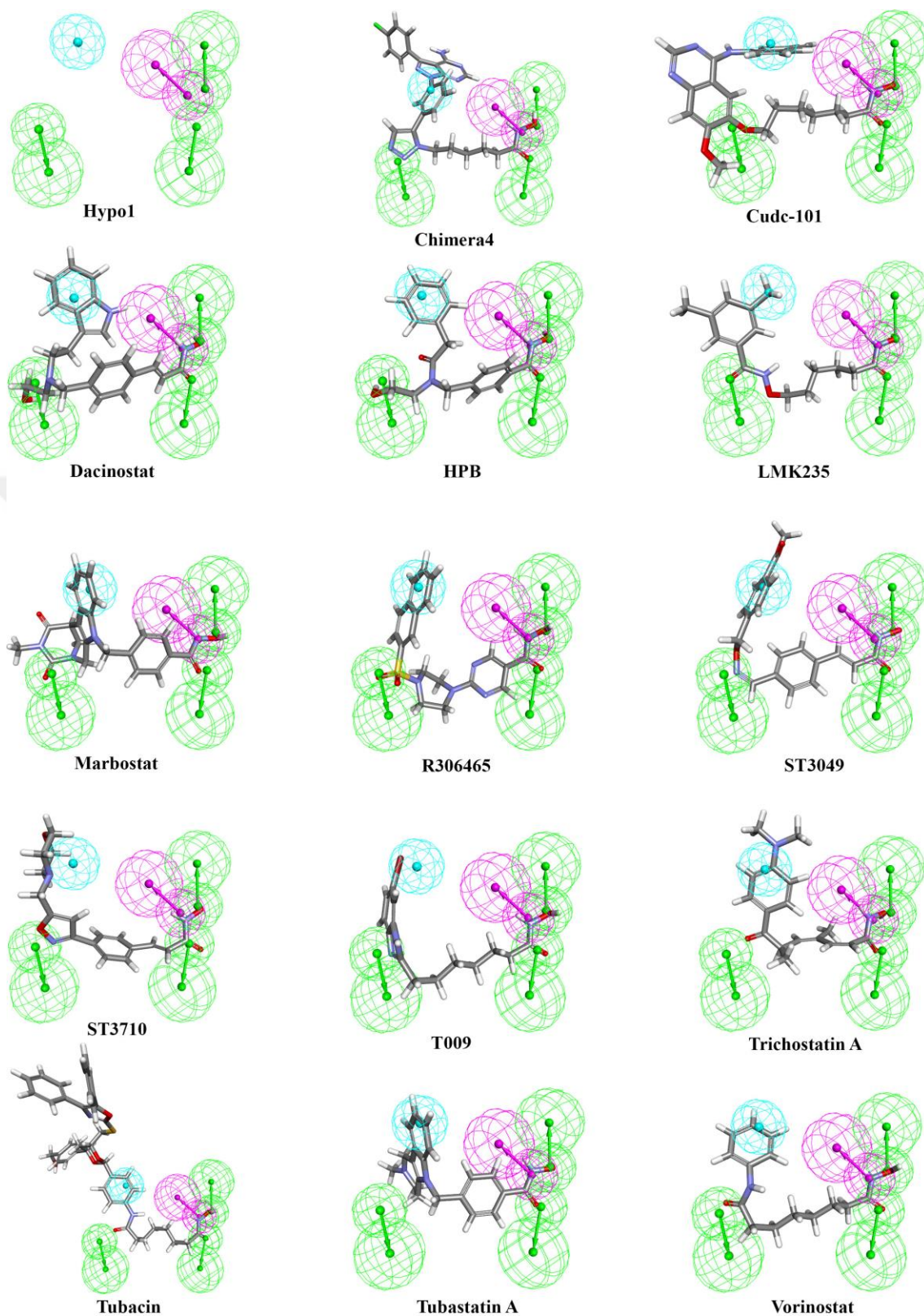


**Figure 3.35.** 14 of selected HDAC5 known inhibitors from the training set mapped onto the generated pharmacophore hypothesis Hypo1.

**Table 3.13.** Common features of the 10 generated pharmacophore hypotheses for the HDAC5 known inhibitors.

Hypotheses	Features	Rank	Max. Fit
1	HDAAA	256.83	5
2	HDAAA	246.53	5
3	HDAAA	246.00	5
4	HDAAA	245.70	5
5	HDAAA	244.02	5
6	HDAAA	243.54	5
7	HDAAA	242.87	5
8	HDAAA	242.79	5
9	HDAAA	241.73	5
10	HDAAA	241.09	5

H: hydrophobic (aromatic/aliphatic); D: hydrogen bond donor; A: hydrogen bond acceptor.

**Table 3.14.** Guner-Henry scoring method results for validating the 10 generated pharmacophore hypotheses based on the HDAC5 known inhibitors.

Hypotheses	D	A	H <sub>t</sub>	H <sub>a</sub>	A%	Y%	E	GH
1	231	21	15	14	66.66	93.33	10.26	0.862
2	231	21	16	13	61.90	81.25	8.93	0.753
3	231	21	18	14	66.66	77.77	8.55	0.735
4	231	21	18	14	66.66	77.77	8.55	0.735
5	231	21	15	13	61.90	86.66	9.53	0.797
6	231	21	21	14	66.66	66.66	7.33	0.644
7	231	21	15	13	61.90	86.66	9.53	0.797
8	231	21	18	14	66.66	77.77	8.55	0.735
9	231	21	17	14	66.66	82.35	9.05	0.773
10	231	21	19	13	61.90	68.42	7.52	0.648

D: the sum of the compounds presents in the decoy set.

A: the sum the of the active compounds in the decoy set.

H<sub>t</sub>: the total number of the hits within the decoy set.

H<sub>a</sub>: the total number of the active compounds shown in the hit list.

A%: the ratio of the active compounds within the hits list.

Y%: the ratio of the active compounds identified by the pharmacophore model from the decoy set.

E: the enrichment factor.

GH: the goodness of hit.

The other 10 generated pharmacophore hypotheses based on HDAD9 known inhibitors consist of several features: ring aromatic, hydrophobic (aromatic/aliphatic), hydrogen bond donor; and hydrogen bond acceptor groups. Although Hypo2 is statistically ranked as the second (Table 3.15), it exhibited the highest GH score (0.87) and enrichment factor (10.13) (Table 3.16). The four generated pharmacophore features of Hypo2 include: 1

ring aromatic; 1 hydrophobic (aromatic/aliphatic); and 2 hydrogen bond acceptor groups. The following four HDAC9 known inhibitors form the training set were found to be well mapped onto Hypo2: BRD4354, BDBM191640, BDBM191641, and TMP269 (Figure 3.36). A total of 21,422 compounds were retrieved from the 3D database search and showed 3 or more fit value and fitted the geometric constrictions of Hypo2 and well represented onto the hypothesis with their characteristic scaffolds.

**Table 3.15.** Common features of the 10 generated pharmacophore hypotheses for the HDAC9 known inhibitors.

Hypotheses	Features	Rank	Max. Fit
1	RHAA	176.23	4
2	RHAA	173.68	4
3	RHAA	169.77	4
4	RHAA	169.26	4
5	RHAA	167.30	4
6	HHDA	166.70	4
7	RHAA	164.71	4
8	RHAA	163.55	4
9	HHAA	162.50	4
10	RHAA	162.43	4

R: aromatic ring; H: hydrophobic (aromatic/aliphatic); D: hydrogen bond donor; A: hydrogen bond acceptor.

**Table 3.16.** Guner-Henry scoring method results for validating the 10 generated pharmacophore hypotheses based on the HDAC9 known inhibitors.

Hypotheses	D	A	H <sub>t</sub>	H <sub>a</sub>	A%	Y%	E	GH
1	231	21	18	15	71.42	83.33	9.166	0.792
2	231	21	16	15	71.42	93.75	10.31	0.877
3	231	21	18	16	76.19	88.88	9.777	0.848
4	231	21	19	15	71.42	78.94	8.684	0.755
5	231	21	19	15	71.42	78.94	8.684	0.755
6	231	21	35	18	85.71	51.42	5.657	0.551
7	231	21	37	19	90.47	51.35	5.648	0.558
8	231	21	20	15	71.42	75.00	8.250	0.723
9	231	21	32	17	80.95	53.12	5.843	0.557
10	231	21	16	14	66.66	87.50	9.625	0.815

D: the sum of the compounds presents in the decoy set. A: the sum the of active compounds in the decoy set. H<sub>t</sub>: the total number of the hits within the decoy set. H<sub>a</sub>: the total number of the active compounds shown in the hit list. A%: the ratio of the active compounds within the hits list. Y%: the ratio of the active compounds identified by the pharmacophore model from the decoy set. E: the enrichment factor. GH: the goodness of hit.

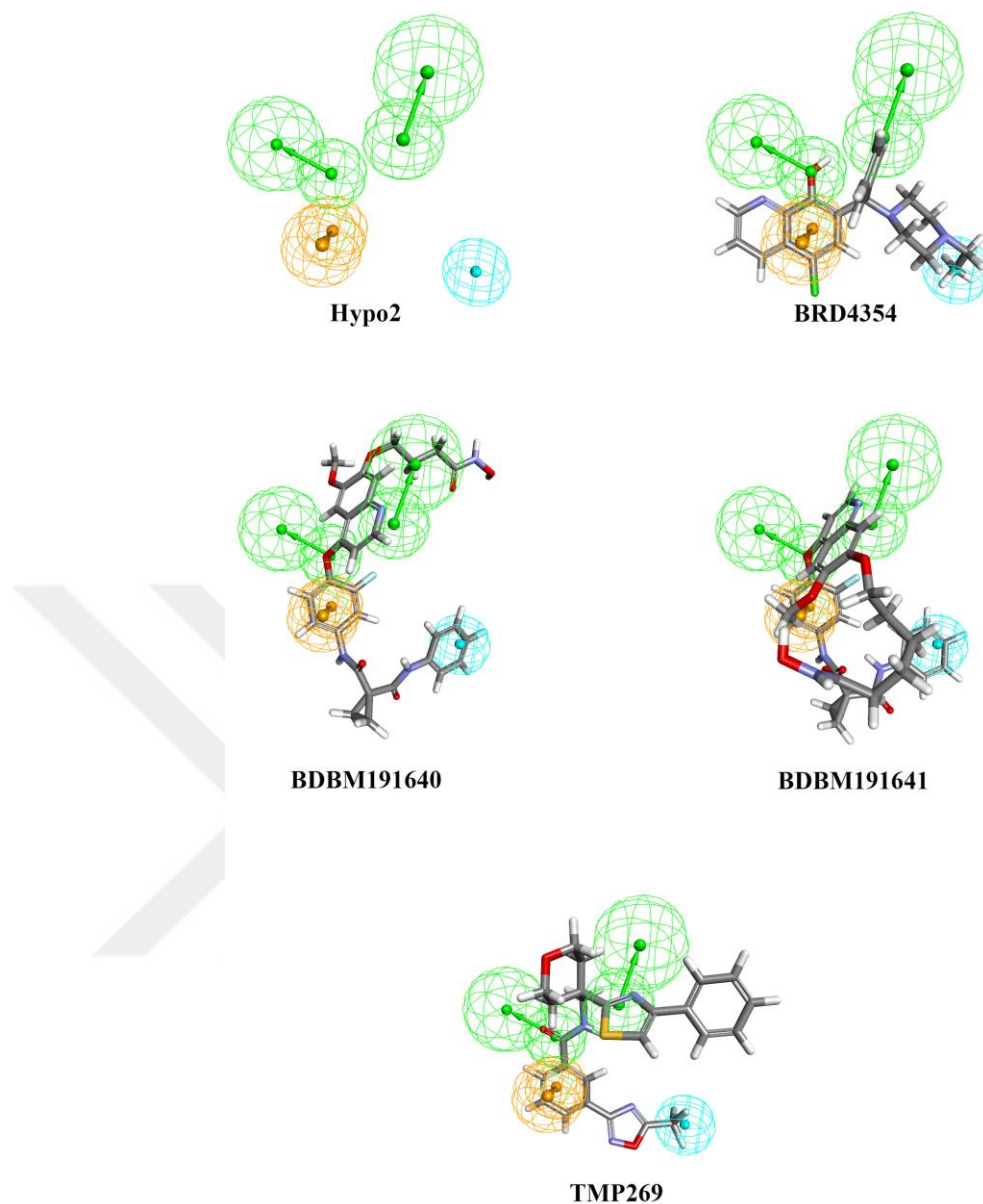


**Figure 3.36.** Four of selected HDAC9 known inhibitors from the training set mapped onto the generated pharmacophore hypothesis Hypo2.

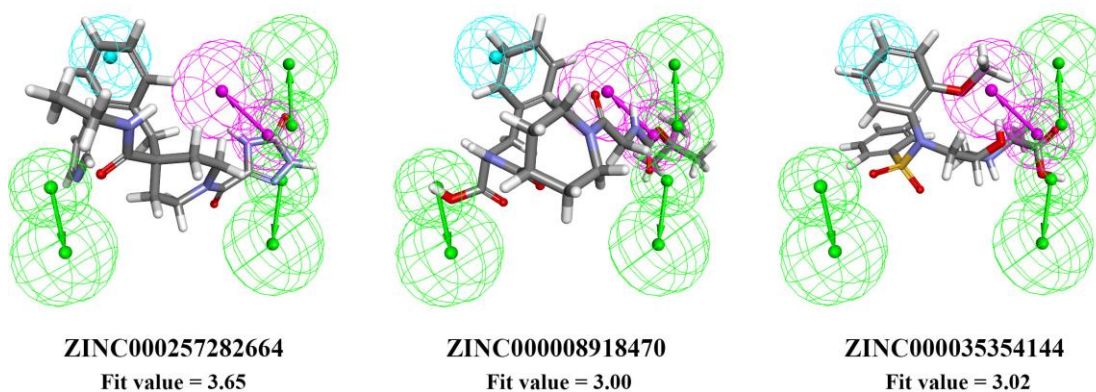
### 3.3.2. Molecular Docking Study

The molecular docking analysis revealed a total of 3 top-ranked isoform selective compounds for each of HDACs 5 and 9 (Table 3.17). All six compounds were well mapped onto their respective pharmacophore hypothesis and their fit values are shown in Figure 3.37.

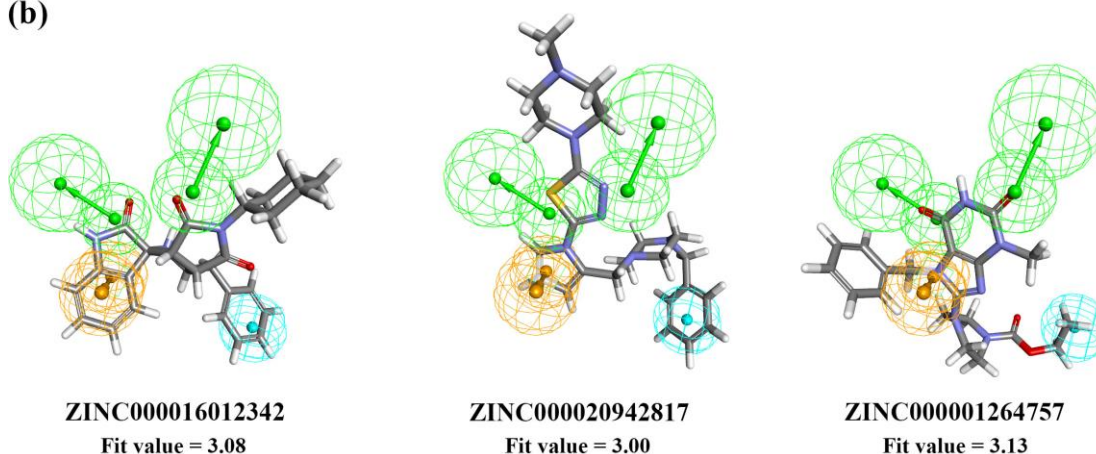
**Table 3.17.** Top ranked compounds with their calculated binding energy using QuickVina 2.0. Selective isoform compounds for HDAC5 are highlighted in green, and selective isoform compounds for HDAC9 are highlighted in yellow.

#	Compound ID	HDAC4	HDAC5	HDAC7	HDAC9
		$\Delta G$ (kcal/mol)	$\Delta G$ (kcal/mol)	$\Delta G$ (kcal/mol)	$\Delta G$ (kcal/mol)
1	ZINC000257282664	-7.4	-8.9	-7.8	-7.7
2	ZINC000008918470	-7.6	-8.9	-7.6	-7.6
3	ZINC000035354144	-7.1	-8.1	-6.5	-7
4	ZINC000016012342	-9.2	-8.7	-8.8	-10.3
5	ZINC000020942817	-8.1	-8.1	-7.3	-9.3
6	ZINC000001264757	-6.8	-7	-6.7	-8

(a)



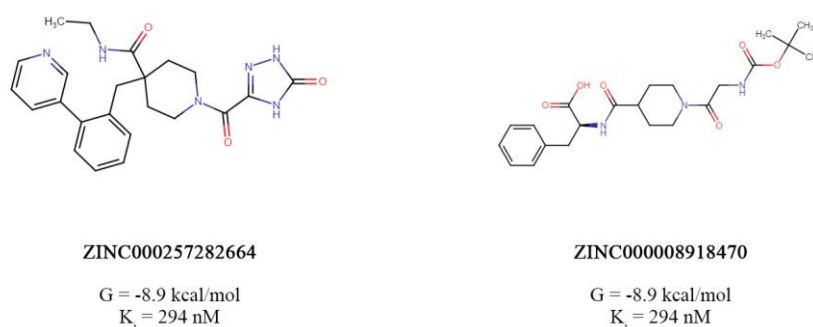
(b)



**Figure 3.37.** The top six selective inhibitors and their mapping onto their respective pharmacophore hypothesis. (a) HDAC5 selective inhibitors mapped onto Hypo1. (b) HDAC9 selective inhibitors mapped onto Hypo2.

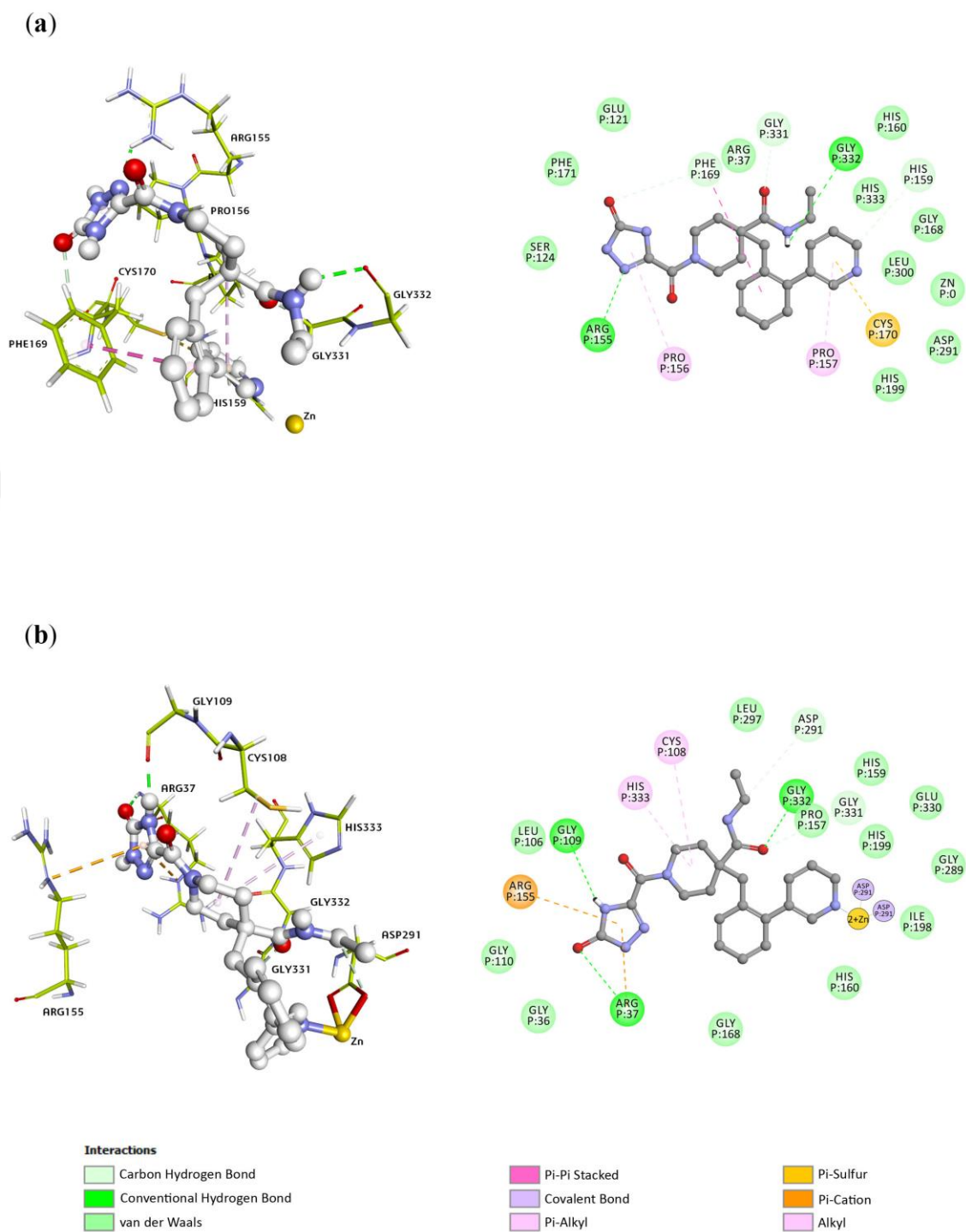


The top two HDAC5 selective compounds, ZINC000257282664 and ZINC000008918470 (Figure 3.38) exhibited the higher binding affinity toward HDAC5 and lowest binding energy with a score of -8.9 kcal/mol and a predicted inhibitory constant ( $K_i$ ) of 294 nM for both compounds (Table 3.17). Both compounds proved to have lower binding energies toward HDAC5 compared to the reference known inhibitor used in this study, the LMK235, which showed a binding energy of -6.8 kcal/mol.



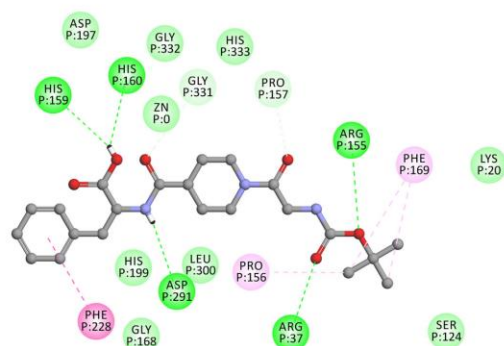
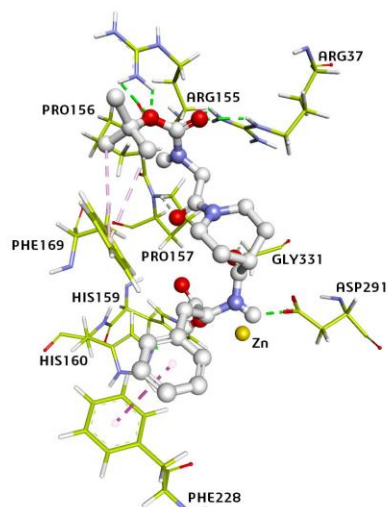
**Figure 3.38.** The two top-ranked HDAC5 selective inhibitors.

Even though these two compounds are not structurally similar to most HDACs known inhibitors with their distinctive zinc binding groups, they both well spanned in the active site of HDAC5. ZINC000257282664 compound was found to be bonded to the active site via several key interactions including five hydrogen bonds with Arg155, His159, Phe169, Gly331 and Gly332; a  $\pi$ -sulfur interaction with Cys170; a  $\pi$ - $\pi$  stacked interaction with Phe169; two  $\pi$ -alkyl interactions with Pro156 and Pro157 in addition to many van der Waals interactions (Figure 3.39). Similarly, binding mode analysis of ZINC000008918470 compound revealed several important chemical interactions with HDAC5 including seven hydrogen bonds with Arg37, Arg155, Pro157, His159, His160, Asp291 and Gly331; a  $\pi$ - $\pi$  stacked interaction with Phe228; two  $\pi$ -alkyl interactions with Phe169; an alkyl interaction with Pro156 and other several van der Waals interactions (Figure 3.40). The catalytic zinc atom was observed to be bonded to both compounds via van der Waals interaction.

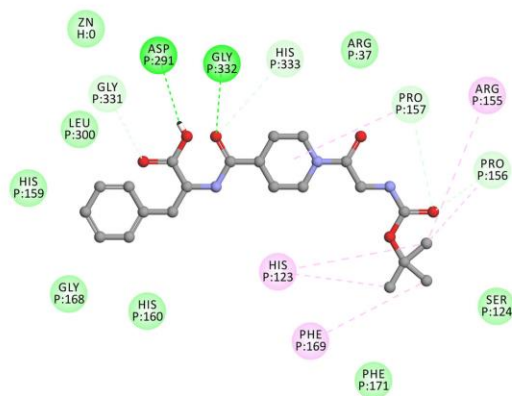
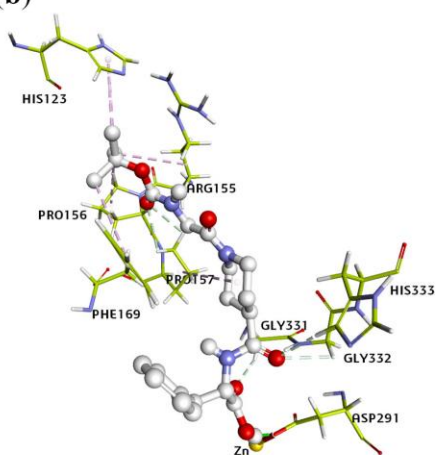


**Figure 3.39.** 3D and 2D presentations of the ZINC000257282664 compound interaction with HDAC5 (a) after molecular docking; and (b) after MD simulation.




(a)




(b)



**Interactions**

-  Carbon Hydrogen Bond
-  Conventional Hydrogen Bond
-  van der Waals

-  Pi-Pi Stacked
-  Alkyl
-  Pi-Alkyl

**Figure 3.40.** 3D and 2D presentations of the ZINC000008918470 compound interaction with HDAC5 (a) after molecular docking; and (b) after MD simulation.

The molecular docking study showed ZINC000016012342 and ZINC000020942817 compounds (Figure 3.41) with the highest binding affinities toward HDAC9 and with the lowest binding energies of -10.3 kcal/mol and -9.3 kcal/mol, respectively (Table 3.17). The predicted inhibitory constants ( $K_i$ ) of ZINC000016012342 and ZINC000020942817



compounds were found to be of 27.64 nM and 149 nM, respectively. Interestingly, both top-ranked compounds displayed lower binding energies in comparison to the reference known inhibitor (BRD4354), which displayed a binding energy of -7.3 kcal/mol.

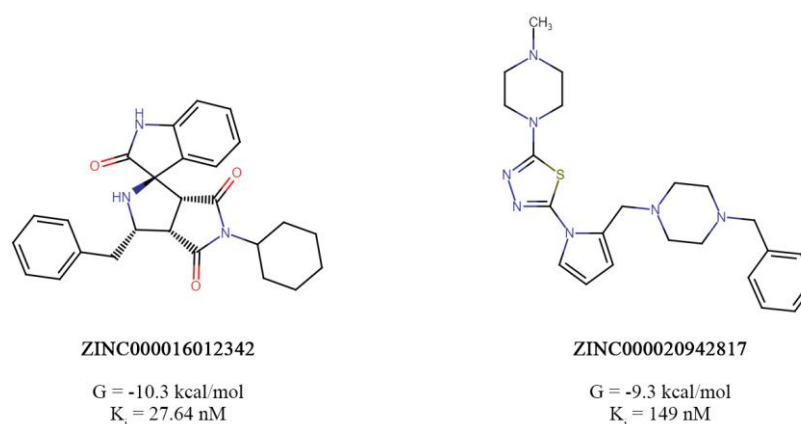
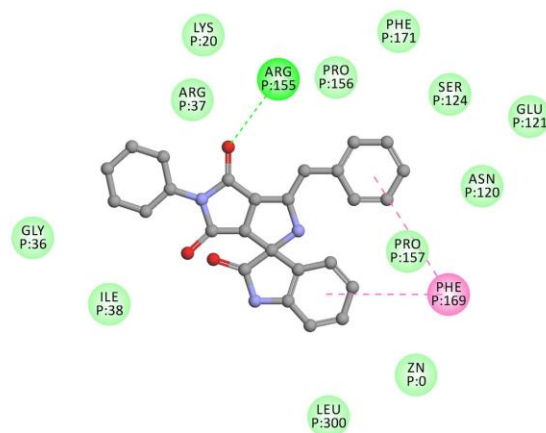
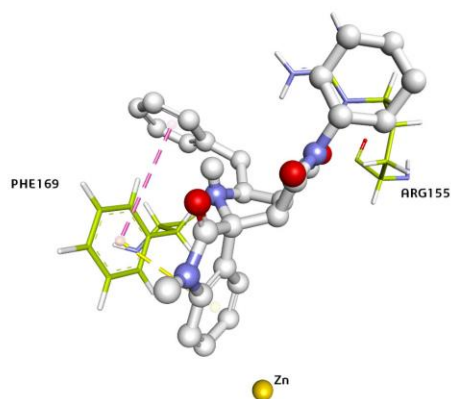


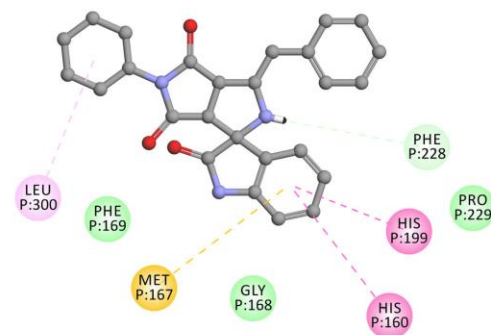
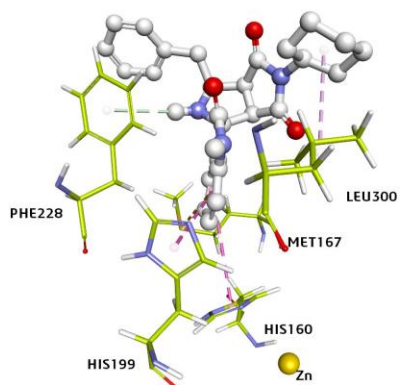
**Figure 3.41.** The two top-ranked HDAC9 selective inhibitors.

ZINC000016012342 binding mode was found to be well fitted into the catalytic pocket of HDAC9 with the following significant interactions: one hydrogen bond with Arg155,  $\pi$ - $\pi$  stacked interaction with Phe169 and one  $\pi$ - $\pi$  T-shaped interaction with Phe169 as well, and many other van der Waals interactions. The catalytic zinc metal atom was not seen involved in any chemical interactions with the ZINC000016012342 compound (Figure 3.42). ZINC000020942817 compound was perfectly spanned into the HDAC9 active site and showed several prominent interactions with the key amino acid residues including hydrogen bonds with Arg37 and Asp291;  $\pi$ -cation interaction with Arg39;  $\pi$ -alkyl interaction with Pro157, Phe169 and His199;  $\pi$ - $\pi$  T-shaped interaction with His199;  $\pi$ - $\pi$  stacked interaction with Phe228; van der Waals interaction with the catalytic zinc atom as well as many other amino acid residues (Figure 3.43).

(a)



(b)



**Interactions**

Light green box: Pi-Donor Hydrogen Bond

Green box: Conventional Hydrogen Bond

Light green box: van der Waals

Pink box: Pi-Pi Stacked

Light pink box: Alkyl

Dark pink box: Pi-Pi T-shaped

Yellow box: Pi-Sulfur

**Figure 3.42.** 3D and 2D presentations of the ZINC000016012342 compound interaction with HDAC9 (a) after molecular docking; and (b) after MD simulation.

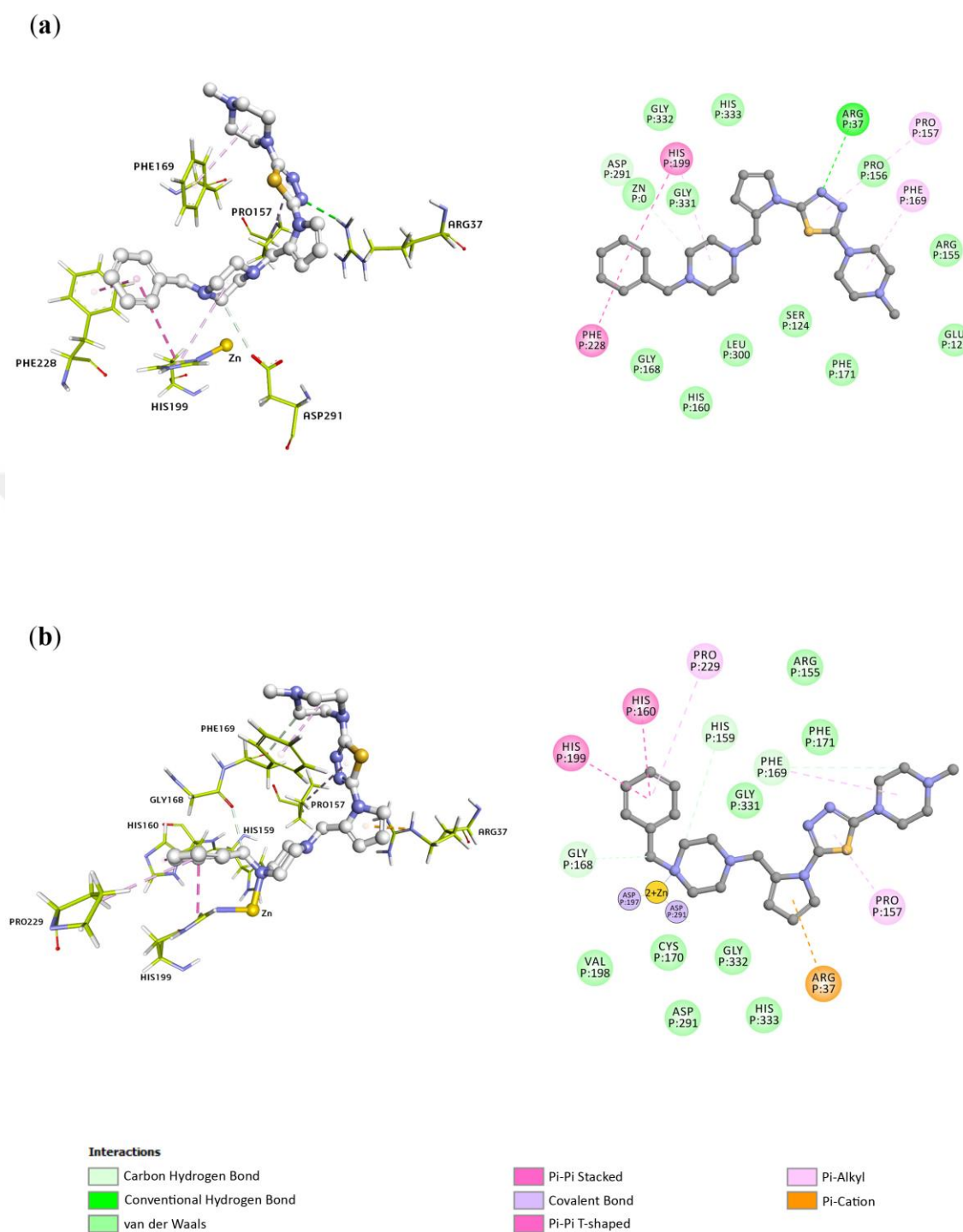


**Figure 3.43.** 3D and 2D presentations of the ZINC00020942817 compound interaction with HDAC9 (a) after molecular docking; and (b) after MD simulation.

In 2008, Bieliauskas and Pflum demonstrated the selectivity index of many different HDACs known inhibitors in their study by comparing the inhibition constant of a particular HDAC protein to other HDAC members (Bieliauskas & Pflum, 2008). Thus,

the selection process of the HDAC-selective inhibitors in the present study was inspired by Bieliauskas and Pflum work. This was achieved by comparing the value of the inhibition constant of a particular inhibitor for a selected HDAC to other inhibition constants of the same inhibitor for other HDAC members. The following formula was applied to obtain the selectivity indices (Equation 3.1), where “x” refers to a selected compound:

$$\text{Selectivity of "x" for HDAC5 or 9} = \frac{K_i \text{ of other HDACs isoform}}{K_i \text{ of HDAC5 or 9}} \quad (3.1)$$

The selectivity indices of HDAC5 and HDAC9 are given in Table 3.18. ZINC000257282664 compound showed a potential selectivity toward HDAC5 ranging between 7 and 13-fold compared to other members of class IIa HDACs. ZINC000008918470 compound displayed a ~9-fold isoform selectivity for HDAC5 over all members of class IIa. ZINC000016012342 compound revealed promising selectivity for HDAC9 ranging between ~7 and 15-fold over the other class IIa HDAC members. Lastly, ZINC000020942817 compound displayed a ~8 to 30-fold isoform selectivity for HDAC9 compared to the rest of the class IIa HDACs.

**Table 3.18.** Selectivity indices of class IIa HDACs. Inhibition constant of one HDAC is compared to the closest inhibition constant of other HDACs for the same inhibitor.

Compounds	HDAC4	HDAC5	HDAC7	HDAC9	Selectivity Index			Selectivity
	$K_i^4$ (nM)	$K_i^5$ (nM)	$K_i^7$ (nM)	$K_i^9$ (nM)	$K_i^4/K_i^5$	$K_i^7/K_i^5$	$K_i^9/K_i^5$	
ZINC000257282664	3713	294	1888	2236	13	7	8	HDAC5/HDAC7
ZINC000008918470	2648	294	2648	2648	9	9	9	HDAC5/All
ZINC000035354144	6164	1137	16989	7299	5	15	6	HDAC5/HDAC4
					$K_i^4/K_i^9$	$K_i^5/K_i^9$	$K_i^7/K_i^9$	
ZINC000016012342	177	412	348	27.64	7	15	13	HDAC9/HDAC4
ZINC000020942817	1137	1137	4396	149	8	8	30	HDAC9/HDAC4
ZINC000001264757	10233	7299	12117	1347	8	5	10	HDAC9/HDAC5

### 3.3.3. Drug-Likeness Prediction and PAINS Filtration

Table 3.19 shows the physicochemical and drug-likeness properties of the isoform selective compounds. All the six selected compounds were found to be within the acceptable reference of oral drugs and thus can be classified as drug-like compounds.

These compounds obeyed the famous Lipinski's rule of five, which states that oral drugs must have a molecular weight (MW) of 500 Da or less, the octanol-water partition coefficient (LogP) should not be more than 5, the total number of hydrogen bond donors should not be more than 5, and the total number of hydrogen acceptors must not be more than 10. Violating two or more of the previous criteria mostly result in poor permeable drugs (Lipinski et al., 2001). According to the collected properties of 90% of 1,700 oral drugs, Di and Kerns proposed the following criteria for identifying drug-like compounds: the water/aqueous solubility (LogS) should be larger than -5.7, the permeability rate in Caco-2 cell line must be faster than 22 nm/s, and lastly, the total number of the primary metabolites must not exceed 7 (Di & Kerns, 2016). The topological polar surface area (TPSA) should not be more than 140 Å<sup>2</sup>. Moreover, the selected six compounds were found to be PAINS free compounds.

**Table 3.19.** The drug-likeness and the physicochemical properties of the 6 isoform selective compounds.

	Compound	Lipinski violations	MW	HA	HD	MLogP	TPSA	HIA	Caco-2	AQ
1	ZINC000257282664	0	434.4	5	3	1.49	123.84	0.953	0.837	-3.059
2	ZINC000008918470	0	433.5	6	3	0.93	125.04	0.860	0.849	-3.146
3	ZINC000035354144	0	408.4	7	3	-1.35	124.55	0.945	0.535	-3.555
4	ZINC000016012342	0	429.5	4	2	3.03	78.51	0.972	0.779	-3.911
5	ZINC000020942817	0	437.6	5	0	2.22	71.91	0.989	0.571	-3.013
6	ZINC000001264757	0	412.4	5	1	1.44	105.46	0.969	0.647	-3.717

MW: Molecular weight, Da.

HA: Total number of H-bond acceptors, O and N.

HD: Total number of H-bond donors, OH and NH.

TPSA: Topological polar surface area, Å<sup>2</sup>.

HIA: Human intestinal absorption.

AQ.: Water solubility, LogS.

### 3.3.4. Analysis of The MD Simulations

The structural stability of the docked complexes of HDAC5 with ZINC000257282664 and ZINC000008918470, HDAC9 with ZINC000016012342 and ZINC000020942817 were analyzed by evaluating their RMSD, RMSF, Rg, potential energy, and by assessing the number of the hydrogen bonds throughout the MD simulations.

- **RMSD analysis:** The root mean squared deviation plots of the free HDAC5 protein and its complex systems with the known inhibitor (LMK235), ZINC000257282664, and ZINC000008918470 are shown in Figure 3.44 (a). All the studied systems exhibited

steady equilibrium state throughout the MD simulations. The RMSD of the apo-protein of HDAC5 (without inhibitor) slightly increased to 3.4 Å around the first 12 ns of the MD run then remained in equilibrium state until the end with an average RMSD of 3.2 Å. The RMSD of HDAC5 complexed with the known inhibitor rose from 0 Å to ~4.8 Å until 39 ns and then the RMSD decreased to an average of 4.1 Å and remained stable to the end. The backbone of the HDAC5-ZINC000257282664 complex showed an increased RMSD profile compared to the apo-protein where the system stabilized with an average RMSD of 4.7 Å after the first 44 ns of the simulation. Interestingly, the backbone RMSD of the HDAC5-ZINC000008918470 complex displayed similar trend with the apo-protein after the first 22 ns and remained stable until the end of the run. HDAC5-ZINC000008918470 complex showed lower RMSD profile over time of the MD run compared to HDAC5-ZINC000257282664 complex.

The RMSD profiles of the free HDAC9 protein and its complex systems with the BRD4354, ZINC000016012342 and ZINC000020942817 are shown in Figure 3.44 (b). The backbone RMSD of the HDAC9 apo-protein initially increased to 5.2 Å around 37 ns and the system seemed to be stabilized till the end of the run with an average RMSD of 4.1 Å. The RMSD examination of ZINC000016012342 and ZINC000020942817 revealed that both systems showed comparable fluctuation after the first 50 ns and restrained their equilibrium state until the end of the MD simulation. HDAC9-ZINC000020942817 complex system gained its stability at earlier stages (around 16 ns) compared to HDAC-ZINC000016012342 and had an average backbone RMSD of 3.9 Å. HDAC-ZINC000016012342 complex system showed a slightly higher fluctuation until the 68 ns, but thereafter showed better equilibrium state till the end of the 100 ns run.

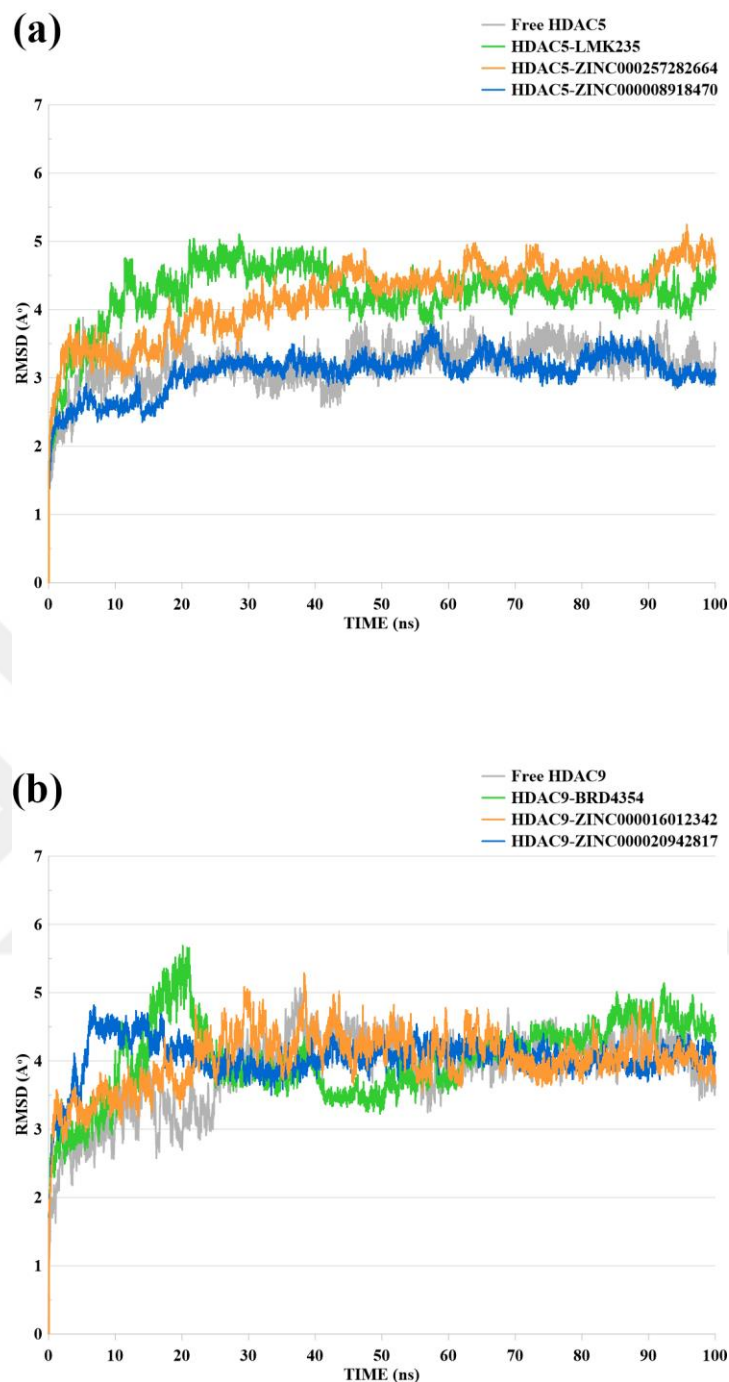


**Figure 3.44.** Presentation of the root mean squared deviation (RMSD) for (a) HDAC5 complex systems; and (b) HDAC9 complex systems.

- RMSF analysis:** The root mean squared fluctuation (RMSF) analysis was conducted for the HDAC5 and HDAC9 complex systems and the results are presented in Figure 3.45 (a) and (b), respectively. RMSF analysis helps in examining the local movements of amino acid residues and their behavior through the MD simulation. Higher backbone RMSF fluctuations were seen in loop regions that are known for their high

flexibility. Overall, HDAC5-ZINC000008918470 complex system exhibited lower RMSF profile compared to the HDAC5-ZINC000257282664 complex system throughout the simulation and this observation agreed with the RMSD profiles of the same complex systems. The RMSF investigation showed that HDAC9-ZINC000020942817 displayed relatively lower amino acid residues fluctuations at major stable regions of the protein compared to the HDAC9-ZINC000016012342 system. This assessment was in agreement with the RMSD profiles of same complex systems.

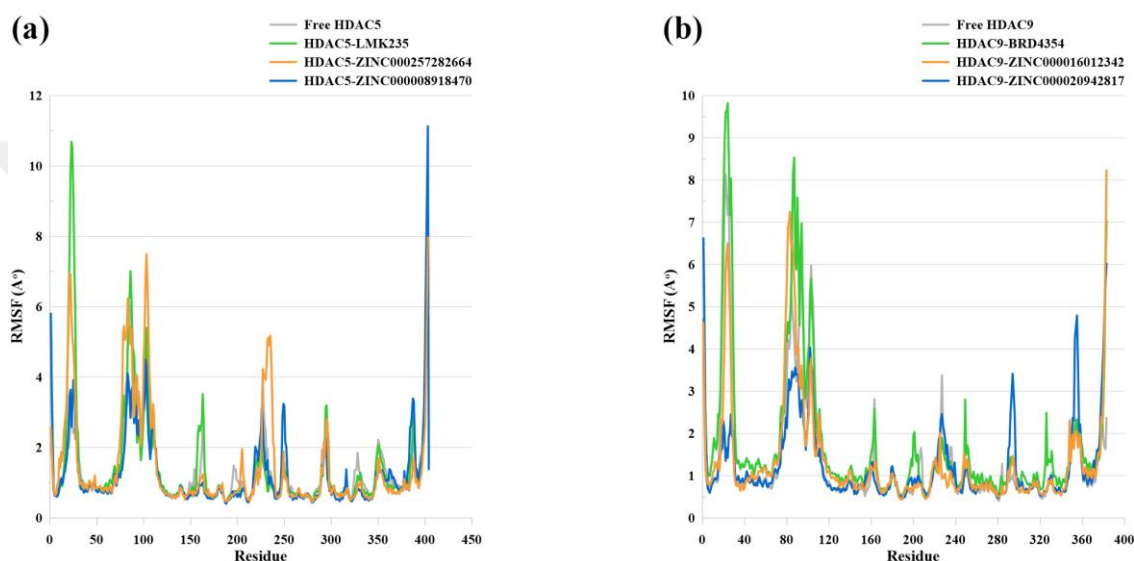


**Figure 3.45.** Illustration of the root mean squared fluctuation (RMSF) for (a) HDAC5 complex systems; and (b) HDAC9 complex systems.

- Rg analysis:** The protein compactness level can be examined via the radius of gyration (Rg) profile which is useful in investigating the protein folding nature throughout the simulation. The Rg of HDAC5 and its complex systems are plotted in Figure 3.46 (a). All studied systems were remained stable over time. Compared to HDAC5-ZINC000257282664 system which has as average RMSF of 1.42 Å during the simulation, HDAC5-ZINC000008918470 system displayed lower Rg profile with a 1.27 Å, suggesting relatively less flexibility levels of the protein. The Rg profiles of HDAC9 systems implying that all complexes were steadily stable during the whole MD run (Figure 3.46 (b)). HDAC9-ZINC000020942817 system exhibited a relatively higher degree of flexibility with an average Rg of 1.39 Å compared to HDAC9-ZINC000016012342 system that showed an average Rg of 1.26 Å during the simulation.



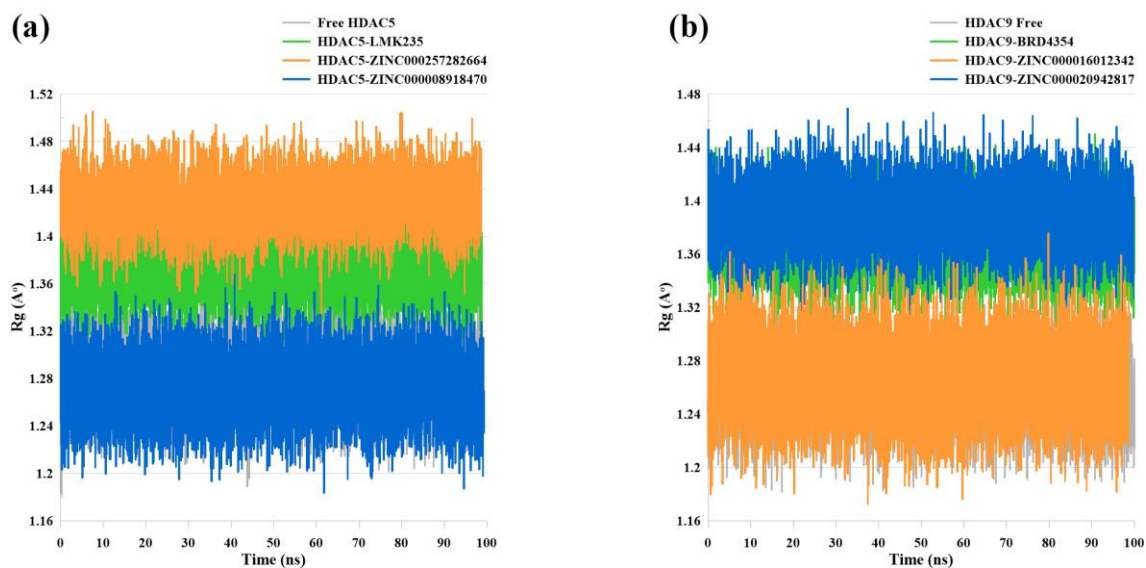


**Figure 3.46.** Representation of the radius of gyration ( $R_g$ ) for (a) HDAC5 complex systems; and (b) HDAC9 complex systems.

- Potential energy analysis:** Another useful measurement for examining the system stability over time is the potential energy profile. All studied systems were found to be stable and physically valid during MD simulations. HDAC5-ZINC000257282664 and HDAC5-ZINC00008918470 systems showed lower energy profiles compared to the apo-protein of HDAC5 and were found to be relatively similar to the energy of HDAC5-LMK235 complex system (Figure 3.47 (a)). This observation was also noted in the HDAC9 complexes with the ZINC000020942817 and ZINC000016012342 compounds, which displayed lower energy profiles than the apo-protein of HDAC9 (Figure 3.47 (b)).

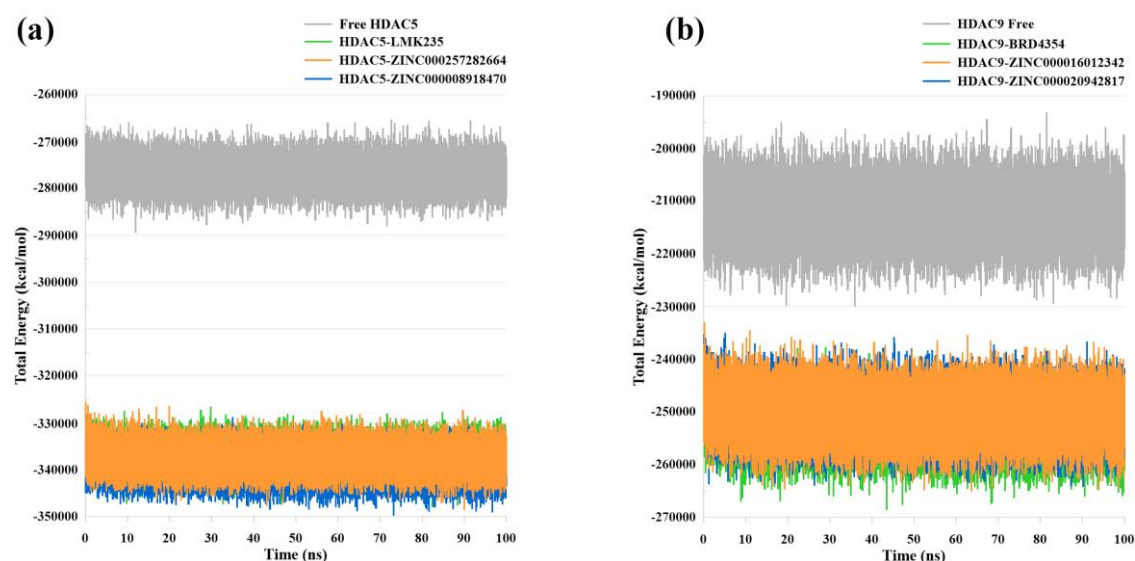


**Figure 3.47.** Potential Energy profiles for (a) HDAC5 complex systems; and (b) HDAC9 complex systems.

- Number of intermolecular hydrogen bonds:** The binding affinity degree in protein-ligand complex is influenced by the number of hydrogen bonds and the more hydrogen bonds number the greater binding affinity level. HDAC5-ZINC000257282664 complex formed maximum of 4 H-bonds during the simulation (Figure 3.48 (a)). The H-bond number gradually increased during the MD run especially after the first 50 ns. The maximum number of H-bonds formed in the HDAC5-ZINC000008918470 complex was found to be 5 (Figure 3.48 (b)). The majority of the complex conformations were found to form 2 H-bonds. HDAC9-ZINC000020942817 complex formed at most 2 H-bonds in very few conformations while the average of the H-bonds was found to be 1 bond during the MD simulation (Figure 3.48 (c)). Most of the conformations in HDAC9-ZINC000016012342 complex formed 1 H-bond throughout the simulation, and notably, the second half of the run showed an increased H-bond number with a maximum of 2 bonds (Figure 3.48 (d)).

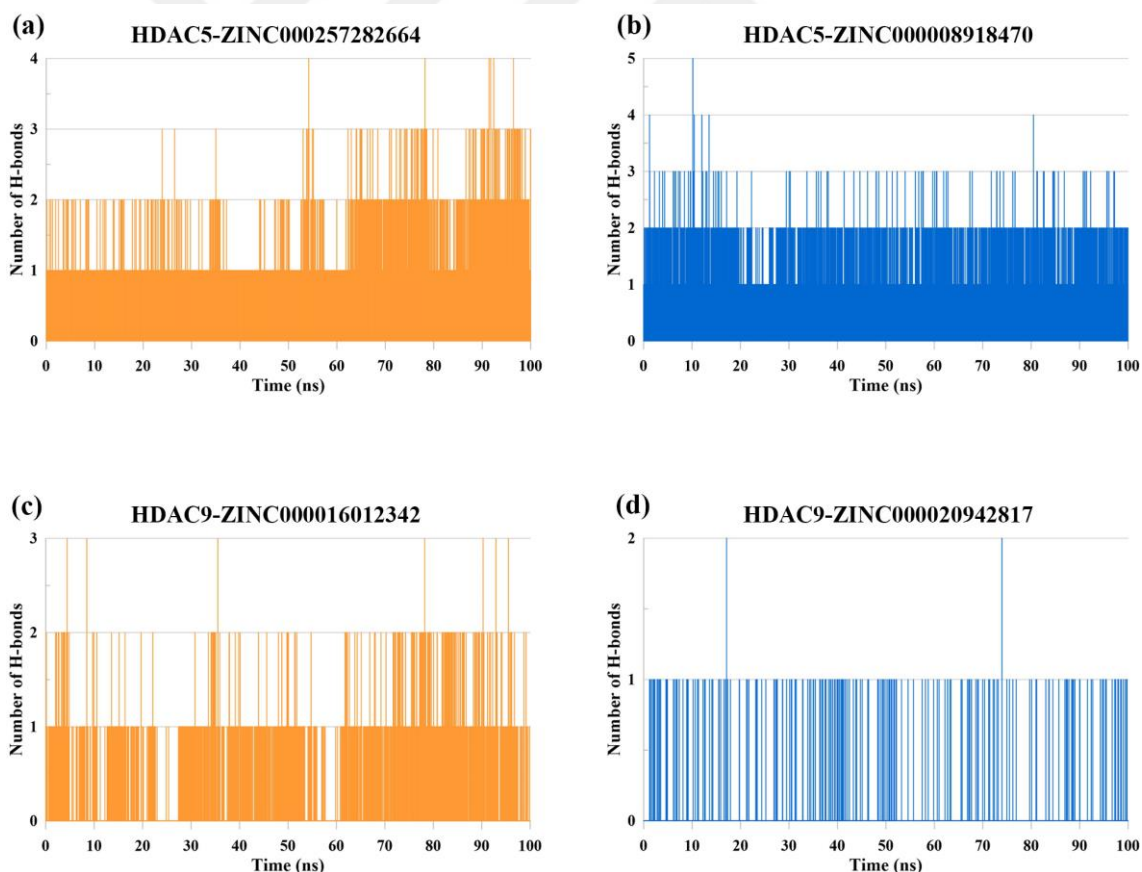


**Figure 3.48.** Number of hydrogen bonds profile of (a) HDAC5-ZINC000257282664 complex; (b) HDAC5-ZINC000008918470 complex; (c) HDAC9-ZINC000016012342 complex; and (d) HDAC9-ZINC000020942817 complex.

- **MM-PBSA calculations:** The average  $\Delta G$  (binding free energy) of the four isoform selective compounds was computed for the last 10 ns applying the MM-PBSA approach. The MM-PBSA calculations showed an average  $\Delta G$  of  $-19.67 \pm 5.66$  kcal/mol for the ZINC000257282664;  $-19.55 \pm 5.08$  kcal/mol for the ZINC000008918470;  $-18.85 \pm 3.77$  kcal/mol for the ZINC000016012342; and  $-16.11 \pm 4.82$  kcal/mol for the ZINC000020942817. Interestingly, the binding free energy calculations were found to be in good agreement with the QuickVina 2.0 ranking (Table 3.17).



## 4. DISCUSSION

### 4.1. HOMOLOGY MODELING OF CLASS IIA HDAC5 AND HDAC9, AND THE DESIGN OF DUAL-ACTING INHIBITORS

It is of a great importance and crucial to validate and assess the reliability and the quality of either the X-ray/NMR resolved protein structures or the generated homology models. ProSA tool and its ProSA-web server are among most commonly used tools to validate the quality of the 3D modeled structures for possible errors (Wiederstein & Sippl, 2007). Herein, ProSA-web was utilized in order to check the quality of both created homology models, M0014 and M0020. ProSA-web calculations of the quality scores of M0014 and M0020 were shown in a graph that illustrates the scores of all available X-ray resolved or NMR identified protein structures that are stored on the Protein Data Bank website (PDB) (Berman et al., 2002). This way, ProSA-web compares and correlates the quality score of a particular 3D model with those scores that were calculated for all experimentally resolved proteins available on the PDB website. The calculated Z-score by ProSA tool identifies the model's overall quality and estimates the total energy variation of the model to be correlated with the energy distribution originated from random structural conformations (Sippl, 1993, 1995). If a Z-score relies outside the characteristic range of native structures, models are believed to have structural errors within. According to ProSA-web calculations, M0014 and M0020 had Z-scores of -8.12 and -8.04, respectively, which are related to the native structural conformations.

PROCHECK tool and its web-based tool are also widely used to evaluate the overall quality of a structure or model (Laskowski et al., 1996). PROCHECK tool offers Ramachandran plot which is one of the most famous and reliable approaches to examine the overall quality of protein structure. It provides a useful method to assess the angle and torsion distribution in the protein structure. In addition, it delivers a summary of undesirable regions that display which rotations of the protein are not favored due to steric hindrance factors and steric collisions between atoms. Ninety percent or more of protein amino acid residues in the allowed regions is an indication of a good model (Laskowski et al., 1996). M0014 and M0020 homology models were found to have 90.4%

and 90.7%, respectively, of their polypeptide residues in the most favored regions, suggesting the good quality of the generated homology modeling 3D structures.

Furthermore, ERRAT program was used to verify the quality of the model by corresponding its structure to experimentally determined proteins. The program calculates the total number of nonbonded interactions among atoms, such as CC, CO, CN, OO, NO, and NN, within a 3.5 Å cutoff distance (Colovos & Yeates, 1993). ERRAT provides an overall quality factor (OQF) for the model structure that is represented as the percentage of the model in which the computed error level is less than 95% rejection threshold. Favored sidechains environment would show an average of 50% confidence or more. Generally, reliable model structure would produce 50 or more of OQF. The ERRAT calculations for M0014 and M0020 showed OQF of 87.34 and 86.4, respectively, suggesting that the majority of the amino acid residues are within an acceptable nonbonded environment.

Moreover, to test the ability of our created homology models to produce a comparable protein-ligand interaction, molecular docking study was carried out using two sets of HDAC known inhibitors respectively to each model. The experimentally calculated IC<sub>50</sub> or K<sub>i</sub> values agreed to the in silico predicted K<sub>i</sub> values that were obtained from AutoDock 4.2. All of those HDAC known inhibitors showed reasonable binding modes and interactions with the corresponding protein. Thus, this observation concluded that our generated models are reliable and could be employed for designing HDAC isoform-selective inhibitors.

To date, there are no available crystal structures for HDAC5 nor HDAC9. Thus, modeling these two enzymes will serve a good purpose to discover novel inhibitors for HDACs 5 and 9 (Elmezayen & Yelekçi, 2020). Therefore, created homology models were used to identify the best complex conformations of the protein-ligand binding modes. The present study aimed to explore promising inhibitors for these important enzymes via employing a variety of computational approaches including the structure-based drug design. Structure-based drug design has been widely utilized for searching for novel potential inhibitors against different HDAC enzymes (Krishna et al., 2015).

In order to accomplish this goal, a total library of ~100,000 molecules were retrieved from ChEMBL website in order to search for dual inhibiting leads against HDAC5 and HDAC9. AutoDock Vina and AutoDock 2.4 were employed to dock the small molecules into their corresponding enzymes, HDAC5 and HDAC9. All compounds were filtered according to their binding energy and affinity toward the enzymes. Four compounds were found to show lower binding energy and higher affinity compared to the selected HDACs known inhibitors. Two of these compounds exhibited closely similar binding affinity toward HDAC5 and HDAC9 and showed potential dual-acting drug property. The physicochemical properties and the drug-likeness profile were tested for these two compounds. The two compounds obeyed the famous Lipinski's rule of five that postulates for any oral drugs the molecular weight (MW) should be  $\leq 500$  Da; the octanol-water partition coefficient (LogP) should be  $\leq 5$ , the total number of hydrogen bond donors must be  $\leq 5$ , and the total number of hydrogen acceptors must be  $\leq 10$  (Lipinski, 2003). Additionally, the compounds were found to be PAINS-free molecules. Furthermore, the compounds were found to be following the well-known Jorgensen's rule of 3 which strictly states that oral drugs should exhibit an aqueous solubility (LogS)  $\geq -5.7$ ; the total number of primary metabolites must be  $\leq 7$ ; and the Caco-2 cell line permeability must be  $\geq 22$  nm/s (Di & Kerns, 2016).

Thorough structural examination of these two compounds exhibited prominent details about their structural properties and their ability to bind tightly to HDACs 5 and 9. Although they differ from other known inhibitors that have hydroxamic acid groups acting as a zinc-binding group, the catalytic  $Zn^{+2}$  atom within the active site of both HDACs was found to interact with the selected compounds. The two compounds proved to have important chemical interactions with the key residues of the binding pockets of the enzymes.

HDAC5 and HDAC9 along with their selected compounds were subjected to molecular dynamics simulations for a reasonable duration to overcome the rigid protein nature that accompanies the molecular docking approach, and to investigate the structural stability of the studied protein-ligand complex. The selected dual-acting compounds remained in the binding pockets of the proteins during the MD simulations and all systems displayed high stability as well. Analysis of the trajectories after the MD simulations provided a

great insight on the structural stability of the complex systems and were found to be consistent with all different measurements including the RMSD, RMSF, Rg, and the potential energy. In general, MM/PBSA calculations do not associate with the absolute values of the experiments; however, it is still able to produce a reasonable calculation for the compounds binding affinity (Chakraborty & Das, 2017; Koukoulitsa et al., 2016; Ngo & Li, 2012). Negatively contribution to the total free binding energy comes from electrostatic and van der Waal interactions along with the energy of nonpolar solvation. On the other hand, the positive contribution only comes from the energy of polar solvation (Verma et al., 2016). Based on the interactions plot and the data obtained from MM-PBSA, it is obvious that hydrophobic interactions are prominent in all complex systems.

According to the *in silico* examination, the two selected dual-acting compounds discovered in the present study showed high binding affinity toward HDACs 5 and 9. Therefore, we strongly recommend that these drug-like inhibitors could be treated as lead compounds and tested *in vitro* for advance optimization to design HDAC5 and HDAC9 dual-acting inhibitor.

#### **4.2. STRUCTURE-BASED DRUG DESIGNING OF ISOFORM SELECTIVE CLASS IIA HDACS INHIBITORS**

Perceptive variations within the active sites and the catalytic channels of HDAC protein members can be beneficial in obtaining isoform-selectivity (Bieliauskas & Pflum, 2008). In attempt to take advantage of that fact, here in the current study, we employed a comprehensive structure-based drug design testing more than 10 million drug-like compounds against class IIa HDAC enzymes.

CHEMBL2177655 and CHEMBL3126309 compounds displayed greater affinity and higher selectivity for HDAC4 over the rest of class IIa HDAC members. Both compounds spanned perfectly in the binding pocket of HDAC4 and formed several important interactions with the key residues in the active site including His158, His159, Gly167, Phe168, Asp196, His198, Asp290, Gly330, and many other residues. Deep in the catalytic channel, the catalytic Zn<sup>2+</sup> metal atom was found to be bonded to the carboxylate

groups of CHEMBL2177655 compound via a covalent bond and an attractive charge interaction; and a covalent bond to the carboxylate group of CHEMBL3126309 compound. This collectively may result in blocking the catalytic site and thus lead to the inhibition of the enzymatic activity.

In HDAC5, ZINC000033260361 and CHEMBL2426361 compounds fitted very well into the binding pocket of the enzyme with great binding affinity compared to the remaining of class IIa HDACs. These two compounds were found to have a variety of chemical interactions with the active amino acid residues lining the binding pocket of the enzyme involving His159, His160, Gly168, Phe169, Asp197, His199, Asp291, Gly331 and other several residues. The catalytic Zn<sup>2+</sup> metal atom was found to be covalently bonded to the fluorobenzene group of the ZINC000033260361 compound; and interacted with CHEMBL2426361 via a van der Waals interaction. These two compounds showed a potential isoform-selectivity for HDAC5 over other class IIa enzymes.

Interestingly, out of the 15 identified compounds, ZINC000009640741 and CHEMBL1968496 compounds exhibited the highest affinity toward HDAC7 compared all other class IIa HDACs, and thus showed promising isoform-selectivity for HDAC7. ZINC000009640741 compound is composed of 4 benzene rings connected with a sulfonyl group and spanned into the catalytic tunnel of HDAC7 forming prominent hydrophobic interactions with the key residues inside the binding pocket. ZINC000009640741 compound was found to be covalently bonded to the catalytic zinc atom. Similarly, CHEMBL1968496 compound contained four benzene rings. It was found to be extended in the binding site of HDAC7 with a great affinity and formed significant chemical interactions with the active amino acid residues in the active site including His166, His167, Gly175, Phe176, Asp204, His206, Asp235, and many other amino acid residues. The carboxylate group of CHEMBL1968496 was found to be covalently bonded to the catalytic zinc atom deep inside the binding pocket of HDAC7.

Although compound CHEMBL1761559 relatively showed the least binding affinity for HDAC9 in comparison to all other 15 tested compounds, the compound displayed modest isoform-selectivity for HDAC9 compared to all other class IIa HDACs. With about 3 to 38-fold selectivity, CHEMBL1761559 compound revealed a higher binding affinity toward HDAC9 compared to the rest of the enzymes. Key amino acid residues lining the



catalytic channel were found to be bonded via important interactions. These residues included His160, Gly168, Phe169, His199, Gly331, and different other residues. CHEMBL1761559 compound was found to be bound to the catalytic zinc atom via  $\pi$ -cation interaction. All the selected compounds seemed to interact with the key amino acids lying within the active site; thus this would interfere with the charge-relay system of HDACs (Somoza et al., 2004), and consequently would interrupt this system which may block the enzymatic activity. The diversity in the structures of the previous tested compounds, considering their pharmacophoric features, along with the subtle variations in the amino acid residues within the active sites of each HDAC member, might have facilitated in their isoform-selectivity.

The 15 top-ranked compounds were tested for their drug-likeness. Their ADMET properties were found to be within the normal range and followed “the rule of three” described by Jorgensen (Di & Kerns, 2016). Although ZINC000514563218 and ZINC000674197814 compounds were found to display a slightly raise in their TPSA values, Lipinski stated that it would still exhibit rational intestinal permeability as oral drugs (Lipinski, 2003). One violation of the Lipinski’s rule of five is still tolerated as Lipinski stated in 2001 as observed in two of the selected compounds, ZINC000033260361 and NSC 23217.

Moreover, molecular dynamics simulations were carried out to examine the binding affinity of the top-ranked compounds and the protein-ligand structural stability. Throughout the MD simulations, all the examined inhibitors were found to be stable and stayed interacted to their respective proteins at physiological condition. MD simulation approach has been effectively performed to assess the stability of different HDACs inhibitors. Several inhibitors were tested for their selectivity against all HDACs classes by performing short MD simulation for 5 ns (Thangapandian et al., 2012). In another study, novel HDAC inhibitors were investigated along with Vorinostat and tested against class II HDACs, in which their structural stability was subjected to short 5 ns MD run (Tambunan et al., 2013). In the present study, all the seven selected compounds-HDAC complex systems, the apo-proteins, and the known-inhibitor-HDACs complexes were subjected to a long 100 ns MD simulation. Analysis of the MD trajectories were found to

be satisfied and all other parameters were consistent throughout the molecular dynamics simulation including the RMSD, RMSF, Rg, and potential energy.

Several approaches that imply further sophisticated energy functions such as MM-PBSA, MM-GBSA, and QM/MM have been widely used in an attempt to enhance the computational calculations of ligands binding (Gleeson & Gleeson, 2009). Despite the fact that quantum mechanical methods like QM/MM are known for their accurate predictions, they require exhaustive computational calculations for virtual screening of large datasets. On the contrary, MM-PBSA or MM-GBSA methods were found to be less computationally intensive and result in improvement outputs when applied in free energy predictions (Lyne et al., 2006; Thompson et al., 2008). Even though the free binding energy calculation using MM-PBSA method is not entirely related to the experiments, this method would still deliver a rational binding affinity for protein-ligand complex (Chakraborty & Das, 2017; Koukoulitsa et al., 2016; Ngo & Li, 2012). Herein, based on the MM-PBSA calculations, CHEMBL2177655 compound displayed more negative energy than CHEMBL3126309 compound when bonded to HDAC4, and thus more binding affinity. The two selective compounds of HDAC5 were re-ranked according to the free binding energy predictions, where CHEMBL2426361 revealed more negative energy than ZINC000033260361. The same observation was seen with the two HDAC7 inhibitors, CHEMBL1968496 showed more negative energy than ZINC000009640741, which was ranked first after the molecular docking study. The MM-PBSA calculations revealed more negative binding energies compared to the molecular docking study suggesting again that the selected compounds could possibly be promising hits in the discovery of class IIa HDACs selective inhibitors.

Up to date, small amount of HDACs isoform-selective inhibitors were identified even though growing attempts in this discipline (Thaler & Mercurio, 2014; S. Zhang et al., 2015). Most of the identified HDACs inhibitors are either categorized as broad spectrum or class selective inhibitors. All the reported compounds in the current study exhibited high to moderate isoform-selectivity toward class IIa HDACs. Based on the above findings, the selected compounds could be used as scaffolds and may undergo additional optimization in attempt to design actual class IIa isoform selective HDAC inhibitors.

Hence, it is highly recommended that these compounds proceed for in vitro and in vivo examinations to evaluate their inhibition effects.

#### **4.3. LIGAND-BASED PHARMACOPHORE MODELING FOR SELECTIVE HDAC5 AND HDAC9 INHIBITORS**

One of the important methods in modern computer-aided drug design is the pharmacophore modeling, which has become a vital tool for the in silico drug discovery. The HipHop method has been widely used in pharmacophore modeling and effectively applied in exploring novel inhibitors against several biological systems (Che et al., 2018; Haidar & Hartmann, 2017; Shahlaei & Doosti, 2016). The 10 created pharmacophore models for HDAC5 contained the same common features; however, all models were found to be varied in their 3D spatial locations. The same observation was seen between the 10 generated pharmacophore hypotheses of HDAC9, in addition to the variations in the common features among the hypotheses. Guner and Henry scoring system was applied in the current study to evaluate all the created hypotheses. Consequently, Hypo1 of HDAC5 displayed the most statistically significance hypothesis where it yielded 93% of the active compounds and showed the highest GH score and enrichment factor with the following values 0.86 and 10.26, respectively. Hypo2 of HDAC9 was found to be the most statistically significance hypothesis as it yielded 93% of the active compounds and displayed 0.87 and 10.13 scores for the GH and the enrichment factor, respectively. Both hypotheses seemed statistically reliable models.

Hypo1 of HDAC5 and Hypo2 of HDAC9 were screened against a total of ~200,000 drug-like diverse structure compounds from ZINC15 database. The 3D database search retrieved ~7,000 compounds for Hypo1 and ~21,000 for Hypo2, all with fit value of 3 and above, which was calculated and ranked by the Catalyst tool in BIOVIA DS 4.5. The yielded compounds were further examined by the molecular docking approach in an attempt to predict their best binding modes. Hypo1 and Hypo2 were found to be in agreement with the classical pharmacophore features of HDAC inhibitors (Mottamal et al., 2015). The cap/linker/chelator characteristic of classic HDAC inhibitors was well exemplified by Hypo1 and Hypo2. Hydrophobic feature was found to be mapped onto the cap group; hydrogen bond acceptor mapped onto the linker of Hypo1, while aromatic

ring onto the linker of Hypo2; hydrogen bond donor and acceptor feature mapped onto the chelator group. These findings agreed with the common pharmacophoric features of HDAC inhibitors (Beckers et al., 2007).

Additionally, the 6 top-ranked compounds obtained in this study were described as drug-like compounds as they passed the Lipinski's rule of 5 and were found to be within the normal range of the ADMET properties, using the admetSAR and SwissADME web-based servers. Aqueous solubility of a drug compound, which is one of the ADMET descriptors, has a great impact on the transportation and the absorption of a drug compound in the biological systems. Quantitative structure–property relationships (QSPR) is effectively utilized to associate organic- and drug compounds to their corresponding water solubility (X. Q. Chen et al., 2002). Another ADMET property is the Caco-2 permeability, that describes the gastrointestinal permeability ration by predicting the degree of a drug compound transportation across the Caco-2 cell line (Peng et al., 2014). Caco-2 permeability level has been predicted in a variety of drug compounds and drug-like molecules *in silico* and *in vitro* (Fossati et al., 2008; Pham-The et al., 2013, 2018; Press, 2011). The physicochemical properties of the 6 top-ranked compounds in the current study were agreed to the previous mentioned ADMET parameters.

Molecular dynamics simulations were carried out to evaluate the binding mode stability of the apo-protein forms of HDAC5 and HDAC9 and their complex with the corresponding known inhibitors and the top-ranked compounds. Throughout the 100 ns MD run, and in addition to the existence of water molecules, all studied systems showed good stability and the small molecules persisted their interaction with the active site of their corresponding targets. HDAC5-ZINC000008918470 complex was found to display overall lower RMSD trend than HDAC5-ZINC000257282664 complex. Whereas HDAC9 complex with ZINC000016012342 and ZINC000020942817 compounds showed relatively similar RMSD profile. Free binding energy predictions employing MM-PBSA method has been successfully used to improve the *in silico* predictions of ligand-protein affinity (Gleeson & Gleeson, 2009). MM-PBSA method requires less exhaustive *in silico* calculations compared to QM/MM approaches (Lyne et al., 2006; Thompson et al., 2008). In MM-PBSA calculations, nonpolar solvation energy, van der Waals, and electrostatic interactions negatively contribute to the total energy of the

system, while positive contribution arises from polar solvation energy (Verma et al., 2016). According to the MM-PBSA calculations, the proposed compounds in the present study showed more negative energy compared to the QuickVina binding energy calculations, suggesting the high affinity of the ligands to their respective targets. More binding affinity in ligand-protein complex is demonstrated by more negative value of the binding free energy, and vice versa. The rank of the selected compounds based on the calculated binding free energy by MM-PBSA method agreed to the molecular docking study.

To the best of our knowledge, although several efforts were made to discover novel HDACs inhibitors against several HDACs targets by pharmacophore modeling (Choubey et al., 2016; N. Gupta et al., 2014; Kandakatla & Ramakrishnan, 2014), our study is the first to apply this approach to identify novel and isoform-selective HDACs 5 and 9 inhibitors. In the current study, training and test sets composed of only HDACs inhibitors that are in clinical trials or with potential inhibition activity for HDACs 5 and 9. Due to the cytotoxicity accompanied by the use of several of the HDACs inhibitors that are already in clinical trials and uses, scientists around the world are paying more attention toward exploring isoform-selective inhibitors. Herein, proposed inhibitors could be used for further optimization as they showed potential isoform-selectivity towards HDAC5 and HDAC9. Hence, further details about the structural features essential for identifying HDACs 5 and 9 selective inhibitors may be offered by the present study, providing opportunities for additional computational (in silico) and in vitro experiments in order to enhance the selectivity and potency of the proposed inhibitors.

## 5. CONCLUSIONS

All efforts that were made to identify potential class IIa HDACs isoform selective inhibitors for cancer treatment are described in this study. The zinc-dependent class IIa HDAC enzymes, which are mainly located in the nucleus and the cytoplasm, are found to be associated with differ types of cancers as they are over expressed, even though they show weaker enzymatic activity compared to class I HDACs. Class IIa HDACs 4, 5, 7, and 9 are found in protein-protein complexes with other transcriptional factor proteins. Class IIa HDACs along with other non-histone proteins control the microtubules and stimulate cancer tissues invasion. The aim of the current study was to apply different in silico approaches in an attempt to identify promising selective inhibitors for each individual enzyme of class IIa HDACs. In order to complete this aim, a variety of molecular modeling methods and computational approaches were carried out including structural and amino acid sequence alignments, homology modeling, virtual screening, molecular dynamics simulation, physicochemical description, and free binding energy calculations.

High amino acid sequence similarity and conserved active sites between class IIa HDACs were examined, which contributed to the difficulties in obtaining isoform-selectivity in the process. HDAC4, HDAC5, and HDAC9 revealed the highest sequence similarity as well as the structural resemblance, increased the challenge in designing specific inhibitors for each of the three isoforms. Being a close ancestor, the active site of HDACs 5 and 9 are found to be very similar to that of HDAC4, whereas HDAC7 slightly differs as being a far relative.

Up to date, and since the beginning of this study, there are no resolved structures for human HDACs 5 nor 9, or for any other organisms. For the completion of the present study, crystal structure of human HDAC4 was retrieved (PDB ID: 2VQM) and used as a template to create the 3D structures of both HDAC5 and HDAC9 due to their high amino acid sequence identity and similarity, particularly between their catalytic domains. The finest created 3D models were checked and validated for their structural conformations. Additionally, the built models were examined by docking sets of corresponding HDACs known inhibitors into their respective catalytic sites. To design novel dual-acting

inhibitors, a library composed of ~100,000 small molecules retrieved from ChEMBL website was docked against the two created models using AutoDock 4.2. According to the highest binding affinity, the two top-ranked compounds showed similar binding affinity for both HDAC5 and HDAC9, suggesting dual-acting effect. Later, MD simulations were conducted to examine the structural dynamics of the created homology models M0014 and M0020 and their complexes with their corresponding known inhibitors and top-ranked compounds. Analysis of trajectories after the MD simulations proved structural stability of all studied systems and the ligands remained bonded to their active sites throughout the simulations. Free binding energy calculations using MM-PBSA method revealed high binding affinity between the dual-acting inhibitors and their respective targets. The reported homology model structures could be useful for further future work and in understanding the dynamics of isoforms structures.

To overcome challenges in drug discovery, structure-based drug design was applied in the present study by in silico screening of ~10,000,000 drug-like compounds retrieved from ZINC15, ChEMBL, and NCI databases against class IIa HDAC enzymes. Combined HTS and molecular docking approaches were performed to guarantee the highest binding affinity and specificity of the studied compounds. A total of 15 compounds obtained from the virtual screening (5 compounds for HDAC4; 3 compounds for HDAC5; 6 compounds for HDAC7; and 1 compound for HDAC9) have displayed specificity for their corresponding isoform by applying similar selectivity criteria employed by other reported studies on selective inhibitors for HDACs. In addition, reported compounds have revealed drug-like properties and their physicochemical properties (ADMET) were found to be in an acceptable range. Moreover, molecular dynamics simulation was carried out to evaluate the structural dynamics and the stability of apo-proteins of the isoforms, the selective inhibitor-protein complexes, and their known inhibitor-protein complexes. While systems are solvated in the presence of water molecules, all the studied compounds persisted bound to their respective isoform throughout the 100 ns MD simulation. Comparative examinations of the trajectories after the MD simulations (including RMSD, RMSD, Rg, and potential energy parameters) in addition to the H-bond number suggested the stability of the complexes over time. The free binding energy predictions using MM-PBSA approach showed high affinity of the selected compounds toward their corresponding HDAC isoforms.

Moreover, to identify further selective inhibitors for HDAC5 and HDAC9 with more diverse scaffolds, ligand-based pharmacophore modeling was employed to generate common features using HipHop method and were statistically examined using the scoring system of Guner-Henry. The first hypothesis (Hypo1) generated for HDAC5 consisted of 1 hydrophobic (aromatic/aliphatic), 1 hydrogen bond donor, and 3 hydrogen bond acceptor features, returned 93% of the active compounds, and revealed of 0.86 for the GH score and 10.26 for the enrichment factor. In addition, the second hypothesis (Hypo2) generated for HDAC9 composed of 1 ring aromatic, 1 hydrophobic (aromatic/aliphatic), and 2 hydrogen bond acceptor features, returned 93% of the active compounds, and showed 0.87 score for the GH and 10.13 score for the enrichment factor. A total of ~200,000 small molecules were obtained from ZINC15 database and screened against Hypo1 and Hypo2 separately, for the search for potential isoform-selective inhibitors for HDACs 5 and 9. The 6 top-ranked compounds with the highest binding affinity were tested for their ADMET properties. They displayed good ADMET properties and were found to be drug-like inhibitors. Molecular docking approach was used to assess the binding affinity of the selected compounds across all class IIa HDACs to examine their isoform-selectivity. ZINC000257282664 and ZINC000008918470 compounds exhibited promising isoform-selectivity for HDAC5, whereas ZINC000016012342 and ZINC000020942817 compounds showed potential specificity for HDAC9. The structural stability of these inhibitors along with apo-protein forms were subjected to 100 ns MD simulations employing NAMD software. The analyses of RMSD, RMSF, radius of gyration, potential energy, hydrogen bonds number, and the MM-PBSA calculations after the MD simulations suggested that all studied inhibitors showed stable trend and remained interacted with the active site of their targets throughout the MD simulation. These findings suggest that the reported inhibitors could be used for further optimization and undergo in vitro examination for designing HDAC5 and HDAC9 isoform specific inhibitors.

Future study may include additional HTS and in silico virtual screening with more small molecules datasets in order to obtain further diverse scaffolds for potentially specific inhibitors against each member of class IIa HDAC enzyme. Additionally, extended molecular dynamics simulations might be carried out to further ascertain the structural dynamics and the stability of the ligand-protein complexes. Moreover, pharmacodynamic



and pharmacokinetic experiments would be performed in vitro to evaluate and examine the safety and toxicity of the candidate isoform selective inhibitors reported in the present study. Consequently, the biological activity of the reported compounds might be validated in vitro and tested against both solid and nonsolid tumor tissues. In addition, after obtaining the isoform selective inhibition, analysis of the molecular mechanisms by applying molecular biology means would be helpful to gain a detailed insight into the functional role of each member of HDAC enzymes in a particular cancer pathophysiology.

In the present study, quick discovery of drug-like compounds that target three-dimensional protein structures of class IIa HDAC isoforms, obtained by either comparative homology modeling or X-ray resolved structure, has been improved by the application of computer-aided drug design.

## REFERENCES

- Adcock, S. A., & McCammon, J. A. (2006). Molecular dynamics: Survey of methods for simulating the activity of proteins. *Chemical Reviews*, *106*(5), 1589–1615. <https://doi.org/10.1021/cr040426m>
- Ago, T., Liu, T., Zhai, P., Chen, W., Li, H., Molkentin, J. D., Vatner, S. F., & Sadoshima, J. (2008). A Redox-Dependent Pathway for Regulating Class II HDACs and Cardiac Hypertrophy. *Cell*, *133*(6), 978–993. <https://doi.org/10.1016/j.cell.2008.04.041>
- Aguilar, C. A., & Craighead, H. G. (2013). Micro- and nanoscale devices for the investigation of epigenetics and chromatin dynamics. *Nature Nanotechnology*, *8*(10), 709–718. <https://doi.org/10.1038/nnano.2013.195>
- Akhter, S. A., Luttrell, L. M., Rockman, H. A., Iaccarino, G., Lefkowitz, R. J., & Koch, W. J. (1998). Targeting the Receptor-G-protein Interface to Inhibit in Vivo Pressure Overload Myocardial Hypertrophy. *Science*, *280*(5363), 574 LP – 577. <https://doi.org/10.1126/science.280.5363.574>
- Alan Kozikowski, Jay H. Kalin, Kyle V. Butler, Joel Bergman, W. W. H. (2016). *Kozikowski, HDAC inhibitors and therapeutic methods using the same* (Patent No. US9249087B2). <https://patents.google.com/patent/US9249087B2/en>
- Albert, M., & Helin, K. (2010). Histone methyltransferases in cancer. *Seminars in Cell & Developmental Biology*, *21*(2), 209–220. <https://doi.org/https://doi.org/10.1016/j.semcd.2009.10.007>
- Alhossary, A., Handoko, S. D., Mu, Y., & Kwoh, C.-K. (2015). Fast, accurate, and reliable molecular docking with QuickVina 2. *Bioinformatics*, *31*(13), 2214–2216. <https://doi.org/10.1093/bioinformatics/btv082>
- Altschul, S. F., Gish, W., Miller, W., Myers, E. W., & Lipman, D. J. (1990). Basic local alignment search tool. *Journal of Molecular Biology*, *215*(3), 403–410. [https://doi.org/10.1016/S0022-2836\(05\)80360-2](https://doi.org/10.1016/S0022-2836(05)80360-2)
- Angibaud, P., Emelen, K. Van, Decrane, L., Brandt, S. van, Holte, P. ten, Pilatte, I., Roux, B., Poncelet, V., Speybrouck, D., Queguiner, L., Gaurrand, S., Mariën, A., Floren, W., Janssen, L., Verdonck, M., Dun, J. van, Gompel, J. van, Gilissen, R., Mackie, C., ... Arts, J. (2010). Identification of a series of substituted 2-piperazinyl-5-pyrimidylhydroxamic acids as potent histone deacetylase inhibitors. *Bioorganic and Medicinal Chemistry Letters*, *20*(1), 294–298. <https://doi.org/10.1016/j.bmcl.2009.10.118>
- Annunziato, A. (2008). DNA packaging: nucleosomes and chromatin. *Nature Education*, *1*(1), 26.
- Arinaminpathy, Y., Sansom, M. S. P., & Biggin, P. C. (2002). Molecular dynamics simulations of the ligand-binding domain of the ionotropic glutamate receptor GluR2. *Biophysical Journal*, *82*(2), 676–683. [https://doi.org/10.1016/S0006-3495\(02\)75430-1](https://doi.org/10.1016/S0006-3495(02)75430-1)

Auzzas, L., Larsson, A., Matera, R., Baraldi, A., Deschênes-Simard, B., Giannini, G., Cabri, W., Battistuzzi, G., Gallo, G., Ciacci, A., Vesci, L., Pisano, C., & Hanessian, S. (2010). Non-natural macrocyclic inhibitors of histone deacetylases: Design, synthesis, and activity. *Journal of Medicinal Chemistry*, 53(23), 8387–8399. <https://doi.org/10.1021/jm101092u>

Azagra, A., Román-González, L., Collazo, O., Rodríguez-Ubreva, J., de Yébenes, V. G., Barneda-Zahonero, B., Rodríguez, J., Castro de Moura, M., Grego-Bessa, J., Fernández-Duran, I., Islam, A. B. M. M. K., Esteller, M., Ramiro, A. R., Ballestar, E., & Parra, M. (2016). In vivo conditional deletion of HDAC7 reveals its requirement to establish proper B lymphocyte identity and development. *Journal of Experimental Medicine*, 213(12), 2591–2601. <https://doi.org/10.1084/jem.20150821>

Azimi, F., Ghasemi\*, J. B., Saghaei, L., Hassanzadeh, F., Mahdavi, M., Sadeghi-Aliabadi, H., & Scotti\*, M. T. S. and L. (2019). Identification of Essential 2D and 3D Chemical Features for Discovery of the Novel Tubulin Polymerization Inhibitors. In *Current Topics in Medicinal Chemistry* (Vol. 19, Issue 13, pp. 1092–1120). <https://doi.org/http://dx.doi.org/10.2174/1568026619666190520083655>

Baba, A. I., & Cătoi, C. (2007). *Comparative Oncology*. <https://pubmed.ncbi.nlm.nih.gov/20806453/>

Backs, J., Song, K., Bezprozvannaya, S., Chang, S., & Olson, E. N. (2006). CaM kinase II selectively signals to histone deacetylase 4 during cardiomyocyte hypertrophy. *The Journal of Clinical Investigation*, 116(7), 1853–1864. <https://doi.org/10.1172/JCI27438>

Backs, J., Worst, B. C., Lehmann, L. H., Patrick, D. M., Jebessa, Z., Kreusser, M. M., Sun, Q., Chen, L., Heft, C., Katus, H. A., & Olson, E. N. (2011). Selective repression of MEF2 activity by PKA-dependent proteolysis of HDAC4. *Journal of Cell Biology*, 195(3), 403–415. <https://doi.org/10.1083/jcb.201105063>

Baell, J. B., & Holloway, G. A. (2010). New substructure filters for removal of pan assay interference compounds (PAINS) from screening libraries and for their exclusion in bioassays. *Journal of Medicinal Chemistry*, 53(7), 2719–2740. <https://doi.org/10.1021/jm901137j>

Baker, E. N. (2006). Hydrogen bonding in biological macromolecules. In M. G. Rossmann & E. Arnold (Eds.), *International Tables for Crystallography* (pp. 546–552). Springer Netherlands. <https://doi.org/10.1107/97809553602060000711>

Baker, N. A., Sept, D., Joseph, S., Holst, M. J., & McCammon, J. A. (2001). Electrostatics of nanosystems: Application to microtubules and the ribosome. *Proceedings of the National Academy of Sciences of the United States of America*, 98(18), 10037–10041. <https://doi.org/10.1073/pnas.181342398>

Bantscheff, M., Hopf, C., Savitski, M. M., Dittmann, A., Grandi, P., Michon, A. M., Schlegl, J., Abraham, Y., Becher, I., Bergamini, G., Boesche, M., Delling, M., Dimpelfeld, B., Eberhard, D., Huthmacher, C., Mathieson, T., Poeckel, D., Reader, V., Strunk, K., ... Drewes, G. (2011). Chemoproteomics profiling of HDAC inhibitors

reveals selective targeting of HDAC complexes. *Nature Biotechnology*, 29(3), 255–268. <https://doi.org/10.1038/nbt.1759>

Barneda-Zahonero, B., Collazo, O., Azagra, A., Fernández-Duran, I., Serra-Musach, J., Islam, A. B. M. M. K., Vega-García, N., Malatesta, R., Camós, M., Gómez, A., Román-González, L., Vidal, A., López-Bigas, N., Villanueva, A., Esteller, M., & Parra, M. (2015). The transcriptional repressor HDAC7 promotes apoptosis and c-Myc downregulation in particular types of leukemia and lymphoma. *Cell Death & Disease*, 6(2), e1635–e1635. <https://doi.org/10.1038/cddis.2014.594>

Barnum, D., Greene, J., Smellie, A., & Sprague, P. (1996). Identification of common functional configurations among molecules. *Journal of Chemical Information and Computer Sciences*, 36(3), 563–571. <https://doi.org/10.1021/ci950273r>

Barrett, A., Santangelo, S., Tan, K., Catchpole, S., Roberts, K., Spencer-Dene, B., Hall, D., Scibetta, A., Burchell, J., & Verdin, E. (2007). Breast cancer associated transcriptional repressor PLU-1/JARID1B interacts directly with histone deacetylases. *International Journal of Cancer*, 121(2), 265–275. <https://doi.org/10.1002/ijc.22673>

Baselga, J., Bhardwaj, N., Cantley, L. C., DeMatteo, R., DuBois, R. N., Foti, M., Gapstur, S. M., Hahn, W. C., Helman, L. J., Jensen, R. A., Paskett, E. D., Lawrence, T. S., Lutzker, S. G., & Szabo, E. (2015). AACR Cancer Progress Report 2015. *Clinical Cancer Research*, 21(19 Supplement), S1 LP-S128. <https://doi.org/10.1158/1078-0432.CCR-15-1846>

Bateman, A. (2019). UniProt: A worldwide hub of protein knowledge. *Nucleic Acids Research*, 47(D1), D506–D515. <https://doi.org/10.1093/nar/gky1049>

Beckers, T., Burkhardt, C., Wieland, H., Gimmnich, P., Ciossek, T., Maier, T., & Sanders, K. (2007). Distinct pharmacological properties of second generation HDAC inhibitors with the benzamide or hydroxamate head group. *International Journal of Cancer*, 121(5), 1138–1148. <https://doi.org/10.1002/ijc.22751>

Beckett, A. H., Harper, N. J., & Clitherow, J. W. (1963). THE IMPORTANCE OF STEREOISOMERISM IN MUSCARINIC ACTIVITY. *Journal of Pharmacy and Pharmacology*, 15(1), 362–371. <https://doi.org/10.1111/j.2042-7158.1963.tb12799.x>

Berg, H. (1989). Molecular Biology of the Gene. *Bioelectrochemistry and Bioenergetics*, 22(1), 85. [https://doi.org/10.1016/0302-4598\(89\)85035-4](https://doi.org/10.1016/0302-4598(89)85035-4)

Bergman, J. A., Woan, K., Perez-Villaruel, P., Villagra, A., Sotomayor, E. M., & Kozikowski, A. P. (2012). Selective histone deacetylase 6 inhibitors bearing substituted urea linkers inhibit melanoma cell growth. *Journal of Medicinal Chemistry*, 55(22), 9891–9899. <https://doi.org/10.1021/jm301098e>

Bergström, C. A. S., & Larsson, P. (2018). Computational prediction of drug solubility in water-based systems: Qualitative and quantitative approaches used in the current drug discovery and development setting. *International Journal of Pharmaceutics*, 540(1–2), 185–193. <https://doi.org/10.1016/j.ijpharm.2018.01.044>

Berman, H. M., Battistuz, T., Bhat, T. N., Bluhm, W. F., Bourne, P. E., Burkhardt, K., Feng, Z., Gilliland, G. L., Iype, L., Jain, S., Fagan, P., Marvin, J., Padilla, D., Ravichandran, V., Schneider, B., Thanki, N., Weissig, H., Westbrook, J. D., & Zardecki, C. (2002). The protein data bank. *Acta Crystallographica Section D: Biological Crystallography*, 58(6 I), 899–907. <https://doi.org/10.1107/S0907444902003451>

Beveridge, D. L., & DiCapua, F. M. (1989). Free energy via molecular simulation: applications to chemical and biomolecular systems. *Annual Review of Biophysics and Biophysical Chemistry*, 18(1), 431–492. <https://doi.org/10.1146/annurev.bb.18.060189.002243>

Bieliauskas, A. V., & Pflum, M. K. H. (2008). Isoform-selective histone deacetylase inhibitors. *Chemical Society Reviews*, 37(7), 1402–1413. <https://doi.org/10.1039/B703830P>

Black, B. L., & Olson, E. N. (1998). TRANSCRIPTIONAL CONTROL OF MUSCLE DEVELOPMENT BY MYOCYTE ENHANCER FACTOR-2 (MEF2) PROTEINS. *Annual Review of Cell and Developmental Biology*, 14(1), 167–196. <https://doi.org/10.1146/annurev.cellbio.14.1.167>

Blaheta, R. A., Nau, H., & Cinatl, Jr, M. M. and J. (2002). Valproate and Valproate-Analogues: Potent Tools to Fight Against Cancer. In *Current Medicinal Chemistry* (Vol. 9, Issue 15, pp. 1417–1433). <https://doi.org/http://dx.doi.org/10.2174/0929867023369763>

Boffa, L. C., Vidali, G., Mann, R. S., & Allfrey, V. G. (1978). Suppression of histone deacetylation in vivo and in vitro by sodium butyrate. *Journal of Biological Chemistry*, 253(10), 3364–3366. <http://www.jbc.org/content/253/10/3364.abstract>

Boron, W. F., & Boulpaep, E. L. (2016). *Medical Physiology* (3rd ed.). Elsevier Health Sciences. <https://www.elsevier.com/books/medical-physiology/boron/978-1-4557-4377-3>

Boskovic, Z. V., Kemp, M. M., Freedy, A. M., Viswanathan, V. S., Pop, M. S., Fuller, J. H., Martinez, N. M., Figueroa Lazú, S. O., Hong, J. A., Lewis, T. A., Calarese, D., Love, J. D., Vetere, A., Almo, S. C., Schreiber, S. L., & Koehler, A. N. (2016). Inhibition of Zinc-Dependent Histone Deacetylases with a Chemically Triggered Electrophile. *ACS Chemical Biology*, 11(7), 1844–1851. <https://doi.org/10.1021/acscchembio.6b00012>

Botta, C. B., Cabri, W., Cini, E., De Cesare, L., Fattorusso, C., Giannini, G., Persico, M., Petrella, A., Rondinelli, F., Rodriguez, M., Russo, A., & Taddei, M. (2011). Oxime amides as a novel zinc binding group in histone deacetylase inhibitors: Synthesis, biological activity, and computational evaluation. *Journal of Medicinal Chemistry*, 54(7), 2165–2182. <https://doi.org/10.1021/jm101373a>

Bottomley, M. J., Lo Surdo, P. Lo, Di Giovine, P. Di, Cirillo, A., Scarpelli, R., Ferrigno, F., Jones, P., Neddermann, P., De Francesco, R., Steinkühler, C., Gallinari, P., & Carff, A. (2008). Structural and functional analysis of the human HDAC4 catalytic domain reveals a regulatory structural zinc-binding domain. *Journal of Biological Chemistry*,

283(39), 26694–26704. <https://doi.org/10.1074/jbc.M803514200>

Boyle, J. (2005). Lehninger principles of biochemistry (4th ed.): Nelson, D., and Cox, M. *Biochemistry and Molecular Biology Education*, 33(1), 74–75. <https://doi.org/10.1002/bmb.2005.494033010419>

Bradner, J. E., West, N., Grachan, M. L., Greenberg, E. F., Haggarty, S. J., Warnow, T., & Mazitschek, R. (2010). Chemical phylogenetics of histone deacetylases. *Nature Chemical Biology*, 6(3), 238–243. <https://doi.org/10.1038/nchembio.313>

Breslow, R., Belvedere, S., & Gershell, L. (2000). Development of Cytodifferentiating Agents for Cancer Chemotherapy. *Helvetica Chimica Acta*, 83(8), 1685–1692. [https://doi.org/10.1002/1522-2675\(20000809\)83:8<1685::AID-HLCA1685>3.0.CO;2-4](https://doi.org/10.1002/1522-2675(20000809)83:8<1685::AID-HLCA1685>3.0.CO;2-4)

Bürli, R. W., Luckhurst, C. A., Aziz, O., Matthews, K. L., Yates, D., Lyons, K. A., Beconi, M., McAllister, G., Breccia, P., Stott, A. J., Penrose, S. D., Wall, M., Lamers, M., Leonard, P., Müller, I., Richardson, C. M., Jarvis, R., Stones, L., Hughes, S., ... Dominguez, C. (2013). Design, synthesis, and biological evaluation of potent and selective class IIa histone deacetylase (HDAC) inhibitors as a potential therapy for huntington's disease. *Journal of Medicinal Chemistry*, 56(24), 9934–9954. <https://doi.org/10.1021/jm4011884>

Cadot, B., Brunetti, M., Coppari, S., Fedeli, S., de Rinaldis, E., Russo, C. Dello, Gallinari, P., De Francesco, R., Steinkühler, C., & Filocamo, G. (2009). Loss of Histone Deacetylase 4 Causes Segregation Defects during Mitosis of p53-Deficient Human Tumor Cells. *Cancer Research*, 69(15), 6074 LP – 6082. <https://doi.org/10.1158/0008-5472.CAN-08-2796>

Cai, X., Zhai, H. X., Wang, J., Forrester, J., Qu, H., Yin, L., Lai, C. J., Bao, R., & Qian, C. (2010). Discovery of 7-(4-(3-Ethynylphenylamino)-7-methoxyquinazolin-6-yloxy)-N-hydroxyheptanamide (CUDC-101) as a potent multi-acting HDAC, EGFR, and HER2 inhibitor for the treatment of cancer. *Journal of Medicinal Chemistry*, 53(5), 2000–2009. <https://doi.org/10.1021/jm901453q>

Campos, E. I., & Reinberg, D. (2009). Histones: Annotating chromatin. *Annual Review of Genetics*, 43(1), 559–599. <https://doi.org/10.1146/annurev.genet.032608.103928>

Cao, X., & Chen, D. (2005). The BMP signaling and in vivo bone formation. *Gene*, 357(1), 1–8. <https://doi.org/https://doi.org/10.1016/j.gene.2005.06.017>

Carrillo, A. K., Guiguemde, W. A., & Guy, R. K. (2015). Evaluation of histone deacetylase inhibitors (HDACi) as therapeutic leads for human African trypanosomiasis (HAT). *Bioorganic and Medicinal Chemistry*, 23(16), 5151–5155. <https://doi.org/10.1016/j.bmc.2014.12.066>

Cavasotto, C. N., & Phatak, S. S. (2009). Homology modeling in drug discovery: current trends and applications. *Drug Discovery Today*, 14(13–14), 676–683. <https://doi.org/10.1016/j.drudis.2009.04.006>

Celeste, A., Fernandez-Capetillo, O., Kruhlak, M. J., Pilch, D. R., Staudt, D. W., Lee, A.,

Bonner, R. F., Bonner, W. M., & Nussenzweig, A. (2003). Histone H2AX phosphorylation is dispensable for the initial recognition of DNA breaks. *Nature Cell Biology*, 5(7), 675–679. <https://doi.org/10.1038/ncb1004>

Cereto-Massagué, A., Guasch, L., Valls, C., Mulero, M., Pujadas, G., & Garcia-Vallvé, S. (2012). DecoyFinder: An easy-to-use python GUI application for building target-specific decoy sets. *Bioinformatics*, 28(12), 1661–1662. <https://doi.org/10.1093/bioinformatics/bts249>

Chakraborty, S., & Das, P. (2017). Emergence of Alternative Structures in Amyloid Beta 1-42 Monomeric Landscape by N-terminal Hexapeptide Amyloid Inhibitors. *Scientific Reports*, 7(1), 9941. <https://doi.org/10.1038/s41598-017-10212-5>

Chang, H. H., Bong, S. J., Kao, H. Y., & Jin, Z. G. (2008). VEGF stimulates HDAC7 phosphorylation and cytoplasmic accumulation modulating matrix metalloproteinase expression and angiogenesis. *Arteriosclerosis, Thrombosis, and Vascular Biology*, 28(10), 1782–1788. <https://doi.org/10.1161/ATVBAHA.108.172528>

Chang, H. H., Wang, W., Bong, S. J., Wong, C., Hausser, A., Pfizenmaier, K., McKinsey, T. A., Olson, E. N., & Jin, Z. G. (2008). Protein kinase D-dependent phosphorylation and nuclear export of histone deacetylase 5 mediates vascular endothelial growth factor-induced gene expression and angiogenesis. *Journal of Biological Chemistry*, 283(21), 14590–14599. <https://doi.org/10.1074/jbc.M800264200>

Che, J., Wang, Z., Sheng, H., Huang, F., Dong, X., Hu, Y., Xie, X., & Hu, Y. (2018). Ligand-based pharmacophore model for the discovery of novel CXCR2 antagonists as anti-cancer metastatic agents. *Royal Society Open Science*, 5(7), 180176. <https://doi.org/10.1098/rsos.180176>

Chen, X. Q., Cho, S. J., Li, Y., & Venkatesh, S. (2002). Prediction of aqueous solubility of organic compounds using a quantitative structure-property relationship. *Journal of Pharmaceutical Sciences*, 91(8), 1838–1852. <https://doi.org/10.1002/jps.10178>

Chen, Y., Wang, X., Xiang, W., He, L., Tang, M., Wang, F., Wang, T., Yang, Z., Yi, Y., Wang, H., Niu, T., Zheng, L., Lei, L., Li, X., Song, H., & Chen, L. (2016). Development of Purine-Based Hydroxamic Acid Derivatives: Potent Histone Deacetylase Inhibitors with Marked in Vitro and in Vivo Antitumor Activities. *Journal of Medicinal Chemistry*, 59(11), 5488–5504. <https://doi.org/10.1021/acs.jmedchem.6b00579>

Cheng, F., Li, W., & Tang, G. L. and Y. (2013). In Silico ADMET Prediction: Recent Advances, Current Challenges and Future Trends. In *Current Topics in Medicinal Chemistry* (Vol. 13, Issue 11, pp. 1273–1289). <https://doi.org/http://dx.doi.org/10.2174/15680266113139990033>

Chien, K. R. (1999). Stress pathways and heart failure. *Cell*, 98(5), 555–558.

Cho, Y., & Cavalli, V. (2012). HDAC5 is a novel injury-regulated tubulin deacetylase controlling axon regeneration. *The EMBO Journal*, 31(14), 3063–3078. <https://doi.org/10.1038/emboj.2012.160>

Cho, Y., Sloutsky, R., Naegle, K. M., & Cavalli, V. (2013). Injury-Induced HDAC5 Nuclear Export Is Essential for Axon Regeneration. *Cell*, 155(4), 894–908. <https://doi.org/10.1016/j.cell.2013.10.004>

Choi, H. S., Choi, B. Y., Cho, Y.-Y., Mizuno, H., Kang, B. S., Bode, A. M., & Dong, Z. (2005). Phosphorylation of Histone H3 at Serine 10 Is Indispensable for Neoplastic Cell Transformation. *Cancer Research*, 65(13), 5818 LP – 5827. <https://doi.org/10.1158/0008-5472.CAN-05-0197>

Choi, M. A., Park, S. Y., Chae, H. Y., Song, Y., Sharma, C., & Seo, Y. H. (2019). Design, synthesis and biological evaluation of a series of CNS penetrant HDAC inhibitors structurally derived from amyloid- $\beta$  probes. *Scientific Reports*, 9(1), 13187. <https://doi.org/10.1038/s41598-019-49784-9>

Chothia, C., & Lesk, A. M. (1986). The relation between the divergence of sequence and structure in proteins. *The EMBO Journal*, 5(4), 823–826. <https://doi.org/10.1002/j.1460-2075.1986.tb04288.x>

Choubey, S. K., Mariadasse, R., Rajendran, S., & Jeyaraman, J. (2016). Identification of novel histone deacetylase 1 inhibitors by combined pharmacophore modeling, 3D-QSAR analysis, in silico screening and Density Functional Theory (DFT) approaches. *Journal of Molecular Structure*, 1125, 391–404. <https://doi.org/10.1016/j.molstruc.2016.06.082>

Choudhary, C., Kumar, C., Gnad, F., Nielsen, M. L., Rehman, M., Walther, T. C., Olsen, J. V., & Mann, M. (2009). Lysine Acetylation Targets Protein Complexes and Co-Regulates Major Cellular Functions. *Science*, 325(5942), 834 LP – 840. <https://doi.org/10.1126/science.1175371>

Christianson, D. W., & Lipscomb, W. N. (1986). The Complex between Carboxypeptidase A and a Possible Transition-State Analogue: Mechanistic Inferences from High-Resolution X-ray Structures of Enzyme-Inhibitor Complexes. *Journal of the American Chemical Society*, 108(16), 4998–5003. <https://doi.org/10.1021/ja00276a048>

Clark, D. E. (2008). What has virtual screening ever done for drug discovery? *Expert Opinion on Drug Discovery*, 3(8), 841–851. <https://doi.org/10.1517/17460441.3.8.841>

Clement, O. O., & Mehl, A. T. (2000). HipHop: pharmacophores based on multiple common-feature alignments. In *Pharmacophore perception, development, and use in drug design*. International University Line La Jolla, CA. <https://books.google.com/books?hl=cs&lr=&id=NWw2aOKIRp8C&pgis=1>

Clocchiatti, A., Di Giorgio, E., Ingrao, S., Meyer-Almes, F.-J., Tripodo, C., & Brancolini, C. (2013). Class IIa HDACs repressive activities on MEF2-dependent transcription are associated with poor prognosis of ER+ breast tumors. *The FASEB Journal*, 27(3), 942–954. <https://doi.org/10.1096/fj.12-209346>

Clocchiatti, A., Florean, C., & Brancolini, C. (2011). Class IIa HDACs: from important roles in differentiation to possible implications in tumourigenesis. *Journal of Cellular and*



*Molecular Medicine*, 15(9), 1833–1846. <https://doi.org/10.1111/j.1582-4934.2011.01321.x>

Colovos, C., & Yeates, T. O. (1993). Verification of protein structures: Patterns of nonbonded atomic interactions. *Protein Science*, 2(9), 1511–1519. <https://doi.org/10.1002/pro.5560020916>

Daina, A., Michielin, O., & Zoete, V. (2017). SwissADME: A free web tool to evaluate pharmacokinetics, drug-likeness and medicinal chemistry friendliness of small molecules. *Scientific Reports*, 7(1), 42717. <https://doi.org/10.1038/srep42717>

Dalrymple, S. L., Becker, R. E., Zhou, H., Deweese, T. L., & Isaacs, J. T. (2012). Tasquinimod prevents the angiogenic rebound induced by fractionated radiation resulting in an enhanced therapeutic response of prostate cancer xenografts. *Prostate*, 72(6), 638–648. <https://doi.org/10.1002/pros.21467>

Darcy, M. J., Calvin, K., Cavnar, K., & Ouimet, C. C. (2010). Regional and subcellular distribution of HDAC4 in mouse brain. *Journal of Comparative Neurology*, 518(5), 722–740. <https://doi.org/10.1002/cne.22241>

Dassault Systèmes. (2016). BIOVIA Discovery Studio Visualizer. In *V16.1.0.15350*.

Davis, I. W., & Baker, D. (2009). RosettaLigand Docking with Full Ligand and Receptor Flexibility. *Journal of Molecular Biology*, 385(2), 381–392. <https://doi.org/10.1016/j.jmb.2008.11.010>

Davoudmanesh, S., & Mosaabadi, J. M. (2018). Investigation of the effect of homocysteinylation of substance P on its binding to the NK1 receptor using molecular dynamics simulation. *Journal of Molecular Modeling*, 24(7), 177. <https://doi.org/10.1007/s00894-018-3695-7>

de Beer, S., Vermeulen, N., & Oostenbrink, C. (2010). The Role of Water Molecules in Computational Drug Design. In *Current Topics in Medicinal Chemistry* (Vol. 10, Issue 1, pp. 55–66). <https://doi.org/10.2174/156802610790232288>

De Ruijter, A. J. M., Van Gennip, A. H., Caron, H. N., Kemp, S., & Van Kuilenburg, A. B. P. (2003). Histone deacetylases (HDACs): Characterization of the classical HDAC family. *Biochemical Journal*, 370(3), 737–749. <https://doi.org/10.1042/BJ20021321>

De Vivo, M., Masetti, M., Bottegoni, G., & Cavalli, A. (2016). Role of Molecular Dynamics and Related Methods in Drug Discovery. *Journal of Medicinal Chemistry*, 59(9), 4035–4061. <https://doi.org/10.1021/acs.jmedchem.5b01684>

De Vreese, R., & D'hooghe, M. (2017). Synthesis and applications of benzohydroxamic acid-based histone deacetylase inhibitors. *European Journal of Medicinal Chemistry*, 135, 174–195. <https://doi.org/10.1016/j.ejmech.2017.04.013>

Delehanty, L. L., Bullock, G. C., & Goldfarb, A. N. (2012). Protein kinase D-HDAC5 signaling regulates erythropoiesis and contributes to erythropoietin cross-talk with GATA1. *Blood*, 120(20), 4219–4228. <https://doi.org/10.1182/blood-2011-10-387050>

Deng, X., Ewton, D. Z., Mercer, S. E., & Friedman, E. (2005). Mirk/dyrk1B Decreases the Nuclear Accumulation of Class II Histone Deacetylases during Skeletal Muscle Differentiation. *Journal of Biological Chemistry*, 280(6), 4894–4905. <http://www.jbc.org/content/280/6/4894.abstract>

Denis, M., Akeila, B., Sophie, P., David, W., Christophe, D., Virginie, L., Rosette, L., & Vincent, C. (2007). Histone Deacetylase 7 Silencing Alters Endothelial Cell Migration, a Key Step in Angiogenesis. *Circulation Research*, 101(12), 1237–1246. <https://doi.org/10.1161/CIRCRESAHA.107.149377>

Dequiedt, F., Kasler, H., Fischle, W., Kiermer, V., Weinstein, M., Herndier, B. G., & Verdin, E. (2003). HDAC7, a Thymus-Specific Class II Histone Deacetylase, Regulates Nur77 Transcription and TCR-Mediated Apoptosis. *Immunity*, 18(5), 687–698. [https://doi.org/10.1016/S1074-7613\(03\)00109-2](https://doi.org/10.1016/S1074-7613(03)00109-2)

Di Giorgio, E., Clocchiatti, A., Piccinin, S., Sgorbissa, A., Viviani, G., Peruzzo, P., Romeo, S., Rossi, S., Dei Tos, A. P., Maestro, R., & Brancolini, C. (2013). MEF2 Is a Converging Hub for Histone Deacetylase 4 and Phosphatidylinositol 3-Kinase/Akt-Induced Transformation. *Molecular and Cellular Biology*, 33(22), 4473 LP – 4491. <https://doi.org/10.1128/MCB.01050-13>

Di, L., & Kerns, E. H. (2016). Drug-Like Properties: Concepts, Structure Design and Methods from ADME to Toxicity Optimization. In *Drug-Like Properties: Concepts, Structure Design and Methods from ADME to Toxicity Optimization*. <https://doi.org/10.1016/C2013-0-18378-X>

Di Pompo, G., Salerno, M., Rotili, D., Valente, S., Zwergel, C., Avnet, S., Lattanzi, G., Baldini, N., & Mai, A. (2015). Novel histone deacetylase inhibitors induce growth arrest, apoptosis, and differentiation in sarcoma cancer stem cells. *Journal of Medicinal Chemistry*, 58(9), 4073–4079. <https://doi.org/10.1021/acs.jmedchem.5b00126>

Dietrich, J.-B., Takemori, H., Grosch-Dirrig, S., Bertorello, A., & Zwiller, J. (2012). Cocaine induces the expression of MEF2C transcription factor in rat striatum through activation of SIK1 and phosphorylation of the histone deacetylase HDAC5. *Synapse*, 66(1), 61–70. <https://doi.org/10.1002/syn.20988>

Dokmanovic, M., Clarke, C., & Marks, P. A. (2007). Histone deacetylase inhibitors: Overview and perspectives. *Molecular Cancer Research*, 5(10), 981–989. <https://doi.org/10.1158/1541-7786.MCR-07-0324>

Downs, J. A., Lowndes, N. F., & Jackson, S. P. (2000). A role for *Saccharomyces cerevisiae* histone H2A in DNA repair. *Nature*, 408(6815), 1001–1004. <https://doi.org/10.1038/35050000>

Duong, V., Bret, C., Altucci, L., Mai, A., Duraffourd, C., Loubersac, J., Harmand, P. O., Bonnet, S., Valente, S., Maudelonde, T., Cavailles, V., & Boulle, N. (2008). Specific activity of class II histone deacetylases in human breast cancer cells. *Molecular Cancer Research*, 6(12), 1908–1919. <https://doi.org/10.1158/1541-7786.MCR-08-0299>

Early Breast Cancer Trialists' Collaborative Group (EBCTCG). (2005). Effects of chemotherapy and hormonal therapy for early breast cancer on recurrence and 15-year survival: an overview of the randomised trials. *The Lancet*, 365(9472), 1687–1717. [https://doi.org/https://doi.org/10.1016/S0140-6736\(05\)66544-0](https://doi.org/https://doi.org/10.1016/S0140-6736(05)66544-0)

Eckschlager, T., Plch, J., Stiborova, M., & Hrabeta, J. (2017). Histone deacetylase inhibitors as anticancer drugs. In *International Journal of Molecular Sciences* (Vol. 18, Issue 7). <https://doi.org/10.3390/ijms18071414>

Egger, G., Liang, G., Aparicio, A., & Jones, P. A. (2004). Epigenetics in human disease and prospects for epigenetic therapy. *Nature*, 429(6990), 457–463. <https://doi.org/10.1038/nature02625>

Ehrlich, P. (1909). Über den jetzigen Stand der Chemotherapie. *Berichte Der Deutschen Chemischen Gesellschaft*, 42(1), 17–47. <https://doi.org/10.1002/cber.19090420105>

El-Beltagi, H. M., Martens, A. C. M., Lelieveld, P., Haroun, E. A., & Hagenbeek, A. (1993). Acetyldinaline: A New Oral Cytostatic Drug with Impressive Differential Activity against Leukemic Cells and Normal Stem Cells Preclinical Studies in a Relevant Rat Model for Human Acute Myelocytic Leukemia. *Cancer Research*, 53(13), 3008–3014. <http://cancerres.aacrjournals.org/content/53/13/3008.abstract>

Ellis, L., & Pili, R. (2010). Histone deacetylase inhibitors: Advancing therapeutic strategies in hematological and solid malignancies. *Pharmaceuticals*, 3(8), 2441–2469. <https://doi.org/10.3390/ph3082441>

Elmezayen, A. D., & Yelekçi, K. (2020). Homology modeling and in silico design of novel and potential dual-acting inhibitors of human histone deacetylases HDAC5 and HDAC9 isozymes. *Journal of Biomolecular Structure and Dynamics*, 1–19. <https://doi.org/10.1080/07391102.2020.1798812>

Estiu, G., Greenberg, E., Harrison, C. B., Kwiatkowski, N. P., Mazitschek, R., Bradner, J. E., & Wiest, O. (2008). Structural origin of selectivity in class II-selective histone deacetylase inhibitors. *Journal of Medicinal Chemistry*, 51(10), 2898–2906. <https://doi.org/10.1021/jm7015254>

FAN, G., & HUTNICK, L. (2005). Methyl-CpG binding proteins in the nervous system. *Cell Research*, 15(4), 255–261. <https://doi.org/10.1038/sj.cr.7290294>

Fass, D. M., Shah, R., Ghosh, B., Hennig, K., Norton, S., Zhao, W. N., Reis, S. A., Klein, P. S., Mazitschek, R., Maglathlin, R. L., Lewis, T. A., & Haggarty, S. J. (2011). Short-chain HDAC inhibitors differentially affect vertebrate development and neuronal chromatin. *ACS Medicinal Chemistry Letters*, 2(1), 39–42. <https://doi.org/10.1021/ml1001954>

Ferrari, A. M., Wei, B. Q., Costantino, L., & Shoichet, B. K. (2004). Soft docking and multiple receptor conformations in virtual screening. *Journal of Medicinal Chemistry*, 47(21), 5076–5084. <https://doi.org/10.1021/jm049756p>

Fielitz, J., Kim, M.-S., Shelton, J. M., Qi, X., Hill, J. A., Richardson, J. A., Bassel-Duby,

R., & Olson, E. N. (2008). Requirement of protein kinase D1 for pathological cardiac remodeling. *Proceedings of the National Academy of Sciences*, 105(8), 3059 LP – 3063. <https://doi.org/10.1073/pnas.0712265105>

Finnin, M. S., Donigian, J. R., Cohen, A., Richon, V. M., Rifkind, R. A., Marks, P. A., Breslow, R., & Pavletich, N. P. (1999). Structures of a histone deacetylase homologue bound to the TSA and SAHA inhibitors. *Nature*, 401(6749), 188–193. <https://doi.org/10.1038/43710>

Fischle, W., Dequiedt, F., Hendzel, M. J., Guenther, M. G., Lazar, M. A., Voelter, W., & Verdin, E. (2002). Enzymatic Activity Associated with Class II HDACs Is Dependent on a Multiprotein Complex Containing HDAC3 and SMRT/N-CoR. *Molecular Cell*, 9(1), 45–57. [https://doi.org/10.1016/S1097-2765\(01\)00429-4](https://doi.org/10.1016/S1097-2765(01)00429-4)

Fiser, Andras. (2010). Template-based protein structure modeling. In D. Fenyö (Ed.), *Methods in molecular biology (Clifton, N.J.)* (Vol. 673, pp. 73–94). Humana Press. [https://doi.org/10.1007/978-1-60761-842-3\\_6](https://doi.org/10.1007/978-1-60761-842-3_6)

Fiser, András. (2004). Protein structure modeling in the proteomics era. *Expert Review of Proteomics*, 1(1), 97–110. <https://doi.org/10.1586/14789450.1.1.97>

Fitzsimons, H. L. (2015). The Class IIa histone deacetylase HDAC4 and neuronal function: Nuclear nuisance and cytoplasmic stalwart? *Neurobiology of Learning and Memory*, 123, 149–158. <https://doi.org/https://doi.org/10.1016/j.nlm.2015.06.006>

Fleming, C. L., Ashton, T. D., Gaur, V., McGee, S. L., & Pfeffer, F. M. (2014). Improved synthesis and structural reassignment of MC1568: A class IIa selective HDAC inhibitor. *Journal of Medicinal Chemistry*, 57(3), 1132–1135. <https://doi.org/10.1021/jm401945k>

Fossati, L., Dechaume, R., Hardillier, E., Chevillon, D., Prevost, C., Bolze, S., & Maubon, N. (2008). Use of simulated intestinal fluid for Caco-2 permeability assay of lipophilic drugs. *International Journal of Pharmaceutics*, 360(1–2), 148–155. <https://doi.org/10.1016/j.ijpharm.2008.04.034>

Frenkel, D., Smit, B., Tobochnik, J., McKay, S. R., & Christian, W. (1997). Understanding Molecular Simulation. In B. Smit (Ed.), *Computers in Physics* (2nd ed., Vol. 11, Issue 4). Academic Press, Inc. PP - USA. <https://doi.org/10.1063/1.4822570>

Frey, N., & Olson, E. N. (2003). Cardiac Hypertrophy: The Good, the Bad, and the Ugly. *Annual Review of Physiology*, 65(1), 45–79. <https://doi.org/10.1146/annurev.physiol.65.092101.142243>

Frey, Norbert, McKinsey, T. A., & Olson, E. N. (2000). Decoding calcium signals involved in cardiac growth and function. *Nature Medicine*, 6(11), 1221–1227. <https://doi.org/10.1038/81321>

Frey, R. R., Wada, C. K., Garland, R. B., Curtin, M. L., Michaelides, M. R., Li, J., Pease, L. J., Glaser, K. B., Marcotte, P. A., Bouska, J. J., Murphy, S. S., & Davidsen, S. K. (2002). Trifluoromethyl ketones as inhibitors of histone deacetylase. *Bioorganic and Medicinal Chemistry Letters*, 12(23), 3443–3447. <https://doi.org/10.1016/S0960->

Frohlich, E. D., Chien, Y., Sesoko, S., & Pegram, B. L. (1993). Relationship between dietary sodium intake, hemodynamics, and cardiac mass in SHR and WKY rats. *American Journal of Physiology-Regulatory, Integrative and Comparative Physiology*, 264(1), R30–R34. <https://doi.org/10.1152/ajpregu.1993.264.1.R30>

Frye, R. A. (2000). Phylogenetic classification of prokaryotic and eukaryotic Sir2-like proteins. *Biochemical and Biophysical Research Communications*, 273(2), 793–798. <https://doi.org/10.1006/bbrc.2000.3000>

Gao, C., Liu, Y., Lam, M., & Kao, H.-Y. (2010). Histone deacetylase 7 (HDAC7) regulates myocyte migration and differentiation. *Biochimica et Biophysica Acta (BBA) - Molecular Cell Research*, 1803(10), 1186–1197. <https://doi.org/10.1016/j.bbamcr.2010.06.008>

Gaulton, A., Hersey, A., Nowotka, M. L., Patricia Bento, A., Chambers, J., Mendez, D., Mutowo, P., Atkinson, F., Bellis, L. J., Cibrian-Uhalte, E., Davies, M., Dedman, N., Karlsson, A., Magarinos, M. P., Overington, J. P., Papadatos, G., Smit, I., & Leach, A. R. (2017). The ChEMBL database in 2017. *Nucleic Acids Research*, 45(D1), D945–D954. <https://doi.org/10.1093/nar/gkw1074>

Geng, L., Cuneo, K. C., Fu, A., Tu, T., Atadja, P. W., & Hallahan, D. E. (2006). Histone deacetylase (HDAC) inhibitor LBH589 increases duration of  $\gamma$ -H2AX foci and confines HDAC4 to the cytoplasm in irradiated non-small cell lung cancer. *Cancer Research*, 66(23), 11298–11304. <https://doi.org/10.1158/0008-5472.CAN-06-0049>

Giannini, G., Marzi, M., Marzo, M. Di, Battistuzzi, G., Pezzi, R., Brunetti, T., Cabri, W., Vesci, L., & Pisano, C. (2009). Exploring bis-(indolyl)methane moiety as an alternative and innovative CAP group in the design of histone deacetylase (HDAC) inhibitors. *Bioorganic and Medicinal Chemistry Letters*, 19(10), 2840–2843. <https://doi.org/10.1016/j.bmcl.2009.03.101>

Giannini, G., Marzi, M., Pezzi, R., Brunetti, T., Battistuzzi, G., Marzo, M. Di, Cabri, W., Vesci, L., & Pisano, C. (2009). N-Hydroxy-(4-oxime)-cinnamide: A versatile scaffold for the synthesis of novel histone deacetylase (HDAC) inhibitors. *Bioorganic and Medicinal Chemistry Letters*, 19(8), 2346–2349. <https://doi.org/10.1016/j.bmcl.2009.02.029>

Gil, V. S., Bhagat, G., Howell, L., Zhang, J., Kim, C. H., Stengel, S., Vega, F., Zelent, A., & Petrie, K. (2016). Deregulated expression of HDAC9 in B cells promotes development of lymphoproliferative disease and lymphoma in mice. *DMM Disease Models and Mechanisms*, 9(12), 1483–1495. <https://doi.org/10.1242/dmm.023366>

Gleeson, M. P., & Gleeson, D. (2009). QM/MM as a tool in fragment based drug discovery. A cross-docking, rescoring study of kinase inhibitors. *Journal of Chemical Information and Modeling*, 49(6), 1437–1448. <https://doi.org/10.1021/ci900022h>

Goldberg, A. D., Allis, C. D., & Bernstein, E. (2007). Epigenetics: A Landscape Takes Shape. *Cell*, 128(4), 635–638. <https://doi.org/10.1016/j.cell.2007.02.006>

Goldblum, J. R., Weiss, S. W., & Folpe, A. L. (2013). *Enzinger and Weiss's soft tissue tumors E-book*. Elsevier Health Sciences.

Graziano, M. J., Spoon, T. A., Cockrell, E. A., Rowse, P. E., & Gonzales, A. J. (2001). Induction of apoptosis in rat peripheral blood lymphocytes by the anticancer drug CI-994 (acetyldinaline). *Journal of Biomedicine and Biotechnology*, 2001(2), 52–61. <https://doi.org/10.1155/S1110724301000146>

Greer, E. L., & Shi, Y. (2012). Histone methylation: a dynamic mark in health, disease and inheritance. *Nature Reviews Genetics*, 13(5), 343–357. <https://doi.org/10.1038/nrg3173>

Grégoire, S., Tremblay, A. M., Xiao, L., Yang, Q., Ma, K., Nie, J., Mao, Z., Wu, Z., Giguère, V., & Yang, X.-J. (2006). Control of MEF2 Transcriptional Activity by Coordinated Phosphorylation and Sumoylation. *Journal of Biological Chemistry*, 281(7), 4423–4433. <http://www.jbc.org/content/281/7/4423.abstract>

Grozinger, C. M., & Schreiber, S. L. (2000). Regulation of histone deacetylase 4 and 5 and transcriptional activity by 14-3-3-dependent cellular localization. *Proceedings of the National Academy of Sciences*, 97(14), 7835 LP – 7840. <https://doi.org/10.1073/pnas.140199597>

Grozinger, C. M., & Schreiber, S. L. (2002). Deacetylase enzymes: Biological functions and the use of small-molecule inhibitors. *Chemistry and Biology*, 9(1), 3–16. [https://doi.org/10.1016/S1074-5521\(02\)00092-3](https://doi.org/10.1016/S1074-5521(02)00092-3)

Gschwend, D. A., Good, A. C., & Kuntz, I. D. (1996). Molecular docking towards drug discovery. *Journal of Molecular Recognition*, 9(2), 175–186. [https://doi.org/10.1002/\(SICI\)1099-1352\(199603\)9:2<175::AID-JMR260>3.0.CO;2-D](https://doi.org/10.1002/(SICI)1099-1352(199603)9:2<175::AID-JMR260>3.0.CO;2-D)

Gu, X., Wang, Y., Wang, M., Wang, J., & Li, N. (2019). Computational investigation of imidazopyridine analogs as protein kinase B (Akt1) allosteric inhibitors by using 3D-QSAR, molecular docking and molecular dynamics simulations. *Journal of Biomolecular Structure and Dynamics*, 1–16. <https://doi.org/10.1080/07391102.2019.1705185>

Guan, Y., Chen, Q., Yang, X., Haines, P., Pei, M., Terek, R., Wei, X., Zhao, T., & Wei, L. (2012). Subcellular relocation of histone deacetylase 4 regulates growth plate chondrocyte differentiation through Ca<sup>2+</sup>/calmodulin-dependent kinase IV. *American Journal of Physiology-Cell Physiology*, 303(1), C33–C40. <https://doi.org/10.1152/ajpcell.00348.2011>

Guerriero, J. L., Sotayo, A., Ponichtera, H. E., Castrillon, J. A., Pourzia, A. L., Schad, S., Johnson, S. F., Carrasco, R. D., Lazo, S., Bronson, R. T., Davis, S. P., Lobera, M., Nolan, M. A., & Letai, A. (2017). Class IIa HDAC inhibition reduces breast tumours and metastases through anti-tumour macrophages. *Nature*, 543(7645), 428–432. <https://doi.org/10.1038/nature21409>

Guner, O., Clement, O., & Kurogi, Y. (2004). Pharmacophore Modeling and Three Dimensional Database Searching for Drug Design Using Catalyst: Recent Advances.

Güner, O. F., & Bowen, J. P. (2014). Setting the Record Straight: The Origin of the Pharmacophore Concept. *Journal of Chemical Information and Modeling*, 54(5), 1269–1283. <https://doi.org/10.1021/ci5000533>

Gupta, N., Sitwala, N., & Patel, K. (2014). Pharmacophore modelling, validation, 3D virtual screening, docking, design and in silico ADMET simulation study of histone deacetylase class-1 inhibitors. *Medicinal Chemistry Research*, 23(11), 4853–4864. <https://doi.org/10.1007/s00044-014-1057-2>

Gupta, S., Kim, S. Y., Artis, S., Molfese, D. L., Schumacher, A., Sweatt, J. D., Paylor, R. E., & Lubin, F. D. (2010). Histone Methylation Regulates Memory Formation. *The Journal of Neuroscience*, 30(10), 3589 LP – 3599. <https://doi.org/10.1523/JNEUROSCI.3732-09.2010>

Ha, C. H., Kim, J. Y., Zhao, J., Wang, W., Jhun, B. S., Wong, C., & Jin, Z. G. (2010). PKA phosphorylates histone deacetylase 5 and prevents its nuclear export, leading to the inhibition of gene transcription and cardiomyocyte hypertrophy. *Proceedings of the National Academy of Sciences*, 107(35), 15467 LP – 15472. <https://doi.org/10.1073/pnas.1000462107>

Haberland, M., Montgomery, R. L., & Olson, E. N. (2009). The many roles of histone deacetylases in development and physiology: implications for disease and therapy. *Nature Reviews Genetics*, 10(1), 32–42. <https://doi.org/10.1038/nrg2485>

Haggarty, S. J., Koeller, K. M., Wong, J. C., Grozinger, C. M., & Schreiber, S. L. (2003). Domain-selective small-molecule inhibitor of histone deacetylase 6 (HDAC6)-mediated tubulin deacetylation. *Proceedings of the National Academy of Sciences of the United States of America*, 100(8), 4389–4394. <https://doi.org/10.1073/pnas.0430973100>

Haidar, S., & Hartmann, R. W. (2017). Computational prediction of new CYP17 inhibitors based on pharmacophore modeling, virtual screening and docking approach. *Pharmazie*, 72(9), 529–536. <https://doi.org/10.1691/ph.2017.7516>

Hanahan, D., & Weinberg, R. A. (2000). The Hallmarks of Cancer. *Cell*, 100(1), 57–70. [https://doi.org/10.1016/S0092-8674\(00\)81683-9](https://doi.org/10.1016/S0092-8674(00)81683-9)

Hansson, T., Marelus, J., & Åqvist, J. (1998). Ligand binding affinity prediction by linear interaction energy methods. *Journal of Computer-Aided Molecular Design*, 12(1), 27–35. <https://doi.org/10.1023/A:1007930623000>

Haus, P., Korbus, M., Schröder, M., & Meyer-Almes, F. J. (2011). Identification of selective class II histone deacetylase inhibitors using a novel dual-parameter binding assay based on fluorescence anisotropy and lifetime. *Journal of Biomolecular Screening*, 16(10), 1206–1216. <https://doi.org/10.1177/1087057111424605>

Haworth, R. S., Konstantina, S., J., C. A., & Metin, A. (2012). Neurohormonal Regulation of Cardiac Histone Deacetylase 5 Nuclear Localization by Phosphorylation-Dependent

and Phosphorylation-Independent Mechanisms. *Circulation Research*, 110(12), 1585–1595. <https://doi.org/10.1161/CIRCRESAHA.111.263665>

Heineke, J., & Molkenin, J. D. (2006). Regulation of cardiac hypertrophy by intracellular signalling pathways. *Nature Reviews Molecular Cell Biology*, 7(8), 589–600. <https://doi.org/10.1038/nrm1983>

Henkes, L. M., Haus, P., Jäger, F., Ludwig, J., & Meyer-Almes, F. J. (2012). Synthesis and biochemical analysis of 2,2,3,3,4,4,5,5,6,6,7,7-dodecafluoro- N-hydroxy-octanediamides as inhibitors of human histone deacetylases. *Bioorganic and Medicinal Chemistry*, 20(2), 985–995. <https://doi.org/10.1016/j.bmc.2011.11.041>

Holoch, D., & Moazed, D. (2015). RNA-mediated epigenetic regulation of gene expression. *Nature Reviews Genetics*, 16(2), 71–84. <https://doi.org/10.1038/nrg3863>

Hsu, K. C., Liu, C. Y., Lin, T. E., Hsieh, J. H., Sung, T. Y., Tseng, H. J., Yang, J. M., & Huang, W. J. (2017). Novel Class Iia-Selective Histone Deacetylase Inhibitors Discovered Using an in Silico Virtual Screening Approach. *Scientific Reports*, 7(1), 3228. <https://doi.org/10.1038/s41598-017-03417-1>

Huang, J., Rauscher, S., Nawrocki, G., Ran, T., Feig, M., De Groot, B. L., Grubmüller, H., & MacKerell, A. D. (2016). CHARMM36m: An improved force field for folded and intrinsically disordered proteins. *Nature Methods*, 14(1), 71–73. <https://doi.org/10.1038/nmeth.4067>

Huang, W. T., Tsai, Y. H., Chen, S. H., Kuo, C. W., Kuo, Y. L., Lee, K. T., Chen, W. C., Wu, P. C., Chuang, C. Y., Cheng, S. M., Lin, C. H., Leung, E. Y., Chang, Y. C., & Cheung, C. H. A. (2017). HDAC2 and HDAC5 up-regulations modulate survivin and miR-125a-5p expressions and promote hormone therapy resistance in estrogen receptor positive breast cancer cells. *Frontiers in Pharmacology*, 8(DEC), 902. <https://doi.org/10.3389/fphar.2017.00902>

Huang, Y., Tan, M., Gosink, M., Wang, K. K. W., & Sun, Y. (2002). Histone Deacetylase 5 Is Not a p53 Target Gene, But Its Overexpression Inhibits Tumor Cell Growth and Induces Apoptosis. *Cancer Research*, 62(10), 2913 LP – 2922. <http://cancerres.aacrjournals.org/content/62/10/2913.abstract>

Hull, E. E., Montgomery, M. R., & Leyva, K. J. (2016). HDAC Inhibitors as Epigenetic Regulators of the Immune System: Impacts on Cancer Therapy and Inflammatory Diseases. *BioMed Research International*, 2016, 8797206. <https://doi.org/10.1155/2016/8797206>

Humphrey, W., Dalke, A., & Schulten, K. (1996). VMD: Visual molecular dynamics. *Journal of Molecular Graphics*, 14(1), 33–38. [https://doi.org/10.1016/0263-7855\(96\)00018-5](https://doi.org/10.1016/0263-7855(96)00018-5)

Hutt, D. M., Herman, D., Rodrigues, A. P. C., Noel, S., Pilewski, J. M., Matteson, J., Hoch, B., Kellner, W., Kelly, J. W., Schmidt, A., Thomas, P. J., Matsumura, Y., Skach, W. R., Gentsch, M., Riordan, J. R., Sorscher, E. J., Okiyonedo, T., Yates, J. R., Lukacs,



G. L., ... Balch, W. E. (2010). Reduced histone deacetylase 7 activity restores function to misfolded CFTR in cystic fibrosis. *Nature Chemical Biology*, 6(1), 25–33. <https://doi.org/10.1038/nchembio.275>

I., G. J., Erhe, G., Xiyang, S., T., P. R., & J., K. W. (2012). Determining the Absolute Requirement of G Protein–Coupled Receptor Kinase 5 for Pathological Cardiac Hypertrophy. *Circulation Research*, 111(8), 1048–1053. <https://doi.org/10.1161/CIRCRESAHA.112.273367>

Illi, B., Russo, C. Dello, Colussi, C., Rosati, J., Pallaoro, M., Spallotta, F., Rotili, D., Valente, S., Ragone, G., Martelli, F., Biglioli, P., Steinkuhler, C., Gallinari, P., Mai, A., Capogrossi, M. C., & Gaetano, C. (2008). Nitric oxide modulates chromatin folding in human endothelial cells via protein phosphatase 2A activation and class II histone deacetylases nuclear shuttling. *Circulation Research*, 102(1), 51–58. <https://doi.org/10.1161/CIRCRESAHA.107.157305>

Isaacs, J. T., Antony, L., Dalrymple, S. L., Brennen, W. N., Gerber, S., Hammers, H., Wissing, M., Kachhap, S., Luo, J., Xing, L., Bjork, P., Olsson, A., Bjork, A., & Leanderson, T. (2013). Tasquinimod is an allosteric modulator of HDAC4 survival signaling within the compromised cancer microenvironment. *Cancer Research*, 73(4), 1386–1399. <https://doi.org/10.1158/0008-5472.CAN-12-2730>

Jaboin, J., Wild, J., Hamidi, H., Khanna, C., Kim, C. J., Robey, R., Bates, S. E., & Thiele, C. J. (2002). MS-27-275, an inhibitor of histone deacetylase, has marked in vitro and in vivo antitumor activity against pediatric solid tumors. *Cancer Research*, 62(21), 6108–6115. <http://cancerres.aacrjournals.org/content/62/21/6108.abstract>

Jang, C.-W., Shibata, Y., Starmer, J., Yee, D., & Magnuson, T. (2015). Histone H3.3 maintains genome integrity during mammalian development. *Genes & Development*, 29(13), 1377–1392. <https://doi.org/10.1101/gad.264150.115>

Jayathilaka, N., Han, A., Gaffney, K. J., Dey, R., Jarusiewicz, J. A., Noridomi, K., Philips, M. A., Lei, X., He, J., Ye, J., Gao, T., Petasis, N. A., & Chen, L. (2012). Inhibition of the function of class IIa HDACs by blocking their interaction with MEF2. *Nucleic Acids Research*, 40(12), 5378–5388. <https://doi.org/10.1093/nar/gks189>

Jensen, E. D., Gopalakrishnan, R., & Westendorf, J. J. (2009). Bone Morphogenic Protein 2 Activates Protein Kinase D to Regulate Histone Deacetylase 7 Localization and Repression of Runx2. *Journal of Biological Chemistry*, 284(4), 2225–2234. <http://www.jbc.org/content/284/4/2225.abstract>

Jiang, F., & Kim, S. H. (1991). “Soft docking”: Matching of molecular surface cubes. *Journal of Molecular Biology*, 219(1), 79–102. [https://doi.org/10.1016/0022-2836\(91\)90859-5](https://doi.org/10.1016/0022-2836(91)90859-5)

Jiang, N., Wang, X., Yang, Y., & Dai, W. (2006). Advances in Mitotic Inhibitors for Cancer Treatment. *Mini Reviews in Medicinal Chemistry*, 6(8), 885–895. <https://doi.org/10.2174/138955706777934955>

Jin, B., Li, Y., & Robertson, K. D. (2011). DNA Methylation: Superior or Subordinate in the Epigenetic Hierarchy? *Genes & Cancer*, 2(6), 607–617. <https://doi.org/10.1177/1947601910393957>

Jinjiang, P., Chen, Y., Kanchana, N., E., C. M., P., M. M., Guoyong, Y., & C., B. B. (2008). GIT1 Mediates HDAC5 Activation by Angiotensin II in Vascular Smooth Muscle Cells. *Arteriosclerosis, Thrombosis, and Vascular Biology*, 28(5), 892–898. <https://doi.org/10.1161/ATVBAHA.107.161349>

Johnson, M., Zaretskaya, I., Raytselis, Y., Merezhuk, Y., McGinnis, S., & Madden, T. L. (2008). NCBI BLAST: a better web interface. *Nucleic Acids Research*, 36(Web Server issue), W5–W9. <https://doi.org/10.1093/nar/gkn201>

Jones, G., Willett, P., & Glen, R. C. (1995). Molecular recognition of receptor sites using a genetic algorithm with a description of desolvation. *Journal of Molecular Biology*, 245(1), 43–53. [https://doi.org/https://doi.org/10.1016/S0022-2836\(95\)80037-9](https://doi.org/https://doi.org/10.1016/S0022-2836(95)80037-9)

Jones, G., Willett, P., Glen, R. C., Leach, A. R., & Taylor, R. (1997). Development and validation of a genetic algorithm for flexible docking. *Journal of Molecular Biology*, 267(3), 727–748. <https://doi.org/10.1006/jmbi.1996.0897>

Jones, P., Bottomley, M. J., Carfi, A., Cecchetti, O., Ferrigno, F., Lo Surdo, P., Ontoria, J. M., Rowley, M., Scarpelli, R., Schultz-Fademrecht, C., & Steinkühler, C. (2008). 2-Trifluoroacetylthiophenes, a novel series of potent and selective class II histone deacetylase inhibitors. *Bioorganic and Medicinal Chemistry Letters*, 18(11), 3456–3461. <https://doi.org/10.1016/j.bmcl.2008.02.026>

Jung, M. (2012). Inhibitors of Histone Deacetylase as New Anticancer Agents. In *Current Medicinal Chemistry* (Vol. 8, Issue 12, pp. 1505–1511). <https://doi.org/10.2174/0929867013372058>

Jung, M., Brosch, G., Kölle, D., Scherf, H., Gerhäuser, C., & Loidl, P. (1999). Amide analogues of trichostatin A as inhibitors of histone deacetylase and inducers of terminal cell differentiation. *Journal of Medicinal Chemistry*, 42(22), 4669–4679. <https://doi.org/10.1021/jm991091h>

Kaletsch, A., Pinkerneil, M., Hoffmann, M. J., Jaguva Vasudevan, A. A., Wang, C., Hansen, F. K., Wiek, C., Hanenberg, H., Gertzen, C., Gohlke, H., Kassack, M. U., Kurz, T., Schulz, W. A., & Niegisch, G. (2018). Effects of novel HDAC inhibitors on urothelial carcinoma cells. *Clinical Epigenetics*, 10(1), 100. <https://doi.org/10.1186/s13148-018-0531-y>

Kalin, J. H., & Bergman, J. A. (2013). Development and therapeutic implications of selective histone deacetylase 6 inhibitors. *Journal of Medicinal Chemistry*, 56(16), 6297–6313. <https://doi.org/10.1021/jm4001659>

Kandakatla, N., & Ramakrishnan, G. (2014). Ligand Based Pharmacophore Modeling and Virtual Screening Studies to Design Novel HDAC2 Inhibitors. *Advances in Bioinformatics*, 2014, 812148. <https://doi.org/10.1155/2014/812148>

Kao, G. D., McKenna, W. G., Guenther, M. G., Muschel, R. J., Lazar, M. A., & Yen, T. J. (2003). Histone deacetylase 4 interacts with 53BP1 to mediate the DNA damage response. *Journal of Cell Biology*, 160(7), 1017–1027. <https://doi.org/10.1083/jcb.200209065>

Kasler, H. G., Lee, I. S., Lim, H. W., & Verdin, E. (2018). Histone Deacetylase 7 mediates tissue-specific autoimmunity via control of innate effector function in invariant Natural Killer T Cells. *ELife*, 7, e32109. <https://doi.org/10.7554/eLife.32109>

Kasler, H. G., Lim, H. W., Mottet, D., Collins, A. M., Lee, I. S., & Verdin, E. (2012). Nuclear export of histone deacetylase 7 during thymic selection is required for immune self-tolerance. *The EMBO Journal*, 31(23), 4453–4465. <https://doi.org/10.1038/emboj.2012.295>

Kasler, H. G., & Verdin, E. (2006). *The Class Iia Histone Deacetylases BT - Histone Deacetylases: Transcriptional Regulation and Other Cellular Functions* (E. Verdin (ed.); pp. 129–163). Humana Press. <https://doi.org/10.1385/1-59745-024-3:129>

Kasler, H. G., Young, B. D., Mottet, D., Lim, H. W., Collins, A. M., Olson, E. N., & Verdin, E. (2011). Histone Deacetylase 7 Regulates Cell Survival and TCR Signaling in CD4/CD8 Double-Positive Thymocytes. *The Journal of Immunology*, 186(8), 4782 LP – 4793. <https://doi.org/10.4049/jimmunol.1001179>

Kehat, I., Accornero, F., Aronow, B. J., & Molkenin, J. D. (2011). Modulation of chromatin position and gene expression by HDAC4 interaction with nucleoporins. *Journal of Cell Biology*, 193(1), 21–29. <https://doi.org/10.1083/jcb.201101046>

Kemp, M. M., Wang, Q., Fuller, J. H., West, N., Martinez, N. M., Morse, E. M., Weïwer, M., Schreiber, S. L., Bradner, J. E., & Koehler, A. N. (2011). A novel HDAC inhibitor with a hydroxy-pyrimidine scaffold. *Bioorganic and Medicinal Chemistry Letters*, 21(14), 4164–4169. <https://doi.org/10.1016/j.bmcl.2011.05.098>

Khan, O., & La Thangue, N. B. (2012). HDAC inhibitors in cancer biology: Emerging mechanisms and clinical applications. *Immunology and Cell Biology*, 90(1), 85–94. <https://doi.org/10.1038/icb.2011.100>

KIER, L. B. (1967). Molecular Orbital Calculation of Preferred Conformations of Acetylcholine, Muscarine, and Muscarone. *Molecular Pharmacology*, 3(5), 487 LP – 494. <http://molpharm.aspetjournals.org/content/3/5/487.abstract>

Kim, H. J., & Bae, S. C. (2011). Histone deacetylase inhibitors: Molecular mechanisms of action and clinical trials as anti-cancer drugs. *American Journal of Translational Research*, 3(2), 166–179. <https://pubmed.ncbi.nlm.nih.gov/21416059>

Klein, D. C., & Hainer, S. J. (2020). Chromatin regulation and dynamics in stem cells. In T. G. B. T.-C. T. in D. B. Fazzio (Ed.), *Current Topics in Developmental Biology* (Vol. 138, pp. 1–71). Academic Press. <https://doi.org/10.1016/bs.ctdb.2019.11.002>

Kolinski, A., Betancourt, M. R., Kihara, D., Rotkiewicz, P., & Skolnick, J. (2001). Generalized comparative modeling (GENECOMP): A combination of sequence

comparison, threading, and lattice modeling for protein structure prediction and refinement. *Proteins: Structure, Function and Genetics*, 44(2), 133–149. <https://doi.org/10.1002/prot.1080>

Kollman, P. A., Massova, I., Reyes, C., Kuhn, B., Huo, S., Chong, L., Lee, M., Lee, T., Duan, Y., Wang, W., Donini, O., Cieplak, P., Srinivasan, J., Case, D. A., & Cheatham, T. E. (2000). Calculating structures and free energies of complex molecules: Combining molecular mechanics and continuum models. *Accounts of Chemical Research*, 33(12), 889–897. <https://doi.org/10.1021/ar000033j>

Komatsu, Y., Tomizaki, K., Tsukamoto, M., Kato, T., Nishino, N., Sato, S., Yamori, T., Tsuruo, T., Furumai, R., Yoshida, M., Horinouchi, S., & Hayashi, H. (2001). Cyclic Hydroxamic-acid-containing Peptide 31, a Potent Synthetic Histone Deacetylase Inhibitor with Antitumor Activity. *Cancer Research*, 61(11), 4459 LP – 4466. <http://cancerres.aacrjournals.org/content/61/11/4459.abstract>

Kong, Y., Jung, M., Wang, K., Grindrod, S., Velena, A., Lee, S. A., Dakshanamurthy, S., Yang, Y., Miessau, M., Zheng, C., Dritschilo, A., & Brown, M. L. (2011). Histone Deacetylase Cytoplasmic Trapping by a Novel Fluorescent HDAC Inhibitor. *Molecular Cancer Therapeutics*, 10(9), 1591 LP – 1599. <https://doi.org/10.1158/1535-7163.MCT-10-0779>

Kontoyianni, M. (2017). *Docking and Virtual Screening in Drug Discovery BT - Proteomics for Drug Discovery: Methods and Protocols* (I. M. Lazar, M. Kontoyianni, & A. C. Lazar (eds.); pp. 255–266). Springer New York. [https://doi.org/10.1007/978-1-4939-7201-2\\_18](https://doi.org/10.1007/978-1-4939-7201-2_18)

Koukoulitsa, C., Villalonga-Barber, C., Csonka, R., Alexi, X., Leonis, G., Dellis, D., Hamelink, E., Belda, O., Steele, B. R., Micha-Screttas, M., Alexis, M. N., Papadopoulos, M. G., & Mavromoustakos, T. (2016). Biological and computational evaluation of resveratrol inhibitors against Alzheimers disease. *Journal of Enzyme Inhibition and Medicinal Chemistry*, 31(1), 67–77. <https://doi.org/10.3109/14756366.2014.1003928>

Kouzarides, T. (2007). Chromatin Modifications and Their Function. *Cell*, 128(4), 693–705. <https://doi.org/10.1016/j.cell.2007.02.005>

Kozhemyakina, E., Cohen, T., Yao, T.-P., & Lassar, A. B. (2009). Parathyroid Hormone-Related Peptide Represses Chondrocyte Hypertrophy through a Protein Phosphatase 2A/Histone Deacetylase 4/MEF2 Pathway. *Molecular and Cellular Biology*, 29(21), 5751 LP – 5762. <https://doi.org/10.1128/MCB.00415-09>

Krishna, S., Kumar, V., & Imran Siddiqi, M. (2015). Recent Advances in Computer-Assisted Structure-Based Identification and Design of Histone Deacetylases Inhibitors. In *Current Topics in Medicinal Chemistry* (Vol. 16, Issue 9, pp. 934–947). <https://doi.org/10.2174/1568026615666150825142310>

Kurdistani, S. K., & Grunstein, M. (2003). Histone acetylation and deacetylation in yeast. *Nature Reviews Molecular Cell Biology*, 4(4), 276–284. <https://doi.org/10.1038/nrm1075>

- Kurogi, Y., & Guner, O. (2001). Pharmacophore Modeling and Three-dimensional Database Searching for Drug Design Using Catalyst. *Current Medicinal Chemistry*, 8(9), 1035–1055. <https://doi.org/10.2174/0929867013372481>
- Lahm, A., Paolini, C., Pallaoro, M., Nardi, M. C., Jones, P., Neddermann, P., Sambucini, S., Bottomley, M. J., Lo Surdo, P., Carfi, A., Koch, U., De Francesco, R., Steinkühler, C., & Gallinari, P. (2007). Unraveling the hidden catalytic activity of vertebrate class IIa histone deacetylases. *Proceedings of the National Academy of Sciences*, 104(44), 17335 LP – 17340. <https://doi.org/10.1073/pnas.0706487104>
- Lamb, M. L., & Jorgensen, W. L. (1997). Computational approaches to molecular recognition. *Current Opinion in Chemical Biology*, 1(4), 449–457. [https://doi.org/10.1016/S1367-5931\(97\)80038-5](https://doi.org/10.1016/S1367-5931(97)80038-5)
- Lang, B., Alrahbeni, T. M. A., Clair, D. S., Blackwood, D. H., Consortium, I. S., McCaig, C. D., & Shen, S. (2011). HDAC9 is implicated in schizophrenia and expressed specifically in post-mitotic neurons but not in adult neural stem cells. *American Journal of Stem Cells*, 1(1), 31–41. <https://pubmed.ncbi.nlm.nih.gov/23671795>
- Langer, T., Hoffmann, R. D., Mannhold, R., Kubinyi, H., & Folkers, G. (2006). *Pharmacophores and Pharmacophore Searches, Volume 32*. Wiley. <https://doi.org/10.1002/3527609164>
- Lapierre, M., Linares, A., Dalvai, M., Duraffourd, C., Bonnet, S., Boulahtouf, A., Rodriguez, C., Jalaguier, S., Assou, S., Orsetti, B., Balaguer, P., Maudelonde, T., Blache, P., Bystricky, K., Boulle, N., & Cavailles, V. (2016). Histone deacetylase 9 regulates breast cancer cell proliferation and the response to histone deacetylase inhibitors. *Oncotarget*; Vol 7, No 15. <https://www.oncotarget.com/article/7564/text/>
- Laskowski, R. A., Rullmann, J. A. C., MacArthur, M. W., Kaptein, R., & Thornton, J. M. (1996). AQUA and PROCHECK-NMR: Programs for checking the quality of protein structures solved by NMR. *Journal of Biomolecular NMR*, 8(4), 477–486. <https://doi.org/10.1007/BF00228148>
- Lau, A. T. Y., Lee, S.-Y., Xu, Y.-M., Zheng, D., Cho, Y.-Y., Zhu, F., Kim, H.-G., Li, S.-Q., Zhang, Z., Bode, A. M., & Dong, Z. (2011). Phosphorylation of Histone H2B Serine 32 Is Linked to Cell Transformation. *Journal of Biological Chemistry*, 286(30), 26628–26637. <http://www.jbc.org/content/286/30/26628.abstract>
- Laubach, J. P., Moreau, P., San-Miguel, J. F., & Richardson, P. G. (2015). Panobinostat for the treatment of multiple myeloma. *Clinical Cancer Research*, 21(21), 4767–4773. <https://doi.org/10.1158/1078-0432.CCR-15-0530>
- Leach, A. R. (1994). Ligand docking to proteins with discrete side-chain flexibility. *Journal of Molecular Biology*, 235(1), 345–356. [https://doi.org/10.1016/S0022-2836\(05\)80038-5](https://doi.org/10.1016/S0022-2836(05)80038-5)
- Leach, A. R., Gillet, V. J., Lewis, R. A., & Taylor, R. (2010). Three-Dimensional Pharmacophore Methods in Drug Discovery. *Journal of Medicinal Chemistry*, 53(2),

539–558. <https://doi.org/10.1021/jm900817u>

Lee, H. Y., Lee, J. F., Kumar, S., Wu, Y. W., HuangFu, W. C., Lai, M. J., Li, Y. H., Huang, H. L., Kuo, F. C., Hsiao, C. J., Cheng, C. C., Yang, C. R., & Liou, J. P. (2017). 3-Aroylindoles display antitumor activity in vitro and in vivo: Effects of N1-substituents on biological activity. *European Journal of Medicinal Chemistry*, *125*, 1268–1278. <https://doi.org/10.1016/j.ejmech.2016.11.033>

Lee, H. Y., Nepali, K., Huang, F. I., Chang, C. Y., Lai, M. J., Li, Y. H., Huang, H. L., Yang, C. R., & Liou, J. P. (2018). (N-Hydroxycarbonylbenzylamino)quinolines as Selective Histone Deacetylase 6 Inhibitors Suppress Growth of Multiple Myeloma in Vitro and in Vivo. *Journal of Medicinal Chemistry*, *61*(3), 905–917. <https://doi.org/10.1021/acs.jmedchem.7b01404>

Lee, H. Z., Kwitkowski, V. E., Del Valle, P. L., Ricci, M. S., Saber, H., Habtemariam, B. A., Bullock, J., Bloomquist, E., Shen, Y. L., Chen, X. H., Brown, J., Mehrotra, N., Dorff, S., Charlab, R., Kane, R. C., Kaminskas, E., Justice, R., Farrell, A. T., & Pazdur, R. (2015). FDA approval: Belinostat for the treatment of patients with relapsed or refractory peripheral T-cell lymphoma. *Clinical Cancer Research*, *21*(12), 2666–2670. <https://doi.org/10.1158/1078-0432.CCR-14-3119>

Lee, J., Cheng, X., Swails, J. M., Yeom, M. S., Eastman, P. K., Lemkul, J. A., Wei, S., Buckner, J., Jeong, J. C., Qi, Y., Jo, S., Pande, V. S., Case, D. A., Brooks, C. L., MacKerell, A. D., Klauda, J. B., & Im, W. (2016). CHARMM-GUI Input Generator for NAMD, GROMACS, AMBER, OpenMM, and CHARMM/OpenMM Simulations Using the CHARMM36 Additive Force Field. *Journal of Chemical Theory and Computation*, *12*(1), 405–413. <https://doi.org/10.1021/acs.jctc.5b00935>

Lei, Y., Liu, L., Zhang, S., Guo, S., Li, X., Wang, J., Su, B., Fang, Y., Chen, X., Ke, H., & Tao, W. (2017). Hdac7 promotes lung tumorigenesis by inhibiting Stat3 activation. *Molecular Cancer*, *16*(1), 170. <https://doi.org/10.1186/s12943-017-0736-2>

Li, X., Tu, Z., Li, H., Liu, C., Li, Z., Sun, Q., Yao, Y., Liu, J., & Jiang, S. (2013). Biological evaluation of new largazole analogues: Alteration of macrocyclic scaffold with click chemistry. *ACS Medicinal Chemistry Letters*, *4*(1), 132–136. <https://doi.org/10.1021/ml300371t>

Liang, X., Wu, Q., Luan, S., Yin, Z., He, C., Yin, L., Zou, Y., Yuan, Z., Li, L., Song, X., He, M., Lv, C., & Zhang, W. (2019). A comprehensive review of topoisomerase inhibitors as anticancer agents in the past decade. *European Journal of Medicinal Chemistry*, *171*, 129–168. <https://doi.org/https://doi.org/10.1016/j.ejmech.2019.03.034>

Lipinski, C. A. (2003). Compound Properties and Drug Quality. In C. G. B. T.-T. P. of M. C. (Second E. Wermuth (Ed.), *The Practice of Medicinal Chemistry: Second Edition* (pp. 341–349). Academic Press. <https://doi.org/10.1016/B978-0127444481-9/50025-8>

Lipinski, C. A., Lombardo, F., Dominy, B. W., & Feeney, P. J. (1997). Experimental and computational approaches to estimate solubility and permeability in drug discovery and development settings. *Advanced Drug Delivery Reviews*, *23*(1), 3–25.

[https://doi.org/https://doi.org/10.1016/S0169-409X\(96\)00423-1](https://doi.org/https://doi.org/10.1016/S0169-409X(96)00423-1)

Lipinski, C. A., Lombardo, F., Dominy, B. W., & Feeney, P. J. (2001). Experimental and computational approaches to estimate solubility and permeability in drug discovery and development settings. *Journal of Pharmaceutical Sciences*, 90(1), 3–26. The article was originally published in *Advanced Drug Delivery Reviews* 23 (1997) 3. *Advanced Drug Delivery Reviews*, 46(1), 3–26. [https://doi.org/https://doi.org/10.1016/S0169-409X\(00\)00129-0](https://doi.org/https://doi.org/10.1016/S0169-409X(00)00129-0)

Little, G. H., Bai, Y., Williams, T., & Poizat, C. (2007). Nuclear Calcium/Calmodulin-dependent Protein Kinase II $\delta$  Preferentially Transmits Signals to Histone Deacetylase 4 in Cardiac Cells. *Journal of Biological Chemistry*, 282(10), 7219–7231. <http://www.jbc.org/content/282/10/7219.abstract>

Liu, F., Dowling, M., Yang, X.-J., & Kao, G. D. (2004). Caspase-mediated Specific Cleavage of Human Histone Deacetylase 4. *Journal of Biological Chemistry*, 279(33), 34537–34546. <http://www.jbc.org/content/279/33/34537.abstract>

Liu, H., & Hou, T. (2016). CaFE: A tool for binding affinity prediction using end-point free energy methods. *Bioinformatics*, 32(14), 2216–2218. <https://doi.org/10.1093/bioinformatics/btw215>

Lobera, M., Madauss, K. P., Pohlhaus, D. T., Wright, Q. G., Trocha, M., Schmidt, D. R., Baloglu, E., Trump, R. P., Head, M. S., Hofmann, G. A., Murray-Thompson, M., Schwartz, B., Chakravorty, S., Wu, Z., Mander, P. K., Kruidenier, L., Reid, R. A., Burkhart, W., Turunen, B. J., ... Nolan, M. A. (2013). Selective class IIa histone deacetylase inhibition via a nonchelating zinc-binding group. *Nature Chemical Biology*, 9(5), 319–325. <https://doi.org/10.1038/nchembio.1223>

Lombardi, P. M., Cole, K. E., Dowling, D. P., & Christianson, D. W. (2011). Structure, mechanism, and inhibition of histone deacetylases and related metalloenzymes. *Current Opinion in Structural Biology*, 21(6), 735–743. <https://doi.org/https://doi.org/10.1016/j.sbi.2011.08.004>

Lu, J., McKinsey, T. A., Nicol, R. L., & Olson, E. N. (2000). Signal-dependent activation of the MEF2 transcription factor by dissociation from histone deacetylases. *Proceedings of the National Academy of Sciences*, 97(8), 4070 LP – 4075. <https://doi.org/10.1073/pnas.080064097>

Lu, W., Zhang, R., Jiang, H., Zhang, H., & Luo, C. (2018). Computer-Aided Drug Design in Epigenetics. In *Frontiers in Chemistry* (Vol. 6, p. 57). <https://www.frontiersin.org/article/10.3389/fchem.2018.00057>

Luckhurst, C. A., Aziz, O., Beaumont, V., Bürli, R. W., Breccia, P., Maillard, M. C., Haughan, A. F., Lamers, M., Leonard, P., Matthews, K. L., Raphy, G., Stott, A. J., Munoz-Sanjuan, I., Thomas, B., Wall, M., Wishart, G., Yates, D., & Dominguez, C. (2019). Development and characterization of a CNS-penetrant benzhydryl hydroxamic acid class IIa histone deacetylase inhibitor. *Bioorganic and Medicinal Chemistry Letters*, 29(1), 83–88. <https://doi.org/10.1016/j.bmcl.2018.11.009>

Luo, G., Lu, F., Qiao, L., Chen, X., Li, G., & Zhang, Y. (2016). Discovery of potential inhibitors of aldosterone synthase from Chinese herbs using pharmacophore modeling, molecular docking, and molecular dynamics simulation studies. *BioMed Research International*, 2016.

Lyne, P. D., Lamb, M. L., & Saeh, J. C. (2006). Accurate prediction of the relative potencies of members of a series of kinase inhibitors using molecular docking and MM-GBSA scoring. *Journal of Medicinal Chemistry*, 49(16), 4805–4808. <https://doi.org/10.1021/jm060522a>

Ma, C., & D'Mello, S. R. (2011). Neuroprotection by Histone Deacetylase-7 (HDAC7) Occurs by Inhibition of c-jun Expression through a Deacetylase-independent Mechanism. *Journal of Biological Chemistry*, 286(6), 4819–4828. <http://www.jbc.org/content/286/6/4819.abstract>

Mai, A., Massa, S., Pezzi, R., Simeoni, S., Rotili, D., Nebbioso, A., Scognamiglio, A., Altucci, L., Loidl, P., & Brosch, G. (2005). Class II (IIa)-selective histone deacetylase inhibitors. 1. Synthesis and biological evaluation of novel (aryloxopropenyl)pyrrolyl hydroxyamides. *Journal of Medicinal Chemistry*, 48(9), 3344–3353. <https://doi.org/10.1021/jm049002a>

Mann, B. S., Johnson, J. R., Cohen, M. H., Justice, R., & Pazdur, R. (2007). FDA Approval Summary: Vorinostat for Treatment of Advanced Primary Cutaneous T-Cell Lymphoma. *The Oncologist*, 12(10), 1247–1252. <https://doi.org/10.1634/theoncologist.12-10-1247>

Marek, L., Hamacher, A., Hansen, F. K., Kuna, K., Gohlke, H., Kassack, M. U., & Kurz, T. (2013). Histone deacetylase (HDAC) inhibitors with a novel connecting unit linker region reveal a selectivity profile for HDAC4 and HDAC5 with improved activity against chemoresistant cancer cells. *Journal of Medicinal Chemistry*, 56(2), 427–436. <https://doi.org/10.1021/jm301254q>

Martí-Renom, M. A., Stuart, A. C., Fiser, A., Sánchez, R., Melo, F., & Šali, A. (2000). Comparative protein structure modeling of genes and genomes. *Annual Review of Biophysics and Biomolecular Structure*, 29(1), 291–325. <https://doi.org/10.1146/annurev.biophys.29.1.291>

Martin, M., Kettmann, R., & Dequiedt, F. (2007). Class IIa histone deacetylases: Regulating the regulators. *Oncogene*, 26(37), 5450–5467. <https://doi.org/10.1038/sj.onc.1210613>

Martin, Maud, Kettmann, R., & Dequiedt, F. (2009). Class IIa histone deacetylases: conducting development and differentiation. *International Journal of Developmental Biology*, 53(2–3), 291–301. <https://doi.org/10.1387/ijdb.082698mm>

Massova, I., & Kollman, P. A. (2000). Combined molecular mechanical and continuum solvent approach (MM-PBSA/GBSA) to predict ligand binding. *Perspectives in Drug Discovery and Design*, 18(1), 113–135. <https://doi.org/10.1023/A:1008763014207>



Mathias, R. A., Greco, T. M., Oberstein, A., Budayeva, H. G., Chakrabarti, R., Rowland, E. A., Kang, Y., Shenk, T., & Cristea, I. M. (2014). Sirtuin 4 Is a Lipoamidase Regulating Pyruvate Dehydrogenase Complex Activity. *Cell*, *159*(7), 1615–1625. <https://doi.org/10.1016/j.cell.2014.11.046>

McGee, S. L., Van Denderen, B. J. W., Howlett, K. F., Mollica, J., Schertzer, J. D., Kemp, B. E., & Hargreaves, M. (2008). AMP-activated protein kinase regulates GLUT4 transcription by phosphorylating histone deacetylase 5. *Diabetes*, *57*(4), 860–867. <https://doi.org/10.2337/db07-0843>

McKinsey, T. A., & Olson, E. N. (2005). Toward transcriptional therapies for the failing heart: chemical screens to modulate genes. *The Journal of Clinical Investigation*, *115*(3), 538–546. <https://doi.org/10.1172/JCI24144>

McKinsey, T. A., Zhang, C.-L., Lu, J., & Olson, E. N. (2000). Signal-dependent nuclear export of a histone deacetylase regulates muscle differentiation. *Nature*, *408*(6808), 106–111. <https://doi.org/10.1038/35040593>

McKinsey, T. A., Zhang, C. L., & Olson, E. N. (2000). Activation of the myocyte enhancer factor-2 transcription factor by calcium/calmodulin-dependent protein kinase-stimulated binding of 14-3-3 to histone deacetylase 5. *Proceedings of the National Academy of Sciences*, *97*(26), 14400 LP – 14405. <https://doi.org/10.1073/pnas.260501497>

McKinsey, T. A., Zhang, C. L., & Olson, E. N. (2001). Control of muscle development by dueling HATs and HDACs. *Current Opinion in Genetics & Development*, *11*(5), 497–504. [https://doi.org/https://doi.org/10.1016/S0959-437X\(00\)00224-0](https://doi.org/https://doi.org/10.1016/S0959-437X(00)00224-0)

McKinsey, T. A., Zhang, C. L., & Olson, E. N. (2002). MEF2: a calcium-dependent regulator of cell division, differentiation and death. *Trends in Biochemical Sciences*, *27*(1), 40–47. [https://doi.org/10.1016/s0968-0004\(01\)02031-x](https://doi.org/10.1016/s0968-0004(01)02031-x)

Melesina, J., Praetorius, L., Simoben, C. V., Robaa, D., & Sippl, W. (2018). Design of selective histone deacetylase inhibitors: Rethinking classical pharmacophore. *Future Medicinal Chemistry*, *10*(13), 1537–1540. <https://doi.org/10.4155/fmc-2018-0125>

Meng, X.-Y., Zhang, H.-X., & Cui, M. M. and M. (2011). Molecular Docking: A Powerful Approach for Structure-Based Drug Discovery. In *Current Computer-Aided Drug Design* (Vol. 7, Issue 2, pp. 146–157). <https://doi.org/http://dx.doi.org/10.2174/157340911795677602>

Mielcarek, M., Landles, C., Weiss, A., Bradaia, A., Seredenina, T., Inuabasi, L., Osborne, G. F., Wadel, K., Touller, C., Butler, R., Robertson, J., Franklin, S. A., Smith, D. L., Park, L., Marks, P. A., Wanker, E. E., Olson, E. N., Luthi-Carter, R., van der Putten, H., ... Bates, G. P. (2013). HDAC4 Reduction: A Novel Therapeutic Strategy to Target Cytoplasmic Huntingtin and Ameliorate Neurodegeneration. *PLOS Biology*, *11*(11), e1001717. <https://doi.org/10.1371/journal.pbio.1001717>

Mihaylova, M. M., Vasquez, D. S., Ravnskjaer, K., Denechaud, P.-D., Yu, R. T., Alvarez,

J. G., Downes, M., Evans, R. M., Montminy, M., & Shaw, R. J. (2011). Class IIa Histone Deacetylases Are Hormone-Activated Regulators of FOXO and Mammalian Glucose Homeostasis. *Cell*, *145*(4), 607–621. <https://doi.org/10.1016/j.cell.2011.03.043>

Miller, M. A. (2002). Chemical database techniques in drug discovery. *Nature Reviews Drug Discovery*, *1*(3), 220–227. <https://doi.org/10.1038/nrd745>

Milne, G. W. A., Nicklaus, M. C., Driscoll, J. S., Wang, S., & Zaharevitz, D. (1994). National Cancer Institute Drug Information System 3D Database. *Journal of Chemical Information and Computer Sciences*, *34*(5), 1219–1224. <https://doi.org/10.1021/ci00021a032>

Minotti, G., Menna, P., Salvatorelli, E., Cairo, G., & Gianni, L. (2004). Anthracyclines: Molecular Advances and Pharmacologic Developments in Antitumor Activity and Cardiotoxicity. *Pharmacological Reviews*, *56*(2), 185 LP – 229. <https://doi.org/10.1124/pr.56.2.6>

Miska, E. A., Karlsson, C., Langley, E., Nielsen, S. J., Pines, J., & Kouzarides, T. (1999). HDAC4 deacetylase associates with and represses the MEF2 transcription factor. *The EMBO Journal*, *18*(18), 5099–5107. <https://doi.org/10.1093/emboj/18.18.5099>

Miska, E. A., Langley, E., Wolf, D., Karlsson, C., Pines, J., & Kouzarides, T. (2001). Differential localization of HDAC4 orchestrates muscle differentiation. *Nucleic Acids Research*, *29*(16), 3439–3447. <https://doi.org/10.1093/nar/29.16.3439>

Moreno, D. A., Scrideli, C. A., Cortez, M. A. A., De Paula Queiroz, R., Valera, E. T., Da Silva Silveira, V., Yunes, J. A., Brandalise, S. R., & Tone, L. G. (2010). research paper: Differential expression of HDAC3, HDAC7 and HDAC9 is associated with prognosis and survival in childhood acute lymphoblastic leukaemia. *British Journal of Haematology*, *150*(6), 665–673. <https://doi.org/10.1111/j.1365-2141.2010.08301.x>

Moresi, V., Marroncelli, N., Coletti, D., & Adamo, S. (2015). Regulation of skeletal muscle development and homeostasis by gene imprinting, histone acetylation and microRNA. *Biochimica et Biophysica Acta - Gene Regulatory Mechanisms*, *1849*(3), 309–316. <https://doi.org/10.1016/j.bbagr.2015.01.002>

Moresi, V., Williams, A. H., Meadows, E., Flynn, J. M., Potthoff, M. J., McAnally, J., Shelton, J. M., Backs, J., Klein, W. H., Richardson, J. A., Bassel-Duby, R., & Olson, E. N. (2010). Myogenin and class II HDACs control neurogenic muscle atrophy by inducing E3 ubiquitin ligases. *Cell*, *143*(1), 35–45. <https://doi.org/10.1016/j.cell.2010.09.004>

Moriguchi, I., Hirono, S., Liu, Q., Nakagome, Izum., & Matsushita, Y. (1992). Simple Method of Calculating Octanol/Water Partition Coefficient. *Chemical and Pharmaceutical Bulletin*, *40*(1), 127–130. <https://doi.org/10.1248/cpb.40.127>

Morris, B., Etoubleau, C., Bourthoumieu, S., Reynaud-Perrine, S., Laroche, C., Lebbar, A., Yardin, C., & Elsea, S. H. (2012). Dose dependent expression of HDAC4 causes variable expressivity in a novel inherited case of brachydactyly mental retardation syndrome. *American Journal of Medical Genetics Part A*, *158A*(8), 2015–2020.

<https://doi.org/10.1002/ajmg.a.35463>

Morris, G. M., Ruth, H., Lindstrom, W., Sanner, M. F., Belew, R. K., Goodsell, D. S., & Olson, A. J. (2009). Software news and updates AutoDock4 and AutoDockTools4: Automated docking with selective receptor flexibility. *Journal of Computational Chemistry*, 30(16), 2785–2791. <https://doi.org/10.1002/jcc.21256>

Mottamal, M., Zheng, S., Huang, T. L., & Wang, G. (2015). Histone deacetylase inhibitors in clinical studies as templates for new anticancer agents. In *Molecules* (Vol. 20, Issue 3, pp. 3898–3941). <https://doi.org/10.3390/molecules20033898>

Mottet, D., Pirote, S., Lamour, V., Hagedorn, M., Javerzat, S., Bikfalvi, A., Bellahcène, A., Verdin, E., & Castronovo, V. (2009). HDAC4 represses p21WAF1/Cip1 expression in human cancer cells through a Sp1-dependent, p53-independent mechanism. *Oncogene*, 28(2), 243–256. <https://doi.org/10.1038/onc.2008.371>

Murcko, M. A. (1995). Computational Methods to Predict Binding Free Energy in Ligand-Receptor Complexes. *Journal of Medicinal Chemistry*, 38(26), 4953–4967. <https://doi.org/10.1021/jm00026a001>

Muthyala, R., Shin, W. S., Xie, J., & Sham, Y. Y. (2015). Discovery of 1-hydroxypyridine-2-thiones as selective histone deacetylase inhibitors and their potential application for treating leukemia. *Bioorganic and Medicinal Chemistry Letters*, 25(19), 4320–4324. <https://doi.org/10.1016/j.bmcl.2015.07.065>

Narita, T., Weinert, B. T., & Choudhary, C. (2019). Functions and mechanisms of non-histone protein acetylation. *Nature Reviews Molecular Cell Biology*, 20(3), 156–174. <https://doi.org/10.1038/s41580-018-0081-3>

Nebbioso, A., Dell'Aversana, C., Bugge, A., Sarno, R., Valente, S., Rotili, D., Manzo, F., Teti, D., Mandrup, S., Ciana, P., Maggi, A., Mai, A., Gronemeyer, H., & Altucci, L. (2010). HDACs class II-selective inhibition alters nuclear receptor-dependent differentiation. *Journal of Molecular Endocrinology*, 45(4), 219–228. <https://doi.org/10.1677/JME-10-0043>

Nebbioso, A., Manzo, F., Miceli, M., Conte, M., Manente, L., Baldi, A., De Luca, A., Rotili, D., Valente, S., Mai, A., Usiello, A., Gronemeyer, H., & Altucci, L. (2009). Selective class II HDAC inhibitors impair myogenesis by modulating the stability and activity of HDAC-MEF2 complexes. *EMBO Reports*, 10(7), 776–782. <https://doi.org/10.1038/embor.2009.88>

Neri, F., Incarnato, D., & Oliviero, S. (2015). DNA methylation and demethylation dynamics. *Oncotarget*, 6(33), 34049–34050. <https://doi.org/10.18632/oncotarget.6039>

Ngo, S. T., & Li, M. S. (2012). Curcumin binds to A $\beta$ 1-40 peptides and fibrils stronger than ibuprofen and naproxen. *Journal of Physical Chemistry B*, 116(34), 10165–10175. <https://doi.org/10.1021/jp302506a>

Nilsson, A. C., Östman, E. M., Knudsen, K. E. B., Holst, J. J., & Björck, I. M. E. (2010). A Cereal-Based Evening Meal Rich in Indigestible Carbohydrates Increases Plasma

Butyrate the Next Morning. *The Journal of Nutrition*, 140(11), 1932–1936. <https://doi.org/10.3945/jn.110.123604>

O’Boyle, N. M., Banck, M., James, C. A., Morley, C., Vandermeersch, T., & Hutchison, G. R. (2011). Open Babel: An open chemical toolbox. *Journal of Cheminformatics*, 3(1), 33. <https://doi.org/10.1186/1758-2946-3-33>

O’Shaughnessy, J. A. (1999). Oral Alkylating Agents for Breast Cancer Therapy. *Drugs*, 58(3), 1–9. <https://doi.org/10.2165/00003495-199958003-00001>

Ohlendorf, D. H. (1994). Accuracy of refined protein structures. II. Comparison of four independently refined models of human interleukin 1beta. *Acta Crystallographica Section D: Biological Crystallography*, 50(6), 808–812. <https://doi.org/10.1107/S09074444994002659>

Olson, D. E., Wagner, F. F., Kaya, T., Gale, J. P., Aidoud, N., Davoine, E. L., Lazzaro, F., Weiwler, M., Zhang, Y. L., & Holson, E. B. (2013). Discovery of the first histone deacetylase 6/8 dual inhibitors. *Journal of Medicinal Chemistry*, 56(11), 4816–4820. <https://doi.org/10.1021/jm400390r>

Olsson, A., Björk, A., Vallon-Christersson, J., Isaacs, J. T., & Leanderson, T. (2010). Tasquinimod (ABR-215050), a quinoline-3-carboxamide anti-angiogenic agent, modulates the expression of thrombospondin-1 in human prostate tumors. *Molecular Cancer*, 9(1), 107. <https://doi.org/10.1186/1476-4598-9-107>

Ontoria, J. M., Altamura, S., Di Marco, A., Ferrigno, F., Laufer, R., Muraglia, E., Palumbi, M. C., Rowley, M., Scarpelli, R., Schultz-Fademrecht, C., Serafini, S., Steinkühler, C., & Jones, P. (2009). Identification of novel, selective, and stable inhibitors of class II histone deacetylases. Validation studies of the inhibition of the enzymatic activity of HDAC4 by small molecules as a novel approach for cancer therapy. *Journal of Medicinal Chemistry*, 52(21), 6782–6789. <https://doi.org/10.1021/jm900555u>

Otto, T., & Sicinski, P. (2017). Cell cycle proteins as promising targets in cancer therapy. *Nature Reviews Cancer*, 17(2), 93–115. <https://doi.org/10.1038/nrc.2016.138>

Ouaïssi, M., Sielezneff, I., Silvestre, R., Sastre, B., Bernard, J.-P., Lafontaine, J. S., Payan, M. J., Dahan, L., Pirrò, N., Seitz, J. F., Mas, E., Lombardo, D., & Ouaiissi, A. (2008). High Histone Deacetylase 7 (HDAC7) Expression Is Significantly Associated with Adenocarcinomas of the Pancreas. *Annals of Surgical Oncology*, 15(8), 2318–2328. <https://doi.org/10.1245/s10434-008-9940-z>

Pajouhesh, H., & Lenz, G. R. (2005). Medicinal chemical properties of successful central nervous system drugs. *NeuroRx*, 2(4), 541–553. <https://doi.org/10.1602/neurorx.2.4.541>

Paluvai, H., Di Giorgio, E., & Brancolini, C. (2018). Unscheduled HDAC4 repressive activity in human fibroblasts triggers TP53-dependent senescence and favors cell transformation. *Molecular Oncology*, 12(12), 2165–2181. <https://doi.org/10.1002/1878-0261.12392>

Papamichos-Chronakis, M., Krebs, J. E., & Peterson, C. L. (2006). Interplay between

Ino80 and Swr1 chromatin remodeling enzymes regulates cell cycle checkpoint adaptation in response to DNA damage. *Genes & Development*, 20(17), 2437–2449. <https://doi.org/10.1101/gad.1440206>

Paris, M., Porcelloni, M., Binaschi, M., & Fattori, D. (2008). Histone deacetylase inhibitors: From bench to clinic. *Journal of Medicinal Chemistry*, 51(6), 1505–1529. <https://doi.org/10.1021/jm7011408>

Paroni, G., Mizzau, M., Henderson, C., Del Sal, G., Schneider, C., & Brancolini, C. (2004). Caspase-dependent Regulation of Histone Deacetylase 4 Nuclear-Cytoplasmic Shuttling Promotes Apoptosis. *Molecular Biology of the Cell*, 15(6), 2804–2818. <https://doi.org/10.1091/mbc.e03-08-0624>

Parra, M., Kasler, H., McKinsey, T. A., Olson, E. N., & Verdin, E. (2005). Protein Kinase D1 Phosphorylates HDAC7 and Induces Its Nuclear Export after T-cell Receptor Activation. *Journal of Biological Chemistry*, 280(14), 13762–13770. <http://www.jbc.org/content/280/14/13762.abstract>

PEDRO, C. M. F., AIZPEA, Z. O., ION, V. S. Y., EIDER, S. A. N. S. L., DORLETA, O. A., CARMEN, M. M. M. D. E. L., & ENEKO, A. A. (2011). *New Histone Deacetylase inhibitors based simultaneously on trisubstituted 1H-pyrroles and aromatic and hetero.* IKERCHEM S L. <https://lens.org/088-094-093-456-51X>

Peng, Y., Yadava, P., Heikkinen, A. T., Parrott, N., & Railkar, A. (2014). Applications of a 7-day Caco-2 cell model in drug discovery and development. *European Journal of Pharmaceutical Sciences*, 56(1), 120–130. <https://doi.org/10.1016/j.ejps.2014.02.008>

Pescatore, G., Kinzel, O., Attenni, B., Cecchetti, O., Fiore, F., Fonsi, M., Rowley, M., Schultz-Fademrecht, C., Serafini, S., Steinkühler, C., & Jones, P. (2008). Optimization of a series of potent and selective ketone histone deacetylase inhibitors. *Bioorganic and Medicinal Chemistry Letters*, 18(20), 5528–5532. <https://doi.org/10.1016/j.bmcl.2008.09.003>

Peters, G. J., van der Wilt, C. L., van Moorsel, C. J. A., Kroep, J. R., Bergman, A. M., & Ackland, S. P. (2000). Basis for effective combination cancer chemotherapy with antimetabolites. *Pharmacology & Therapeutics*, 87(2), 227–253. [https://doi.org/https://doi.org/10.1016/S0163-7258\(00\)00086-3](https://doi.org/https://doi.org/10.1016/S0163-7258(00)00086-3)

Pevsner, J. (2009). *Bioinformatics and Functional Genomics: Second Edition*. In *Bioinformatics and Functional Genomics: Second Edition* (3rd ed., Vol. 3, Issue 2). John Wiley & Sons. <https://doi.org/10.1002/9780470451496>

Pham-The, H., Cabrera-Pérez, M. Á., Nam, N.-H., Castillo-Garit, J. A., Rasulev, B., Le-Thi-Thu, H., & Casañola-Martin, G. M. (2018). In Silico Assessment of ADME Properties: Advances in Caco-2 Cell Monolayer Permeability Modeling. In *Current Topics in Medicinal Chemistry* (Vol. 18, Issue 26, pp. 2209–2229). <https://doi.org/10.2174/1568026619666181130140350>

Pham-The, H., Garrigues, T., Bermejo, M., González-Álvarez, I., Monteagudo, M. C., &

Cabrera-Pérez, M. Á. (2013). Provisional classification and in silico study of biopharmaceutical system based on Caco-2 cell permeability and dose number. *Molecular Pharmaceutics*, 10(6), 2445–2461. <https://doi.org/10.1021/mp4000585>

Phiel, C. J., Zhang, F., Huang, E. Y., Guenther, M. G., Lazar, M. A., & Klein, P. S. (2001). Histone Deacetylase Is a Direct Target of Valproic Acid, a Potent Anticonvulsant, Mood Stabilizer, and Teratogen. *Journal of Biological Chemistry*, 276(39), 36734–36741. <https://doi.org/10.1074/jbc.M101287200>

Phillips, J. C., Hardy, D. J., Maia, J. D. C., Stone, J. E., Ribeiro, J. V., Bernardi, R. C., Buch, R., Fiorin, G., Hémin, J., Jiang, W., McGreevy, R., Melo, M. C. R., Radak, B. K., Skeel, R. D., Singharoy, A., Wang, Y., Roux, B., Aksimentiev, A., Luthey-Schulten, Z., ... Tajkhorshid, E. (2020). Scalable molecular dynamics on CPU and GPU architectures with NAMD. *The Journal of Chemical Physics*, 153(4), 044130. <https://doi.org/10.1063/5.0014475>

Picot, J., Cooper, K., Bryant, J., & Clegg, A. J. (2011). The clinical effectiveness and cost-effectiveness of bortezomib and thalidomide in combination regimens with an alkylating agent and a corticosteroid for the first-line treatment of multiple myeloma: a systematic review and economic evaluation. *Health Technology Assessment (Winchester, England)*, 15(41), 1–204. <https://doi.org/10.3310/hta15410>

Pirhadi, S., & Ghasemi, F. S. and J. B. (2013). Methods and Applications of Structure Based Pharmacophores in Drug Discovery. In *Current Topics in Medicinal Chemistry* (Vol. 13, Issue 9, pp. 1036–1047). <https://doi.org/http://dx.doi.org/10.2174/1568026611313090006>

Pirinen, E., Lo Sasso, G., & Auwerx, J. (2012). Mitochondrial sirtuins and metabolic homeostasis. *Best Practice & Research Clinical Endocrinology & Metabolism*, 26(6), 759–770. <https://doi.org/https://doi.org/10.1016/j.beem.2012.05.001>

Ponder, J. W., & Case, D. A. (2003). Force fields for protein simulations. In *Advances in Protein Chemistry* (Vol. 66, pp. 27–85). Academic Press. [https://doi.org/10.1016/S0065-3233\(03\)66002-X](https://doi.org/10.1016/S0065-3233(03)66002-X)

Popov, S., Venetsanou, K., Chedrese, P. J., Pinto, V., Takemori, H., Franco-Cereceda, A., Eriksson, P., Mochizuki, N., Soares-da-Silva, P., & Bertorello, A. M. (2012). Increases in intracellular sodium activate transcription and gene expression via the salt-inducible kinase 1 network in an atrial myocyte cell line. *American Journal of Physiology-Heart and Circulatory Physiology*, 303(1), H57–H65. <https://doi.org/10.1152/ajpheart.00512.2011>

Poulsen, R. C., Knowles, H. J., Carr, A. J., & Hulley, P. A. (2014). Cell differentiation versus cell death: extracellular glucose is a key determinant of cell fate following oxidative stress exposure. *Cell Death & Disease*, 5(2), e1074–e1074. <https://doi.org/10.1038/cddis.2014.52>

Press, B. (2011). Optimization of the Caco-2 permeability assay to screen drug compounds for intestinal absorption and efflux. In K. Turksen (Ed.), *Methods in*

*Molecular Biology* (Vol. 763, pp. 139–154). Humana Press. [https://doi.org/10.1007/978-1-61779-191-8\\_9](https://doi.org/10.1007/978-1-61779-191-8_9)

Raepfel, S., Zhou, N., Gaudette, F., Leit, S., Paquin, I., Larouche, G., Moradei, O., Fréchette, S., Isakovic, L., Delorme, D., Fournel, M., Kalita, A., Lu, A., Trachy-Bourget, M. C., Yan, P. T., Liu, J., Rahil, J., Wang, J., Besterman, J. M., ... Vaisburg, A. (2009). SAR and biological evaluation of analogues of a small molecule histone deacetylase inhibitor N-(2-aminophenyl)-4-((4-(pyridin-3-yl)pyrimidin-2-ylamino)methyl)benzamide (MGCD0103). *Bioorganic and Medicinal Chemistry Letters*, 19(3), 644–649. <https://doi.org/10.1016/j.bmcl.2008.12.048>

Rahman, M., Murad, G. J. A., Bova, F., Friedman, W. A., & Mocco, J. (2009). Stereotactic radiosurgery and the linear accelerator: accelerating electrons in neurosurgery. *Neurosurgical Focus FOC*, 27(3), E13. <https://doi.org/10.3171/2009.7.FOCUS09116>

Rajendran, P., Williams, D. E., Ho, E., & Dashwood, R. H. (2011). Metabolism as a key to histone deacetylase inhibition. *Critical Reviews in Biochemistry and Molecular Biology*, 46(3), 181–199. <https://doi.org/10.3109/10409238.2011.557713>

Redon, C., Pilch, D., Rogakou, E., Sedelnikova, O., Newrock, K., & Bonner, W. (2002). Histone H2A variants H2AX and H2AZ. *Current Opinion in Genetics & Development*, 12(2), 162–169. [https://doi.org/https://doi.org/10.1016/S0959-437X\(02\)00282-4](https://doi.org/https://doi.org/10.1016/S0959-437X(02)00282-4)

Rester, U. (2008). From virtuality to reality - Virtual screening in lead discovery and lead optimization: a medicinal chemistry perspective. *Current Opinion in Drug Discovery & Development*, 11(4), 559–568. <http://europepmc.org/abstract/MED/18600572>

Richon, V. M., Webb, Y., Merger, R., Sheppard, T., Jursic, B., Ngo, L., Civoli, F., Breslow, R., Rifkind, R. A., & Marks, P. A. (1996). Second generation hybrid polar compounds are potent inducers of transformed cell differentiation. *Proceedings of the National Academy of Sciences*, 93(12), 5705 LP – 5708. <https://doi.org/10.1073/pnas.93.12.5705>

Risau, W. (1997). Mechanisms of angiogenesis. *Nature*, 386(6626), 671–674. <https://doi.org/10.1038/386671a0>

Rodgers, G. M., Becker, P. S., Blinder, M., Cella, D., Chanan-Khan, A., Cleeland, C., Coccia, P. F., Djulbegovic, B., Gilreath, J. A., & Kraut, E. H. (2012). Cancer-and chemotherapy-induced anemia. *Journal of the National Comprehensive Cancer Network*, 10(5), 628–653. <https://doi.org/10.6004/jnccn.2012.0064>

Ropero, S., & Esteller, M. (2007). The role of histone deacetylases (HDACs) in human cancer. *Molecular Oncology*, 1(1), 19–25. <https://doi.org/10.1016/j.molonc.2007.01.001>

Rossetto, D., Truman, A. W., Kron, S. J., & Côté, J. (2010). Epigenetic Modifications in Double-Strand Break DNA Damage Signaling and Repair. *Clinical Cancer Research*, 16(18), 4543 LP – 4552. <https://doi.org/10.1158/1078-0432.CCR-10-0513>

Saito, A., Yamashita, T., Mariko, Y., Nosaka, Y., Tsuchiya, K., Ando, T., Suzuki, T.,

Tsuruo, T., & Nakanishi, O. (1999). A synthetic inhibitor of histone deacetylase, MS-27-275, with marked in vivo antitumor activity against human tumors. *Proceedings of the National Academy of Sciences of the United States of America*, 96(8), 4592–4597. <https://doi.org/10.1073/pnas.96.8.4592>

Šali, A., & Blundell, T. L. (1993). Comparative protein modelling by satisfaction of spatial restraints. *Journal of Molecular Biology*, 234(3), 779–815. <https://doi.org/10.1006/jmbi.1993.1626>

Schäfer, M., & Werner, S. (2008). Cancer as an overhealing wound: an old hypothesis revisited. *Nature Reviews Molecular Cell Biology*, 9(8), 628–638. <https://doi.org/10.1038/nrm2455>

Schmieder, R. E., Messerli, F. H., Garavaglia, G. E., & Nunez, B. D. (1988). Dietary salt intake. A determinant of cardiac involvement in essential hypertension. *Circulation*, 78(4), 951–956. <https://doi.org/10.1161/01.CIR.78.4.951>

Schölz, C., Weinert, B. T., Wagner, S. A., Beli, P., Miyake, Y., Qi, J., Jensen, L. J., Streicher, W., McCarthy, A. R., Westwood, N. J., Lain, S., Cox, J., Matthias, P., Mann, M., Bradner, J. E., & Choudhary, C. (2015). Acetylation site specificities of lysine deacetylase inhibitors in human cells. *Nature Biotechnology*, 33(4), 415–425. <https://doi.org/10.1038/nbt.3130>

Schones, D. E., Cui, K., & Cuddapah, S. (2011). Genome-wide approaches to studying yeast chromatin modifications. In J. I. Castrillo & S. G. Oliver (Eds.), *Methods in Molecular Biology* (Vol. 759, pp. 61–71). Humana Press. [https://doi.org/10.1007/978-1-61779-173-4\\_4](https://doi.org/10.1007/978-1-61779-173-4_4)

Schueler, F. W. (1961). Chemobiodynamics and Drug Design. *Journal of Pharmaceutical Sciences*, 50(1), 92. <https://doi.org/10.1002/jps.2600500143>

Schuetz, A., Min, J., Allali-Hassani, A., Schapira, M., Shuen, M., Loppnau, P., Mazitschek, R., Kwiatkowski, N. P., Lewis, T. A., Maglathin, R. L., McLean, T. H., Bochkarev, A., Plotnikov, A. N., Vedadi, M., & Arrowsmith, C. H. (2008). Human HDAC7 Harbors a Class IIa Histone Deacetylase-specific Zinc Binding Motif and Cryptic Deacetylase Activity. *Journal of Biological Chemistry*, 283(17), 11355–11363. <http://www.jbc.org/content/283/17/11355.abstract>

Scott, F. L., Fuchs, G. J., Boyd, S. E., Denault, J.-B., Hawkins, C. J., Dequiedt, F., & Salvesen, G. S. (2008). Caspase-8 Cleaves Histone Deacetylase 7 and Abolishes Its Transcription Repressor Function. *Journal of Biological Chemistry*, 283(28), 19499–19510. <http://www.jbc.org/content/283/28/19499.abstract>

Seelig, M. H., & Berger, M. R. (1996). Efficacy of dinaline and its methyl and acetyl derivatives against colorectal cancer in vivo and in vitro. *European Journal of Cancer Part A*, 32(11), 1968–1976. [https://doi.org/10.1016/0959-8049\(96\)00217-1](https://doi.org/10.1016/0959-8049(96)00217-1)

Sekizawa, H., Amaike, K., Itoh, Y., Suzuki, T., Itami, K., & Yamaguchi, J. (2014). Late-stage C-H coupling enables rapid identification of HDAC inhibitors: Synthesis and



evaluation of NCH-31 analogues. *ACS Medicinal Chemistry Letters*, 5(5), 582–586. <https://doi.org/10.1021/ml500024s>

Sellmer, A., Stangl, H., Beyer, M., Grünstein, E., Leonhardt, M., Pongratz, H., Eichhorn, E., Elz, S., Striegl, B., Jenei-Lanzl, Z., Dove, S., Straub, R. H., Krämer, O. H., & Mahboobi, S. (2018). Marbostat-100 Defines a New Class of Potent and Selective Antiinflammatory and Antirheumatic Histone Deacetylase 6 Inhibitors. *Journal of Medicinal Chemistry*, 61(8), 3454–3477. <https://doi.org/10.1021/acs.jmedchem.7b01593>

Shah, P., Jogani, V., Bagchi, T., & Misra, A. (2006). Role of Caco-2 cell monolayers in prediction of intestinal drug absorption. *Biotechnology Progress*, 22(1), 186–198. <https://doi.org/10.1021/bp050208u>

Shahlaei, M., & Doosti, E. (2016). Virtual screening based on pharmacophore model followed by docking simulation studies in search of potential inhibitors for p38 map kinase. *Biomedicine and Pharmacotherapy*, 80, 352–372. <https://doi.org/10.1016/j.biopha.2016.02.041>

Shoichet, B. K., McGovern, S. L., Wei, B., & Irwin, J. J. (2002). Lead discovery using molecular docking. *Current Opinion in Chemical Biology*, 6(4), 439–446. [https://doi.org/10.1016/S1367-5931\(02\)00339-3](https://doi.org/10.1016/S1367-5931(02)00339-3)

Shuttleworth, S. J., & Tomassi, C. D. (2014). *Scriptaid isosteres and their use in therapy*. KARUS THERAPEUTICS LTD OP - GB 0901406 A 20090128 OP - GB 0912383 A 20090716. <https://lens.org/064-943-743-970-856>

Singh, B. N., Zhang, G., Hwa, Y. L., Li, J., Dowdy, S. C., & Jiang, S. W. (2010). Nonhistone protein acetylation as cancer therapy targets. *Expert Review of Anticancer Therapy*, 10(6), 935–954. <https://doi.org/10.1586/era.10.62>

Singh, E. K., Nazarova, L. A., Lapera, S. A., Alexander, L. D., & McAlpine, S. R. (2010). Histone deacetylase inhibitors: synthesis of cyclic tetrapeptides and their triazole analogs. *Tetrahedron Letters*, 51(33), 4357–4360. <https://doi.org/https://doi.org/10.1016/j.tetlet.2010.06.050>

Sinha, S., Goyal, S., Somvanshi, P., & Grover, A. (2017). Mechanistic Insights into the Binding of Class IIa HDAC Inhibitors toward Spinocerebellar Ataxia Type-2: A 3D-QSAR and Pharmacophore Modeling Approach. In *Frontiers in Neuroscience* (Vol. 10, p. 606). <https://www.frontiersin.org/article/10.3389/fnins.2016.00606>

Sippl, M. J. (1993). Recognition of errors in three-dimensional structures of proteins. *Proteins: Structure, Function, and Bioinformatics*, 17(4), 355–362. <https://doi.org/10.1002/prot.340170404>

Sippl, M. J. (1995). Knowledge-based potentials for proteins. *Current Opinion in Structural Biology*, 5(2), 229–235. [https://doi.org/10.1016/0959-440X\(95\)80081-6](https://doi.org/10.1016/0959-440X(95)80081-6)

Sitkoff, D., Sharp, K. A., & Honig, B. (1994). Accurate calculation of hydration free energies using macroscopic solvent models. *Journal of Physical Chemistry*, 98(7), 1978–1988. <https://doi.org/10.1021/j100058a043>

Somoza, J. R., Skene, R. J., Katz, B. A., Mol, C., Ho, J. D., Jennings, A. J., Luong, C., Arvai, A., Buggy, J. J., Chi, E., Tang, J., Sang, B.-C., Verner, E., Wynands, R., Leahy, E. M., Dougan, D. R., Snell, G., Navre, M., Knuth, M. W., ... Tari, L. W. (2004). Structural Snapshots of Human HDAC8 Provide Insights into the Class I Histone Deacetylases. *Structure*, *12*(7), 1325–1334. <https://doi.org/10.1016/j.str.2004.04.012>

Steindl, T., Laggner, C., & Langer, T. (2005). Human Rhinovirus 3C Protease: Generation of Pharmacophore Models for Peptidic and Nonpeptidic Inhibitors and Their Application in Virtual Screening. *Journal of Chemical Information and Modeling*, *45*(3), 716–724. <https://doi.org/10.1021/ci049638a>

Stephen Joseph Shuttleworth, C. D. T. (2014). *Shuttleworth, Scriptaid isosteres and their use in therapy* (Patent No. US8748458B2). <https://patents.google.com/patent/US8748458B2/en?q=8748458>

Sterling, T., & Irwin, J. J. (2015). ZINC 15--Ligand Discovery for Everyone. *Journal of Chemical Information and Modeling*, *55*(11), 2324–2337. <https://doi.org/10.1021/acs.jcim.5b00559>

Stronach, E. A., Alfraidi, A., Rama, N., Datler, C., Studd, J. B., Agarwal, R., Guney, T. G., Gourley, C., Hennessy, B. T., Mills, G. B., Mai, A., Brown, R., Dina, R., & Gabra, H. (2011). HDAC4-Regulated STAT1 Activation Mediates Platinum Resistance in Ovarian Cancer. *Cancer Research*, *71*(13), 4412 LP – 4422. <https://doi.org/10.1158/0008-5472.CAN-10-4111>

Struhl, K. (1998). Histone acetylation and transcriptional regulatory mechanisms. *Genes and Development*, *12*(5), 599–606. <https://doi.org/10.1101/gad.12.5.599>

Suzuki, T., Ando, T., Tsuchiya, K., Fukazawa, N., Saito, A., Mariko, Y., Yamashita, T., & Nakanishi, O. (1999). Synthesis and histone deacetylase inhibitory activity of new benzamide derivatives. *Journal of Medicinal Chemistry*, *42*(15), 3001–3003. <https://doi.org/10.1021/jm980565u>

Swanson, J. M. J., Henchman, R. H., & McCammon, J. A. (2004). Revisiting Free Energy Calculations: A Theoretical Connection to MM/PBSA and Direct Calculation of the Association Free Energy. *Biophysical Journal*, *86*(1 I), 67–74. [https://doi.org/10.1016/S0006-3495\(04\)74084-9](https://doi.org/10.1016/S0006-3495(04)74084-9)

Tambunan, U., Bakri, R., Prasetya, T., Parikesit, A. A., & Kerami, D. (2013). Molecular dynamics simulation of complex Histones Deacetylase (HDAC) Class II Homo Sapiens with suberoylanilide hydroxamic acid (SAHA) and its derivatives as inhibitors of cervical cancer. *Bioinformatics*, *9*(13), 696–700. <https://doi.org/10.6026/97320630009696>

Tang, J., Yan, H., & Zhuang, S. (2013). Histone deacetylases as targets for treatment of multiple diseases. *Clinical Science*, *124*(11), 651–662. <https://doi.org/10.1042/CS20120504>

Taniguchi, M., Carreira, M. B., Smith, L. N., Zirlin, B. C., Neve, R. L., & Cowan, C. W. (2012). Histone Deacetylase 5 Limits Cocaine Reward through cAMP-Induced Nuclear

Import. *Neuron*, 73(1), 108–120. <https://doi.org/10.1016/j.neuron.2011.10.032>

Tessier, P., Smil, D. V., Wahhab, A., Leit, S., Rahil, J., Li, Z., Déziel, R., & Besterman, J. M. (2009). Diphenylmethylene hydroxamic acids as selective class IIa histone deacetylase inhibitors. *Bioorganic and Medicinal Chemistry Letters*, 19(19), 5684–5688. <https://doi.org/10.1016/j.bmcl.2009.08.010>

Thaler, F., & Mercurio, C. (2014). Towards selective inhibition of histone deacetylase isoforms: What has been achieved, where we are and what will be next. *ChemMedChem*, 9(3), 523–536. <https://doi.org/10.1002/cmdc.201300413>

Thangapandian, S., John, S., & Lee, K. W. (2012). Molecular dynamics simulation study explaining inhibitor selectivity in different class of histone deacetylases. *Journal of Biomolecular Structure and Dynamics*, 29(4), 677–698. <https://doi.org/10.1080/07391102.2012.10507409>

Thompson, D. C., Humblet, C., & Joseph-McCarthy, D. (2008). Investigation of MM-PBSA rescoring of docking poses. *Journal of Chemical Information and Modeling*, 48(5), 1081–1091. <https://doi.org/10.1021/ci700470c>

Totrov, M., & Abagyan, R. (2008). Flexible ligand docking to multiple receptor conformations: a practical alternative. *Current Opinion in Structural Biology*, 18(2), 178–184. <https://doi.org/10.1016/j.sbi.2008.01.004>

Trott, O., & Olson, A. J. (2009). AutoDock Vina: Improving the speed and accuracy of docking with a new scoring function, efficient optimization, and multithreading. *Journal of Computational Chemistry*, 31(2), NA-NA. <https://doi.org/10.1002/jcc.21334>

Tsuji, N., Kobayashi, M., Nagashima, K., Wakisaka, Y., & Koizumi, K. (1976). A new antifungal antibiotic, trichostatin. *The Journal of Antibiotics*, 29(1), 1–6. <https://doi.org/10.7164/antibiotics.29.1>

Vannini, A., Volpari, C., Filocamo, G., Casavola, E. C., Brunetti, M., Renzoni, D., Chakravarty, P., Paolini, C., De Francesco, R., Gallinari, P., Steinkühler, C., & Di Marco, S. (2004). Crystal structure of a eukaryotic zinc-dependent histone deacetylase, human HDAC8, complexed with a hydroxamic acid inhibitor. *Proceedings of the National Academy of Sciences of the United States of America*, 101(42), 15064 LP – 15069. <https://doi.org/10.1073/pnas.0404603101>

Vanommeslaeghe, K., Hatcher, E., Acharya, C., Kundu, S., Zhong, S., Shim, J., Darian, E., Guvench, O., Lopes, P., Vorobyov, I., & Mackerell, A. D. (2010). CHARMM general force field: A force field for drug-like molecules compatible with the CHARMM all-atom additive biological force fields. *Journal of Computational Chemistry*, 31(4), 671–690. <https://doi.org/10.1002/jcc.21367>

Veber, D. F., Johnson, S. R., Cheng, H.-Y., Smith, B. R., Ward, K. W., & Kopple, K. D. (2002). Molecular Properties That Influence the Oral Bioavailability of Drug Candidates. *Journal of Medicinal Chemistry*, 45(12), 2615–2623. <https://doi.org/10.1021/jm020017n>

Vega, R. B., Harrison, B. C., Meadows, E., Roberts, C. R., Papst, P. J., Olson, E. N., &

McKinsey, T. A. (2004). Protein Kinases C and D Mediate Agonist-Dependent Cardiac Hypertrophy through Nuclear Export of Histone Deacetylase 5. *Molecular and Cellular Biology*, 24(19), 8374 LP – 8385. <https://doi.org/10.1128/MCB.24.19.8374-8385.2004>

Vega, R. B., Matsuda, K., Oh, J., Barbosa, A. C., Yang, X., Meadows, E., McAnally, J., Pomajzl, C., Shelton, J. M., Richardson, J. A., Karsenty, G., & Olson, E. N. (2004). Histone Deacetylase 4 Controls Chondrocyte Hypertrophy during Skeletogenesis. *Cell*, 119(4), 555–566. <https://doi.org/10.1016/j.cell.2004.10.024>

Venza, I., Visalli, M., Oteri, R., Cucinotta, M., Teti, D., & Venza, M. (2013). Class II-specific histone deacetylase inhibitors MC1568 and MC1575 suppress IL-8 expression in human melanoma cells. *Pigment Cell and Melanoma Research*, 26(2), 193–204. <https://doi.org/10.1111/pcmr.12049>

Verdin, E., Dequiedt, F., & Kasler, H. G. (2003). Class II histone deacetylases: versatile regulators. *Trends in Genetics*, 19(5), 286–293. [https://doi.org/10.1016/S0168-9525\(03\)00073-8](https://doi.org/10.1016/S0168-9525(03)00073-8)

Verma, S., Grover, S., Tyagi, C., Goyal, S., Jamal, S., Singh, A., & Grover, A. (2016). Hydrophobic interactions are a key to MDM2 inhibition by polyphenols as revealed by molecular dynamics simulations and MM/PBSA free energy calculations. *PLoS ONE*, 11(2), e0149014. <https://doi.org/10.1371/journal.pone.0149014>

Vernal, J., Fiser, A., Šali, A., Müller, M., José Cazzulo, J., & Nowicki, C. (2002). Probing the specificity of a trypanosomal aromatic  $\alpha$ -hydroxy acid dehydrogenase by site-directed mutagenesis. *Biochemical and Biophysical Research Communications*, 293(1), 633–639. [https://doi.org/10.1016/S0006-291X\(02\)00270-X](https://doi.org/10.1016/S0006-291X(02)00270-X)

Vieth, M., Siegel, M. G., Higgs, R. E., Watson, I. A., Robertson, D. H., Savin, K. A., Durst, G. L., & Hipskind, P. A. (2004). Characteristic Physical Properties and Structural Fragments of Marketed Oral Drugs. *Journal of Medicinal Chemistry*, 47(1), 224–232. <https://doi.org/10.1021/jm030267j>

Villavicencio-Lorini, P., Klopocki, E., Trimborn, M., Koll, R., Mundlos, S., & Horn, D. (2013). Phenotypic variant of Brachydactyly-mental retardation syndrome in a family with an inherited interstitial 2q37.3 microdeletion including HDAC4. *European Journal of Human Genetics*, 21(7), 743–748. <https://doi.org/10.1038/ejhg.2012.240>

Vissing, K., McGee, S. L., Roepstorff, C., Schjerling, P., Hargreaves, M., & Kiens, B. (2008). Effect of sex differences on human MEF2 regulation during endurance exercise. *American Journal of Physiology-Endocrinology and Metabolism*, 294(2), E408–E415. <https://doi.org/10.1152/ajpendo.00403.2007>

Vogelauer, M., Krall, A. S., McBrian, M. A., Li, J.-Y., & Kurdistani, S. K. (2012). Stimulation of Histone Deacetylase Activity by Metabolites of Intermediary Metabolism. *Journal of Biological Chemistry*, 287(38), 32006–32016. <http://www.jbc.org/content/287/38/32006.abstract>

Von Blume, J., Knippschild, U., Dequiedt, F., Giamas, G., Beck, A., Auer, A., Van Lint,

J., Adler, G., & Seufferlein, T. (2007). Phosphorylation at Ser244 by CK1 determines nuclear localization and substrate targeting of PKD2. *EMBO Journal*, 26(22), 4619–4633. <https://doi.org/10.1038/sj.emboj.7601891>

Von Langen, J., Fritzemeier, K. H., Diekmann, S., & Hillisch, A. (2005). Molecular basis of the interaction specificity between the human glucocorticoid receptor and its endogenous steroid ligand cortisol. *ChemBioChem*, 6(6), 1110–1118. <https://doi.org/10.1002/cbic.200400361>

Vuorinen, A., Nashev, L. G., Odermatt, A., Rollinger, J. M., & Schuster, D. (2014). Pharmacophore model refinement for 11 $\beta$ -hydroxysteroid dehydrogenase inhibitors: Search for modulators of intracellular glucocorticoid concentrations. *Molecular Informatics*, 33(1), 15–25. <https://doi.org/10.1002/minf.201300063>

Wada, C. K., Frey, R. R., Ji, Z., Curtin, M. L., Garland, R. B., Holms, J. H., Li, J., Pease, L. J., Guo, J., Glaser, K. B., Marcotte, P. A., Richardson, P. L., Murphy, S. S., Bouska, J. J., Tapang, P., Magoc, T. J., Albert, D. H., Davidsen, S. K., & Michaelides, M. R. (2003).  $\alpha$ -Keto amides as inhibitors of histone deacetylase. *Bioorganic and Medicinal Chemistry Letters*, 13(19), 3331–3335. [https://doi.org/10.1016/S0960-894X\(03\)00685-1](https://doi.org/10.1016/S0960-894X(03)00685-1)

Wagner, A., Ploder, O., Enislidis, G., Truppe, M., & Ewers, R. (1995). Virtual image guided navigation in tumor surgery—technical innovation. *Journal of Cranio-Maxillofacial Surgery*, 23(5), 271–273. [https://doi.org/doi.org/10.1016/S1010-5182\(05\)80155-6](https://doi.org/doi.org/10.1016/S1010-5182(05)80155-6)

Wagner, F. F., Olson, D. E., Gale, J. P., Kaya, T., Weïwer, M., Aidoud, N., Thomas, M., Davoine, E. L., Lemercier, B. C., Zhang, Y. L., & Holson, E. B. (2013). Potent and selective inhibition of histone deacetylase 6 (HDAC6) does not require a surface-binding motif. *Journal of Medicinal Chemistry*, 56(4), 1772–1776. <https://doi.org/10.1021/jm301355j>

Wagner, F. F., Weïwer, M., Steinbacher, S., Schomburg, A., Reinemer, P., Gale, J. P., Campbell, A. J., Fisher, S. L., Zhao, W. N., Reis, S. A., Hennig, K. M., Thomas, M., Müller, P., Jefson, M. R., Fass, D. M., Haggarty, S. J., Zhang, Y. L., & Holson, E. B. (2016). Kinetic and structural insights into the binding of histone deacetylase 1 and 2 (HDAC1, 2) inhibitors. *Bioorganic and Medicinal Chemistry*, 24(18), 4008–4015. <https://doi.org/10.1016/j.bmc.2016.06.040>

Walter, M. W., Felici, A., Galleni, M., Soto, R. P., Adlington, R. M., Baldwin, J. E., Frère, J. M., Gololobov, M., & Schofield, C. J. (1996). Trifluoromethyl alcohol and ketone inhibitors of metallo- $\beta$ -lactamases. *Bioorganic and Medicinal Chemistry Letters*, 6(20), 2455–2458. [https://doi.org/10.1016/0960-894X\(96\)00453-2](https://doi.org/10.1016/0960-894X(96)00453-2)

Walters, W. P., Stahl, M. T., & Murcko, M. A. (1998). Virtual screening—an overview. *Drug Discovery Today*, 3(4), 160–178. [https://doi.org/https://doi.org/10.1016/S1359-6446\(97\)01163-X](https://doi.org/https://doi.org/10.1016/S1359-6446(97)01163-X)

Wan, M., & Cao, X. (2005). BMP signaling in skeletal development. *Biochemical and Biophysical Research Communications*, 328(3), 651–657.

<https://doi.org/https://doi.org/10.1016/j.bbrc.2004.11.067>

Wang, E., Sun, H., Wang, J., Wang, Z., Liu, H., Zhang, J. Z. H., & Hou, T. (2019). End-Point Binding Free Energy Calculation with MM/PBSA and MM/GBSA: Strategies and Applications in Drug Design. *Chemical Reviews*, *119*(16), 9478–9508. <https://doi.org/10.1021/acs.chemrev.9b00055>

Wang, G. M., Sevick, E. M., Mittag, E., Searles, D. J., & Evans, D. J. (2002). Experimental Demonstration of Violations of the Second Law of Thermodynamics for Small Systems and Short Time Scales. *Physical Review Letters*, *89*(5), 50601. <https://doi.org/10.1103/PhysRevLett.89.050601>

Wang, J., Morin, P., Wang, W., & Kollman, P. A. (2001). Use of MM-PBSA in reproducing the binding free energies to HIV-1 RT of TIBO derivatives and predicting the binding mode to HIV-1 RT of efavirenz by docking and MM-PBSA. *Journal of the American Chemical Society*, *123*(22), 5221–5230. <https://doi.org/10.1021/ja003834q>

Wang, S., Li, X., Parra, M., Verdin, E., Bassel-Duby, R., & Olson, E. N. (2008). Control of endothelial cell proliferation and migration by VEGF signaling to histone deacetylase 7. *Proceedings of the National Academy of Sciences of the United States of America*, *105*(22), 7738–7743. <https://doi.org/10.1073/pnas.0802857105>

Wang, T., Sepulveda, M., Gonzales, P., & Gately, S. (2013). Identification of novel HDAC inhibitors through cell based screening and their evaluation as potential anticancer agents. *Bioorganic and Medicinal Chemistry Letters*, *23*(17), 4790–4793. <https://doi.org/10.1016/j.bmcl.2013.07.001>

Wang, W., Ha, C. H., Jhun, B. S., Wong, C., Jain, M. K., & Jin, Z. G. (2010). Fluid shear stress stimulates phosphorylation-dependent nuclear export of HDAC5 and mediates expression of KLF2 and eNOS. *Blood*, *115*(14), 2971–2979. <https://doi.org/10.1182/blood-2009-05-224824>

Wang, Y., Xing, J., Xu, Y., Zhou, N., Peng, J., Xiong, Z., Liu, X., Luo, X., Luo, C., Chen, K., Zheng, M., & Jiang, H. (2015). In silico ADME/T modelling for rational drug design. *Quarterly Reviews of Biophysics*, *48*(4), 488–515. <https://doi.org/DOI:10.1017/S0033583515000190>

Waszkowycz, B., Perkins, T. D. J., Sykes, R. A., & Li, J. (2001). Large-scale virtual screening for discovering leads in the postgenomic era. *IBM Systems Journal*, *40*(2), 360–376. <https://doi.org/10.1147/sj.402.0360>

Webb, B., & Sali, A. (2016). Comparative protein structure modeling using MODELLER. *Current Protocols in Bioinformatics*, *2016*(1), 5.6.1-5.6.37. <https://doi.org/10.1002/cpbi.3>

Wei, J.-W., Huang, K., Yang, C., & Kang, C.-S. (2017). Non-coding RNAs as regulators in epigenetics (Review). *Oncol Rep*, *37*(1), 3–9. <https://doi.org/10.3892/or.2016.5236>

Wei, Y., Yu, L., Bowen, J., Gorovsky, M. A., & Allis, C. D. (1999). Phosphorylation of Histone H3 Is Required for Proper Chromosome Condensation and Segregation. *Cell*,

97(1), 99–109. [https://doi.org/10.1016/S0092-8674\(00\)80718-7](https://doi.org/10.1016/S0092-8674(00)80718-7)

Wermuth, C. G., Ganellin, C. R., Lindberg, P., & Mitscher, L. A. (1998). Glossary of terms used in medicinal chemistry (IUPAC Recommendations 1998). *Pure and Applied Chemistry*, 70(5), 1129–1143. <https://doi.org/10.1351/pac199870051129>

Wiech, N. L., Fisher, J. F., & Wiest, P. H. and O. (2009). Inhibition of Histone Deacetylases: A Pharmacological Approach to the Treatment of Non-Cancer Disorders. In *Current Topics in Medicinal Chemistry* (Vol. 9, Issue 3, pp. 257–271). <https://doi.org/http://dx.doi.org/10.2174/156802609788085241>

Wiederstein, M., & Sippl, M. J. (2007). ProSA-web: Interactive web service for the recognition of errors in three-dimensional structures of proteins. *Nucleic Acids Research*, 35(SUPPL.2), W407–W410. <https://doi.org/10.1093/nar/gkm290>

Williams, G. H., & Stoeber, K. (2012). The cell cycle and cancer. *Journal of Pathology*, 226(2), 352–364. <https://doi.org/10.1002/path.3022>

Williams, S. R., Aldred, M. A., Der Kaloustian, V. M., Halal, F., Gowans, G., McLeod, D. R., Zondag, S., Toriello, H. V., Magenis, R. E., & Elsea, S. H. (2010). Haploinsufficiency of HDAC4 Causes Brachydactyly Mental Retardation Syndrome, with Brachydactyly Type E, Developmental Delays, and Behavioral Problems. *The American Journal of Human Genetics*, 87(2), 219–228. <https://doi.org/10.1016/j.ajhg.2010.07.011>

Wilson, A. J., Byun, D. S., Nasser, S., Murray, L. B., Ayyanar, K., Arango, D., Figueroa, M., Melnick, A., Kao, G. D., Augenlicht, L. H., & Mariadason, J. M. (2008). HDAC4 promotes growth of colon cancer cells via repression of p21. *Molecular Biology of the Cell*, 19(10), 4062–4075. <https://doi.org/10.1091/mbc.E08-02-0139>

Wu, H.-C., Chang, D.-K., & Huang, C.-T. (2006). Targeted therapy for cancer. *J Cancer Mol*, 2(2), 57–66.

Xiangbin, X., Chang-Hoon, H., Chelsea, W., Weiye, W., Angelika, H., Klaus, P., N., O. E., A., M. T., & Zheng-Gen, J. (2007). Angiotensin II Stimulates Protein Kinase D-Dependent Histone Deacetylase 5 Phosphorylation and Nuclear Export Leading to Vascular Smooth Muscle Cell Hypertrophy. *Arteriosclerosis, Thrombosis, and Vascular Biology*, 27(11), 2355–2362. <https://doi.org/10.1161/ATVBAHA.107.151704>

Yang, H., Lou, C., Sun, L., Li, J., Cai, Y., Wang, Z., Li, W., Liu, G., & Tang, Y. (2019). AdmetSAR 2.0: Web-service for prediction and optimization of chemical ADMET properties. *Bioinformatics*, 35(6), 1067–1069. <https://doi.org/10.1093/bioinformatics/bty707>

Yang, S. Y. (2010). Pharmacophore modeling and applications in drug discovery: Challenges and recent advances. *Drug Discovery Today*, 15(11–12), 444–450. <https://doi.org/10.1016/j.drudis.2010.03.013>

Yang, X. J., & Seto, E. (2008). The Rpd3/Hda1 family of lysine deacetylases: From bacteria and yeast to mice and men. *Nature Reviews Molecular Cell Biology*, 9(3), 206–

218. <https://doi.org/10.1038/nrm2346>

Yang, Z., Wang, T., Wang, F., Niu, T., Liu, Z., Chen, X., Long, C., Tang, M., Cao, D., Wang, X., Xiang, W., Yi, Y., Ma, L., You, J., & Chen, L. (2016). Discovery of Selective Histone Deacetylase 6 Inhibitors Using the Quinazoline as the Cap for the Treatment of Cancer. *Journal of Medicinal Chemistry*, 59(4), 1455–1470. <https://doi.org/10.1021/acs.jmedchem.5b01342>

Yao, Y., Tu, Z., Liao, C., Wang, Z., Li, S., Yao, H., Li, Z., & Jiang, S. (2015). Discovery of Novel Class i Histone Deacetylase Inhibitors with Promising in Vitro and in Vivo Antitumor Activities. *Journal of Medicinal Chemistry*, 58(19), 7672–7680. <https://doi.org/10.1021/acs.jmedchem.5b01044>

Yeh, I. C., & Hummer, G. (2004). System-size dependence of diffusion coefficients and viscosities from molecular dynamics simulations with periodic boundary conditions. *Journal of Physical Chemistry B*, 108(40), 15873–15879. <https://doi.org/10.1021/jp0477147>

Yoshida, M. (2007). Potent and specific inhibition of mammalian histone deacetylase both in vivo and in vitro by trichostatin A. *Tanpakushitsu Kakusan Koso. Protein, Nucleic Acid, Enzyme*, 52(13 Suppl), 1788–1789. <http://www.jbc.org/content/265/28/17174.abstract>

Youngson, R. M. (2006). *Collins Dictionary of Human Biology*. Collins. <https://books.google.com.tr/books?id=EcRf1G4y76oC>

Zhang, C. L., McKinsey, T. A., Chang, S., Antos, C. L., Hill, J. A., & Olson, E. N. (2002). Class II Histone Deacetylases Act as Signal-Responsive Repressors of Cardiac Hypertrophy. *Cell*, 110(4), 479–488. [https://doi.org/10.1016/S0092-8674\(02\)00861-9](https://doi.org/10.1016/S0092-8674(02)00861-9)

Zhang, C. L., McKinsey, T. A., & Olson, E. N. (2001). The transcriptional corepressor MITR is a signal-responsive inhibitor of myogenesis. *Proceedings of the National Academy of Sciences*, 98(13), 7354 LP – 7359. <https://doi.org/10.1073/pnas.131198498>

Zhang, K., & Dent, S. Y. R. (2005). Histone modifying enzymes and cancer: Going beyond histones. *Journal of Cellular Biochemistry*, 96(6), 1137–1148. <https://doi.org/10.1002/jcb.20615>

Zhang, S., Huang, W., Li, X., Yang, Z., & Feng, B. (2015). Synthesis, Biological Evaluation, and Computer-Aided Drug Designing of New Derivatives of Hyperactive Suberoylanilide Hydroxamic Acid Histone Deacetylase Inhibitors. *Chemical Biology and Drug Design*, 86(4), 795–804. <https://doi.org/10.1111/cbdd.12554>

Zhang, T., Kohlhaas, M., Backs, J., Mishra, S., Phillips, W., Dybkova, N., Chang, S., Ling, H., Bers, D. M., Maier, L. S., Olson, E. N., & Brown, J. H. (2007). CaMKII $\delta$  Isoforms Differentially Affect Calcium Handling but Similarly Regulate HDAC/MEF2 Transcriptional Responses. *Journal of Biological Chemistry*, 282(48), 35078–35087. <http://www.jbc.org/content/282/48/35078.abstract>

Zhao, Y.-X., Wang, Y.-S., Cai, Q.-Q., Wang, J.-Q., & Yao, W.-T. (2015). Up-regulation



of HDAC9 promotes cell proliferation through suppressing p53 transcription in osteosarcoma. *International Journal of Clinical and Experimental Medicine*, 8(7), 11818–11823. <https://pubmed.ncbi.nlm.nih.gov/26380023>

Zhong, L., Sun, S., Yao, S., Han, X., Gu, M., & Shi, J. (2018). Histone deacetylase 5 promotes the proliferation and invasion of lung cancer cells. *Oncology Reports*, 40(4), 2224–2232. <https://doi.org/10.3892/or.2018.6591>

Zhu, C., Chen, Q., Xie, Z., Ai, J., Tong, L., Ding, J., & Geng, M. (2011). The role of histone deacetylase 7 (HDAC7) in cancer cell proliferation: regulation on c-Myc. *Journal of Molecular Medicine*, 89(3), 279–289. <https://doi.org/10.1007/s00109-010-0701-7>

Zhu, Y., Yan, Y., Gius, D. R., & Vassilopoulos, A. (2013). Metabolic regulation of Sirtuins upon fasting and the implication for cancer. *Current Opinion in Oncology*, 25(6). [https://journals.lww.com/co-oncology/Fulltext/2013/11000/Metabolic\\_regulation\\_of\\_Sirtuins\\_upon\\_fasting\\_and.8.aspx](https://journals.lww.com/co-oncology/Fulltext/2013/11000/Metabolic_regulation_of_Sirtuins_upon_fasting_and.8.aspx)

Ziwei YUN, H. W. (2012). *Yun, Quinolyl-containing hydroxamic acid compound and preparation method thereof, and pharmaceutical composition containing this compound and use thereof* (Patent No. CA2858033C). <https://patents.google.com/patent/CA2858033C/en?q=2858033>

## CURRICULUM VITAE

### Personal Information

Name Surname : Ammar Dawoud Elmezayen

### Education

Undergraduate Education : Bachelor of Allied Medical Sciences in Medical Technology, Zarqa University, Jordan, September 1999 – June 2004.

Graduate Education : Master of Science degree in Human Genetics, Medical Research Institute, Egypt, September 2008 – March 2011.

Foreign Language Skills : Arabic (native), English.

### Publications:

1. **Ammar D. Elmezayen** & Kemal Yelekçi (2020) Homology modeling and in silico design of novel and potential dual-acting inhibitors of human histone deacetylases HDAC5 and HDAC9 isozymes, *Journal of Biomolecular Structure and Dynamics*, DOI: 10.1080/07391102.2020.1798812
2. **Ammar D. Elmezayen**, Anas Al-Obaidi, Alp Tegin Şahin & Kemal Yelekçi (2020) Drug repurposing for coronavirus (COVID-19): in silico screening of known drugs against coronavirus 3CL hydrolase and protease enzymes, *Journal of Biomolecular Structure and Dynamics*, DOI: 10.1080/07391102.2020.1758791
3. Anas Al-Obaidi, **Ammar D. Elmezayen** & Kemal Yelekçi (2020) Homology modeling of human GABA-AT and devise some novel and potent inhibitors via computer-aided drug design techniques, *Journal of Biomolecular Structure and Dynamics*, DOI: 10.1080/07391102.2020.1774417
4. Erensoy G, Ding K, Zhan CG, **Elmezayen A**, Yelekçi K, Duracık M, Bingöl-Özakpınar Ö, Küçükgülzel İ. Synthesis, in silico studies and cytotoxicity evaluation of novel 1,3,4-oxadiazole derivatives designed as potential mPGES-1 inhibitors. *J Res Pharm.* 2020; 24(4): 436-451. DOI: 10.35333/jrp.2020.187
5. **Ammar D. Elmezayen**, MSc, Samia M. Kotb, PhD, Nadia A. Sadek, MD, Ebtesam M. Abdalla, PhD,  $\beta$ -Globin Mutations in Egyptian Patients With  $\beta$ -Thalassemia, *Laboratory Medicine*, Volume 46, Issue 1, Winter 2015, Pages 8–13, <https://doi.org/10.1309/LM1AYKG6VE8MLPHG>

## ANNEX A

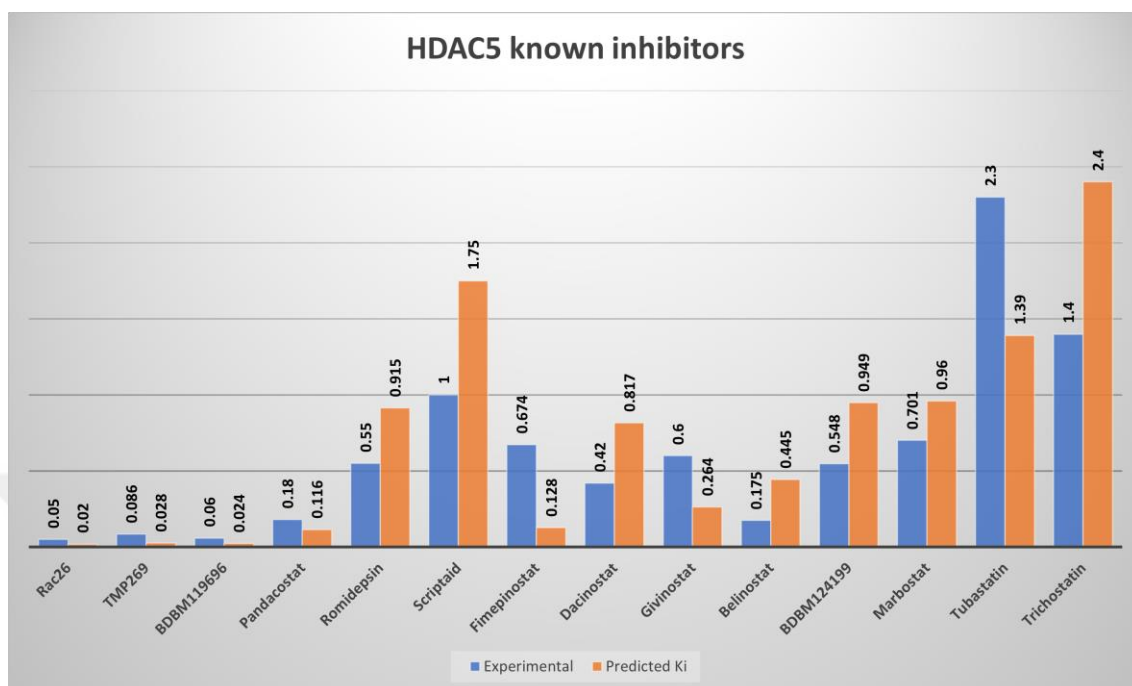


**Figure 0.1.** Correlation between the experimental catalytic activities ( $K_i$  or  $IC_{50}$ ) of HDAC5 known inhibitors with the in silico predicted  $K_i$  values for the same inhibitors. Experimental values are presented in blue color, while in silico calculations are given in orange color.

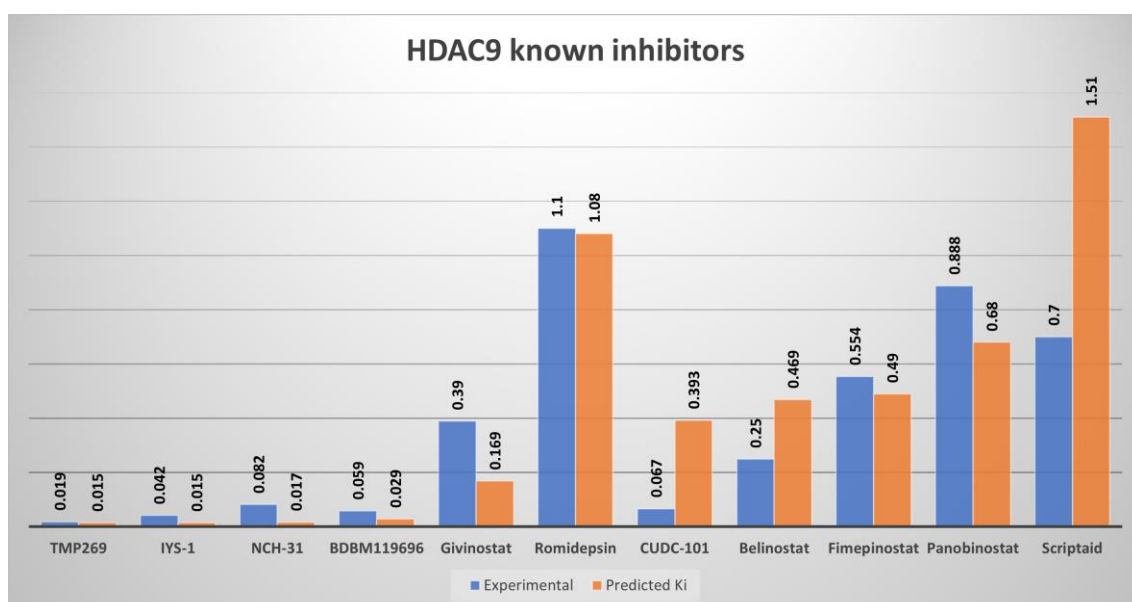


**Figure 0.2.** A comparison chart between the experimental catalytic activities ( $K_i$  or  $IC_{50}$ ) of the HDAC9 known inhibitors and their corresponding in silico predicted  $K_i$  values.